

# **Impact of anthropogenic stressors on the estuarine nitrogen cycle**

Dissertation

zur Erlangung des Doktorgrades

an der Fakultät für Mathematik, Informatik und Naturwissenschaften

Fachbereich Erdsystemwissenschaften

der Universität Hamburg

vorgelegt von

Gesa Schulz

Hamburg, 2023



Fachbereich Erdsystemwissenschaften

Datum der Disputation:

29.08.2023

Gutachter/innen der Dissertation:

Dr. Kirstin Dähnke

Dr. habil. Birgit Gaye

Zusammensetzung der Prüfungskommission:

Vorsitz Dr. habil. Birgit Gaye

Dr. Kirstin Dähnke

PD Dr. Eva Spieck

Prof. Dr. Hermann W. Bange

Prof. Dr. Kai Jensen

Vorsitzender des Fach-Promotionsausschusses

Erdsystemwissenschaften:

Prof. Dr. Hermann Held

Dekan der Fakultät MIN:

Prof. Dr.-Ing. Norbert Ritter



---

## **Eidesstattliche Versicherung | Declaration on Oath**

Hiermit erkläre ich an Eides statt, dass ich die vorliegende Dissertationsschrift selbst verfasst und keine anderen als die angegebenen Quellen und Hilfsmittel benutzt habe.

I hereby declare upon oath that I have written the present dissertation independently and have not used further resources and aids than those stated.

Hamburg, den

Gesa Schulz



---

## Abstract

Eutrophication due to excessive nutrient inputs poses a massive threat to water quality and biodiversity in many inland waters and in oceans. Estuaries can significantly alter riverine nutrient loads before they reach adjacent coastal oceans. As nutrient filters, they can either be sinks or additional sources of reactive nitrogen. The biogeochemistry of estuaries and their filter function are strongly affected by anthropogenic impacts and activities. In this thesis, the effects of different stressors on nitrogen retention, nitrogen turnover, and the production of the atmospheric trace gas nitrous oxide were examined in two heavily anthropogenically impacted estuaries in Germany: Elbe and Ems.

For the Elbe, the close coupling of river discharge with the riverine nitrogen cycle was shown using long-term measurements of nutrient concentrations and nitrate stable isotopes. The riverine nitrogen loads decreased disproportionately to the concurrent reduction in nutrient inputs. This decrease was caused by intensified nitrogen retention in the Elbe River basin and fueled phytoplankton growth under low discharge conditions. At present, decreasing nitrogen inputs and intensified nitrate retention result in nitrate depletion upstream of the Hamburg Port region and an upstream shift in heterotrophic respiration and remineralization processes. In contrast, a reverse effect is seen in the Port of Hamburg: the synergetic effects of enhanced phytoplankton blooms and altered suspended particulate matter dynamics increase nitrate production at low discharges.

The spatiotemporal variability of nitrous oxide in the Elbe Estuary revealed the drivers of nitrous oxide production and emissions in estuaries with high agricultural nutrient inputs. The Elbe Estuary is a year-round source of nitrous oxide, with the highest emissions in winter along with high nitrogen loads and wind speeds. However, despite significantly reduced nitrogen loads in spring and summer, nitrous oxide saturations and emissions do not decrease to the same extent during this period. High nutrient loads from agriculture promote phytoplankton blooms, leading to high organic matter availability that fuels nitrification. This leads to year-round high nitrous oxide emissions and a decoupling from dissolved inorganic nitrogen loads.

In the hyper-turbid Ems Estuary, suspended particulate matter concentrations and the linked oxygen deficits controlled nitrogen turnover and nitrous oxide production. Transect measurements revealed distinct biogeochemical zones along the estuary. High suspended particulate matter loads enhance denitrification but also trigger nitrous oxide production and enhance oxygen-depleted zones. As turbidity decreases, nitrification gains importance.

Altogether, this study highlights the synergistic effects of multiple stressors on nitrogen cycling in highly anthropogenically influenced estuaries. Thus, it emphasizes the need for a holistic approach to water quality improvement, nutrient reduction, and sediment management, which must also include possible impacts of climate change.

---

## Zusammenfassung

Eutrophierung aufgrund überhöhter Nährstoffeinträge gefährdet massiv die Wasserqualität und Artenvielfalt in vielen Binnengewässern und Meeren. Dabei können Ästuar die Nährstoffbelastung von Flüssen erheblich verändern, bevor diese die angrenzenden Küstenmeere erreichen. Als Nährstofffilter fungieren sie entweder als Senken oder zusätzliche Quellen für reaktiven Stickstoff. Dabei wird die Biogeochemie der Ästuar und ihre Filterfunktion durch anthropogene Einflüsse und Veränderungen stark beeinflusst. In dieser Arbeit wurden die Auswirkungen verschiedener Stressoren auf die Stickstoffretention, den Stickstoffumsatz und die Produktion des atmosphärischen Spurengases „Lachgas“ in zwei stark anthropogen geprägten Ästuar in Deutschland untersucht: der Elbe und der Ems.

Für die Elbe wurde die enge Kopplung des Durchflusses mit dem aquatischen Stickstoffkreislauf anhand von Langzeitmessungen der Nährstoffkonzentrationen und stabilen Nitratisotopen gezeigt. Bei einer Verringerung der Nährstoffeinträge nahmen die Stickstofffrachten der Elbe überproportional ab. Dieser Rückgang ist zurückzuführen auf einen verstärkten Stickstoffrückhalt im Elbeeinzugsgebiet mit verstärktem Phytoplanktonwachstum bei niedrigen Durchflüssen. Gegenwärtig führen abnehmende Stickstoffeinträge und verstärkter Nitratrückhalt zu niedrigen Nitratkonzentrationen stromaufwärts des Hamburger Hafens, und einer stromaufwärts gerichteten Verlagerung der heterotrophen Respirations- und Remineralisierungsprozesse. Im Hamburger Hafen zeigt sich dagegen ein umgekehrter Effekt: Das Zusammenwirken von der verstärkten Phytoplanktonblüte mit einer veränderten Schwebstoffdynamik erhöht die Nitratproduktion bei niedrigen Durchflüssen.

Die räumliche und zeitliche Variabilität der Lachgas Konzentration im Elbeästuar zeigt die Treiber der Lachgasproduktion und -emissionen in Ästuar mit hohem Nährstoffeinträgen aus der Landwirtschaft. Das Elbeästuar ist eine ganzjährige Lachgasquelle mit den höchsten Emissionen im Winter. Getrieben wird dies durch hohe Stickstofffrachten und hohe Windgeschwindigkeiten. Trotz deutlich reduzierter Stickstofffrachten im Frühjahr und Sommer nehmen die Sättigungen und Emissionen von Lachgas in dieser Zeit jedoch nicht in dem gleichen Maße ab. Hohe Nährstoffeinträge aus der Landwirtschaft fördern hier Phytoplanktonblüten, was zu einer hohen Verfügbarkeit organischen Materials führt, die die Nitrifikation erhöht. Das Ergebnis sind weiterhin hohe Lachgasemissionen und eine Entkopplung von den gelösten anorganischen Stickstofffrachten.

Im sehr trüben Emsästuar bestimmen die Schwebstoffkonzentrationen und die damit verbundenen Sauerstoffdefizite den Stickstoffumsatz und die Lachgasproduktion. Transektmessungen machten

hier eine deutliche biogeochemische Zoneneinteilung des Ästuars möglich. Die hohen Schwebstofffrachten fördern die Denitrifikation, verstärken aber auch die Lachgasproduktion und die Ausbildung von sauerstoffarmen Zonen. Mit abnehmender Trübung gewinnt die Nitrifikation an Bedeutung.

Insgesamt verdeutlicht diese Arbeit das synergetische Zusammenwirken mehrerer Stressfaktoren auf den Stickstoffkreislauf in stark anthropogen beeinflussten Ästuaren. Sie unterstreicht damit die Notwendigkeit eines ganzheitlichen Ansatzes zur Nährstoffreduktion, zum Sedimentmanagement und zur Verbesserung der Wasserqualität, bei dem auch mögliche Auswirkungen des Klimawandels berücksichtigt werden müssen.

---

## Table of contents

Eidesstaatliche Erklärung   Declaration of Oath.....	III
Abstract.....	V
Zusammenfassung .....	VII
Table of contents .....	IX
List of figures.....	X
List of tables .....	XII
1 Introduction .....	1
2 Low discharges intensify nitrogen retention in rivers – a case study in the Elbe River .....	13
3 How low discharges affect estuarine nitrogen turnover – a case study in the freshwater Elbe Estuary .....	31
4 Seasonal variability of nitrous oxide concentrations and emissions along a temperate estuary .....	49
5 Suspended particulate matter drives the spatial segregation of nitrogen turnover along the hyper-turbid Ems Estuary .....	73
6 Conclusions and outlook.....	97
Abbreviations.....	101
References .....	103
Appendix .....	127
List of publications .....	159
Acknowledgments .....	161

---

## List of figures

<b>Figure 1.1.</b> Schematic illustration of the nitrogen cycle.....	3
<b>Figure 1.2.</b> Isotope effect of nitrogen turnover processes central for estuarine environments.....	7
<b>Figure 2.1.</b> Discharge measured at the gauge Neu Darchau from 1985 to 2021.....	18
<b>Figure 2.2.</b> Annual and seasonal variation of nitrogen concentrations at weir Geesthacht from 1985 to 2019.....	19
<b>Figure 2.3.</b> Annual and seasonal variation of nutrient concentrations and nitrate stable isotopes at weir Geesthacht from June 2011 to June 2021.....	20
<b>Figure 2.4.</b> Annual nitrogen loads at weir Geesthacht from 1985 to 2021.....	21
<b>Figure 2.5.</b> Average annual total nitrogen concentrations plotted against annual total nitrogen emissions from Germany and annual average discharge from 1985 to 2016.....	22
<b>Figure 2.6.</b> Regression based analysis of fraction of annual German TN emissions to surface water reaching the Elbe Estuary at the weir in Geesthacht 1985 to 2019.....	25
<b>Figure 2.7.</b> Seasonal variation of total organic nitrogen fractions in total nitrogen concentration from 1980s to 2010s.....	28
<b>Figure 3.1.</b> The Elbe Estuary.....	33
<b>Figure 3.2.</b> Annual average discharge and daily discharge measured at the gauge in Neu Darchau from 2011 to 2022.....	36
<b>Figure 3.3.</b> Suspended particulate matter dynamic in the Port of Hamburg at station Seemanshoef from 2011 to 2022.....	37
<b>Figure 3.4.</b> Near surface water column properties from 17 summer transect cruises done from 2011 to 2022 along the freshwater Elbe Estuary.....	39
<b>Figure 3.5.</b> Nitrate stable isotopes plotted against concentrations upstream of the Hamburg Port in the Elbe Estuary.....	41
<b>Figure 3.6.</b> Exemplary comparison of two summer cruises along the freshwater Elbe Estuary in 2013 and 2019.....	43
<b>Figure 3.7.</b> Nitrate gain along the freshwater Elbe Estuary.....	45

---

<b>Figure 4.1.</b> Map of the Elbe Estuary .....	52
<b>Figure 4.2.</b> Near surface water column properties from eleven transect cruises done from 2015 to 2022 along the Elbe Estuary .....	57
<b>Figure 4.3.</b> Plots of excess nitrous oxide vs apparent oxygen utilization along the Elbe Estuary ...	61
<b>Figure 4.4.</b> Succession of nitrogen bearing substances coming from the North Sea and in the Port of Hamburg in September 2020 .....	64
<b>Figure 4.5.</b> Seasonal variability of average nitrous oxide saturations, average nitrous oxide emissions, average dissolved inorganic nitrogen loads and ratio of nitrous oxide emissions and dissolved inorganic nitrogen loads. ....	70
<b>Figure 5.1.</b> Map of the Ems Estuary .....	76
<b>Figure 5.2.</b> Near surface water column properties along the Ems Estuary .....	82
<b>Figure 5.3.</b> Dissolved oxygen concentration 0.5 m above riverbed during our research cruises along the Ems Estuary in 2014 and 2020 .....	84
<b>Figure 5.4.</b> Nitrate concentrations and isotope values of nitrate plotted versus salinity in the Ems Estuary for 2014 and 2020.....	85
<b>Figure 5.5.</b> PCA results for the Ems Estuary in 2014 and 2020. ....	86

---

## List of tables

<b>Table 3.1.</b> Length, area and typical residence time upstream and downstream of the Port of Hamburg as a function of low and medium discharge .....	46
<b>Table 4.1.</b> Campaign dates with the sampled Elbe Estuary sections shown via stream kilometers, average discharge during each cruise, averages and standard deviations for water temperature, wind speed at 10 m height, dissolved inorganic nitrogen concentrations for each campaign .....	52
<b>Table 4.2.</b> Calculated average nitrous oxide saturation, sea-to-air fluxes calculated and atmospheric nitrous oxide dry mole fractions during cruises in the Elbe Estuary .....	59
<b>Table 4.3.</b> Annual nitrous oxide emission estimates from the Elbe Estuary .....	60
<b>Table 4.4.</b> Pearson correlation coefficients for nitrous oxide saturation with temperature, pH value, oxygen, ammonium concentrations, nitrite concentrations, nitrate concentrations, suspended particulate matter concentrations, C/N values, particulate carbon fraction and particulate nitrogen fraction within sections of the Elbe Estuary .....	62
<b>Table 4.5.</b> Pearson correlation coefficients for average nitrous oxide saturation with average discharge, temperature, pH value, oxygen, ammonium concentrations, nitrite concentrations, nitrate concentrations, suspended particulate matter concentrations, C/N values, particulate carbon fraction and particulate nitrogen fraction within sections of the Elbe Estuary .....	62

---

# 1 Introduction

## 1.1 Estuaries as coastal nutrient filters

Estuaries are situated in the land-ocean interface and can be defined as the tidally influenced transition zone between marine and riverine environments. Their ecosystems have some of the highest diversity and productivity in the world (Hobbie 2000; Bianchi 2007; Kennish 2017), with physical and biogeochemical coupling taking place on many spatial and temporal scales (Bianchi 2007; Voss et al. 2011; Chilton et al. 2021). Estuaries act as potential nutrient filters that can significantly alter riverine nutrient loads before they reach adjacent coastal oceans (Crossland et al. 2005; Bianchi 2007; Bouwman et al. 2013). Thereby, they can either be sinks or additional sources of reactive nitrogen, which is one of the main drivers of eutrophication (Middelburg and Nieuwenhuize 2000; Dähnke et al. 2008; Voss et al. 2011).

Over the last 150 years, the excessive input of nutrients, primarily nitrogen and phosphorus from point and diffuse sources (Galloway et al. 2003; Kennish 2017), has caused eutrophication (Galloway et al. 2003; Howarth 2008; van Beusekom et al. 2019), one of the major threats to coastal ecosystems worldwide (Howarth and Marino 2006; Voss et al. 2011). Eutrophication may result in harmful algae blooms (Anderson et al. 2002; Brockmann et al. 2003; Heisler et al. 2008), oxygen depletion (Diaz and Rosenberg 2008), loss of seagrass meadows (Orth et al. 2006; Burkholder et al. 2007) and shifts in species abundances (Cadée and Hegeman 1974, 2002).

Enhanced nutrient loads also stimulate biogeochemical turnover processes, including production of nitrous oxide (N<sub>2</sub>O; Seitzinger 1988; Bianchi 2007; Bange 2008), an important atmospheric trace gas. With a global warming potential of approximately 300 times that of carbon dioxide over a 100-year time span (IPCC 2007), nitrous oxide contributes to global warming and stratospheric ozone depletion (WMO 2018; IPCC 2022). Nitrous oxide is accountable for at least 6 % of the 1.5 °C global temperature increase, with an average tropospheric concentration of  $332.1 \pm 0.4$  ppb in 2019 and a continuous increase of  $0.85 \pm 0.03$  ppb yr<sup>-1</sup> during the period from 1995 to 2019 (IPCC 2021). Estuaries are potential sources of nitrous oxide (e.g., Bange 2006; Barnes and Upstill-Goddard 2011; Murray et al. 2015; Bange et al. 2019), contributing, together with coastal wetlands, between 0.17 and 0.95 Tg N<sub>2</sub>O-N of the annual global budget of 16.9 Tg N<sub>2</sub>O-N (Murray et al. 2015; Tian et al. 2020).

Several resolutions to combat eutrophication were enacted in the 1980s, including decisions at the second Ministerial Conference on the Protection of the North Sea in 1987 (INSC-2) and the

Convention for the Protection of Marine Environment of the North-East Atlantic in 1988 (OSPAR). Their aim was to reduce riverine nutrient loads by 50 % from 1985 to 1995 (INSC 1987; OSPAR 1988; de Jong 2007). According to OSPAR, a healthy marine environment in which eutrophication no longer occurs should have been established by 2010 (de Jong 2007). Indeed, riverine nutrient loads have decreased since the late 1980s, but the 50 % reduction in nutrient loads of continental European rivers was not reached until the 2010s (van Beusekom et al. 2019), and nutrient pollution remains an urgent problem to this day (EEA 2019). The OSPAR strategy for 2020 to 2030 aims to combat eutrophication by limiting nutrient inputs to avoid adverse eutrophication effects and also takes into consideration the effects of climate change (OSPAR 2021).

### **1.2 The aquatic nitrogen cycle and its production of nitrous oxide**

Nitrogen is an essential nutrient for all organisms. It exists in multiple chemical forms and can rapidly be converted by microorganisms. Its most abundant form is triple bonded unreactive dinitrogen gas ( $N_2$ ), composing nearly 78 % of the atmosphere. It is unavailable for most microorganisms, making nitrogen a limiting nutrient for biological use. Through  $N_2$ -fixation, nitrogen is reduced into a reactive form. In aquatic ecosystems, these are primarily organic nitrogen and dissolved inorganic nitrogen (DIN), which include ammonium ( $NH_4^+$ ), nitrite ( $NO_2^-$ ) and nitrate ( $NO_3^-$ ). The cycle closes when nitrogen returns to the atmosphere as gaseous dinitrogen or nitrous oxide ( $N_2O$ ; Figure 1.1; e.g., Gruber 2008; Damashek and Francis 2018). In aquatic ecosystems, sources and sinks of nitrogen are widely recognized (Gruber 2008; Damashek and Francis 2018). In particular, the processes of remineralization with coupled nitrification and denitrification are important (Figure 1.1). Both processes are also known to be the main producers of nitrous oxide in aquatic ecosystems (e.g., Bange 2008; Murray et al. 2015; Quick et al. 2019).

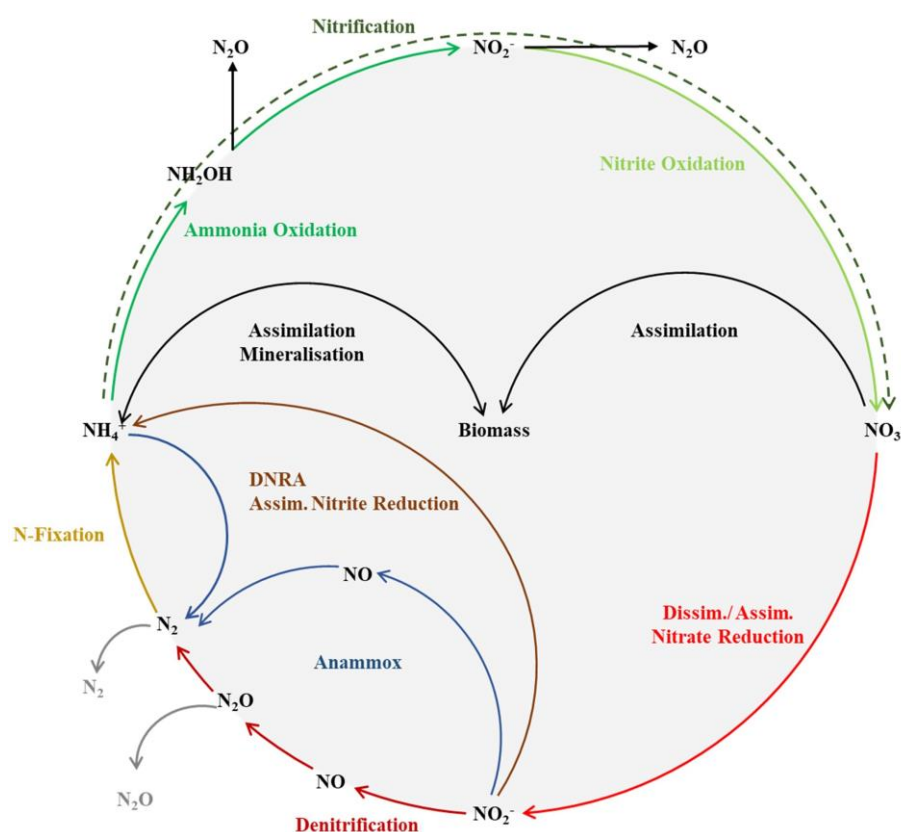


**Figure 1.1.** Schematic illustration of the nitrogen cycle modified from Daims et al. (2016).

As an important process in the aquatic nitrogen cycle, denitrification leads to a loss of reactive nitrogen by the stepwise heterotrophic dissimilatory reduction of nitrate to dinitrogen. Nitrite, nitric oxide (NO) and nitrous oxide are intermediate products of this process (Figure 1.1; Knowles 1982; Tiedje 1988). A wide range of facultative anaerobic bacteria perform denitrification that reduces nitrate when oxygen becomes limited (Knowles 1982; Tiedje 1988; Bothe et al. 2000; Damashek and Francis 2018). Since nitrous oxide is an intermediate product, its concentration produced by denitrification depends on the balance of its production and consumption (Tiedje 1988; Bange 2008).

Nitrification is an aerobic, autotrophic process linking organic matter input with reactive nitrogen removal by remineralization. It describes the microbial-catalyzed oxidation of ammonium to nitrate with hydroxylamine ( $NH_2OH$ ) and nitrite as intermediate products (Figure 1.1). The first step is performed by ammonia-oxidizing bacteria (AOB) and ammonia-oxidizing archaea (AOA), while the second step is mainly performed by nitrite-oxidizing bacteria (NOB; Wrage et al. 2001; Ward 2008). Recently, nitrifying bacteria were discovered that completely oxidize ammonium to nitrate (= comammox; Daims et al. 2015; van Kessel et al. 2015). During nitrification, two subpathways possibly lead to nitrous oxide production. First, hydroxylamine oxidation produces nitrous oxide (Bremner 1997; Otte et al. 1999). The second pathway, chemodenitrification, describes the reduction

of nitrite to nitrous oxide (Tiedje 1988; Bremner 1997). Both processes can also produce nitric oxide or  $N_2$ . Under low oxygen conditions, nitrifier denitrification may occur, in which nitrifiers first oxidize ammonia to nitrite followed by its reduction to nitric oxide, nitrous oxide and  $N_2$  (Wrage et al. 2001).

During assimilation, phytoplankton use either nitrate or ammonium to build biomass (Figure 1.1). Phytoplankton usually prefer ammonium over nitrate because nitrate conversion requires a two-step reaction in the cell. The first is a reduction to nitrite and the second to ammonium before it can be converted to biomass. Therefore, nitrate uptake is more energy consuming and generally less favorable (Dortch 1990; Kirchman 1994; Gruber 2008).

Remineralization (= ammonification) transforms labile organic nitrogen to ammonium, reversing the reaction of ammonium assimilation (Figure 1.1). Heterotrophic bacteria release ammonium during their energy production by the oxidation of organic carbon to carbon dioxide ( $CO_2$ ; Nixon 1981; Gruber 2008).

Other processes of the nitrogen cycle are (Figure 1.1): anaerobic ammonium oxidation (anammox) combining ammonium and nitrite to  $N_2$  (Strous et al. 1999; Trimmer et al. 2003), dissimilatory nitrate reduction to ammonium (DNRA) reducing nitrate to produce ammonium (Tiedje 1988; Damashek and Francis 2018) and biological  $N_2$  fixation converting  $N_2$  to reactive nitrogen (Karl et al. 1997; Capone et al. 2005; Damashek and Francis 2018).

### 1.3 Stable isotopes as a tool to disentangle the nitrogen cycle

Isotopes are atoms of the same element with the same number of protons and electrons but different quantities of neutrons and different atomic masses. Nitrogen has two stable isotopes:  $^{14}N$  and  $^{15}N$ . In the global nitrogen pool, lighter  $^{14}N$  (99.635 %) is more abundant than heavier  $^{15}N$  (0.365 %). Oxygen is composed of three isotopes, with the commonly studied isotopes being  $^{16}O$  (99.759 %) and  $^{18}O$  (0.204 %) and the least abundant isotope being  $^{17}O$  (0.037 %; e.g., Sulzman 2007; Hoefs 2018).

Variation in the natural abundance of stable isotopes is shown in the relative differences in isotope ratios. The isotope ratio  $R$  is the ratio of heavy to light isotopes (Eq. 1.1). Since isotope differences are very small, the delta- $\delta$ -notation is used to describe the isotopic composition of samples (Eq. 1.2). The isotope ratio of a sample ( $R_{\text{Sample}}$ ) is reported relative to the isotope ratio of an internationally accepted reference material ( $R_{\text{Reference}}$ ). The reference material for  $\delta^{15}N$  is atmospheric  $N_2$ , and for  $\delta^{18}O$ , it is Vienna Standard Mean Ocean Water (VSMOW). The values are expressed in parts per thousands (e.g., Sulzman 2007; Coplen 2011; Hoefs 2018).

$$R = \frac{\text{abundance of heavier isotopes}}{\text{abundance of lighter isotopes}} \quad (1.1)$$

$$\delta (\text{‰}) = \left( \frac{R_{\text{Sample}} - R_{\text{Reference}}}{R_{\text{Reference}}} \right) \times 1000 \quad (1.2)$$

The number of electrons determines the chemical properties of an atom. Hence, the chemical properties of isotopes are qualitatively equal. However, atomic masses determine the vibrational energy of neutrons and protons, resulting in different reaction rates and bond strengths. As a result, the chemical bonds of heavier isotopes are stronger (Sulzman 2007; Hoefs 2018), leading to a discrimination of physical, chemical and biological processes between isotopes (e.g., Sulzman 2007; Casciotti 2016; Hoefs 2018). Equilibrium and unidirectional processes lead to “equilibrium fractionation” and “kinetic fractionation”, respectively. The latter usually dominates during the conversions of nitrogen in oceans (Sigman and Fripiat 2019). The kinetic isotope effect ( $\epsilon$ ) is defined as the ratio of reaction rates with which the heavy and light isotopes are converted (Eq. 1.3; Sigman and Fripiat 2019):

$$\epsilon (\text{‰}) = \left( \frac{{}^{14}k}{{}^{15}k} - 1 \right) \times 1000 \quad (1.3)$$

where  ${}^{14}k$  and  ${}^{15}k$  are the rate coefficients for the  ${}^{14}\text{N}$ - and  ${}^{15}\text{N}$ -containing reactants, respectively. Kinetic fractionation leads to predictable changes between the isotope ratios of the substrate and product that help to identify the individual production processes (Figure 1.2; e.g., Mariotti et al. 1981; Granger et al. 2004; Buchwald and Casciotti 2010; Sigman and Fripiat 2019).

The kinetic isotope effect ( $\epsilon$ ) can either be calculated using a Rayleigh model (closed-system) or a steady-state model (open-system). The closed-system approach is used for transformations that proceed with a constant isotope effect without a resupply of nitrogen. Thus, the isotope effect can be calculated when the reactant and substrate are neither lost nor replenished (Eq. 1.4; Sigman and Fripiat 2019):

$$\epsilon_{\text{substrate}} = \frac{\delta^{15}N_{\text{substrate}} - \delta^{15}N_{\text{initial}}}{\ln(f)} \quad (1.4)$$

where  $f$  is the remaining fraction with  $f = ([C]/[C_{\text{initial}}])$ . The  $\delta^{15}\text{N}$  value of the substrate and the initial value are denoted by  $\delta^{15}N_{\text{substrate}}$  and  $\delta^{15}N_{\text{initial}}$ .

The open-system approach is used to quantify processes where supply and uptake occur simultaneously and are relatively time-invariant. Thus, the isotope effect can be calculated if a steady state is assumed in which the reactant nitrate is continuously supplied and partially consumed (Eq. 1.5 and Eq. 1.6). This results in a linear relationship between nitrate isotope values and fraction  $f$ , where  $f = ([C]/[C_{initial}])$ . The isotope effects correspond to the slope of the regression (Sigman and Fripiat 2019):

$$\varepsilon_{substrate} = \frac{\delta^{15}N_{substrate} - \delta^{15}N_{initial}}{(1 - f)} \quad (1.5)$$

$$\varepsilon_{product} = \frac{\delta^{15}N_{product} - \delta^{15}N_{initial}}{f} \quad (1.6)$$

where  $\delta^{15}N_{substrate}$ ,  $\delta^{15}N_{product}$ , and  $\delta^{15}N_{initial}$  denote the  $\delta^{15}N$  values of the substrate and product at the time of sampling and the initial value, respectively. The remaining fraction of substrate at the time of sampling is described by  $f$ .

The fractionation occurring during specific turnover processes leads to nitrate stable isotopes being source specific, producing distinct isotopic values, e.g., different fertilizers, wastewater and sewage, atmospheric deposition or marine nitrogen. Thus, they can be used for source attribution. The nitrate dual approach (simultaneous analysis of nitrogen and oxygen isotopes) allows to distinguish processes that overlap with each other in  $\delta^{15}N$ -nitrate alone, leading to a more precise source determination (Kendall 1998; Kendall et al. 2007; Xue et al. 2009). Overall, dual stable isotope analysis of nitrate is a powerful tool to disentangle the nitrogen cycle and assess anthropogenic impacts (e.g., Deutsch et al. 2005; Wankel et al. 2006; Gaye et al. 2013; Korth et al. 2014; Buchwald et al. 2015; Dähnke et al. 2022; Tian et al. 2022).

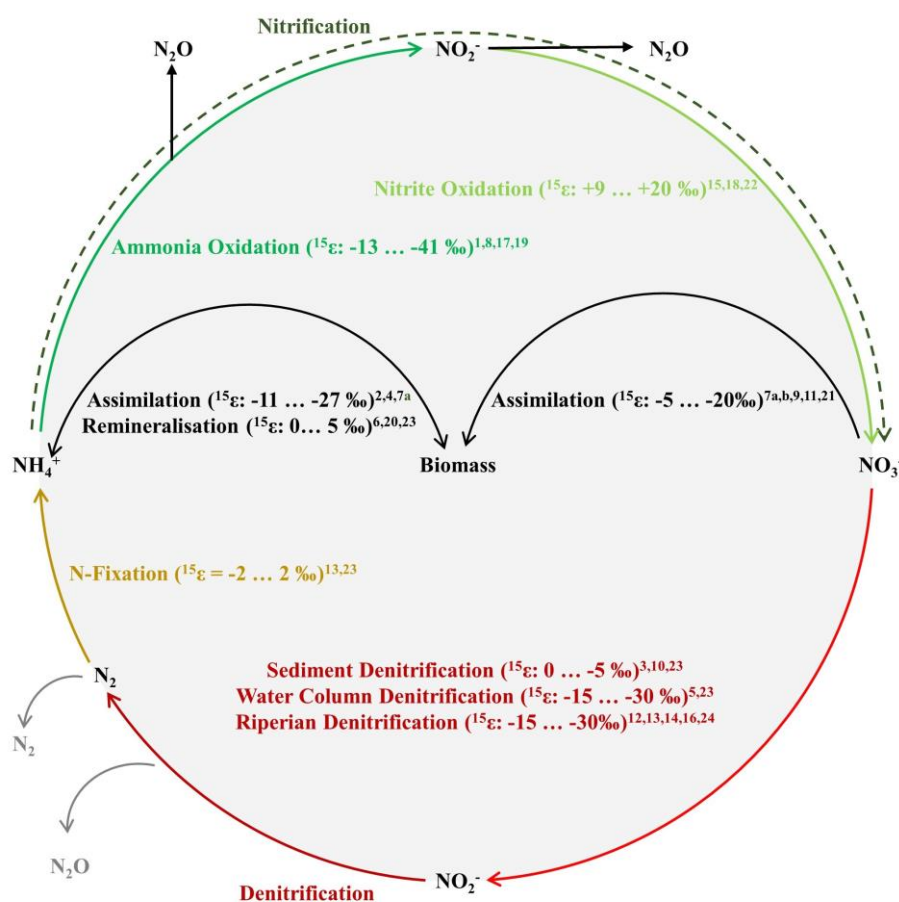


**Figure 1.2.** Isotope effect ( $^{15}\epsilon$ ) of nitrogen turnover processes central for estuarine environments. Negative isotope effects represent preference for the lighter  $^{14}\text{N}$  isotope whereas inverse isotope effects show a  $^{15}\text{N}$  preference. The range of the isotope effects were derived from literature: 1 - (Mariotti et al. 1981; Casciotti et al. 2003; Sigman et al. 2009; Santoro and Casciotti 2011), 2 - (Casciotti 2009; Buchwald and Casciotti 2010; Jacob et al. 2017), 3 - (Waser et al. 1998b; a; Granger et al. 2004; Needoba and Harrison 2004; Rohde et al. 2015), 4 - (Brandes and Devol 1997; Lehmann et al. 2004; Sigman and Fripiat 2019), 5 - (Brandes et al. 1998; Sigman and Fripiat 2019), 6 - (Deutsch et al. 2005; Kendall et al. 2007; Granger et al. 2008; Houlton and Bai 2009; Lutz et al. 2020), 7 - (Kendall et al. 2007; Sigman and Fripiat 2019), 8 - (Hoch et al. 1992; Voss et al. 1997; Waser et al. 1998a), 9 - (Kendall 1998; Möbius 2013; Sigman and Fripiat 2019)

#### 1.4 Anthropogenic impacts - estuaries under pressure

With approximately 23 % to 37 % of the global population living within 100 kilometers of a coast (Cohen et al. 1997; Nicholls and Small 2002; McMichael et al. 2020), estuarine biogeochemistry and the estuarine filter function are heavily affected by anthropogenic impacts and activities (Bianchi 2007; Kennish 2017; IPCC 2022), making estuaries an area of conflict among ecological, economic and social demands. Kennish (2017) summarized anthropogenic stressors on estuarine ecosystems and organized them into twelve categories, including nutrient enrichment, human-induced sediment/particulate inputs, dredging and disposal of dredged-material, human-altered hydrological regimes and climate change effects.

Urbanization, as well as local and global trading, has led to extensive modification of estuarine morphology (Kempe 1988; Bianchi 2007; Kennish 2017). Channel deepening, draining, damming, diking and land draining led to significant regime changes, including hyper-turbid conditions, tidal amplifications and loss of habitats (Winterwerp et al. 2013; de Jonge et al. 2014; Kennish 2017). Increased suspended particulate matter concentrations possibly result in light attenuation inhibiting primary production and causing extensive oxygen depletion (Talke et al. 2009; Kennish 2017). Changing salinity regimes and residence times can significantly affect the structure and function of microbial communities, as well as the estuarine nutrient filter function (Kennish 2017).

Climate change has multilayered effects on estuarine systems, as it affects not only environmental factors such as temperature and sea levels but also social and economic problems such as food production, urbanization, shipping and energy systems, naming only a few examples (Brasseur et al. 2017; Kennish 2017; IPCC 2022). Without further adaptation, the IPCC (2022) predicted increased flood risks as well as reduced freshwater inflow into estuaries due to more frequent droughts. These changes in discharge, combined with land use changes, can alter the salinity gradients, water quality and sediment dynamics. Alterations in residence times and warming can impact microbial communities and biogeochemical turnover processes, potentially increasing acidification and hypoxia in estuarine environments. Eutrophication further complicates these problems by decreasing both oxygen and pH and therefore exacerbating the occurrence and impact of dead zones (IPCC 2022).

### **1.5 Two heavily stressed estuaries: Elbe and Ems**

The two German estuaries Elbe and Ems are both heavily affected by anthropogenic impacts. Both have high population densities (ARGE-Elbe 2001; FGG Ems 2015a), receive high nutrient inputs from agriculture (Johannsen et al. 2008; FGG Elbe 2018; FGE Ems 2022) and are heavily modified in their morphologies (Winterwerp et al. 2013; Boehlich and Strotmann 2019).

The Elbe River stretches over 1094 km from its spring in the Giant Mountains (Czech Republic) to the North Sea (Cuxhaven, Germany) and is the second largest river discharging into the North Sea. The mean annual discharge is  $712 \text{ m}^3 \text{ s}^{-1}$  (measured at gauge Neu Darchau from 1926 to 2014; HPA and Freie und Hansestadt Hamburg 2017). The catchment of the Elbe River covers  $140\,268 \text{ km}^2$  with 74 % urban/agricultural land use (Johannsen et al. 2008) and an average population density of 167 inhabitants per  $\text{km}^2$  (ARGE-Elbe 2001).

The Elbe Estuary begins at a weir in Geesthacht and flows through the Port of Hamburg, entering the North Sea near Cuxhaven. The Elbe Estuary serves as an important shipping fairway and hosts the third largest port in Europe (Port of Hamburg 2021). To accommodate for large container ships, the

estuary is continuously deepened and dredged throughout the entire year (Boehlich and Strotmann 2019; Hein et al. 2021). Construction work for further deepening of the fairway was carried out from 2019 to early 2022.

High nutrient inputs from agriculture lead to an annual nitrogen load of 84 Gg-N (2011-2015; FGG Elbe 2018), making the Elbe Estuary the largest source of nitrogen in the German Bight (Brockmann and Pfeiffer 1990), which is heavily affected by eutrophication (van Beusekom et al. 2019). After the reunification of Germany in 1990, the closing of East German industries and the implementation of wastewater treatment (e.g., Bergemann et al. 1996; Guhr et al. 2000) led to improved oxygen concentrations. This, in combination with high nutrient loads, allowed for phytoplankton growth to reestablish (Kerner 2000; Amann et al. 2012; Hillebrand et al. 2018; Rewrie et al. submitted), and a shift of predominant denitrification to significant nitrification transformed the Elbe Estuary from a nitrate sink to a nitrate source (Dähnke et al. 2008). A hotspot of nitrification exists in the Port of Hamburg (Sanders et al. 2018), which results from a sudden change in morphology. The increase in water depth leads to light limitation and decomposition of phytoplankton entering the port from the upper estuary and river (Kerner 2000; Schöl et al. 2014; Hein et al. 2016). As a consequence, substrate is available for coupled remineralization and nitrification (Sanders et al. 2018; Dähnke et al. 2022), and intense respiration leads to oxygen depletion as well as low-oxygen zones in the Port of Hamburg (Kerner 2000; Schöl et al. 2014).

The Ems River has a length of 370 km and discharges into the Wadden Sea, a part of the southern North Sea (van Beusekom and de Jonge 1994; Krebs and Weilbeer 2008). It has an average discharge of  $79 \text{ m}^3 \text{ s}^{-1}$  (measured at gauge Versen from 1942 to 2015, NLWKN 2018). The catchment of the Ems is  $17\,934 \text{ km}^2$  (Krebs and Weilbeer 2008), with dominant agricultural (80 %) and 8 % urban land use (FGG Ems 2015b). The population density of the catchment is approximately 200 inhabitants per  $\text{km}^2$  (FGG Ems 2015c).

The Ems Estuary is situated on the Dutch-German border with an annual nitrogen load of 12 Gg-N between 2013 and 2018 (FGE Ems 2022). The estuary is approximately 100 km long and stretches from the weir at Herbrum to the island Borkum. The Ems Estuary is also an important waterway with ports in Delfzijl and Emden and is used for the transport of large vessels from the shipyard in Papenburg to the North Sea (Talke and de Swart 2006). Bos et al. (2012) classified the Ems Estuary as a degraded ecological system with high nutrient loads.

Dredging and channel deepening led to tidal amplification and to a significant increase in suspended particulate matter concentrations and hyper-turbid conditions in the Ems Estuary (Winterwerp et al. 2013; de Jonge et al. 2014; van Maren et al. 2015a). As a result, shifts in species abundances (Compton et al. 2017), anoxic conditions in the water column (Schuchardt et al. 2007; Talke et al.

2009), and reduced primary production due to light limitation (Bos et al. 2012; de Jonge and Schückel 2019) were reported.

## 1.6 Main focus and thesis outline

Estuaries are sites of intense human activity with increasing anthropogenic impacts due to ongoing population growth, heavy recreational and commercial use, and development in coastal regions (Bianchi 2007; Bouwman et al. 2013; Kennish 2017). Anthropogenic changes may significantly alter the estuarine nitrogen filter function (Horrigan et al. 1990; Soetaert et al. 2006; Dähnke et al. 2008; Voss et al. 2011). Although the individual nitrogen turnover processes are well understood, the responses of estuarine nitrogen turnover to anthropogenic stressors need to be assessed. The interplay between two or more stressors may be synergetic, causing a more serious impact when the stressors are combined than when they are alone (Kennish 2017). Thus, a profound understanding of estuarine nitrogen turnover processes and their controls is crucial to assess complex management studies (Bianchi 2007; Kennish 2017). Ultimately, this thesis focused on the effects of different stressors on nitrogen retention, nitrogen turnover and nitrous oxide production in the two heavily anthropogenically impacted Elbe and Ems estuaries by addressing three main research questions:

- 1) How do low discharge conditions affect riverine nitrogen input, nitrogen retention, and nitrogen turnover in heavily anthropogenically impacted estuaries?
- 2) What are the drivers of nitrous oxide production, and emissions in heavily anthropogenically impacted estuaries with high nutrient inputs?
- 3) How do suspended particulate matter concentrations affect nitrogen turnover and retention, including nitrous oxide production, in hyper-turbid estuaries?

This thesis consists of four chapters that were either published, have been submitted or are in preparation for submission to a peer-reviewed scientific journals (Chapters 2-5). Detailed information on author contributions is given in *List of publications*. In Chapter 6, the findings of the thesis are summarized, leading to a main conclusion and an outlook for future research.

## Chapter 2: “Low discharges intensify nitrogen retention in rivers – a case study in the Elbe River”

Gesa Schulz, Justus E. E. van Beusekom, Juliane Jacob, Sina Bold, Andreas Schöl, Markus Ankele, Tina Sanders and Kirstin Dähnke, *Science of The Total Environment*, 904, 166740, <https://doi.org/10.1016/j.scitotenv.2023.166740>, 2023.

The impact of low freshwater discharge on riverine nitrogen input and nitrogen retention was studied for the Elbe River, the largest source of nitrogen in the German Bight. From 1985 to 2019, the nitrogen input into the estuary at the weir in Geesthacht was characterized by using data provided by

the River Basin Community Elbe. Additionally, from 2011 to 2021, surface water samples were taken regularly to analyze dissolved inorganic nutrient concentrations and nitrate stable isotope compositions. We found that with decreasing discharge, the nitrogen retention of the Elbe Estuary increased, potentially doubling the retention compared to average discharge conditions. Longer residence times and more light availability due to lower water levels fueled phytoplankton uptake. This suggests that the recent reduction in Elbe River nitrogen loads was not a result of successful management alone but was amplified by persisting low discharge conditions in the catchment.

### **Chapter 3: “How low discharges affect estuarine nitrogen turnover – a case study in the freshwater Elbe Estuary”**

*Gesa Schulz, Tina Sanders, Vanessa Russnak, Justus E. E. van Beusekom, and Kirstin Dähnke [in preparation]*

The effects of low freshwater discharge on nitrate retention and nitrate turnover in heavily anthropogenically impacted estuaries were studied for the freshwater section of the Elbe Estuary based on 17 summer cruises (May to August) from 2011 to 2022. Intensified nitrate retention due to low freshwater discharge led to nitrate depletion upstream of the Hamburg Port region and an early collapse of the phytoplankton bloom. This resulted in an upstream shift of heterotrophic processes with accumulated ammonium concentrations and oxygen depletion. In Hamburg Port, low discharges fueled the synergetic effects of enhanced phytoplankton blooms and altered suspended particulate matter dynamics, leading to high nitrate gains and reversing the effect of increased retention in the upstream areas. Overall, our findings highlighted the need for a holistic approach to water quality improvement, nutrient mitigation and sediment management in heavily anthropogenically impacted estuaries.

### **Chapter 4: “Seasonal variability of nitrous oxide concentrations and emissions along a temperate estuary”**

*Gesa Schulz, Tina Sanders, Yoana G. Voynova, Hermann W. Bange, and Kirstin Dähnke, Biogeosciences, 20, 3229-3247, <https://doi.org/10.5194/bg-20-3229-2023>, 2023.*

To identify drivers of nitrous oxide production and emissions in heavily managed estuaries, we studied the spatiotemporal variability of nitrous oxide in the Elbe Estuary. During nine research cruises performed between 2017 and 2022, we measured dissolved nitrous oxide concentrations, dissolved nutrients and oxygen concentrations along the estuary and calculated nitrous oxide saturation and emissions. We found the estuary to be a year-round source of nitrous oxide, with the highest emissions in winter along with high DIN loads and wind speeds. However, in spring and

summer, nitrous oxide saturation and emission did not decrease in scale with DIN loads, suggesting that in-situ production is important regardless of the season. Two hot-spot areas of nitrous oxide production existed: the Port of Hamburg and the mesohaline estuary near the estuarine turbidity maximum (MTZ), with production being fueled by the decomposition of either riverine (in the Hamburg Port) or marine organic matter (in the MTZ). Previous measurements in the Elbe Estuary revealed that nitrous oxide saturation was decoupled from DIN loads after an improvement in water quality in the 1990s that allowed phytoplankton growth to reestablish. This, combined with the overarching control of organic matter on nitrous oxide production, highlighted the linkage between eutrophication and nitrous oxide emissions in estuaries with high agricultural inputs.

### **Chapter 5: “SPM drives the spatial segregation of nitrogen turnover along the hyper-turbid Ems Estuary”**

*Gesa Schulz, Tina Sanders, Justus E. E. van Beusekom, Yoana G. Voynova, Andreas Schöl, and Kirstin Dähnke, Biogeosciences, 19, 2007–2024, <https://doi.org/10.5194/bg-19-2007-2022>, 2022.*

The hyper-turbid Ems Estuary served as the study area to assess the interplay of suspended particulate matter and nitrogen turnover and nitrous oxide emissions. During two research cruises in August 2014 and June 2020, we measured water column properties, dissolved inorganic nitrogen, dual stable isotopes of nitrate and dissolved nitrous oxide concentrations along the estuary. We found that three distinct biogeochemical zones existed along the estuary. A strong fractionation of nitrate stable isotopes pointed toward nitrate removal via water column denitrification in the hyper-turbid tidal river, driven by anoxic conditions in deeper water layers. In the middle reaches of the estuary, nitrification gained importance, turning this section into a net nitrate source. The outer reaches were dominated by mixing, with nitrate uptake in 2020. We found that the overarching control on biogeochemical nitrogen cycling, zonation and nitrous oxide production in the Ems Estuary was exerted by suspended particulate matter concentrations and the linked oxygen deficits.

---

## 2 Low discharges intensify nitrogen retention in rivers – a case study in the Elbe River

*Schulz, G., van Beusekom, J. E. E., Jacob, J., Bold, S., Schöl, A., Ankele, M., Sanders, T., and Dähnke, K.: Low discharges intensifies nitrogen retention in rivers – a case study in the Elbe River, Science of The Total Environment, 904, 166740, <https://doi.org/10.1016/j.scitotenv.2023.166740>, 2023.*

### Abstract

Eutrophication due to excessive nutrient inputs is a major threat to coastal ecosystems worldwide, leading among others to harmful algae blooms, seagrass loss and hypoxia. Decisions to combat eutrophication in the North Sea were made in the 1980s. Despite significant improvements in recent decades, high nitrogen loads and resulting eutrophication remain problematic. In this study, we characterize nitrogen inputs to the Elbe Estuary (Germany) at a weir separating the river from the estuary based on nitrogen data provided by the Elbe River Basin Community Elbe from 1985 to 2019. In surface water samples taken at regular intervals from 2011 to 2021, we analyze dissolved inorganic nitrogen concentrations and nitrate stable isotope compositions. Our findings highlight the close coupling of river discharge with the riverine nitrogen cycle. Moreover, we find that nitrogen loads decreased disproportionately with decreasing discharge. This decrease is due to intensified nitrogen retention in the Elbe catchment, potentially doubling the retention compared to average discharge conditions. Phytoplankton growth was enhanced by long residence times and high light availability at low water levels. This suggests that the recent decreases in nitrogen loads in the Elbe River were not only a result of management measures in the catchment but were also amplified by a recent long-lasting drought in the catchment. Based on projections from the Intergovernmental Panel on Climate Change, we anticipate more frequent and extensive droughts, which may lead to future seasonal shift from a silicate/phosphate limitation to nitrate limitation in the lower Elbe River.

### 2.1 Introduction

For more than 150 years, the growing use of synthetic fertilizers has led to high nutrient loads in rivers and coastal regions (Galloway et al. 2003). This has caused eutrophication (Galloway et al. 2003; Howarth 2008; van Beusekom et al. 2019), a major threat to coastal ecosystems worldwide (Howarth and Marino 2006; Voss et al. 2011). Some possible consequences are harmful algae blooms (Anderson et al. 2002; Heisler et al. 2008), oxygen depletion (Diaz and Rosenberg 2008), loss of

seagrass meadows (Orth et al. 2006; Burkholder et al. 2007) and shifts in species abundance (Cloern 2001; Brockmann et al. 2003). In the North Sea, enhanced algae blooms, shifts in phytoplankton composition (Cadée and Hegeman 1974, 2002) and anoxic events in bottom water (von Westernhagen et al. 1986) have been observed since the early 1970s. Consequently, decisions were made to combat eutrophication, for example, goals were set to reduce riverine nutrient loads by 50 % from 1985 to 1995 (de Jong 2007). In fact, riverine nutrient loads have decreased since the late 1980s, but the set goal of a 50 % load reduction in continental European rivers was only reached in the 2010s (e.g., van Beusekom et al. 2019) and, nutrient pollution remains an urgent problem to this day (EEA 2019).

Biological nitrogen (N) transformation in rivers alters the composition of the total nitrogen (TN) load that is transported to adjacent coastal zone. Phytoplankton assimilation of dissolved inorganic nitrogen (DIN) results in addition of nitrogen to the organic nitrogen pool (Ritz and Fischer 2019), whereas riparian or sediment denitrification reduces the total nitrogen load. The relative contribution of transformation processes within a river is governed by environmental factors such as temperature, discharge, oxygen and organic matter availability (e.g., Nixon 1981; Thornton et al. 2007; Diaz and Rosenberg 2008; Voss et al. 2011; Carstensen et al. 2014).

In particular, discharge conditions have a clear effect on riverine nutrient loads (van Beusekom et al. 2019), with wet years leading to enhanced nutrient dynamics compared to dry years (van Beusekom and de Jonge 2002). Long-term observations can help to disentangle the individual effects of discharge or nutrient retention and to determine environmental corridors or trends driven by climate change or management measures (e.g., Bianchi 2007).

In addition to nutrient measurements, dual nitrate stable isotopes are a powerful tool to disentangle the effects of nitrogen uptake and removal. Biological turnover processes favor lighter isotopes, leading to an enrichment in the remaining nitrate pool and a process-specific isotope effect used to identify nitrate uptake and production processes (e.g., Granger et al. 2004; Wankel et al. 2006; Dähnke et al. 2010; Sigman and Fripiat 2019). Both phytoplankton assimilation and denitrification lead to an increase in  $\delta^{15}\text{N}$ -nitrate and  $\delta^{18}\text{O}$ -nitrate values. Assimilation increases  $\delta^{15}\text{N}$ -nitrate and  $\delta^{18}\text{O}$ -nitrate in parallel, following a 1:1 slope (Granger et al. 2004), whereas isotope enrichment during denitrification follows a 0.5:1 slope (Böttcher et al. 1990; Mengis et al. 1999; Granger and Wankel 2016; Wong et al. 2020). Thus, it is possible to distinguish between both processes based on nitrate dual stable isotope analysis.

We investigated nitrogen input and retention in the Elbe River (Germany) at the river/estuarine transition. We used nitrogen data provided by the River Basin Community Elbe (FGG Elbe) between 1985 and 2019, and additional surface water samples were taken at the weir at stream kilometer 589

from 2011 to 2021. In these samples, we analyzed the dissolved inorganic nitrogen concentrations and nitrate dual stable isotope composition. With this study we want to investigate the effect of altered freshwater discharge on riverine nitrogen retention. We further evaluate potential changes in seasonal nitrogen turnover over the past decade, and address the possibility of a future nitrate limitation in this heavily managed estuary.

## **2.2 Methods**

### **2.2.1 Study site**

The Elbe River spans over 1094 km from its spring in the Giant Mountains (Czech Republic) to the North Sea (Cuxhaven, Germany). The catchment of the Elbe River is 140 268 km<sup>2</sup>, with 74 % urban/agricultural land use (Johannsen et al. 2008) and an average population density of 167 inhabitants per km<sup>2</sup> (ARGE-Elbe 2001). The Elbe River is the second largest German river (Brockmann and Pfeiffer 1990), with an average annual freshwater discharge of 712 m<sup>3</sup> s<sup>-1</sup> (measured at gauge Neu Darchau at stream kilometer 536 and calculated from 1926 to 2014; HPA and Freie und Hansestadt Hamburg 2017). A weir at stream kilometer 585 separates the river from the tidal estuary. The Elbe is the largest source of dissolved nitrogen for the German Bight (Brockmann and Pfeiffer 1990), with an annual nitrogen load of 84 kT-N at stream kilometer 628.9 between 2011 and 2015 (FGG Elbe 2018).

### **2.2.2 FGG Elbe data**

Total nitrogen (TN) and dissolved inorganic nitrogen concentrations (DIN) at the weir in Geesthacht (stream kilometer 585.9) were obtained from the FGG Elbe data portal (FGG Elbe 2022). They took weekly water samples from 1985 to 1987, biweekly from 1994 to 2006, and monthly samples from 2006 to 2019. The data were supplemented by longitudinal sampling campaigns along the estuary that were performed three to eleven times a year from 1990 to 2019. The sample data are listed in Table A1.1 and Table A1.2. The total organic nitrogen (TON) concentration in the data was calculated from the difference between TN and DIN.

### **2.2.3 Water sampling at the weir in Geesthacht**

Starting in 2011, we took surface water samples at regular intervals from a location upstream of the weir (585, 53°25'31''N, 10°20'10''E) between the riverine and estuarine sections of the Elbe River. Generally, samples were taken once or twice per month. Water temperature was measured immediately after sampling. The water was then transferred into 2 L PE bottles for immediate transport to the laboratory. Within an hour, samples were filtered through pre-combusted and weighed GF/F filters (450 °C, 4.5 h) and stored in acid-washed (10 % HCl, overnight) PE bottles

at -20°C for subsequent analysis of nitrate, phosphate, silicate, particulate nitrogen and nitrate stable isotopes as described below (Section 2.2.4).

For nutrient concentrations, triplicates of filtered water samples were measured with a continuous flow auto analyzer (AA3, SEAL Analytics) and standard colorimetric and fluorometric techniques (Hansen and Koroleff 1999). The detection limits were 0.05 µmol L<sup>-1</sup> for nitrate (NO<sub>3</sub><sup>-</sup>), 0.05 µmol L<sup>-1</sup> for nitrite (NO<sub>2</sub><sup>-</sup>), 0.07 µmol L<sup>-1</sup> for ammonium (NH<sub>4</sub><sup>+</sup>), 0.03 µmol L<sup>-1</sup> for silicate (Si) and 0.13 µmol L<sup>-1</sup> for phosphate (PO<sub>4</sub><sup>3-</sup>). Particulate nitrogen concentrations were measured with an Elemental Analyzer (Eurovector EA 3000) with a certified acetanilide standard (IVA Analysetechnik, Germany) as the reference material.

#### 2.2.4 Isotopic analysis of nitrate

To measure the stable isotope composition of nitrate in the filtered water samples, the denitrifier method was used (Sigman et al. 2001; Casciotti et al. 2002). The method is based on the analysis of nitrous oxide (N<sub>2</sub>O), which is produced by denitrifying *Pseudomonas aureofaciens* (ATCC#13985) from nitrate (NO<sub>3</sub><sup>-</sup>) and nitrite (NO<sub>2</sub><sup>-</sup>) in the filtered water samples. A GasBench II coupled with an isotope ratio mass spectrometer (Delta XP Plus, Thermo Fisher Scientific) measured the produced nitrous oxide. For calibration, two international standards (USGS34, δ<sup>15</sup>N-nitrate -1.8 ‰, δ<sup>18</sup>O-nitrate -27.9 ‰; IAEA, δ<sup>15</sup>N-nitrate +4.7 ‰, δ<sup>18</sup>O-nitrate +25.6 ‰) and one internal standard (δ<sup>15</sup>N-nitrate +7.6 ‰) were measured during each run. The standard deviation for standards and samples was <0.2 ‰ (n= 4) for δ<sup>15</sup>N-nitrate and <0.5 ‰ (n=4) for δ<sup>18</sup>O-nitrate. If the nitrite concentration in the samples exceeded 5 % of the combined concentrations of nitrite and nitrate (NO<sub>x</sub><sup>-</sup>), nitrite was removed before performing the measurement using Sulfamic Acid (4 % Sulfamic Acid in 10 % HCl (Granger and Sigman 2009)).

Nitrogen turnover processes lead to a specific isotope effect in the nitrogen isotope ratios that can be used to identify individual turnover process pathways (e.g., Kendall et al. 2007). We assumed steady-state and calculated the isotope effect with an open-system approach (Eq. 2.1), in which the reactant nitrate is continuously supplied and partially consumed, leading to a linear relationship between nitrogen isotopes and the fraction *f*. The isotope effect  $\epsilon$  corresponds to the slope of the regression line (Sigman et al. 2009).

$$\epsilon_{substrate} = \frac{\delta^{15}N_{substrate} - \delta^{15}N_{initial}}{1 - f} \quad (2.1)$$

Where δ<sup>15</sup>N values of the substrate and initial values are δ<sup>15</sup>N<sub>substrate</sub> and δ<sup>15</sup>N<sub>initial</sub>, respectively. The fraction of substrate remaining at the time of sampling is denoted by *f*, where  $f = [C]/[C_{initial}]$ , with *C*

and  $C_{initial}$  being the nitrate concentration of the sample and initial values, respectively. In our study, we used average winter isotope values as initial values.

### 2.2.5 Calculations of annual loads

From the FGG Elbe dataset and our measured nutrient concentrations, we calculated the annual and seasonal loads ( $L$ ) of total nitrogen, dissolved inorganic nitrogen and total organic nitrogen as in Eq. 2.2:

$$L = \sum_{i=1}^k c_i^{II} Q_i \quad (2.2)$$

Where  $c_i^{II}$  is the concentration data of day  $i$  (from available concentration data or linearly temporal interpolation).  $Q_i$  is the discharge measured on day  $i$  in Neu Darchau (stream kilometer 536). The annual load is the sum of the daily loads within one year (Pätsch and Lenhart 2011).

## 2.3 Results

### 2.3.1 Discharge conditions

The average discharge from 1985 to 2021 was  $653 \text{ m}^3 \text{ s}^{-1}$ , which is below the long-term average annual freshwater discharge of  $712 \text{ m}^3 \text{ s}^{-1}$  calculated from 1926 to 2014 (HPA and Freie und Hansestadt Hamburg 2017). Seasonal dynamics are characterized by high discharges from January to March and low discharges from June to August. Since 2013, the annual discharges has been low with an average annual discharge of  $539 \text{ m}^3 \text{ s}^{-1}$ . A similar situation occurred in the years 1989 to 1993 with five successive years of low discharge conditions (Figure 2.1a; Weilbeer et al. 2021). Over the observation period (1985 to 2021), the daily discharge was below the long-term mean low water discharge of  $276 \text{ m}^3 \text{ s}^{-1}$  (1924 to 2014; HPA and Freie und Hansestadt Hamburg 2017) over 10 % of days. Forty-four percent of these days occurred over the last eight years, i.e., since 2014. The years 2015, 2018, 2019 and 2020 were particularly dry, with more than 68 days of low discharge ( $276 \text{ m}^3 \text{ s}^{-1}$ ). Major flood events occurred in spring 1988, summer 2002, spring 2006, winter 2011 and summer 2013 (Figure 2.1b; HPA and Freie und Hansestadt Hamburg 2017).

For the time period from 2010 to 2019, the Federal Maritime and Hydrographic Agency provided mean annual residence times for the Elbe River in summer (June to August; Table A1.3). We found a significant correlation of residence time with logarithmic annual summer discharge ( $R = -0.95$ ,  $p < 0.001$ ; Figure A1.1), leading to increased retention times with low discharge conditions in the Elbe River (e.g., Hein et al. 2016).

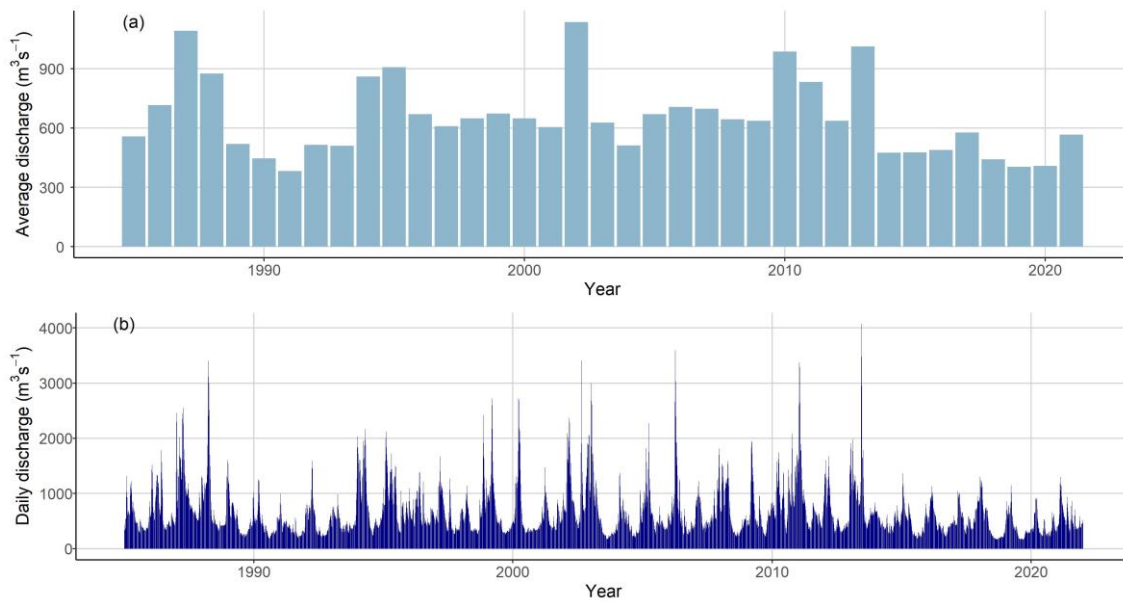


**Figure 2.1.** Discharge measured at the gauge Neu Darchau at stream kilometer 536 from 1985 to 2021: (a) annual average discharge and (b) daily discharge (FGG Elbe 2022).

### 2.3.2 Annual nitrogen dynamics

To investigate the development of the annual nitrogen dynamics at the weir in Geesthacht, we used two datasets: (1) FGG Elbe data including TN, DIN and calculated TON concentrations and (2) our own sample set, collected from the weir Geesthacht starting in 2011. Both datasets match in terms of nutrient concentration, ensuring comparability (Figure A1.2).

Since 1985, TN and DIN concentrations have decreased significantly (FGG Elbe data). The mean annual TN concentrations ranged from  $546.9 \mu\text{mol L}^{-1}$  in 1985 to  $173.8 \mu\text{mol L}^{-1}$  in 2018 (Figure 2.2a). The highest mean annual DIN concentrations were measured in 1986 ( $444.7 \mu\text{mol L}^{-1}$ ), and decreased to  $111.8 \mu\text{mol L}^{-1}$  in 2018 (Figure 2.2c). The mean annual TON concentrations remained relatively stable over the observation period, varying between  $109.9 \mu\text{mol L}^{-1}$  in 1985 and  $38.0 \mu\text{mol L}^{-1}$  in 2010 (Figure 2.2e).

The DIN and TON concentrations showed opposite seasonal dynamics, with the lowest DIN and highest DON values in summer (Figure 2.2d, f). Since DIN was usually the dominant nitrogen form, seasonal TN dynamics followed the same pattern as DIN (Figure 2.2b, d). However, in the later years, TON concentrations exceeded DIN concentrations in midsummer (June to July, Figure 2.7).

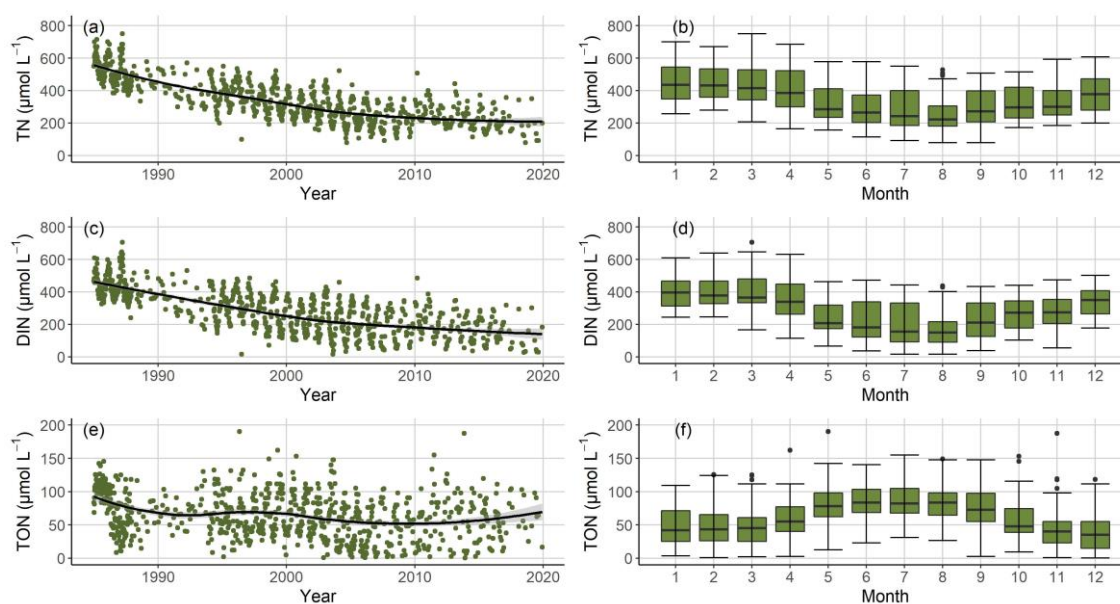


**Figure 2.2.** FGG Elbe dataset showing annual (left) and seasonal (right) variations in (a, b) TN concentrations, (c, d) DIN concentrations and (e, f) TON concentrations from 1985 to 2019 (Section 2.2.2; FGG Elbe 2022). The black line displays local regression fittings (loess method) for the annual data. In the boxplots, the lines indicate median values, boxes show the 25th and 75th percentiles and whiskers indicate the data range without outliers.

In our weir samples (2011 to 2021), nitrate was the predominant form of DIN, with the highest concentrations in winter (maximum  $377.8 \mu\text{mol L}^{-1}$  in February 2021) and the lowest in summer (approaching  $0.2 \mu\text{mol L}^{-1}$  in August 2019; Figure 2.3a, b). Nitrite was mostly below  $1 \mu\text{mol L}^{-1}$  (Figure 2.3c, d) and only reached an unusually high maximum of  $5.7 \mu\text{mol L}^{-1}$  during a flood event in June 2013. The ammonium concentration ranged from not detectable (mostly March to May) to  $24.4 \mu\text{mol L}^{-1}$  in August 2018 (Figure 2.3e, f). The ammonium and nitrite concentrations peaked in winter and summer, whereas the concentrations were low in spring and autumn. The highest silicate concentrations occurred in winter and ranged from  $202.9 \mu\text{mol L}^{-1}$  in March 2012 to  $<1 \mu\text{mol L}^{-1}$  in late spring, with the lowest monthly average of  $9.2 \mu\text{mol L}^{-1}$  in May (Figure 2.3i, j). The phosphate concentration ranged from not detectable in summer to  $5.8 \mu\text{mol L}^{-1}$  in October 2016 or  $8.7 \mu\text{mol L}^{-1}$  during the flood event in June 2013 (Figure 2.3k, l).

Nitrate stable isotope values varied seasonally, with the lowest values in winter and highest values in summer (Figure 2.3m, n and Figure 2.3o, p). The lowest  $\delta^{15}\text{N}$ -nitrate was measured in February 2016 at  $4.3 \text{‰}$  and  $\delta^{18}\text{O}$ -nitrate was measured in December 2014 at  $0.3 \text{‰}$ . The highest values were  $30.0 \text{‰}$  in July 2018 and  $22.0 \text{‰}$  in July 2019 for  $\delta^{15}\text{N}$ -nitrate and  $\delta^{18}\text{O}$ -nitrate, respectively.

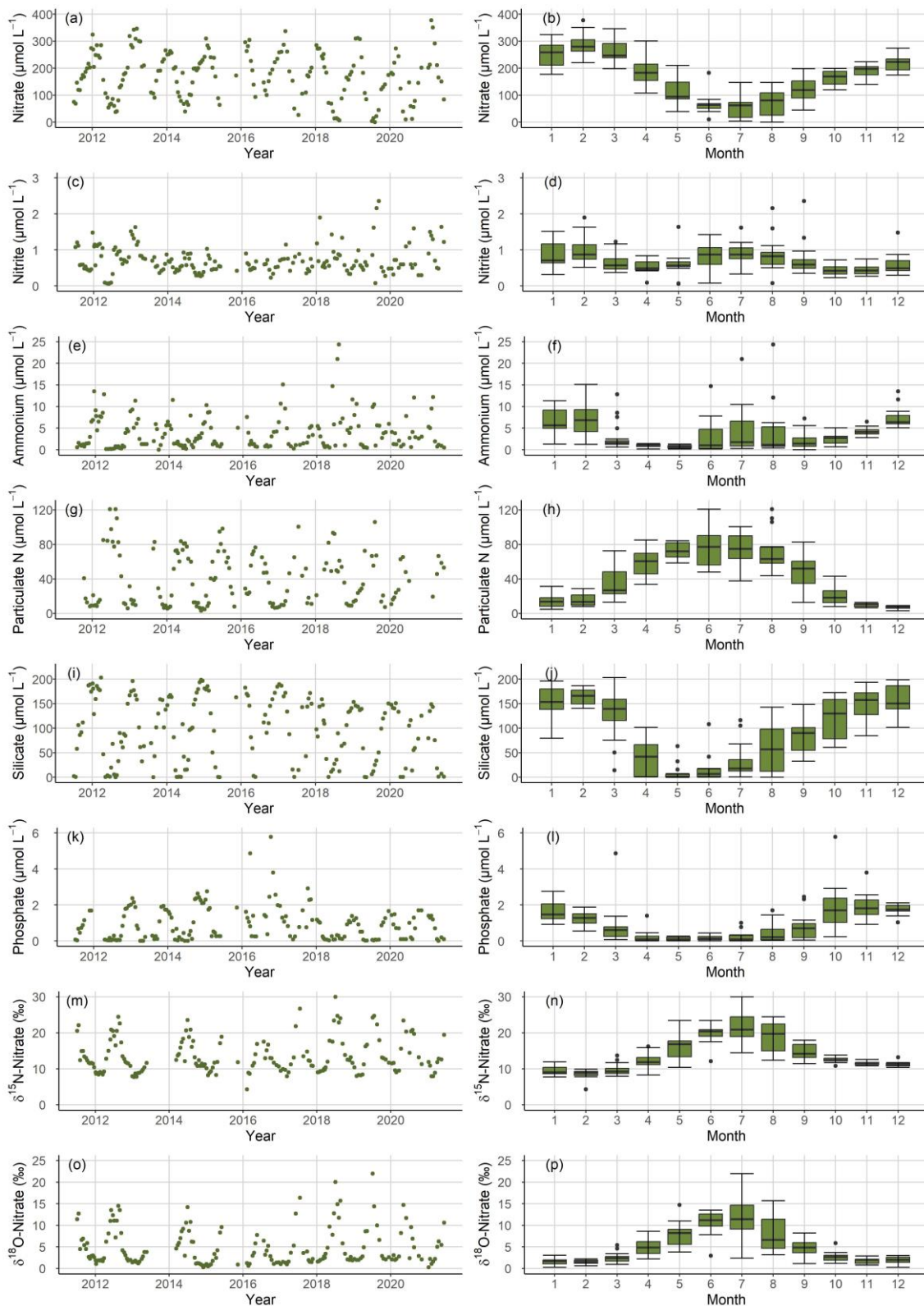


**Figure 2.3.** Weir sampling dataset showing annual (left) and seasonal (right) variations in (a, b) nitrate concentrations, (c, d) nitrite concentrations, (e, f) ammonium concentrations, (g, h) particulate nitrogen (PN) concentrations, (i, j) silicate concentrations, (k, l) phosphate concentrations, (m, n)  $\delta^{15}\text{N}$ -nitrate and (o, p)  $\delta^{18}\text{O}$ -nitrate measured at weir Geesthacht from June 2011 to June 2021 (Section 2.2.3). In the boxplots, we excluded data from the flood event in summer 2013 to illustrate typical seasonal patterns. In the boxplots, the lines indicate median values, boxes show the 25th and 75th percentiles and whiskers indicate the data range without outliers.

### 2.3.3 Annual nitrogen loads

To calculate annual loads, we used the FGG Elbe data (Section 2.2.2) and data from our sampling campaign at weir Geesthacht (Section 2.2.3). Annual total nitrogen (TN) loads clearly decreased over our observation period (Figure 2.4a), with a maximum of 252.9 kt in 1987 and a minimum load of 39.2 kt in 2019 (Figure 2.4a). The dissolved inorganic nitrogen (DIN) load also decreased over time and was highest in 1987 (227.3 kt) and lowest in 2020 (29.0 kt; Figure 2.4b). For total organic nitrogen (TON), the decrease in loads was less evident. A maximum load of 27.0 kt was observed in 2002, and the minimum load was 8.1 kt in 2004 (Figure 2.4c).

Total annual TN loads decreased. This can be attributed to decreasing inputs as well as to interannual changes or trends in discharge. To separate both factors, we divided the annual TN loads by the annual discharge, yielding a discharge-weighted mean concentration. This weighted concentration shows a clear decrease from below 600  $\mu\text{mol L}^{-1}$  to approximately 250  $\mu\text{mol L}^{-1}$  (Figure 2.4d).

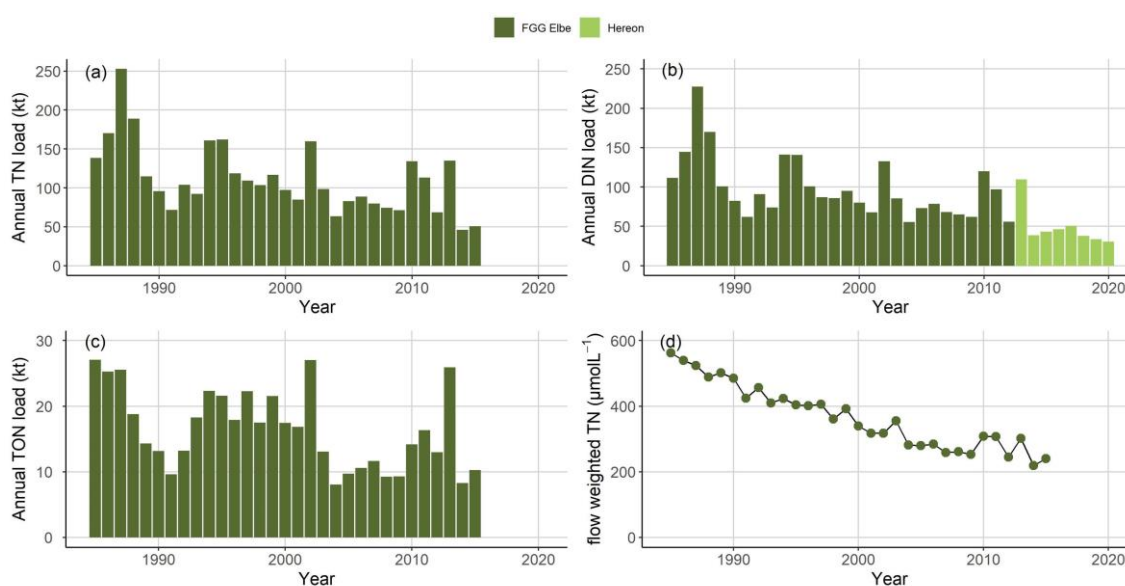


**Figure 2.4.** (a) Annual total nitrogen loads (TN), (b) annual dissolved inorganic nitrogen (DIN) loads, (c) annual total organic nitrogen (TON) loads, and (d) flow-weighted TN load (annual TN load/annual discharge). Loads calculated using the FGG Elbe dataset are shown in dark green, and loads derived from our sampling campaign (Hereon) are light green.

## 2.4 Discussion

### 2.4.1 Impact of discharge on nitrogen retention in the Elbe Basin

Since the first signs of coastal eutrophication along the Dutch and German coasts were observed in the 1970s (e.g., de Jonge and Postma 1974; Gieskes and Kraay 1977), a government-established target to reduce nutrient input was set in 1988 (de Jong 2007). In Germany, a reduction in nitrogen loads occurred after reunification in 1990 due to the collapse of eastern German industries (e.g., Guhr

et al. 2000), leading to large changes in both oxygen dynamics and dominant nitrogen forms. Reduced nitrogen input from agriculture (UBA 2017; BMEL 2022) and the implementation of wastewater treatment (UBA 2015, 2020) also contributed to the observed decrease in nitrogen loads. Rewrie et al. (submitted) identified three ecosystem states in the Elbe Estuary: polluted (up to 1990), transitional (1991-1996) and recovery (since 1997) based on dissolved inorganic carbon concentrations. The FGG Elbe dataset shows that the total nitrogen loads into the Elbe River clearly decreased over this period (Figure 2.4). However, the flow-normalized concentrations do not show a clear difference between the three ecosystems states but rather continuous decline.

To separate the effects of annual differences in discharge or management measures on the TN concentrations and loads, we used five-year moving averages of total nitrogen input to surface water bodies in Germany (TN Germany) in the time period from 1987 to 2016 provided by UBA (2020; Figure A1.3). These management measures have clearly decreased the overall annual national nitrogen emissions in Germany, and the average annual nitrogen concentrations of the Elbe River obviously reflected this general decrease in earlier years (Figure 2.4a and Figure 2.5a). From 1985 to 2004, average annual TN concentrations correlated significantly with annual German TN emissions (Figure 2.5a;  $R = 0.93$ ,  $p < 0.001$ ). In this time period, TN concentrations showed no clear correlation with discharge (Figure 2.5c). However, starting in 2005, we observe a shift, so TN concentrations are no longer significantly correlated with German TN emissions (Figure 2.5b) but rather correlate with average annual discharge (Figure 2.5d;  $R = 0.85$ ,  $p < 0.001$ ). This suggests that recent changes in average annual TN concentrations reflect annual variabilities in discharge.

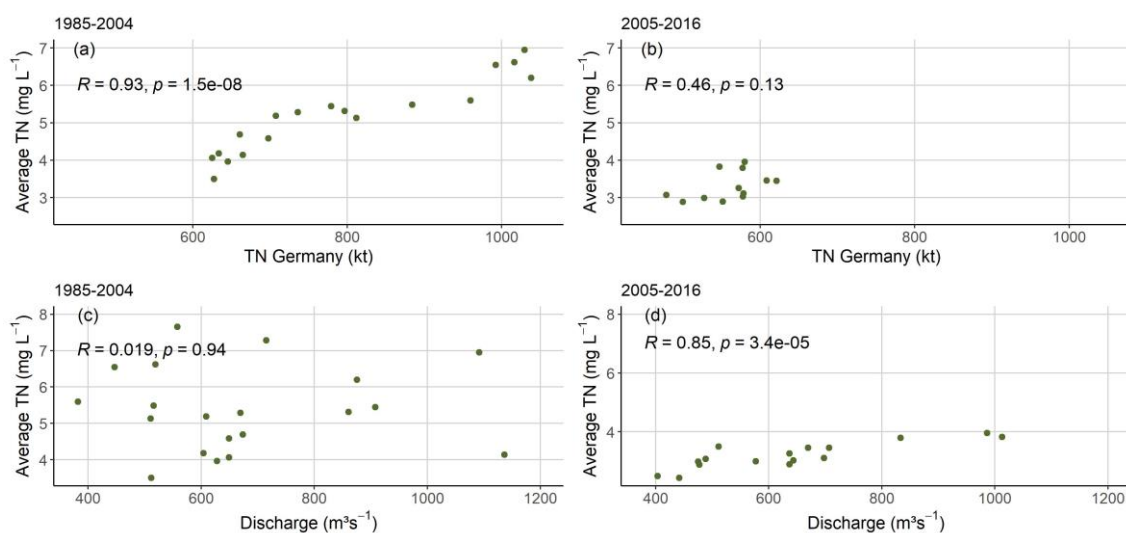


**Figure 2.5.** Average annual TN concentrations plotted against annual total nitrogen emissions from Germany (data provided by UBA 2020) from (a) 1985 to 2004 and (b) 2005 to 2016. Average annual TN concentrations plotted against annual average discharge from (c) 1985 to 2004 and (d) 2005 to 2016. Pearson’s correlations ( $R$ ) and  $p$ -values are shown.

To further investigate the interaction between discharge and nitrogen dynamic, we developed a regression-based analysis on a significant correlation between the fraction ( $f$ ) of annual German TN emissions reaching the Elbe Estuary and discharge (Figure 2.6a;  $R = 0.96$ ,  $p < 0.001$ ; Eq. 2.3). In a second step, this regression was used to predict annual nitrogen loads using discharge and national nitrogen emissions (Figure 2.6b; Eq. 2.4). We performed the same analysis using five-year moving averages for TN loads from the Elbe River, leading to similar results, which we present in Figure A1.5.

$$f = \frac{TN_{Elbe,observed}}{TN_{Germany}} = m \times Q_{Elbe} + b \quad (2.3)$$

$$TN_{Elbe,model} = b \times TN_{Germany} + m \times TN_{Germany} \times Q_{Elbe} \quad (2.4)$$

Where  $f$  denotes the fraction of annual German TN emission reaching the Elbe Estuary,  $TN_{Elbe,observed}$  are the calculated TN loads at the weir in Geesthacht (Section 2.3.3),  $TN_{Germany}$  is the annual TN emission in Germany (UBA 2020) and  $Q_{Elbe}$  is the discharge of the Elbe Estuary measured at the gauge in Neu Darchau (stream kilometer 536). The slope and intercept of the regression are denoted as  $m$  and  $b$ , respectively.

We did not consider nitrogen input from the Czech Republic in our regression-based analysis, which contributes ~30 % of the total Elbe River catchment. A report of the International Commission for the Protection of the Elbe (IKSE 2018) determined a relative share of total nitrogen load from the Czech Republic of 46 % in the time period of 1997 to 2011, which increased to 54 % in the period of 2011 to 2015. However, we considered the nitrogen input from the Czech Republic as a baseline for nitrogen loads in the Elbe River and due to the good fit of our regression (Figure 2.6a), we assume this assumption is valid.

Our calculation suggests that on average, 14.8 % of Germany's nitrogen inputs into surface water reached the Elbe Estuary. This is lower than the proportion of the Elbe catchment area in Germany of 27 % of Germany (Statistisches Bundesamt 2023). The share of Germanys nitrogen input into surface waters rose to >20 % in wet years (1994, 1995 or 2010) and in years with extreme flood events (2002, 2013, Figure 2.6a). Schlarbaum et al. (2011) and Jacob et al. (2016) showed that flood led to high nitrogen loads and low nitrate isotope ratios. This highlights the effect of discharge on the Elbe River nitrogen loads, with increased input from tributaries and reduced biological turnover jointly increasing DIN loads. However, the robust correlation in our analysis (Figure 2.6a) suggests that average annual discharge is a more suitable predictor of nitrogen loads than the occurrence of individual extreme events like floods.

Conversely, during low discharge conditions, a lower proportions of nitrogen emissions reach the estuary. This is clearly visible in years starting in 2013, when low discharge conditions prevailed in the Elbe River, with an average discharge level of about  $200 \text{ m}^3 \text{ s}^{-1}$  below the long term average. A similar situation occurred from 1989 to 1993 with five successive years of low discharge conditions (Weilbeer et al. 2021). In these dry years, less than 10 % of the national nitrogen emissions reached the weir at Geesthacht. This analysis shows that nitrogen retention in the catchment (i.e., the relative difference between annual German TN emissions and the proportion of N inputs that reach the estuary) strongly depends on discharge.

This effect remains visible in discharged-weighted calculations (Figure 2.4d) because higher residence times at low discharge conditions promote denitrification (Nixon et al. 1996; Pind et al. 1997; Silvennoinen et al. 2007) but also increase sedimentation (Reynolds and Descy 1996; Köhler et al. 2002), leading to nitrogen retention within the catchment, tributaries and river. Kamjunke et al. (2022) showed reduced TN and chlorophyll a concentrations just upstream of the weir in Geesthacht during their sampling campaign of a drought in September 2019, which they attributed to intensified sedimentation caused by low flow velocity. We cannot distinguish the contribution of denitrification and sedimentation to overall nitrogen retention, but enhanced organic matter availability in riverine sediments along with sufficient nitrate availability enhance denitrification (Cornwell et al. 1999; Megonigal et al. 2004; Opdyke et al. 2006; Devol 2008). Under these circumstances, low discharges can increase nitrogen removal from the catchment.

We found a very good fit between the annual loads predicted from the UBA data and the discharge and measured annual nitrogen loads from the Elbe Estuary (Figure 2.6b). We conclude that low discharges have a twofold effect on reducing the transfer of TN emissions into German surface waters leading to the Elbe Estuary by (1) increased retention of nitrogen (reduced concentrations) in the Elbe River catchment and (2) as a direct effect of water volume reduction (Figure 2.4d).

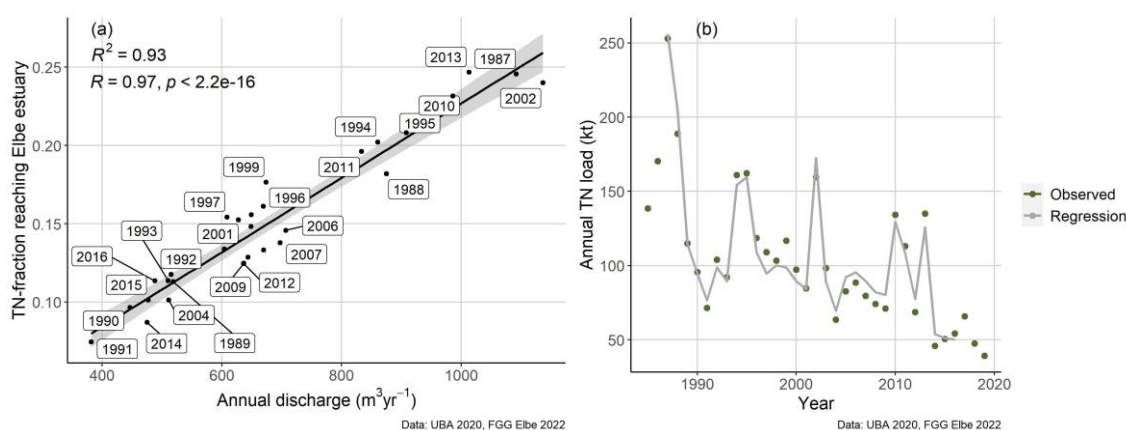


**Figure 2.6.** (a) Fraction of annual German TN emissions to surface water reaching the Elbe Estuary at the weir in Geesthacht with a regression line (Eq. 2.3), p-value, Pearson’s correlation coefficient and R<sup>2</sup>-value, (b) Annual TN loads at the weir Geesthacht, the points show the calculated loads based on the FGG Elbe (2022) dataset (Section 2.3.3). The gray line indicates the results derived from our regression-based analysis (Eq. 2.4). Please note that UBA (2020) only provided data from 1987 to 2016, and we calculated TN loads from 1985 to 2019.

## 2.4.2 Seasonal changes in nitrogen turnover

We observed enhanced nitrogen retention with decreased freshwater discharge from 2005 to 2016 (Figure 2.5). Next to enhanced denitrification (Section 2.4.1), this can lead to intensified phytoplankton growth due to longer residence times and lower water levels improving the light supply of phytoplankton (Scharfe et al. 2009; Quiel et al. 2011; Hein et al. 2016). To further investigate these autotrophic seasonal nitrate uptake processes in the river, we use our nitrate stable isotope measurements from the weir at Geesthacht, which marks the end of the riverine part and hence integrates the river signal.

We observe a distinct seasonal signal of nitrate stable isotopes with enriched values in summer and lighter isotopes in winter as well as a strong negative correlation between nitrate isotopes and nitrate concentration ( $R = -0.92$ ,  $p < 0.001$ ). This indicates fractionation due to biological nitrogen turnover, with an isotope effect for nitrate consumption of  $^{15}\epsilon = -14$  ‰ ( $R = 0.92$ ,  $p < 0.001$ ). This fits well with reported values for nitrate assimilation ( $^{15}\epsilon = -5$  to  $-20$  ‰; Waser et al. 1998b; a; Granger et al. 2004; Needoba and Harrison 2004; Sigman et al. 2009) but also with riparian denitrification ( $^{15}\epsilon = \sim -15$  to  $-30$  ‰; Deutsch et al. 2005; Kendall et al. 2007; Lutz et al. 2020). Furthermore, we found a significant correlation between  $\delta^{15}\text{N}$ -nitrate and  $\delta^{18}\text{O}$ -nitrate, with a ratio  $\delta^{18}\text{O}$ -nitrate vs.  $\delta^{15}\text{N}$ -nitrate of 0.77:1 ( $R = 0.91$ ,  $p < 0.001$ ; Figure A1.6). Phytoplankton assimilation usually results in a ratio of  $\delta^{18}\text{O}$ -nitrate vs.  $\delta^{15}\text{N}$ -nitrate of 1:1 (Granger et al. 2004) and denitrification in an increase of 0.5:1 (Böttcher et al. 1990; Mengis et al. 1999; Granger and Wankel 2016; Wong et al. 2020). Hence, based on our calculated isotope effects, we assume that nitrate consumption likely is caused by a combination of assimilation and denitrification.

The relation between particulate nitrogen (PN) and DIN concentrations (PN/DIN ratios) strongly varied with season (Figure A1.6), with the exception of the summer flood in 2013 that we excluded from this analysis. To analyze the seasonal succession of nitrate consumption processes, we separated our data into seasons (Figure A1.6). In spring (March – May), increasing PN/DIN ratios along with decreasing silicate concentrations (Figure 2.3j) indicated the impact of the spring phytoplankton bloom in the Elbe River. Nitrate isotope values showed significant correlations with both particulate nitrogen concentrations ( $R = 0.86$ ,  $p < 0.001$  for  $\delta^{15}\text{N}$ -nitrate and  $R = 0.84$ ,  $p < 0.001$  for  $\delta^{18}\text{O}$ -nitrate) and silicate concentrations ( $R = -0.84$ ,  $p < 0.001$  for  $\delta^{15}\text{N}$ -nitrate and  $R = -0.85$ ,  $p < 0.001$  for  $\delta^{18}\text{O}$ -nitrate). During this spring bloom, we calculated an  $^{15}\epsilon$  isotope effect of  $-11\text{‰}$ , which fits with lab-based assessments (Waser et al. 1998b; Granger et al. 2004; Needoba and Harrison 2004; Rohde et al. 2015) and suggests dominance of phytoplankton uptake.

The spring blooms were followed by high but relatively stable PN/DIN ratios in summer (June to August). Phytoplankton growth seems to be at least partly limited by low concentrations of silicate and/or phosphate, as reflected in the elevated ammonium concentrations. Over the entire year, we regard in-stream remineralization of suspended particulate organic matter as the main source of ammonium. This ammonium is immediately assimilated during algae blooms in spring but accumulates in summer (Figure 2.3e, f). This accumulation of ammonium in the water column points toward reduced uptake by phytoplankton, possibly due to a limitation of diatom growth by silicate concentrations  $< 2.8\ \mu\text{mol L}^{-1}$  and phosphate concentrations  $< 0.6\ \mu\text{mol L}^{-1}$  (Schöl et al. 2014), which we observed during several days in later spring/summer. Reduced nitrogen assimilation is also reflected in the calculated  $^{15}\epsilon$  isotope effect of  $-22\text{‰}$ . This isotope effect is outside the previously reported values for nitrate assimilation ( $-5$  to  $-20\text{‰}$ ; see above) and may indicate increasing importance of riparian denitrification in mid-summer, with an isotope effect of up to  $-30\text{‰}$  (e.g., Granger et al. 2008; Wunderlich et al. 2012; Lutz et al. 2020).

To estimate the overall importance of phytoplankton uptake in the Elbe River for the entire year, we compared our initial isotope effect of  $^{15}\epsilon = -14\text{‰}$  calculated from the entire dataset with isotope effect estimates for phytoplankton uptake ( $^{15}\epsilon = -10\text{‰}$ ) and riparian denitrification ( $^{15}\epsilon = -26\text{‰}$ ), leading to an estimate of 73 % assimilation and 27 % denitrification. This is in line with previous studies that suggested that phytoplankton assimilation is the dominant nitrate removal pathway within the Elbe River. Estimates for the proportion of assimilation range from 53% (Ritz and Fischer 2019) to 75% (Deutsch et al. 2009). Kamjunke et al. (2021) suggested that nitrate removal was almost completely explained from phytoplankton assimilation, with only a negligible contribution by denitrification. However, they did not measure nitrate stable isotopes, which showed clear denitrification signals in both our measurements and measurements performed by Deutsch et al. (2009). In line with observations by Scharfe et al. (2009), Kamjunke et al. (2021) found that high

light availability at low water levels and low discharge were important drivers enhancing phytoplankton growth in the Elbe.

### **2.4.3 A nitrate limitation ahead?**

During dry periods in August 2018 and 2019, we measured extraordinarily low nitrate concentrations of  $7.0 \mu\text{mol L}^{-1}$  and  $0.2 \mu\text{mol L}^{-1}$ , respectively. Low discharges not only enhance denitrification and sedimentation but also increase phytoplankton growth due to longer residence times and increased light availability (Scharfe et al. 2009; Kamjunke et al. 2021). Can such intensified nitrogen retention and increasing nitrogen uptake cause shifts to a future limitation in the Elbe River?

At present, phytoplankton growth in the Elbe Estuary is limited by silicate and phosphate concentrations (Karrasch et al. 2001; Böhme et al. 2006). In March/April, spring blooms develop with diatoms as the most abundant phytoplankton group in the Elbe River. Low silicate concentrations in spring but high concentrations of nitrogen enable the development of a second bloom in the Elbe River in late summer, which is dominated by nonsilicifying algae, including green algae (Karrasch et al. 2001). In less eutrophic rivers, green algae play a subordinate role (Gosselain et al. 1994), as was the case in the Elbe River in the past (Karrasch et al. 2001; Böhme et al. 2006; Hein et al. 2016).

Management measures introduced in the 1980s and 1990s have led to improved water quality, which in turn caused a significant increase in phytoplankton growth (Kerner 2000; Amann et al. 2012; Hillebrand et al. 2018). Before the German reunification, organic nitrogen mainly originated from industries and wastewater inputs. High organic matter concentrations, high pollutant levels and low light availability inhibited the developments of algal blooms in the 1980s, as shown by the lack of seasonal variability in TON concentration (Figure 2.7). The water quality in the Elbe River has improved since the 1990s and enabled the development of phytoplankton blooms with seasonal oscillations (Figure 2.7; Kerner 2000; Amann et al. 2012; Hillebrand et al. 2018).

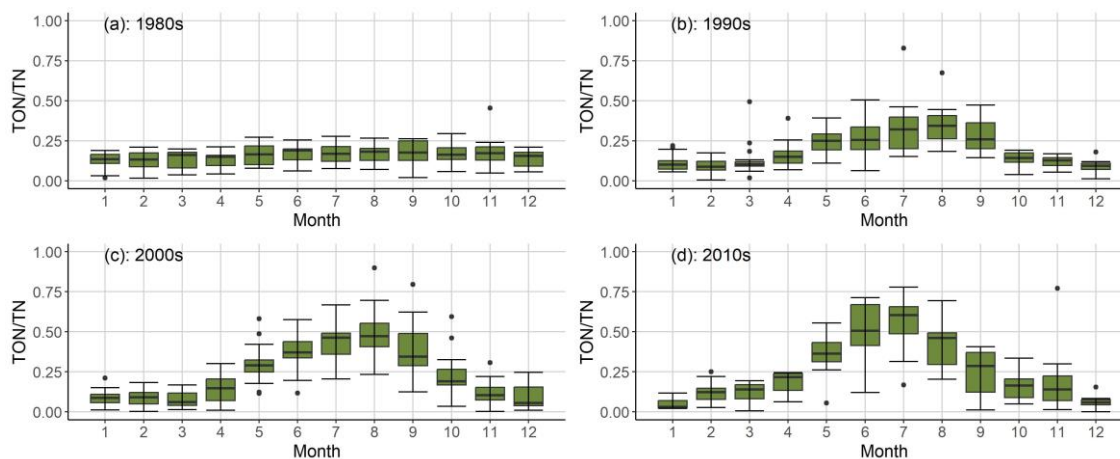


**Figure 2.7.** Seasonal variation in TON fractions in TN concentration (a) in the 1980s, (b) in the 1990s, (c) in the 2000s and (d) in the 2010s. In the boxplots, the lines indicate median values, boxes show the 25th and 75th percentiles and whiskers indicate the data range without outliers.

We anticipate that low discharge conditions will occur more frequently in the future with ongoing climate change (Brasseur et al. 2017; IPCC 2022). Due to lower discharges and higher water temperatures, nitrogen loads and concentrations in the Elbe River will very likely further decrease in summer, leading to pronounced retention in the catchment upstream. This could decrease eutrophication effects both in the adjacent coastal estuary and the coastal zone. However, our data and those from several other studies (Guhr et al. 2000; Deutsch et al. 2009; Ritz and Fischer 2019; Kamjunke et al. 2021) revealed that phytoplankton uptake is an important nitrate sink in the Elbe River. Low discharge conditions will intensify this sink by enhancing algal blooms. As this organic material is remineralized, it has the potential to increase recycled nutrient loads later in the year or further downstream in the estuary, increasing the loads of dissolved inorganic nitrogen and oxygen depletion. Sanders et al. (2018) found that presently, remineralization and nitrification in summer almost doubled the estuarine nitrate concentration. Whether and how estuarine nitrogen turnover is affected by low nitrogen input from rivers still needs to be investigated.

The coupling of reduced nitrogen inputs into surface waters, pronounced nitrogen retention in the catchment and intensified algae blooms under low discharge conditions may lead to more frequent and longer periods of nearly depleted DIN concentrations in the water column at the end of the riverine part of the Elbe River, as already observed in summer 2018 and 2019. A possible nitrate limitation of phytoplankton growth could lead to an early collapse of algal blooms within the riverine stretch, an upstream shift in heterotrophic processes and subsequent intense oxygen depletion, as suggested by Quiel et al. (2011), leading to an upstream shift in low-oxygen conditions in the upper Elbe estuary and river. Such a spatiotemporal coupling of management effects and nutrient cascade effects (Galloway et al. 2003) calls for integrated management approaches that consider the river system as a whole.

## 2.5 Conclusions

In our heavily managed study site, we find that reduction in nitrogen emissions is mirrored in river loads, but that in addition discharge conditions were responsible for the strong variability in total nitrogen loads reaching the Elbe Estuary. With decreasing discharge, nitrogen retention in the Elbe River and catchment increased, at times doubling nitrogen reduction in comparison to years with average discharge. Nitrogen retention was enhanced due to sedimentation and denitrification in the river and catchment. Prolonged residence times and higher light availability also fueled phytoplankton growth and microbial turnover. This increased both DIN uptake and particulate nitrogen transport downstream. This particulate nitrogen is recycled in-stream to ammonium or nitrate and supports the development of a riverine phytoplankton blooms. At present, decreasing nitrogen input and enhanced phytoplankton growth during low discharge conditions cause low nitrate concentrations or even complete nitrate depletion in the upper estuary.

Overall, we conclude that the recent decreases in nitrogen loads in the Elbe River were not only driven by management measures, but were amplified by long-lasting low discharge conditions in the catchment. In light of future decreasing summer discharge conditions as predicted by climate scenarios, a future nitrate limitation in phytoplankton growth appears possible. The consequences for phytoplankton bloom dynamics are unclear, but nutrient depletion may lead to a collapse in phytoplankton blooms and subsequent oxygen depletion in the upstream river.

## Acknowledgments

We thank all the involved colleagues in sampling at the Weir Geesthacht, e.g., Fabian Jung, Lisa Brase and Vanessa Russnak. For measuring the nutrient concentrations of the Hereon data set, we thank Leon Schmidt and Verena Küppers.



---

### **3 How low discharges affect estuarine nitrogen turnover – a case study in the freshwater Elbe Estuary**

*Schulz, G., Sanders, T., Russnak, V., van Beusekom, J. E. E., and Dähnke, K.: How low discharges affect estuarine nitrogen turnover – a case study in the freshwater Elbe Estuary, [in preparation].*

#### **Abstract**

Estuaries are widely recognized as important nutrient filters. Their potential filter function depends on residence time. The Intergovernmental Panel on Climate Change anticipates more frequent and extensive droughts, which will significantly impact water residence times in estuaries. Since 2013, persisting low freshwater discharge amounts in the catchment of the Elbe River (Germany) have dominated transport to the coastal zone. In this study, we investigated how these low discharges have affected nitrate turnover within the freshwater section of the estuary. In a total of 17 summer research cruises (May to August) from 2011 to 2022, we measured nutrient concentrations, stable isotopes of nitrate, oxygen saturation, and suspended particulate matter composition. We observed that intensified nitrate retention due to low freshwater discharges led to nitrate depletion upstream of the Hamburg Port region, accompanied by a collapse of the phytoplankton bloom. This collapse resulted in an upstream shift of heterotrophic respiration and remineralization processes, visible in ammonium accumulation and oxygen depletion. In the Port of Hamburg, low discharge amounts have fueled the synergetic effects of enhanced phytoplankton blooms in the river and altered suspended particulate matter dynamics, causing high nitrate production within the estuary, an inverse effect to the increased retention in upstream areas. Overall, our findings highlight the need for a holistic approach to water quality improvement: Nutrient mitigation and sediment management in estuaries under stress must be harmonized along the entire river continuum for an optimal reduction strategy.

#### **3.1 Introduction**

Estuaries are situated at the land-ocean interface (e.g., Bianchi 2007; Kennish 2017) and can significantly alter riverine nutrient loads before they reach adjacent coastal oceans (e.g., Crossland et al. 2005; Bouwman et al. 2013). Their nutrient filter capacity depends on various factors, such as geomorphological conditions and oxygen and light availability (e.g., Middelburg and Nieuwenhuize 2000; Dähnke et al. 2008; Voss et al. 2011). Residence time is considered to be one of the key controls on the extent of reactive nitrogen processed within estuaries, which is mainly controlled by riverine

freshwater inflow, estuarine volume, and tidal exchange with coastal waters (e.g., Middelburg and Nieuwenhuize 2000; Voss et al. 2011).

The Elbe Estuary is the largest riverine source of dissolved nitrogen in the German Bight, with nitrogen input mainly linked to agricultural land use in the catchment (Radach and Pätsch 2007; Johannsen et al. 2008). Since 2013, the Elbe Estuary has experienced frequent low freshwater inflows, leading to discharge levels that are approximately  $200 \text{ m}^3 \text{ s}^{-1}$  below the long-term average (Weilbeer et al. 2021). Projections from the Intergovernmental Panel on Climate Change predict more frequent and extensive droughts in the future, highlighting the need to understand the interaction between climate change and estuarine biogeochemical processes (IPCC 2022).

The recent low freshwater discharges in the Elbe have significantly altered riverine nitrogen input into the estuary by enhancing nitrogen retention through denitrification, sedimentation and enhanced phytoplankton blooms (Scharfe et al. 2009; Kamjunke et al. 2021; Schulz et al. submitted). This scenario has increased dissolved inorganic nitrogen (DIN) uptake and led to low riverine nitrate concentrations entering the estuary. However, enhanced phytoplankton growth also increased the downstream transport of particulate nitrogen, which can be remineralized and increase DIN loads and oxygen depletion further downstream in the estuary.

The freshwater Elbe Estuary hosts the Port of Hamburg, a hotspot of biogeochemical turnover processes within the estuary (e.g., Brase et al. 2017; Sanders et al. 2018; Dähnke et al. 2022; Norbistrath et al. 2022) with severe oxygen depletion and low oxygen zones in summer ( $<3 \text{ mg L}^{-1}$ ; Schroeder 1997; Gaumert and Bergemann 2007; Schöl et al. 2014). Sanders et al. (2018) found that intense remineralization and nitrification in the Port of Hamburg nearly doubled the estuarine nitrate concentration in summer, highlighting the need to understand the linkage between freshwater discharges and estuarine nitrogen turnover.

To investigate this nitrogen turnover, dual stable isotope analysis of nitrate is a frequently used tool. Biological turnover processes usually favor lighter isotopes. This leads to predictable changes in the isotope ratios of the substrate and the product of a reaction that helps to identify the individual uptake and production processes of nitrate (e.g., Granger et al. 2004; Wankel et al. 2006; Dähnke et al. 2010; Sigman and Fripiat 2019).

From 2011 to 2022, we performed 17 summer research cruises within the freshwater section of the heavily managed Elbe Estuary (Germany) to study water column nutrient concentrations, stable isotopes of nitrate, oxygen saturation and particulate matter composition. We aimed to investigate the effects of low discharges on estuarine nitrogen turnover in summer by addressing the following

research questions: How does freshwater discharge impact (1) nitrate retention and (2) nitrogen turnover in the upper freshwater estuary and (3) in the Port of Hamburg?

## 3.2 Methods

### 3.2.1 Study site

The Elbe Estuary begins at the weir in Geesthacht (stream kilometer 586), flows through the Port of Hamburg, which is the third largest port in Europe (Port of Hamburg 2021), and enters the North Sea near Cuxhaven (stream kilometer 727; Figure 3.1). The catchment of the Elbe is 140 268 km<sup>2</sup> (Boehlich and Strotmann 2019) and is dominated by urban/agricultural land use (74 %; Johannsen et al. 2008). Point sources play a minor role in the annual nitrogen load of 84 kT-N of the Elbe Estuary (Hofmann et al. 2005; FGG Elbe 2018; IKSE 2018). The Elbe has a mean annual discharge of 712 m<sup>3</sup> s<sup>-1</sup> varying between the average low discharge amount of 276 m<sup>3</sup> s<sup>-1</sup> to the average high discharge amount of 1960 m<sup>3</sup> s<sup>-1</sup> (measured at gauge Neu Darchau at stream kilometer 536; HPA and Freie und Hansestadt Hamburg 2017). The water residence time ranges from ~79 days during low discharge (300 m<sup>3</sup> s<sup>-1</sup>) to <19 days during high discharge (2000 m<sup>3</sup> s<sup>-1</sup>) and is in average ~30 days (stream kilometer 585 to 730; Amann et al. 2015).

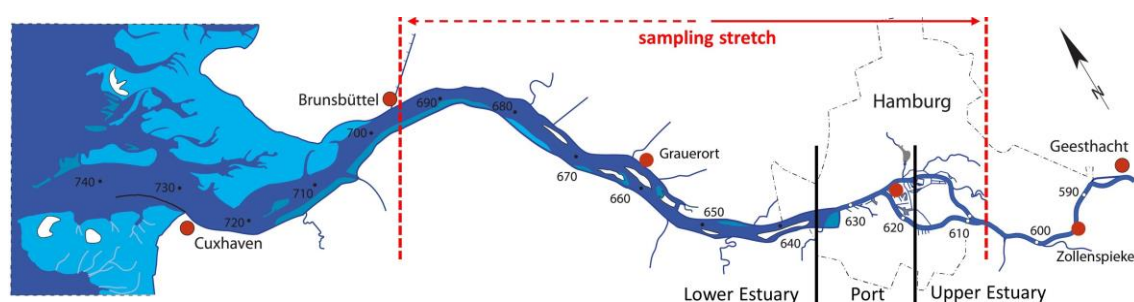


**Figure 3.1.** The Elbe Estuary: the sampling stretch is marked in red with the dashed line indicating the range of the onset of the salinity gradient, the vertical black lines indicate the Port of Hamburg (stream kilometer 615-635). Sections upstream of the Port of Hamburg are defined as “upper estuary” and downstream of it as “lower estuary”.

### 3.2.2 FGG Elbe data

The River Basin Community Elbe portal (FGG Elbe 2022) provides daily discharge measurements, concentration data on different nitrogen forms and suspended particulate matter concentrations for several stations along the Elbe. Discharge was measured at the gauge in Neu Darchau (stream kilometer 536). Nitrate concentrations were obtained from discrete water samples at the Zollenspieker station (stream kilometer 598.7) for comparison with our transect measurements (Figure A2.2). Furthermore, we used the suspended particulate matter concentrations from the Seemanshoeft station (stream kilometer 628.9) located in Hamburg Port (Figure 3.1) to study the impact of discharge on suspended particulate matter dynamics.

### 3.2.3 Transect sampling and measurements

From 2011 to 2022, we performed a total of 17 summer research cruises (May to August) in the freshwater Elbe Estuary, mainly with the research vessel *Ludwig Prandtl*. For other research vessels used, see Sanders et al. (2018). Usually, sampling of the freshwater section of the estuary started at the onset of the salinity gradient (salinity <1, ranging between stream kilometers 650 and 690 depending on discharge, Table A2.1), continued through the Port of Hamburg (stream kilometer 635-620) and ended in Oortkaten (stream kilometer ~610, Figure 3.1). We started sampling downstream against the outgoing tide to prevent tidal effects on our measurements.

An online in-situ FerryBox system continuously measured water temperature, salinity, oxygen concentrations and turbidity and was provided with water from 1.2 m depth from an onboard membrane pump. Since 2017, we corrected the oxygen measurements using the salinity-corrected optode measurements in comparison to Winkler titrations according to Schulz et al. (2023).

Approximately every 20 min, discrete water samples were collected from a bypass of the FerryBox system. For nutrient analysis, water samples were filtered immediately through combusted, pre-weighted GF/F filters (4 h, 450 °C) and stored frozen in acid-washed PE bottles until analysis. The filters were stored frozen (-20 °C) and used for the later analysis of suspended particulate matter (SPM; Röttgers et al. 2014), particulate nitrogen (PN), particulate carbon (PC) and C/N ratios (Figure A2.1).

For nutrient analysis, triplicates of filtered water samples were measured by a continuous flow auto analyzer (AA3, SEAL Analytics) and standard colorimetric and fluorometric methods (Hansen and Koroleff 1999). The detection limits were 0.05  $\mu\text{mol L}^{-1}$ , 0.05  $\mu\text{mol L}^{-1}$ , 0.07  $\mu\text{mol L}^{-1}$ , 0.03  $\mu\text{mol L}^{-1}$  and 0.13  $\mu\text{mol L}^{-1}$  for dissolved nitrate, nitrite, ammonium, silicate, and phosphate concentrations, respectively. PN and PC fractions were measured by an Elemental Analyzer (Eurovector EA 3000) calibrated against a certified acetanilide standard (IVA Analysentechnik, Germany). The standard deviation was 0.05 % for carbon and 0.005 % for nitrogen.

Due to varying objectives during cruise planning and staff limitations, data coverage of the set of all 17 research cruises varied. Tables with campaign dates, measured parameters, sampling transects, average water temperatures, discharges and DIN loads for each cruise are listed in Table A2.1.

### 3.2.4 Isotopic analysis

The stable isotope composition of nitrate in the filtered water samples was measured using the denitrifier method (Sigman et al. 2001; Casciotti et al. 2002). Denitrifying *Pseudomonas aureofaciens* (ATCC#13985) lacks nitrous oxide reductase and produces nitrous oxide as a final product from the denitrification of nitrate and nitrite in filtered water samples. The nitrous oxide was

analyzed by an isotope ratio mass spectrometer (Delta XP Plus, Thermo Fisher Scientific) coupled with a GasBench II. In each run, two international standards (USGS34,  $\delta^{15}\text{N}$ -nitrate: -1.8 ‰,  $\delta^{18}\text{O}$ -nitrate: -27.9 ‰; IAEA,  $\delta^{15}\text{N}$ -nitrate: +4.7 ‰,  $\delta^{18}\text{O}$ -nitrate: +25.6 ‰) and one internal standard were measured for standardization. The standard deviations for the standards and samples were <0.2 ‰ (n= 4) for  $\delta^{15}\text{N}$ -nitrate and <0.5 ‰ (n=4) for  $\delta^{18}\text{O}$ -nitrate.  $\text{N}_2$  and Vienna Standard Mean Ocean Water (VSMOW) were the standards for nitrogen and oxygen, respectively.

We performed  $\delta^{15}\text{N}$ -SPM analysis with an elemental analyzer (Carlo Erba NA 2500) coupled with an isotope ratio mass spectrometer (Finnigan MAT 252). As reference materials IAEA N1 ( $\delta^{15}\text{N} = +0.4$  ‰), IAEA N2 ( $\delta^{15}\text{N} = +20.3$  ‰) and a certified sediment standard (IVA Anlaysetechnik, Germany) were used.

### 3.2.5 Statistical analysis

All statistical analyses were performed using R packages. The packages ggpubr v.0.6.0 (Kassambara 2023) and stats v.4.0.2 (R Core Team and contributors worldwide 2020) were used to calculate Pearson correlations (R) and p-values.

## 3.3 Results

### 3.3.1 Discharge conditions

From 2011 to 2022, the annual average discharge was  $564 \text{ m}^3 \text{ s}^{-1}$ , which was clearly below the long-term average of  $712 \text{ m}^3 \text{ s}^{-1}$  (1926-2014; HPA and Freie und Hansestadt Hamburg 2017). In summer 2013, a flood event led to the highest recorded discharge of  $4070 \text{ m}^3 \text{ s}^{-1}$  (HPA and Freie und Hansestadt Hamburg 2017). In the following years, low discharge conditions persisted in the Elbe (Figure 3.2). For the observation period from May to August, average discharges ranged from  $263 \text{ m}^3 \text{ s}^{-1}$  in 2019 to  $1188 \text{ m}^3 \text{ s}^{-1}$  in 2013. In total, 384 days had discharges below the average low water discharge of  $276 \text{ m}^3 \text{ s}^{-1}$  (1926-2014; HPA and Freie und Hansestadt Hamburg 2017), with all days occurring after 2013. The years 2015, 2018, 2019, 2020 and 2022 all had more than 68 days with discharges below this average low water discharge.

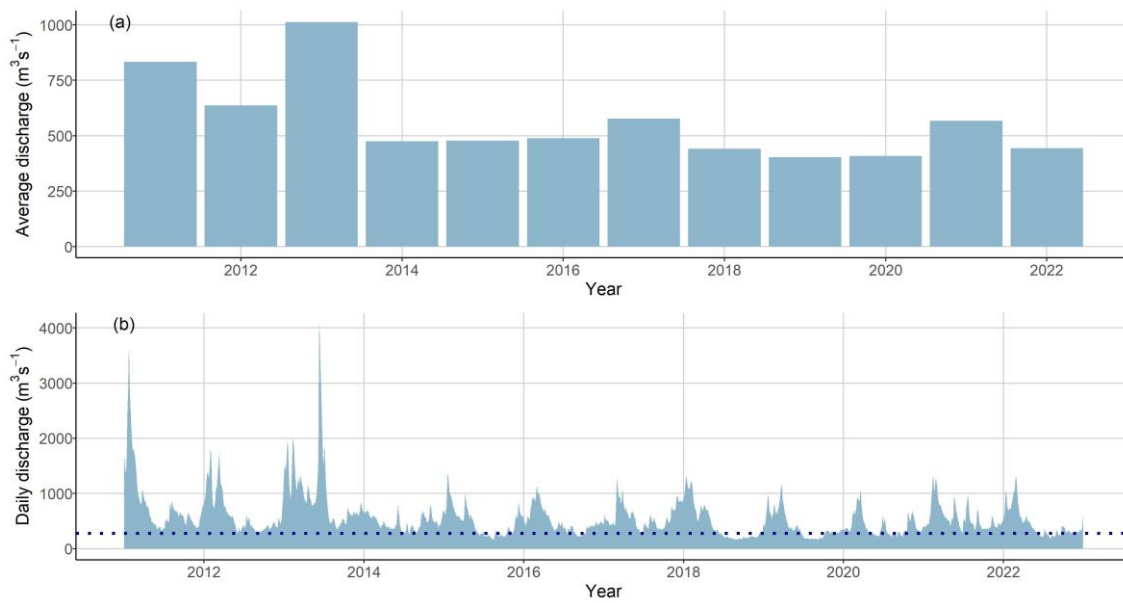


**Figure 3.2.** Annual average discharge and (b) daily discharge measured at the gauge in Neu Darchau (stream kilometer 536; FGG Elbe 2022). The dotted line shows the long-term average low discharge of  $276 \text{ m}^3 \text{ s}^{-1}$  (calculated from 1926 to 2014; HPA and Freie und Hansestadt Hamburg 2017).

### 3.3.2 FGG Elbe data

From 2011 to 2022, the suspended particulate matter concentrations increased in Hamburg Port (Figure 3.3a), showing a significant relationship with logarithmic daily discharge ( $p < 0.001$ , Figure 3.3b). The correlation improved using a long-term average of the present daily discharge amounts and discharge amounts from the previous 120 days ( $\sim 4$  month average,  $p < 0.001$ , Figure 3.3c). In later years (2018-2022), the suspended particulate matter concentrations measured during the transect cruises were significantly lower than the suspended particulate matter concentrations measured by the FGG Elbe (Figure 3.3a). The reason for this finding may have been differences in the suspended particulate matter concentrations between the main channel as measured during the transect cruises and riverbanks as measured by the FGG Elbe, which could have occurred due to enhanced sedimentation rates due to lower current velocities near the banks (e.g., Nunes and Simpson 1985; Schuchardt and Scholle 2017).

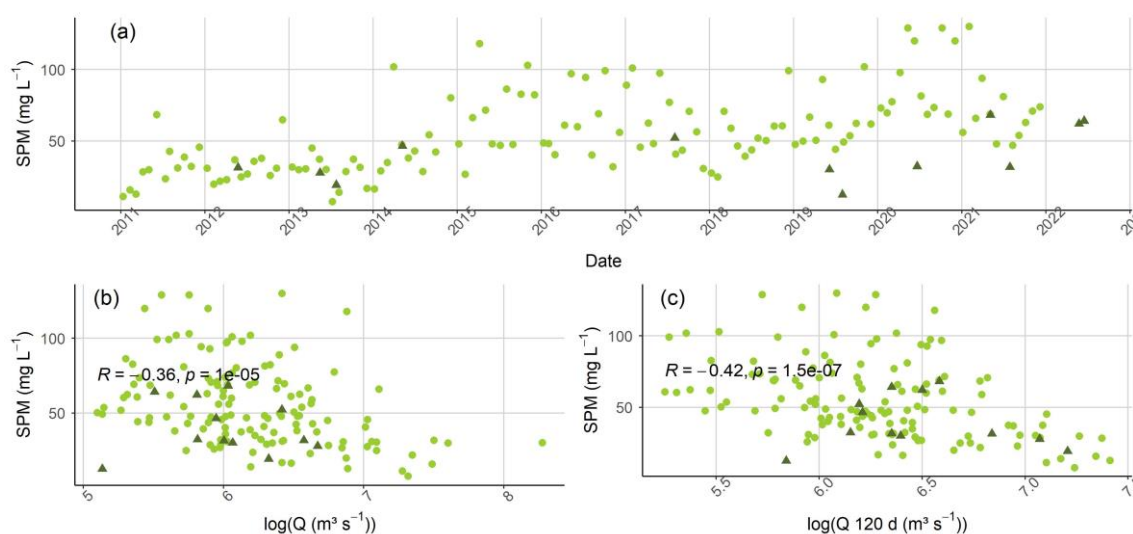


**Figure 3.3.** Suspended particulate matter (SPM) dynamic in the Port of Hamburg measured by the FGG Elbe at station Seemanshoeft from 2011 to 2022: (a) temporal evolution of suspended particulate matter concentrations, suspended particulate matter concentrations plotted against discharge: (b) logarithmic daily discharge and (c) logarithmic mean of present and 120 previous days measured at Neu Darchau. In plots (b) and (c) Pearson correlation coefficients ( $R$ ) and  $p$ -values are shown. Green circles show measurements done by the FGG Elbe. Transect cruise concentrations are displayed by dark green triangles.

### 3.3.3 Transect sampling

In the following sections, the area upstream of the Port of Hamburg is referred to as “the upper estuary”. In the upper estuary, the ammonium concentrations were generally low ( $<2 \mu\text{mol L}^{-1}$ ) but showed elevated values in August 2019, June 2020 and June 2022 of  $8.2 \mu\text{mol L}^{-1}$ ,  $18.3 \mu\text{mol L}^{-1}$  and  $4.5 \mu\text{mol L}^{-1}$ , respectively. The ammonium concentrations peaked in the Port of Hamburg, with maximum values ranging between  $6.7 \mu\text{mol L}^{-1}$  in July 2021 and  $23.6 \mu\text{mol L}^{-1}$  in June 2012. Downstream of the port, the ammonium concentrations decreased (Figure 3.4a-d).

Nitrite concentrations  $<1 \mu\text{mol L}^{-1}$  were usually measured in the most upstream part of the estuary, with the exception of August 2017 with  $1.2 \mu\text{mol L}^{-1}$  and June 2020 with  $2.3 \mu\text{mol L}^{-1}$ . The highest nitrite concentrations ranged between  $1.9 \mu\text{mol L}^{-1}$  in June 2015 and  $12.9 \mu\text{mol L}^{-1}$  in July 2013 and occurred in or slightly downstream of the Port of Hamburg (Figure 3.4e-h).

At stream kilometer  $\sim 610$ , the nitrate concentrations ranged from  $1.9 \mu\text{mol L}^{-1}$  in June 2022 to  $200.6 \mu\text{mol L}^{-1}$  in July 2021. The nitrate concentrations usually increased along our sampling transects, but some cruises exhibited a slight decrease or relatively stable nitrate concentrations (e.g., May 2013, August 2017 and July 2021). At the end of the freshwater part of the estuary, the nitrate concentrations ranged between  $84.2 \mu\text{mol L}^{-1}$  in June 2020 to  $251.5 \mu\text{mol L}^{-1}$  in May 2013 (Figure 3.4i-l).

The  $\delta^{15}\text{N}$ -nitrate values in the most upstream samples (~stream kilometers 610) varied between 10.3 ‰ in August 2019 and 25.4 ‰ in May 2022. The  $\delta^{18}\text{O}$ -nitrate values ranged from 1.7 ‰ to 15.5 ‰ measured in August 2019 and May 2022, respectively. During most cruises, nitrate isotopes decreased with increasing nitrate concentrations, indicating nitrate production within the freshwater part of the estuary. However, during some cruises (e.g., August 2017, July 2019, June 2020 and June 2022), we measured increasing nitrate stable isotopes in the Port of Hamburg (Figure 3.4m-t).

Oxygen was usually >100 % saturation in the upper estuary. We measured undersaturation in August 2019, June 2020 and June 2022. In the Port of Hamburg, oxygen decreased significantly, leading to oxygen minima that varied between 31 % (June 2012) and 71.6 % saturation (May 2021; Figure 3.4u-x). Note that oxygen data from cruises prior to 2017 were not corrected by Winkler titrations.

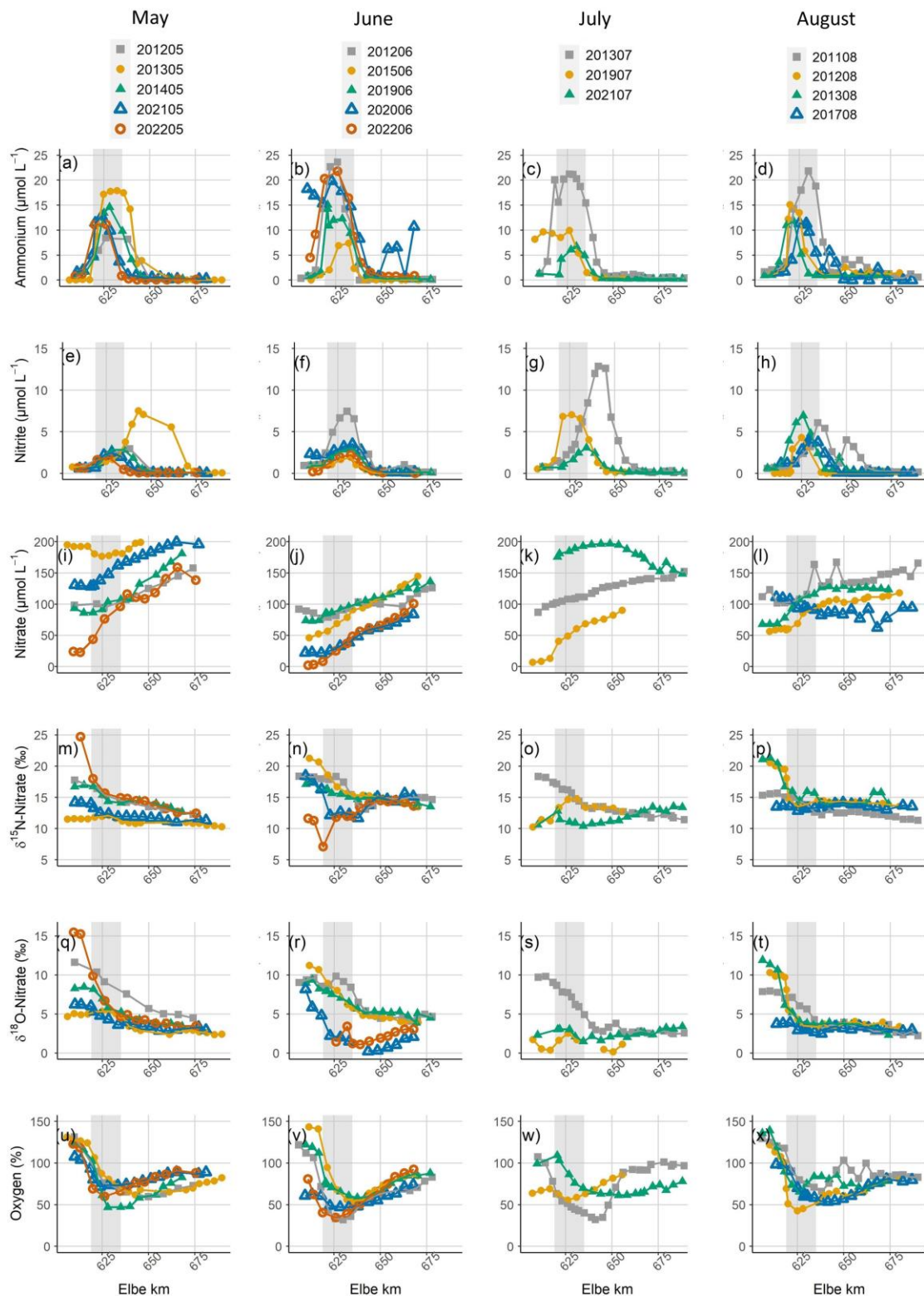


**Figure 3.4.** Dissolved inorganic nitrogen forms concentrations, nitrate stable isotopes and oxygen concentrations plotted against stream kilometers during the transect cruises ordered by months: Ammonium concentrations in (a) May, (b) June, (c) July and (d) August; Nitrite concentrations in (e) May, (f) June, (g) July and (h) August; Nitrate concentrations in (i) May, (j) June, (k) July and (l) August;  $\delta^{15}\text{N}$ -nitrate concentrations in (m) May, (n) June, (o) July and (p) August;  $\delta^{18}\text{O}$ -nitrate concentrations in (q) May, (r) June, (s) July and (t) August; Oxygen saturation in (u) May, (v) June, (w) July and (x) August. The grey background indicates the Port of Hamburg.

### 3.3.4 Statistical analysis

We performed statistical analysis to check for relations between the positions of ammonium and nitrite concentration peaks and the oxygen minimum. We found significant correlations between discharge and the position of the nitrite maximum ( $R = 0.58$ ,  $p = 0.015$ ) and oxygen minimum ( $R = 0.76$ ,  $p < 0.001$ ), showing that the nitrite concentration maximum and oxygen minimum moved upstream at lower discharges. The position of the nitrite maximum showed a weak positive relation with the location of the ammonium maximum ( $R = 0.47$ ,  $p = 0.055$ ) and a strongly significant relation with the position of the oxygen minimum ( $R = 0.77$ ,  $p < 0.001$ ). Respective Figures for the relations are shown in Figure A2.4.

Particulate nitrogen loads (as observed at the most upstream station) correlated with maximum ammonium ( $\text{NH}_4^+$ ) and nitrite ( $\text{NO}_2^-$ ) loads ( $R = 0.76$  and  $p = 0.007$  for  $\text{NH}_4^+$  loads,  $R = 0.76$  and  $p = 0.007$  for  $\text{NO}_2^-$  loads, Figure A2.3).

## 3.4 Discussion

### 3.4.1 Nitrate depletion in the upper estuary

The Intergovernmental Panel on Climate Change predicts more frequent and extensive droughts in the future (IPCC 2022). In the Elbe Estuary, frequent low amounts of freshwater inflows have occurred since 2013 (Figure 3.2; Weilbeer et al. 2021). Schulz et al. (submitted) described the effect of discharge on riverine nitrogen turnover in the Elbe River. River loads mirrored the decline in German nitrogen emissions since 1990 due to the collapse of eastern German industries (e.g., Guhr et al. 2000), reduced nitrogen input from agriculture (UBA 2017; BMEL 2022) and the implementation of wastewater treatment (UBA 2015, 2020). However, discharge conditions were responsible for the strong variability in annual nitrogen loads. Low discharges enhanced denitrification and sedimentation in the river and its catchments but also fueled phytoplankton growth (Scharfe et al. 2009; Kamjunke et al. 2021).

We extended the observations conducted by Schulz et al. (submitted) from the Elbe River to the upper estuary, where we observed a significant correlation between discharge and nitrate concentrations in the most upstream samples of our transects (~stream kilometer 610;  $R = 0.85$ ,  $p < 0.001$ ). Extraordinarily low nitrate concentrations occurred in July 2019, June 2020, May 2022 and June 2022 ( $< 24 \mu\text{mol L}^{-1}$ , Figure 3.4 and Figure 3.5). Minima were confirmed in a comparison with monitoring data provided by FGG Elbe (stream kilometer 598.7; Figure A2.2). In particular, the extraordinarily low concentrations in July 2019 ( $6.9 \mu\text{mol L}^{-1}$ ) and June 2022 ( $1.9 \mu\text{mol L}^{-1}$ ) were striking.

Usually, nitrate isotopes become progressively enriched with decreasing concentrations due to uptake of lighter isotopes by phytoplankton (Figure 3.5; Schulz et al. submitted). However, light nitrate isotopes occurred with extraordinarily low nitrate concentrations in July 2019, June 2020 and June 2022 (Figure 3.5a, b). Isotopic compositions were similar to average winter values with  $\delta^{15}\text{N}$ -nitrate at 7.8 ‰ - 9.5 ‰ and  $\delta^{18}\text{O}$ -nitrate at 2.7 ‰ - 3.1 ‰ (Johannsen et al. 2008; Schlarbaum et al. 2011;  $\delta^{18}\text{O}$ -nitrate values corrected for a change in the IAEA reference material, see Appendix A2 for details), suggesting nitrate production by coupled remineralization and nitrification. This finding is intriguing, as it indicates the complete consumption of the isotopic enriched riverine nitrate pool and recent nitrate production within the estuary from particulate plankton detritus. In addition to light nitrate isotopes, heavier isotopic signatures of particulate nitrogen (11.2 ‰ in July 2018 and 12.1 ‰ in June 2022) indicated an isotopic enrichment of approximately 4 ‰ compared to other summer values (ranging from 5 ‰ to 8 ‰; Figure A2.1), an offset that corresponds to literature values for remineralization (Kendall 1998; Möbius 2013; Sigman and Fripiat 2019). Overall, isotope changes suggest that low discharge intensified nitrate uptake in the river and nitrogen recycling in the freshwater section of the estuary.

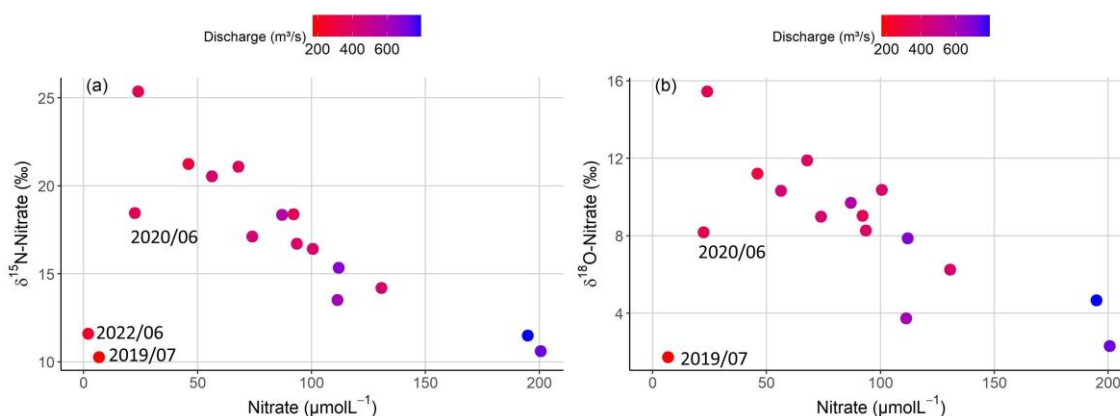


**Figure 3.5.** Nitrate stable isotopes plotted against concentrations for the most upstream samples (stream kilometer ~610):(a)  $\delta^{15}\text{N}$ -nitrate plotted against nitrate concentration and (b)  $\delta^{18}\text{O}$ -nitrate plotted against nitrate concentration with cruises as labels and point color indicating discharge conditions with low discharges shown in red and high discharges shown in blue.

### 3.4.2 Upstream shift in heterotrophic processes

An upward shift towards dominating heterotrophic processes due to reduced freshwater discharge amounts was predicted by Quiel et al. (2011) and was already shown for dissolved inorganic carbon concentrations in the Elbe Estuary by Rewrie et al. (2023). In our data, the significant correlations between discharge, nitrite maximum and oxygen minimum (Section 3.3.4) also reflected an upstream longitudinal shift in the dominant processes, leading to the question of how this shift affects nitrogen turnover processes.

In the Elbe Estuary, nitrate turnover in summers without nitrate depletion in the upper estuary (exemplary shown for July 2013 in Figure 3.6) has been described by Sanders et al. (2018) and Dähnke et al. (2022) and is briefly outlined here. Enriched nitrate entered the estuary at the weir in Geesthacht (Figure 3.6g,i; Schulz et al. submitted). Ongoing phytoplankton uptake in the upstream river (e.g., Deutsch et al. 2009) led to low silicate and phosphate concentrations (Figure 3.6b, d). Any nitrite and ammonium released during the degradation of phytoplankton detritus (e.g., Kerner and Spitzky 2001) was immediately assimilated (Figure 3.6a, c). Oxygen saturation was high (>100 %; Figure 3.6k), indicating that production exceeded respiration. Entering the Hamburg Port region, remineralization processes resulted in oxygen depletion (Schöl et al. 2014; Hein et al. 2016) and a shift from autotrophy to heterotrophy.

In summers with nitrate depletion in the upper estuary (July 2019, June 2020 and June 2022, example shown for July 2019 in Figure 3.6), riverine nitrate was either completely or nearly depleted at the weir in Geesthacht due to enhanced retention by denitrification and phytoplankton uptake caused by low freshwater discharges (Schulz et al. submitted). Low nitrate concentrations measured at stream kilometer 606 were freshly produced by coupled remineralization and nitrification (Section 3.4.1). The remineralization of phytoplankton already led to increasing ammonium, silicate and phosphate concentrations (Figure 3.6a, b, d) upstream of the port region. In the upper estuary, an undersaturation of oxygen (63 % saturation at stream kilometer 607) also indicated that in contrast to nitrate-replete conditions, primary production was lower than respiration (Figure 3.6k). Further downstream, a nitrite maximum developed, located approximately at stream kilometer 620 (Figure 3.6c), showing the stepwise succession of nitrogen turnover with remineralization followed by nitrification. This scenario also led to enriched  $\delta^{15}\text{N}$ -SPM up to 13 ‰ (Figure 3.6l). Thus, our results indicate an early collapse of the phytoplankton bloom in the riverine transect upstream of the port, where shallow depths preclude a light limitation as inferred for the deep Hamburg Port (e.g., Schöl et al. 2014). One possible explanation for the collapse is an increased grazing pressure by zooplankton. Due to the drought-induced longer residence time in the river, the zooplankton population may have increased to a level where grazing rates exceeded the growth rate, leading to a collapse of the phytoplankton. Another explanation is that due to the low nitrate concentrations, the phytoplankton community had to adapt to low nitrate concentrations. This may have caused a shift in the community and a transient drop in productivity, leading to a dominance of heterotrophic processes. In either case, low discharge amounts ultimately led to a collapse of the phytoplankton bloom and a switch heterotrophic dominance upstream of the port.

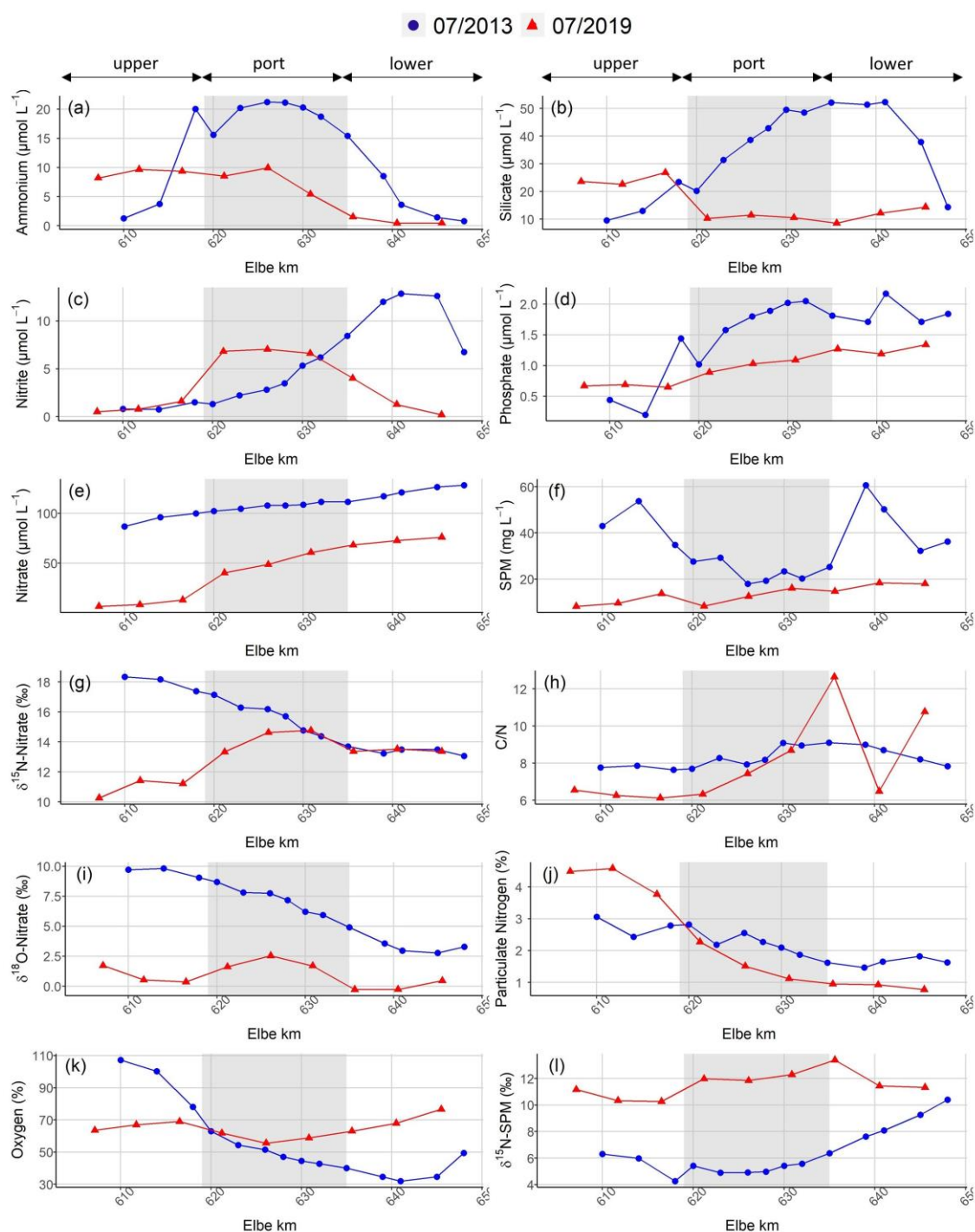


**Figure 3.6.** Exemplary comparison of July 2013 to August 2019 plotted against stream kilometers: (a) ammonium concentrations, (b) silicate concentrations, (c) nitrite concentrations, (d) phosphate concentrations, (e) nitrate concentrations, (f) suspended particulate matter concentrations, (g)  $\delta^{15}\text{N}$ -nitrate, (h) C/N ratios, (i)  $\delta^{18}\text{O}$ -nitrate, (j) particulate nitrogen content, (k) oxygen saturation and (l)  $\delta^{15}\text{N}$ -SPM.

### 3.4.3 Enhanced nitrogen turnover in the Hamburg Port area

The difference between nitrate at the onset of the salinity gradient and the riverine nitrate input (stream kilometer 610) revealed a higher nitrate gain with low freshwater discharges (Figure 3.7).

Low discharge amounts enhanced algae blooms in the upper Elbe River based on favorable light availability and longer residence times (Scharfe et al. 2009; Kamjunke et al. 2021), providing organic matter for downstream remineralization and fueling eutrophication in a cascade effect (Galloway et al. 2003). Prolonged residence times in the estuary enable that a larger part of organic matter is remineralized and nitrified along the Elbe Estuary.

In the Elbe Estuary, the Hamburg Port area is a hotspot of organic matter turnover and nitrogen cycling (e.g., Brase et al. 2017; Sanders et al. 2018; Zander et al. 2020, 2022; Dähnke et al. 2022), with high nitrification rates leading to high nitrate gains within the estuary (Sanders et al. 2018). The nitrogen budget is driven by the settling and resuspension of particulate matter, with its reactivity being the main control of nitrogen turnover (Dähnke et al. 2022). Both settling and resuspension are processes that are affected by flow conditions (Winterscheid et al. 2014). A reduction in freshwater inflow results in higher sedimentation rates of fine particles and an accumulation of organic material (de Haas et al. 2002; Giles et al. 2007). We found a logarithmic relation between suspended particulate matter concentrations from the Seemanshoeft station in the Port of Hamburg and long-term discharge conditions (4-month average), showing increasing suspended particulate matter accumulation with low freshwater discharges (Figure 3.3c). This result is in line with those from Winterscheid et al. (2014), who found a continuous increase in turbidity and sedimentation rates in periods of persisting low-discharge conditions.

Zander et al. (2020, 2022) identified a strong spatial gradient in labile suspended organic matter availability, showing that riverine organic matter becomes trapped in the upstream part of the Port of Hamburg. With reduced freshwater discharge, tidal exchange gains in importance, which shows in upstream shifts of the estuarine maximum turbidity zone and salinity gradient but also in increased tidal pumping (Bergemann 2004; Boehlich and Strotmann 2008; Winterscheid et al. 2014) and longer residence times in the port area (Table 3.1; Bergemann et al. 1996; Amann et al. 2015). Accumulated organic material can thus, in combination with prolonged residence times, lead to intensified remineralization in the Hamburg Port under low discharge conditions, which we see in the enhanced nitrate gain at low discharge amounts (Figure 3.7c).

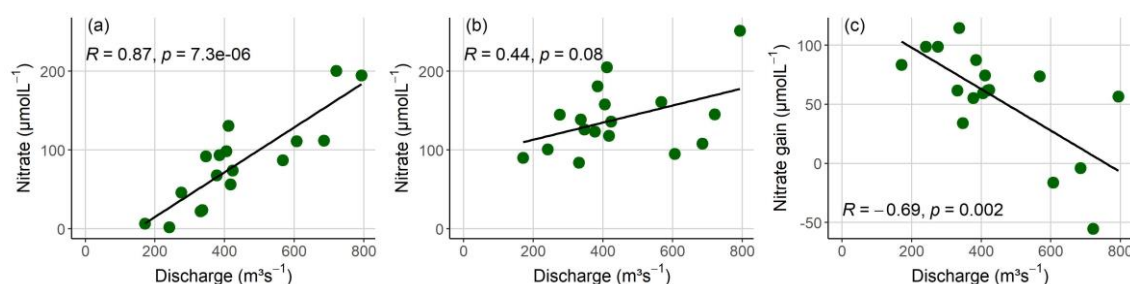


**Figure 3.7.** Nitrate gain along the estuary: (a) Nitrate concentrations in the most upstream samples (~stream kilometer 610), (b) nitrate concentrations at the onset of the salinity gradient (salinity <1) and (c) nitrate gain along the freshwater estuary plotted against discharge.

### 3.4.4 Limitations of our sampling campaign

Low discharge amounts fueled remineralization in the Port of Hamburg, leading to higher nitrate gains within the estuary (Figure 3.7; Section 3.4.3), but prolonged residence times also limited the interpretation of our sampling transects. In the campaigns, we sampled the freshwater estuary over one to two days, but during low discharges, residence times were well above one week (Table 3.1). As a consequence, the nitrate concentrations at stream kilometer 650 did not necessarily correspond to the concentrations at stream kilometer 610 measured on the same day. The downstream samples represented mixed signals from riverine input one to two weeks prior to the campaign.

In July 2019 (Figure 3.4 and Figure 3.6), June 2020 and June 2022 (Figure 3.4), both nitrate concentrations and nitrate stable isotopes increased in the freshwater transect. The reason for this could have been a strongly fractionating process that reduces nitrate (e.g., water column denitrification) simultaneously occurring with nitrate production, overshadowing the lighter isotopes added via nitrification. In summer 2013, water column denitrification was shown by Dähnke et al. (2022) in Hamburg Port. However, since nitrate concentrations increase within the freshwater estuary, production must strongly exceed reduction, making this scenario unlikely. For example, in July 2019, the nitrate concentration increased from  $6.7 \mu\text{mol L}^{-1}$  at stream kilometer 607 to  $136.1 \mu\text{mol L}^{-1}$  with a simultaneous increase in  $\delta^{15}\text{N}$ -nitrate from 10.3 ‰ to 13.5 ‰. If this increase was an effect of simultaneous nitrification and water column denitrification, then 40 % of the freshly produced nitrate would have been reduced within the sampling transect (estimated by the mapping approach by Schulz et al. (2022); Appendix A4). Considering the low suspended particulate matter concentrations ( $<22 \text{ mg L}^{-1}$ ; Figure A2.1) and oxygen concentrations above the threshold of denitrification in the water column ( $>146 \mu\text{mol L}^{-1}$ ), this scenario is highly unlikely.

We suggest that the increase in nitrate isotopes along the estuary reflected the origin of the nitrate. Given the long residence times at low discharges, the nitrate had entered the estuary a few weeks before our sampling. At that time, nitrate was not depleted yet and nitrate uptake by phytoplankton would

have enriched the isotopes of remaining nitrate. At the time of sampling, all nitrate was consumed by the phytoplankton and new, low isotope nitrate was produced from freshly degraded phytoplankton detritus. This intensified the observed gradient in the isotopic composition of the nitrate from light (newly produced) to more heavy (older) nitrate (Figure 3.5).

Thus, to properly assess the impact of longer residence times on nitrate production and the isotopic changes in the Port of Hamburg and Elbe Estuary, transect measurements need to be combined with high-resolution observations at the head of the estuary and residence time calculations within the estuary. Together, these data can be used to track the entering riverine nitrogen concentrations and isotopic composition from the river along the estuary and to determine nitrogen turnover processes in more detail. Our data nonetheless provide solid evidence for the observed upstream shifts in heterotrophy and processing intensification, but the quantification of the nitrate gain in the port region remains difficult.

**Table 3.1.** Length, area and typical residence time upstream and downstream of the Port of Hamburg as a function of low and medium discharge (Q) derived from Bergemann et al. (1996) and Amann et al. (2015).

Zone	Stream km	Length	Area	Residence time		
				Q=250 m <sup>3</sup> s <sup>-1</sup>	Q=700 m <sup>3</sup> s <sup>-1</sup>	Q=1200 m <sup>3</sup> s <sup>-1</sup>
Pre-Port	585-620	35 km	11.8 km <sup>2</sup>	3	1	<1
Port	620-650	30 km	27.5 km <sup>2</sup>	11	4	2

### 3.5 Conclusion

Low freshwater discharge intensified nitrate retention, leading to complete consumption of the riverine nitrate pool and a collapse of the phytoplankton bloom upstream of the Hamburg Port region. Consequently, heterotrophic processes moved upstream, resulting in accumulated ammonium and oxygen depletion upstream of the port. In Hamburg Port, nitrogen turnover is controlled by particulate matter, which accumulates in the port under persist low discharge conditions, fueling nitrate production and leading to high nitrate gains. However, prolonged residence times limited the quantification of the gain along our sampling transects. A combined approach using high-resolution steady-state data, transect measurements, and residence time calculations is needed to track nitrate inputs from the river to the estuary and to assess the effects of low discharges on the estuarine nutrient filter function.

Our results highlighted the complex interplay between various stressors on the estuarine nitrogen cycle. While nitrate is increasingly retained in upstream regions with low discharge conditions, the synergetic effects of altered suspended particulate matter dynamics (Bergemann 2004; Boehlich and Strotmann 2008; Winterscheid et al. 2014) and fueled phytoplankton blooms (Scharfe et al. 2009;

Kamjunke et al. 2021; Schulz et al. submitted) have led to a reversed effect in the Port of Hamburg. This findings highlights the need for a holistic approach to water quality improvement, nutrient mitigation and sediment management in heavily anthropogenically impacted estuaries.

### **Acknowledgments**

We thank all the involved colleagues in sampling the Elbe Estuary, e.g., Markus Ankele, Andreas Neumann, Fabrizio Minutolo, Leon Schmidt and many others. Yoana G. Voynova and our colleagues from KOI provided the FerryBox data. Thanks to Andreas Schöl and the staff of the BfG for providing us with data from their research cruises. Many thanks to the crew of the *R/V Ludwig Prandtl* and *Vogelsand* for their support on board. For measuring the nutrient concentrations, we thank Leon Schmidt and Verena Küppers. The working group of Biogeochemistry at the Institute for Geology measured C/N ratios and  $\delta^{15}\text{N}$ -SPM values.



---

## 4 Seasonal variability of nitrous oxide concentrations and emissions along a temperate estuary

*Schulz, G., Sanders, T., Voynova, Y. G., Bange, H. W., and Dähnke, K.: Seasonal variability of nitrous oxide concentrations and emissions in a temperate estuary, Biogeosciences, 20, 3229–3247, <https://doi.org/10.5194/bg-20-3229-2023>, 2023.*

### Abstract

Nitrous oxide is a greenhouse gas, with a global warming potential 298 times that of carbon dioxide. Estuaries can be sources of nitrous oxide, but their emission estimates have significant uncertainties due to limited data availability and high spatiotemporal variability. We investigated the spatial and seasonal variability of dissolved nitrous oxide and its emissions along the Elbe Estuary (Germany), a well-mixed temperate estuary with high nutrient loading from agriculture. During nine research cruises performed between 2017 and 2022, we measured dissolved nitrous oxide concentrations, as well as dissolved nutrients and oxygen concentrations along the estuary and calculated nitrous oxide saturations, flux densities and emissions. We found that the estuary was a year-round source of nitrous oxide, with highest emissions in winter when dissolved inorganic nitrogen (DIN) loads and wind speeds are high. However, in spring and summer, nitrous oxide saturations and emissions did not decrease alongside lower riverine nitrogen loads, suggesting that estuarine in-situ nitrous oxide production is an important source of nitrous oxide. We identified two hot-spots areas of nitrous oxide production: the Port of Hamburg, a major port region, and the mesohaline estuary near the maximum turbidity zone (MTZ). Nitrous oxide production was enhanced by warmer temperatures and was fueled by decomposition of riverine organic matter in the Hamburg Port and by marine organic matter in the MTZ. A comparison with previous measurements in the Elbe Estuary revealed that nitrous oxide saturation did not decrease alongside with DIN concentrations after a significant improvement of water quality in the 1990s that allowed for phytoplankton growth to reestablish in the river and estuary. This effect of phytoplankton growth and the overarching control of organic matter on nitrous oxide production, highlights that eutrophication and agricultural nutrient input can increase nitrous oxide emissions in estuaries.

### 4.1 Introduction

Nitrous oxide (N<sub>2</sub>O) is an important atmospheric trace gas that contributes to global warming and stratospheric ozone depletion (WMO 2018; IPCC 2021). Estuaries are important regions of nitrogen

turnover (Middelburg and Nieuwenhuize 2000; Crossland et al. 2005; Bouwman et al. 2013), and a potential source of nitrous oxide (Bange 2006; Barnes and Upstill-Goddard 2011; Murray et al. 2015). Together with coastal wetlands, estuaries contribute between 0.17 and 0.95 Tg N<sub>2</sub>O-N of the annual global budget of 16.9 Tg N<sub>2</sub>O-N (Murray et al. 2015; Tian et al. 2020). Nitrous oxide emission estimates from estuaries are associated with significant uncertainties due to limited data availability and high spatiotemporal variability (e.g., Bange 2006; Barnes and Upstill-Goddard 2011; Maavara et al. 2019), presenting a big challenge for the global nitrous oxide emission estimates.

Nitrification and denitrification are the most important nitrous oxide production pathways in estuaries. Under oxic conditions, nitrous oxide is produced as a side product during the first step of nitrification, the oxidation of ammonia to nitrite (e.g., Wrage et al. 2001; Barnes and Upstill-Goddard 2011). At low oxygen (but not anoxic) conditions, nitrifier-denitrification may occur, during which nitrifiers reduce nitrite to nitrous oxide (e.g., Wrage et al. 2001; Bange 2008). Denitrification takes place under anoxic conditions and mostly acts as a source of nitrous oxide, but can also reduce nitrous oxide to N<sub>2</sub> (e.g., Knowles 1982; Bange 2008). In estuaries, denitrification can occur in anoxic sediments, the anoxic water column or anoxic microsites of particles, whereas nitrification and nitrifier-denitrification take place in the oxygenated water column (e.g., Beaulieu et al. 2011; Murray et al. 2015; Ji et al. 2018; Tang et al. 2022).

In estuaries, the most important factor controlling nitrous oxide emissions are considered to be oxygen availability and dissolved inorganic nitrogen loads (Murray et al. 2015). Since nitrous oxide measurements in estuaries are scarce, global nitrous oxide emissions can be estimated by using emission factors and considering dissolved inorganic nitrogen (DIN) or total nitrogen (TN) loads, where it is assumed that higher loads lead to higher nitrous oxide emissions (Kroeze et al. 2005, 2010; Ivens et al. 2011; Hu et al. 2016). However, several studies instead reported no obvious relationship between nitrogen concentrations and nitrous oxide emissions (Borges et al. 2015; Marzadri et al. 2017; Wells et al. 2018), highlighting the need to understand the causes for variability of the relationship between nitrogen loads and nitrous oxide emissions (Wells et al. 2018).

The Elbe Estuary is a heavily managed estuary with high agricultural nitrogen inputs that hosts the third largest port in Europe (e.g., Radach and Pätsch 2007; Bergemann and Gaumert 2008; Pätsch et al. 2010; Quiel et al. 2011). It has been identified as a nitrous oxide source, with a hotspot of nitrous oxide production in the Port of Hamburg (Hanke and Knauth 1990; Brase et al. 2017). We aimed to investigate drivers for nitrous oxide emissions along the estuary, specifically the nitrous oxide and DIN ratio (N<sub>2</sub>O:DIN). To do so, we (1) looked for potential long-term changes in nitrous oxide saturations, (2) investigated potential production hotspots as well as the spatial and temporal

distribution of nitrous oxide saturations, and (3) used the  $\text{N}_2\text{O}:\text{DIN}$  ratio for a comparison with other estuaries that receive similar high agricultural nutrient inputs.

## 4.2 Methods

### 4.2.1 Study site

The Elbe River stretches over 1094 km from the Giant Mountains (Czech Republic) to the North Sea (Cuxhaven, Germany). The catchment of the Elbe River is 140 268 km<sup>2</sup> (Boehlich and Strotmann 2019), with 74 % urban and agricultural land use (Johannsen et al. 2008). The Elbe is the second largest German river discharging into the North Sea, as well as the largest source of dissolved nitrogen for the German Bight, which is heavily affected by eutrophication (van Beusekom et al. 2019).

The Elbe Estuary is a well-mixed temperate estuary, which begins at stream kilometer 586 at a weir in Geesthacht and stretches through the Port of Hamburg, entering the North Sea near Cuxhaven at stream kilometer 727 (Figure 4.1). Estuaries are commonly structured along their salinity gradient into an oligohaline (salinity: 0.5-5.0), a mesohaline (salinity: 5.0-18.0) and polyhaline (salinity >18.0) (US EPA 2006). The Elbe Estuary has a length of 142 km (Boehlich and Strotmann 2019) and a mean annual discharge of 712 m<sup>3</sup> s<sup>-1</sup> (measured at gauge Neu Darchau at stream kilometer 536; HPA and Freie und Hansestadt Hamburg 2017). The average water residence time is ~32 days, ranging from ~72 days during times of low discharge (300 m<sup>3</sup> s<sup>-1</sup>) to ~10 days during times of high discharge (2000 m<sup>3</sup> s<sup>-1</sup>; Boehlich and Strotmann 2008). The estuary has an annual nitrogen load of 84 Gg-N (FGG Elbe 2018). Point sources along the estuary provide only small part of the total nitrogen input to the Elbe Estuary (Hofmann et al. 2005; IKSE 2018). Oxygen concentrations in the Elbe Estuary vary seasonally, with oxygen depletion during the summer months and oxygen minimum zones regularly experiencing concentrations below 94  $\mu\text{mol O}_2 \text{ L}^{-1}$  (Schroeder 1997; Gaumert and Bergemann 2007; Schöl et al. 2014).

The Elbe Estuary is dredged year-round to maintain a water depth of 15-20 m and to grant access for large container ships to the Port of Hamburg (Boehlich and Strotmann 2019; Hein et al. 2021). Construction work for further deepening of the fairway was carried out during our study period, from 2019 to early 2022. Upstream of the Port of Hamburg water depth is less than 10 m (Hein et al. 2021).

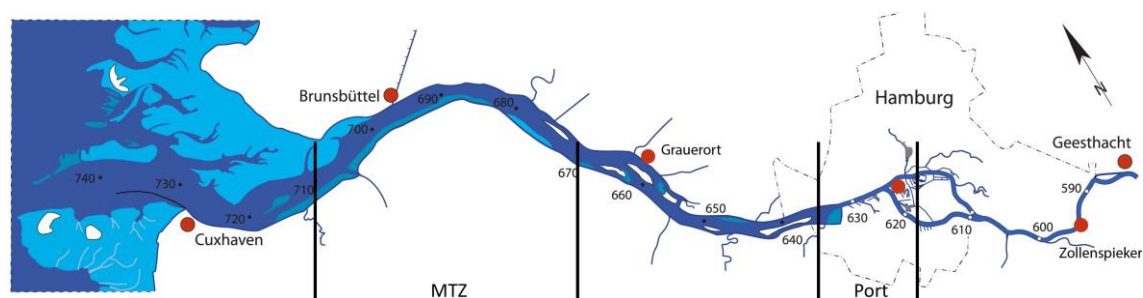


**Figure 4.1.** Map of the Elbe Estuary sampled during our research cruises with stream kilometers. The vertical black lines indicate the Hamburg Port region and a typical position for the maximum turbidity zone (MTZ; Bergemann 2004).

#### 4.2.2 Transect sampling and measurements

We performed nine sampling campaigns along the estuary with the research vessel *Ludwig Prandtl* (Table 4.1). Most cruises took place during spring and summer, with water temperatures  $>10\text{ }^{\circ}\text{C}$  (May to September), two cruises were conducted during winter (early March; water temperature  $<6\text{ }^{\circ}\text{C}$ ; Table 4.1). Transects started in the German Bight, and continued along the salinity gradient, through the Port of Hamburg to Oortkaten (stream kilometer 609). To ensure comparable current and mixing conditions, transect sampling was always done after high-tide, with the ship travelling upstream against the tide. For comparison to previous measurements, we included summer data from a previous study in 2015 (Brase et al. 2017).

**Table 4.1.** Campaign dates with the sampled Elbe Estuary sections shown via stream kilometers, average discharge during each cruise measured at the Neu Darchau gauging station, averages and standard deviations for water temperature, wind speed at 10 m height, dissolved inorganic nitrogen (DIN) concentrations for each campaign.

Campaign Dates	Stream kilometers (km)	Water temperature ( $^{\circ}\text{C}$ )	Wind speed 10 m ( $\text{m s}^{-1}$ )	Average discharge ( $\text{m}^3 \text{s}^{-1}$ )	Average DIN load ( $\mu\text{mol L}^{-1}$ )
28.-29.04.2015	627 – 741	$12.3 \pm 1.0$	$7.4 \pm 2.3$	595	$191.0 \pm 45.0$
02.-04.06.2015	609 – 739	$17.4 \pm 1.7$	$5.0 \pm 1.3$	276	$105.9 \pm 36.2$
01.-02.08.2017	621 – 749	$20.9 \pm 0.7$	$3.6 \pm 1.5$	607	$79.2 \pm 30.2$
04.-05.06.2019	610 – 750	$18.7 \pm 2.2$	$4.0 \pm 1.7$	423	$108.3 \pm 35.9$
30.07.-01.08.2019	609 – 752	$22.6 \pm 1.0$	$4.2 \pm 1.4$	171	$60.8 \pm 38.6$
19.-20.06.2020	609 – 747	$19.8 \pm 1.4$	$5.8 \pm 1.2$	331	$74.6 \pm 33.8$
09.-11.09.2020	607 – 745	$18.9 \pm 0.6$	$5.9 \pm 2.8$	305	$93.1 \pm 32.7$
10.-12.03.2021	609 – 748	$5.4 \pm 0.5$	$9.3 \pm 2.6$	862	$324.4 \pm 83.8$
04.-05.05.2021	610 – 751	$10.5 \pm 0.8$	$11.0 \pm 3.1$	411	$85.7 \pm 36.6$
27.-28.07.2021	621 – 751	$22.2 \pm 0.7$	$5.2 \pm 1.3$	721	$139.8 \pm 58.4$
01.-02.03.2022	610 – 752	$5.6 \pm 0.2$	$2.9 \pm 1.0$	1282	$238.0 \pm 74.7$

An onboard membrane pump continuously provided water at 1.2 m depth to an on-line in-situ FerryBox system and to an equilibrator used for the measurements of nitrous oxide dry mole fraction (Section 4.2.4). The FerryBox system continuously measured water temperature, salinity, oxygen concentrations, pH and turbidity. We corrected the salinity corrected optode measurements using comparisons to Winkler titrations of distinct samples. See Table A3.1 for further details.

Discrete water samples (30-40 samples for each cruise) were collected every 20 min from a bypass of the FerryBox system. For nutrient analysis, water samples were filtered immediately through combusted, pre-weighted GF/F Filters (4 h, 450 °C), and were frozen in acid washed PE bottles until analysis. The filters were also stored frozen (-20 °C) and subsequently analyzed for suspended particulate matter (SPM), particulate nitrogen (PN), particulate carbon (PC) and C/N ratios (Figure A3.1).

#### 4.2.3 Nutrient measurements

Filtered water samples were measured in triplicates with a continuous flow auto analyzer (AA3, SEAL Analytics) using standard colorimetric and fluorometric methods (Hansen and Koroleff 1999) for dissolved nitrate ( $\text{NO}_3^-$ ), nitrite ( $\text{NO}_2^-$ ) and ammonium ( $\text{NH}_4^+$ ) concentrations. Detection limits were  $0.05 \mu\text{mol L}^{-1}$ ,  $0.05 \mu\text{mol L}^{-1}$ , and  $0.07 \mu\text{mol L}^{-1}$  for nitrate, nitrite and ammonium, respectively.

#### 4.2.4 Equilibrator based nitrous oxide measurements and calculations

Equilibrated dry mole fractions of nitrous oxide were measured by a nitrous oxide analyzer based on off-axis integrated cavity output (OA-ICOS) absorption spectroscopy (Model 914-0022, Los Gatos Res. Inc., San Jose, CA, USA), which was coupled with a sea water/gas equilibrator using off-axis cavity output spectroscopy. Brase et al. (2017) described the set-up and instrument precision in detail. Twice a day, two standard gas mixtures of nitrous oxide in synthetic air ( $500.5 \text{ ppb} \pm 5 \%$  and  $321.2 \text{ ppb} \pm 3 \%$ ) were analyzed to validate our measurements. No drift was detected during our cruises.

We calculated the dissolved nitrous oxide concentrations in water with the Bunsen solubility function of Weiss and Price (1980), using 1 min averages of the measured nitrous oxide dry mole fraction (ppb). Temperature differences between the sample inlet and the equilibrator were taken into account for the calculation of the final nitrous oxide concentrations (Rhee et al. 2009). Nitrous oxide saturation were calculated based on nitrous oxide concentrations in water ( $N_2O_{cw}$ ) and the atmospheric equilibration concentrations ( $N_2O_{eq}$ ; Eq. 4.1). Atmospheric nitrous oxide dry mole fractions were measured before and after each transect cruises using an air duct from the deck of the research vessel.

$$s = 100 \times \frac{N_2O_{cw}}{N_2O_{eq}} \quad (4.1)$$

The gas transfer coefficients ( $k$ ) were determined based on Borges et al. (2004; Eq. 4.2), Nightingale et al. (2000), Wanninkhof (1992) and Clark et al. (1995), using the Schmidt number ( $Sc$ ) and wind speeds ( $u_{10}$ ) measured at 10 m height (Eq. 4.2). The Schmidt number was calculated as ratio of the kinematic viscosity in water (Siedler and Peters 1986) to the nitrous oxide diffusivity in water (Rhee 2000). Cruise wind speeds (Table 4.1) varied significantly from average annual wind speeds of the two federal states, in which the Elbe Estuary is located ( $4.7 \text{ m s}^{-1}$ ; Hereon and DWD 2023), and also compared to seasonal average wind speeds determined for the stations Cuxhaven and Hamburg (Rosenhagen et al. 2011). Thus, to estimate uncertainties due to varying wind conditions during our cruises, we used 1) the in-situ wind speeds measured on board the *R/V Ludwig Prandtl* at 10 m height by a MaxiMet GMX600 (Gill Instruments Limited, Hampshire, UK), 2) the average annual wind speed (Hereon and DWD 2023), and 3) the seasonally averaged wind speeds (Rosenhagen et al. 2011). The flux densities ( $f$ ) in the main text were calculated using Eq. 4.2 and Eq. 4.3 and the wind speeds measured on board the vessel. Results of the other calculations are listed in Table A3.2, Table A3.3 and Table A3.4.

$$k = 0.24 \times (4.045 + 2.58u_{10}) \times \left(\frac{Sc}{600}\right)^{-0.5} \quad (4.2)$$

$$f = k \times (N_2O_{cw} - N_2O_{eq}) \quad (4.3)$$

To estimate nitrous oxide emissions, we separated the Elbe Estuary into five regions: limnic (stream kilometer 585 to 615), Port of Hamburg (stream kilometer 615 to 632), oligohaline (stream kilometer 632 to 704), mesohaline (stream kilometer 704 to 727) and polyhaline (stream kilometer 727 to 750), see Table A3.5. Respective areas were provided by the German Federal Waterways Engineering and Research Institute (BAW, pers. Comm., Oritz, 2023) and Geerts et al. (2012). In order to account for seasonality, cruises were defined as: winter (March), spring (April and May), summer (June and July) and late summer/autumn (August and September). We then calculated daily nitrous oxide emissions per section and season. For upscaling, we used calculated monthly emissions to estimate annual emissions (winter: November to March, spring: April to May, summer: June to July and late summer/autumn: August to October). To address uncertainties, we calculated nitrous oxide emissions based on different parametrizations and wind speeds as described above.

#### 4.2.5 Excess nitrous oxide and apparent oxygen utilization

The correlation between excess nitrous oxide ( $N_2O_{xs}$ ) and apparent oxygen utilization ( $AOU$ ) can provide insights into nitrous oxide production (Nevison et al. 2003; Walter et al. 2004). We calculated  $N_2O_{xs}$  as the difference between the nitrous oxide concentration in water ( $N_2O_w$ ) and the theoretical equilibrium concentration ( $N_2O_{eq}$ ; Eq. 4.4).  $AOU$  was determined using Eq. 4.5, where  $O_2$  is the measured dissolved oxygen concentration, and  $O_2'$  is the theoretical equilibrium concentration between water and atmosphere calculated according to Weiss (1970).

$$N_2O_{xs} = N_2O_w - N_2O_{eq} \quad (4.4)$$

$$AOU = O_2' - O_2 \quad (4.5)$$

A linear relationship between  $AOU$  and  $N_2O_{xs}$  is usually an indicator for nitrification (Nevison et al. 2003; Walter et al. 2004).

#### 4.2.6 Statistical analysis

All statistical analyses were done using R packages. The packages `ggpubr` v.0.6.0 (Kassambara 2023) and `stats` v.4.0.2 (R Core Team and contributors worldwide 2020) were used to calculate Pearson correlations (R) and p-values.

### 4.3 Results

#### 4.3.1 Hydrographic properties and DIN distribution

Discharge ranged between  $171 \text{ m}^3 \text{ s}^{-1}$  and  $1282 \text{ m}^3 \text{ s}^{-1}$  during our cruises (ZDM 2022), with higher discharge in winter and lower discharge in summer (Table 4.1). Average water temperature over the entire estuary ranged from  $5.4 \pm 0.5 \text{ }^\circ\text{C}$  in March 2021 to  $22.6 \pm 1.0 \text{ }^\circ\text{C}$  in August 2017 (Table 4.1). For further evaluation, March 2021 and 2022 cruises were regarded as winter cruises (water temperature  $<6^\circ\text{C}$ ), whereas all cruises with higher water temperature were jointly regarded as spring and summer conditions.

Nitrate was the major form of DIN during all cruises. In winter, high nitrogen concentrations entered the estuary from the river. Towards summer, the riverine input of nitrate (stream kilometer  $<620$ ) decreased, but along the estuary nitrate concentrations increased up to  $\sim$ stream kilometer 700, then decreased towards the North Sea. Nitrate concentrations were highest during both March cruises with averages of  $319.0 \pm 85.7 \text{ } \mu\text{mol L}^{-1}$  and  $230.9 \pm 76.2 \text{ } \mu\text{mol L}^{-1}$  in 2021 and 2022, respectively. During summer, nitrate concentrations were lower, with averages between  $151.0 \pm 58.1 \text{ } \mu\text{mol L}^{-1}$  in May 2021 and  $63.3 \pm 38.8 \text{ } \mu\text{mol L}^{-1}$  in July 2019 (Figure 4.2a, b).

Nitrite and ammonium concentrations were usually low ( $<1 \mu\text{mol L}^{-1}$ ) throughout the Elbe Estuary, but peaked in the Hamburg Port region and around stream kilometer 720 (Figure 4.2c, e). We measured pronounced variations in nitrite concentrations during most of our cruises, ranging from  $>6.0 \mu\text{mol L}^{-1}$  (July 2019) to concentrations below the detection limit (Figure 4.2c, d). The highest ammonium concentration was measured in March 2021 at  $23.5 \mu\text{mol L}^{-1}$  (Figure 4.2e, f).

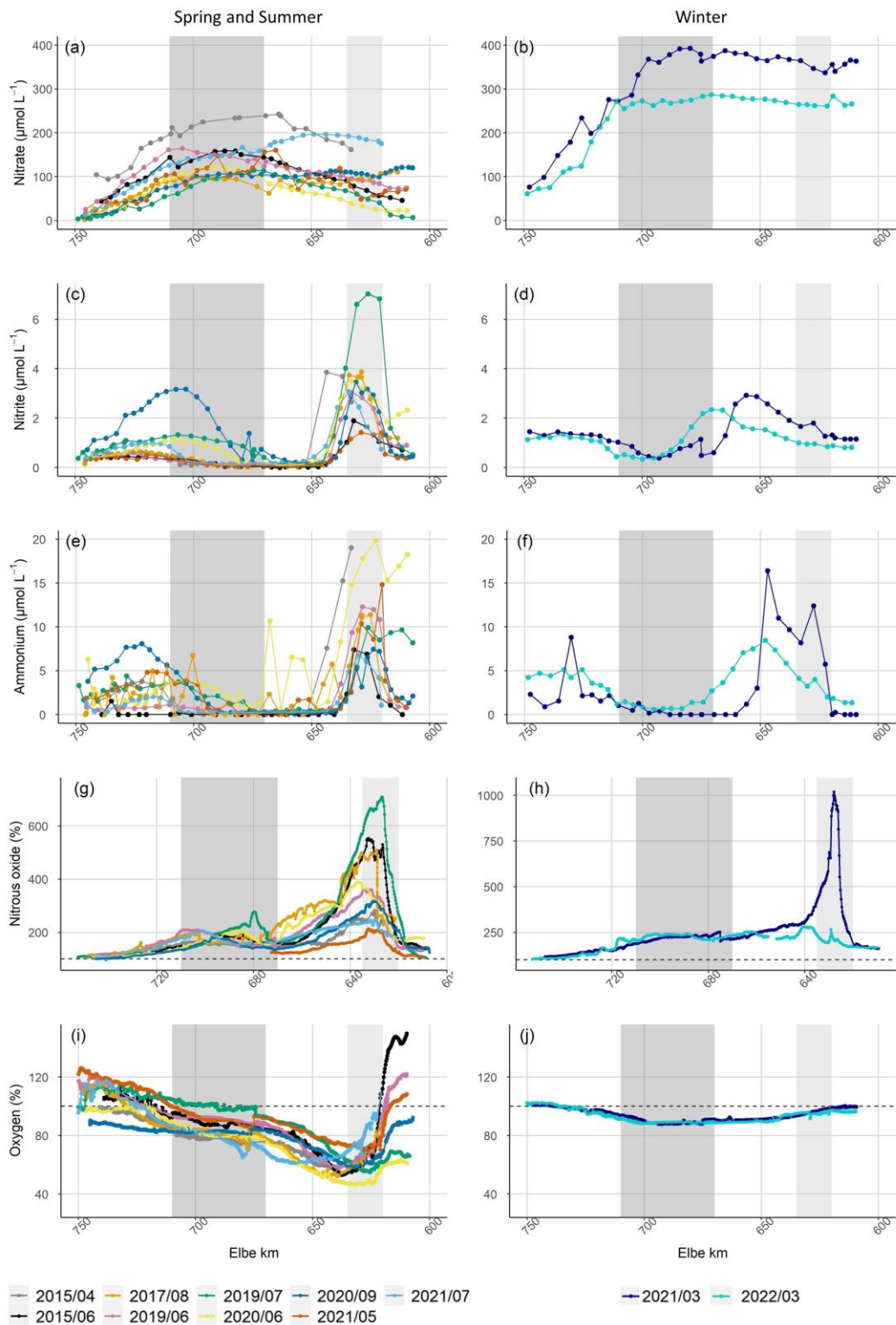


**Figure 4.2.** Nitrate concentration along the Elbe Estuary (a) in spring/summer, (b) in winter. Nitrite concentration along the Elbe Estuary (c) in spring/summer and (d) in winter. Ammonium concentration along the Elbe Estuary (e) in spring/summer and (f) in winter. Nitrous oxide in % saturation along the Elbe Estuary (g) in spring/summer, (h) in winter. Dissolved oxygen in % saturation along the Elbe Estuary (i) in spring/summer and (j) in winter. All variables are plotted against Elbe stream kilometers (Elbe km). Light grey shading denotes the Hamburg Port region, dark grey shading the typical position of the maximum turbidity zone (MTZ, Bergemann, 2004). Note the difference in Y axis scales for the plots of (g) and (h). The dashed black lines in (g) and (h), as well as (i) and (j) indicate saturation of 100 % for nitrous oxide and dissolved oxygen, respectively.

### 4.3.2 Atmospheric nitrous oxide and nitrous oxide saturation

The average atmospheric nitrous oxide dry mole fractions ranged from 325 ppb in June 2015 to 336 ppb in July 2022 (Table 4.2). The differences between our measurements and the mean monthly nitrous oxide mole fraction measured at the Mace Head atmospheric monitoring station (Ireland; Dlugokencky et al. 2022) were always less than 1.5 %, indicating a good agreement with the monitoring data.

During all cruises, the Elbe Estuary was supersaturated in nitrous oxide in the freshwater region (Figure 4.2g, h). The average nitrous oxide saturation over the entire transect ranged between 146 % and 243 % with an overall average of 197 % for all cruises. Highest nitrous oxide occurred in the Hamburg Port region in spring and summer with an average nitrous oxide peak of 402 % saturation and a maximum supersaturation of 710 % in July 2019. The distributions of nitrous oxide during winter cruises were significantly different: In March 2022, highest nitrous oxide (280 % saturation) occurred at stream kilometer 640. In contrast, in March 2021, we found an extraordinarily high peak with a saturation of 1018 % at stream kilometer 627. Between stream kilometer 680 and 720, a supersaturation of up to 277 % occurred in spring and summer. Further towards the North Sea, nitrous oxide decreased, approaching equilibrium with the atmosphere.

### 4.3.3 Nitrous oxide flux densities and nitrous oxide emissions

For nitrous oxide flux densities, we in the following present calculated values after Borges et al. (2004; Table 4.2). See Table A3.2, Table A3.3 and Table A3.4 for results of other parametrizations. The nitrous oxide flux densities were usually highest in the Hamburg Port area, with an average of  $95.0 \pm 97.9 \mu\text{mol m}^{-2} \text{d}^{-1}$  and lowest towards the North Sea, with an average of  $3.9 \pm 3.0 \mu\text{mol m}^{-1} \text{d}^{-1}$  (Elbe stream kilometers >735). The average nitrous oxide flux density of all cruises was  $39.9 \pm 46.9 \mu\text{mol m}^{-2} \text{d}^{-1}$  (calculated with in-situ wind speeds measured during the cruises).

**Table 4.2.** Calculated average nitrous oxide saturation, sea-to-air fluxes calculated following Borges et al. (2004) and atmospheric nitrous oxide dry mole fractions during our cruises in the Elbe Estuary

Campaign Dates	Average saturation (%)	Nitrous oxide flux densities ( $\mu\text{mol m}^{-2} \text{d}^{-1}$ )			Average atmospheric dry mole fraction (ppb)
		In-situ wind	Annual wind	Seasonal wind	
28.-29.04.15	$160.8 \pm 37.9$	$33.1 \pm 21.0$	$23.1 \pm 14.7$	$25.4 \pm 16.1$	$331 \pm 0.5$
02.-04.06.15	$203.8 \pm 112.7$	$39.0 \pm 42.7$	$37.2 \pm 40.7$	$37.8 \pm 41.4$	$325 \pm 0.8$
01.-02.08.17	$221.0 \pm 106.5$	$35.6 \pm 31.8$	$43.2 \pm 38.5$	$44.1 \pm 39.3$	$331 \pm 1.2$
04.-05.06.19	$192.6 \pm 66.0$	$29.7 \pm 21.5$	$33.5 \pm 24.2$	$34.0 \pm 24.6$	$332 \pm 0.2$
30.07.-01.08.19	$232.5 \pm 155.3$	$42.0 \pm 50.1$	$45.7 \pm 54.5$	$47.4 \pm 56.4$	$327 \pm 1.0$
19.-20.06.20	$193.9 \pm 74.1$	$39.2 \pm 31.6$	$33.3 \pm 26.9$	$33.9 \pm 27.3$	$330 \pm 0.6$
09.-11.09.20	$160.5 \pm 53.6$	$26.0 \pm 23.5$	$21.8 \pm 19.7$	$24.5 \pm 22.1$	$331 \pm 0.7$
10.-12.03.21	$242.5 \pm 141.6$	$100.7 \pm 101.2$	$58.1 \pm 58.4$	$71.0 \pm 71.4$	$331 \pm 1.3$
04.-05.05.21	$145.6 \pm 28.8$	$35.6 \pm 22.5$	$17.8 \pm 11.2$	$18.5 \pm 11.7$	$331 \pm 0.8$
27.-28.07.21	$172.6 \pm 37.2$	$28.0 \pm 14.6$	$25.9 \pm 13.6$	$26.9 \pm 14.1$	$334 \pm 3.8$
01.-02.03.22	$196.5 \pm 47.0$	$27.8 \pm 13.9$	$39.0 \pm 19.5$	$47.7 \pm 23.8$	$333 \pm 0.7$

Nitrous oxide emission estimates varied significantly depending on the used parametrization and wind speeds. Note that we calculated emission twice: 1) including (w 03/2021) and 2) deliberately excluding (w/o 03/2021) the nitrous oxide peak saturation measured in the Port of Hamburg in March 2021, using a linear interpolated concentrations in the respective. Highest emissions were calculated following methods by Borges et al. (2004) and using in-situ wind speeds, resulting in emissions of  $0.25 \pm 0.16 \text{ Gg-N}_2\text{O yr}^{-1}$  and  $0.23 \pm 0.12 \text{ Gg-N}_2\text{O yr}^{-1}$  with and without the nitrous oxide peak in March 2021, respectively. Lowest emissions of  $0.08 \text{ Gg-N}_2\text{O yr}^{-1}$  arose with parametrization of Nightingale et al. (2000) and Wanninkhof (1992), and using annual wind speeds (Table 4.3).

**Table 4.3.** Annual nitrous oxide emission estimates in Gg-N<sub>2</sub>O yr<sup>-1</sup> calculated with different parametrizations and wind speeds

		Emissions in Gg-N <sub>2</sub> O yr <sup>-1</sup>			
		Borges et al. (2004)	Nightingale et al. (2000)	Wanninkhof (1992)	Clark et al. (1995)
w	In-situ wind	0.25 ± 0.16	0.14 ± 0.12	0.17 ± 0.15	0.16 ± 0.12
03/2021	Annual wind	0.21 ± 0.11	0.08 ± 0.04	0.09 ± 0.05	0.09 ± 0.05
	Seasonal wind	0.24 ± 0.12	0.11 ± 0.06	0.13 ± 0.06	0.12 ± 0.06
w/o	In-situ wind	0.23 ± 0.12	0.13 ± 0.09	0.15 ± 0.11	0.14 ± 0.09
03/2021	Annual wind	0.20 ± 0.08	0.08 ± 0.03	0.08 ± 0.03	0.09 ± 0.04
	Seasonal wind	0.22 ± 0.09	0.11 ± 0.04	0.12 ± 0.04	0.12 ± 0.04

#### 4.3.4 Dissolved oxygen saturation

Average oxygen varied between 76 and 95 % saturation with an oxygen minimum in the Hamburg Port area. Winter cruises varied little, with oxygen remaining relatively constant along the estuary (>88 % saturation). During most spring and summer cruises, water from the river coming into the estuary was supersaturated in oxygen (>100 % saturation). In the Hamburg Port region, oxygen saturation generally decreased. Lowest values occurred in June 2020 with 47 % saturation. The along-estuary oxygen minimum in summer months (June to August) was always below 61 % saturation. In spring and summer, oxygen increased towards the North Sea and reached 100 % saturation (Figure 4.2i, j).

Plots of N<sub>2</sub>O<sub>xs</sub> and AOU revealed excess nitrous oxide along the entire estuary (Figure 4.3). During all cruises, elevated riverine N<sub>2</sub>O<sub>xs</sub> entered the estuary (stream kilometer <620). A linear positive relationship between N<sub>2</sub>O<sub>xs</sub> and AOU suggested nitrification as main production pathway in large sections of the estuary (Nevison et al. 2003; Walter et al. 2004). However, in summer, a change of slope in the Port of Hamburg as well as in the mesohaline section of the estuary suggested either increased in-situ nitrous oxide production or external nitrous oxide input. In winter, we found an increasing slope in the Hamburg Port region and in the oligohaline part of the Elbe Estuary (Figure 4.3h, k).

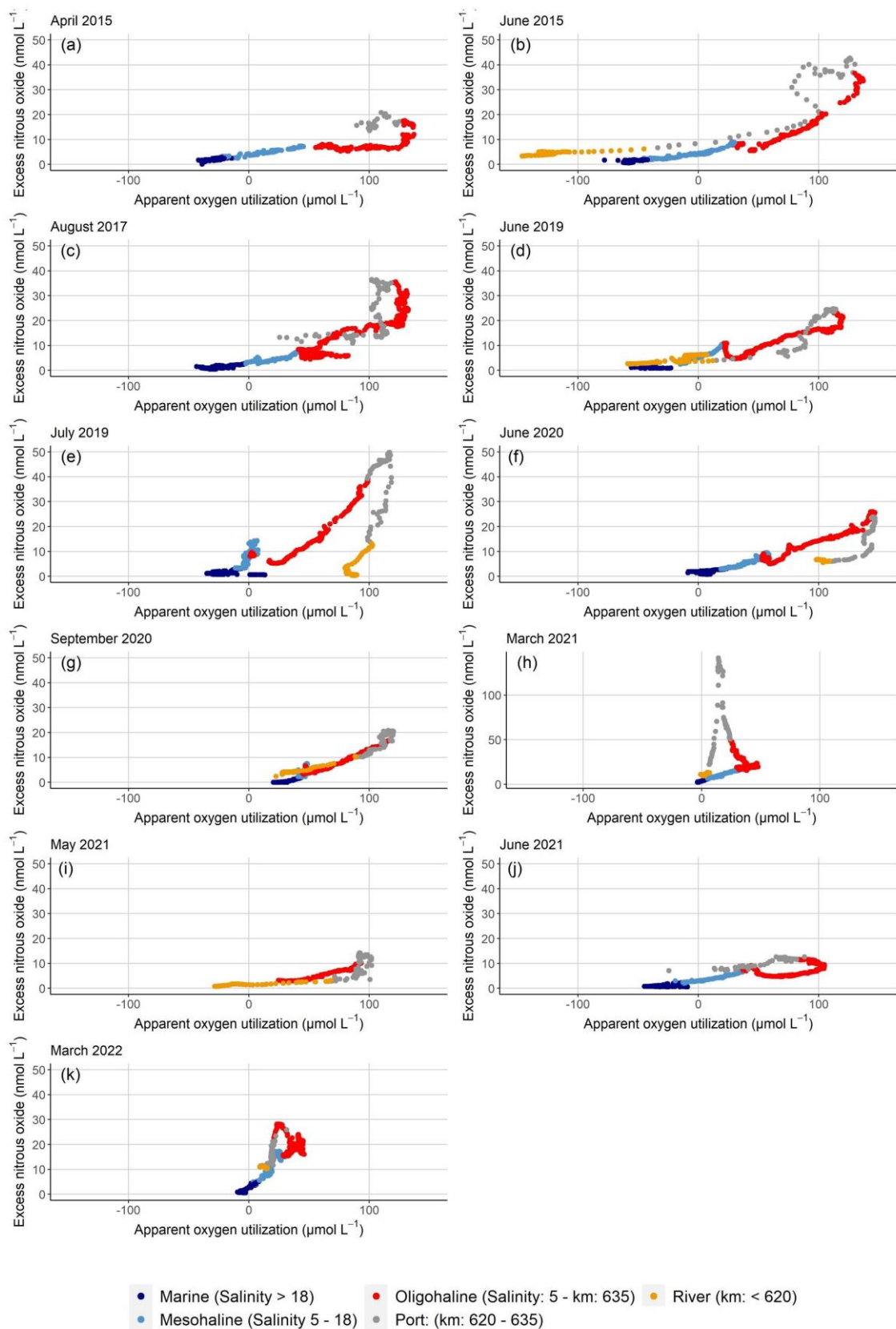


**Figure 4.3.** Plots of  $\text{N}_2\text{O}_{\text{xs}}$  vs AOU for (a) April 2015, (b) June 2015, (c) August 2017, (d) June 2019, (e) July 2019, (f) June 2020, (g) September 2020, (h) March 2021, (i) May 2021, (j) June 2021 and (k) March 2022. The values are colored to distinguish between different regions of the estuary. Y-axis scale differ for Figure 4.3h.

#### 4.3.5 Statistical analysis

We performed a statistical analyses to identify potential nitrous oxide production pathways and controlling factors. Table 4.4 summarizes the results for the entire data set with further separation into spring and summer cruises (sp/su), as well as separation according to presence of a salinity gradient (salinity >1) or freshwater regions (salinity <1). Further, we performed corresponding analysis to assess the significance of correlations between for average values of different parameters for each cruise (Table 4.5).

**Table 4.4.** Pearson correlation coefficients (R) for nitrous oxide saturation (%) with temperature (T in °C), pH value, oxygen (O<sub>2</sub> in % saturation), ammonium concentrations (NH<sub>4</sub><sup>+</sup> in μmol L<sup>-1</sup>), nitrite concentrations (NO<sub>2</sub><sup>-</sup> in μmol L<sup>-1</sup>), nitrate concentrations (NO<sub>3</sub><sup>-</sup> in μmol L<sup>-1</sup>), suspended particulate matter concentrations (SPM in mg L<sup>-1</sup>), C/N values, particulate carbon fraction (PC in %) and particulate nitrogen fraction (PN in %) for the entire data set, spring and summer cruises (sp/su), data with salinity >1, spring and summer cruises with salinity >1, data with salinity <1 and spring and summer cruises with salinity <1. The significance is shown as “ for p-value <0.001, \* for p-values <0.01 and + for p-values <0.05.

N <sub>2</sub> O	T	pH	O <sub>2</sub>	NH <sub>4</sub> <sup>+</sup>	NO <sub>2</sub> <sup>-</sup>	NO <sub>3</sub> <sup>-</sup>	SPM	C/N	PC	PN
%	°C		%	μM	μM	μM	mg		%	%
Entire data	0.06	-0.47“	-0.56“	0.27“	0.48“	0.23	0.10	0.60	-0.05	-0.13 <sup>+</sup>
sp/su	0.33*	-0.59“	-0.65“	0.23“	0.53“	0.09	0.02	0.24“	-0.09	-0.13 <sup>+</sup>
Sal>1	0.03	-0.40“	-0.53“	-0.32“	-0.05	0.71“	0.32“	0.11*	-0.24	-0.39“
Sal<1,	0.01	-0.41“	-0.42“	0.28“	0.51“	-0.00	-0.08	0.15	-0.25*	-0.24*
Sal>1, sp/su	-0.10	-0.21 <sup>+</sup>	-0.52“	-0.28“	0.01	0.62“	0.02	0.39“	-0.31“	-0.41“
Sal<1, sp/su	0.30“	-0.60“	-0.57“	0.21 <sup>+</sup>	0.58“	-0.23*	-0.16 <sup>+</sup>	0.11	-0.30*	-0.27*

**Table 4.5.** Pearson correlation coefficients (R) for average nitrous oxide saturation (%) with average discharge (Q in m<sup>3</sup> s<sup>-1</sup>) temperature (T in °C), pH value, oxygen (O<sub>2</sub> in % saturation), ammonium concentrations (NH<sub>4</sub><sup>+</sup> in μmol L<sup>-1</sup>), nitrite concentrations (NO<sub>2</sub><sup>-</sup> in μmol L<sup>-1</sup>), nitrate concentrations (NO<sub>3</sub><sup>-</sup> in μmol L<sup>-1</sup>), suspended particulate matter concentrations (SPM in mg L<sup>-1</sup>), C/N values, particulate carbon fraction (PC in %) and particulate nitrogen fraction (PN in %) for the entire data set, spring and summer cruises (sp/su), data with salinity >1, spring and summer cruises with salinity >1, data with salinity <1 and spring and summer cruises with salinity <1. The significance is shown as “ for p-value <0.001, \* for p-values <0.01 and + for p-values <0.05.

N <sub>2</sub> O	Q	T	pH	O <sub>2</sub>	NH <sub>4</sub> <sup>+</sup>	NO <sub>2</sub> <sup>-</sup>	NO <sub>3</sub> <sup>-</sup>	SPM	C/N	PC	PN
%	m <sup>3</sup> s <sup>-1</sup>	°C		%	μM	μM	μM	mg		%	%
Entire data	0.13	0.06	-0.65	-0.39	0.02	0.48	0.27	-0.31	0.53	0.12	-0.16
sp/su	-0.26	0.76 <sup>+</sup>	-0.82 <sup>+</sup>	-0.32	0.01	0.35	-0.40	-0.92*	0.15	0.18	0.31
Sal>1	-0.07	-0.14	-0.38	-0.43	-0.18	0.23	0.52	-0.19	0.46	-0.18	-0.38
Sal<1,	-0.21	0.29	-0.59	-0.39	0.26	0.76*	-0.11	-0.57	0.12	0.61	0.47
Sal>1, sp/su	-0.07	-0.70 <sup>+</sup>	-0.41	-0.26	-0.42	0.03	0.05	-0.81 <sup>+</sup>	-0.04	-0.10	0.14
Sal<1, sp/su	-0.48	0.72 <sup>+</sup>	-0.80	-0.46	0.29	0.77 <sup>+</sup>	-0.58	-0.87 <sup>+</sup>	-0.17	0.69	0.67

## 4.4 Discussion

### 4.4.1 Nitrous oxide saturation and flux densities of the Elbe Estuary

The average nitrous oxide saturation and flux density were 197 % and  $39.9 \pm 46.9 \mu\text{mol m}^{-2} \text{d}^{-1}$ , respectively. The nitrous oxide flux densities from the Elbe Estuary were in the mid-range of flux densities of other European estuaries ranging from  $2.9 \mu\text{mol m}^{-2} \text{d}^{-1}$  to  $96.5 \mu\text{mol m}^{-2} \text{d}^{-1}$  (Garnier et al. 2006; Gonçalves et al. 2010; Murray et al. 2015) and average nitrous oxide saturations fitted to values determined by Reading et al. (2020) for highly modified urban systems. The relationship of  $\text{N}_2\text{O}_{\text{xs}}$  and AOU (Figure 4.3), with changing slopes in the Port of Hamburg and mesohaline estuary, was determined by either initial riverine nitrous oxide production, or in-situ production along the estuary. During spring and summer, we found increasing nitrous oxide concentrations in the Hamburg Port region (see also Brase et al. 2017), and in the salinity gradient (stream kilometer 680-700, salinity  $\sim 5$ ). Both nitrous oxide peaks varied in magnitude and spatial extension, suggesting in-situ biological production (Figure 4.2g). This matches earlier research linking estuarine nitrous oxide fluxes to in-situ generation (e.g., Bange 2006; Barnes and Upstill-Goddard 2011; Murray et al. 2015).

Previous measurements of nitrous oxide saturation and flux densities in the Elbe Estuary between the 1980s and 2015 (Hanke and Knauth 1990; Barnes and Upstill-Goddard 2011; Brase et al. 2017) showed a significant reduction of nitrous oxide saturation due to the reduced riverine nutrient load and higher dissolved oxygen concentrations (Brase et al. 2017). However, since the BIOGEST study in 1997 (Barnes and Upstill-Goddard 2011), nitrous oxide remained relatively stable at  $\sim 200$  % saturation despite a concurrent decrease in TN concentration from  $\sim 400 \mu\text{mol L}^{-1}$  to around  $200 \mu\text{mol L}^{-1}$  (Figure A3.2; Hanke and Knauth 1990; Barnes and Upstill-Goddard 2011; Brase et al. 2017; FGG Elbe 2022). As nitrous oxide saturation did not decrease in scale with riverine nitrogen input this suggests that in-situ nitrous oxide production along the estuary is important. Dähnke et al. (2008) showed a shift from dominating denitrification towards significant nitrification in the Elbe Estuary due to the significant improvement of water quality after the reunification of Germany in 1990. In the following sections, we investigate the biogeochemical controls of this in-situ production. For this purpose, we discuss the two zones of intense nitrous oxide nitrous oxide production separately and also distinguish between cruises in spring and summer (water temperature  $>10$  °C) and in winter (water temperature  $<6$  °C).

### 4.4.2 Nitrous oxide production in spring and summer in the mesohaline estuary

The nitrous oxide peak in the transition between oligohaline and mesohaline estuary was accompanied by a sudden change in the slope of the AOU vs  $\text{N}_2\text{O}_{\text{xs}}$  plots, (Figure 4.3), pointing towards nitrous oxide production in the oxic water column. Peaks of nitrite and ammonium concentrations coincided with the elevated nitrous oxide saturations between Elbe km 680 -700, with

an ammonium peak around stream kilometer  $\sim 720$ , and a nitrite peak at  $\sim 700$  (Figure 4.4). Highest nitrous oxide concentrations were usually measured between the nitrite peak and the region with highest turbidity (Figure 4.4a; September 2020, and Figure A3.3-Figure A3.13). This co-occurrence of nitrite accumulation and increased nitrous oxide saturation has been interpreted as signs for nitrous oxide production via denitrification (Wertz et al. 2018; Sharma et al. 2022). However, denitrification does not seem likely in this oxic water column. Such a succession of nitrite and ammonium peaks is also typical for remineralization and nitrification, and the slight decrease of oxygen concentrations around the higher nitrous oxide saturation (Figure 4.2g, i) suggests oxygen consumption, possibly caused by these two processes. Sanders et al. (2018) measured small but detectable nitrification rates ( $1\text{--}2 \mu\text{mol L}^{-1} \text{d}^{-1}$ ) for this region of the Elbe Estuary, suggesting that nitrous oxide may be a side product of nitrification.

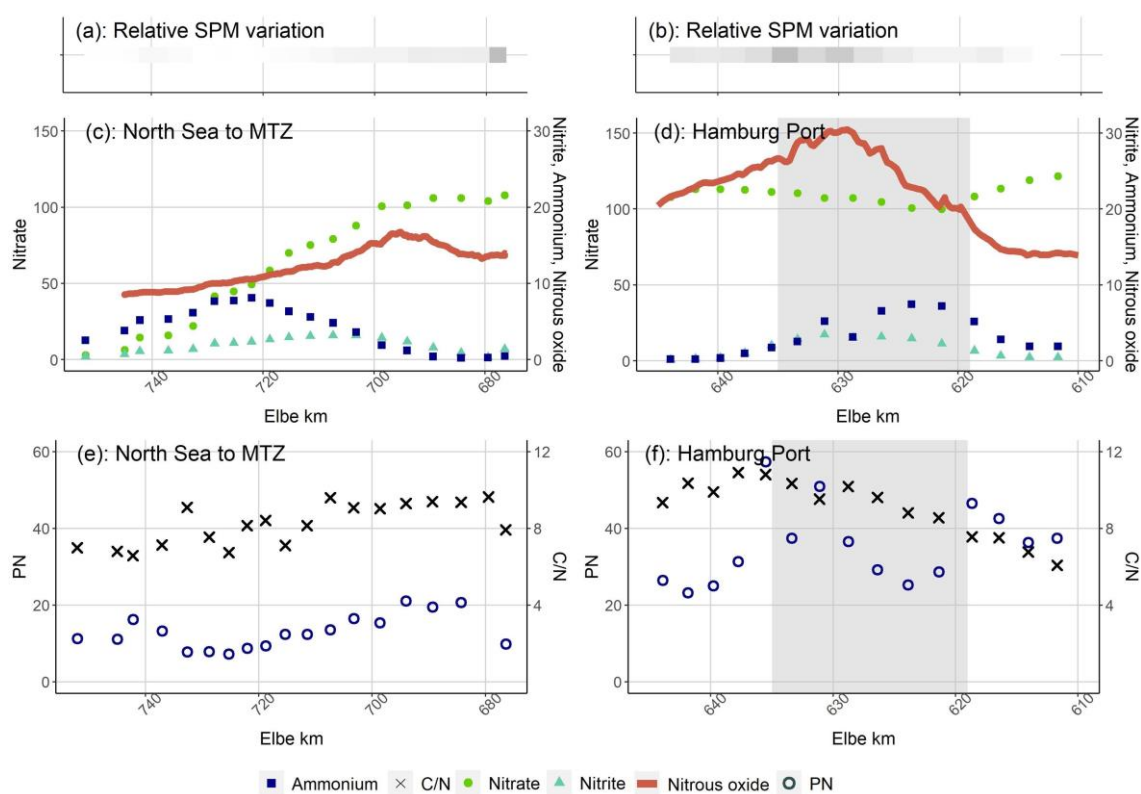


**Figure 4.4.** Succession of N-bearing substances coming from the North Sea and in the Port of Hamburg in September 2020: Relative change of suspended particulate matter concentrations (a) from the North Sea and (b) in the Port of Hamburg. Nitrate in  $\mu\text{mol L}^{-1}$ , nitrite in  $\mu\text{mol L}^{-1}$ , ammonium in  $\mu\text{mol L}^{-1}$  and nitrous oxide concentrations in  $\text{nmol L}^{-1}$  plotted against Elbe stream kilometers (c) from the North Sea and (d) in the Port of Hamburg. Particulate nitrogen concentrations in  $\mu\text{mol L}^{-1}$  and C/N values plotted against stream kilometers (e) from the North Sea and (f) in the Port of Hamburg. The grey area in (f) and (f) shows the position of the Port of Hamburg.

This suggests input of particulate matter from the North Sea and upstream particle transport towards the maximum turbidity zone of the estuary (MTZ). This transport mechanism is in line with Wolfstein and Kies (1999), who explained organic matter contents and chlorophyll a concentrations in the

polyhaline part of the Elbe Estuary by input of freshly produced particulate matter of marine origin. Generally, maximum turbidity zones are generated by the balance between river-induced flushing and upstream transport of marine suspended particulate matter, as a function of estuarine geomorphology, gravitational circulation and tidal flow, trapping the particles in the MTZ (Bianchi 2007; Sommerfield and Wong 2011; Winterwerp and Wang 2013). Other studies detected nitrous oxide production from water column nitrification in estuarine MTZs (e.g., Barnes and Owens 1999; de Wilde and de Bie 2000; Bange 2006; Barnes and Upstill-Goddard 2011; Harley et al. 2015), caused by high bacterial numbers, particulate nitrogen availability and long residence times (Murray et al. 2015).

For the selected dataset, we calculated a negative correlation between average suspended particulate matter concentrations and nitrous oxide saturation ( $R = -0.81$ ; Table 4.5), and found that the nitrous oxide peak was located downstream of the MTZ, and upstream of increasing nitrite and ammonium concentrations (Figure 4.4). This suggests that (1) the mere concentration of suspended particulate matter is not the driving factor of nitrification as a source of nitrous oxide, but that organic matter quality is key to biological turnover (Dähnke et al. 2022), and (2) the material transport from the North Sea upstream towards the MTZ (Schoer 1990; Kappenberg and Fanger 2007) is a main mechanism for nitrous oxide generation. We find organic matter with low C/N ratios, and with relatively high PN and PC contents in the outermost samples (ranging from 5.9 in June 2020 to 8.8 August 2017), indicating fresh and easily degradable organic matter (Figure A3.1; e.g., Redfield et al. 1963; Fraga et al. 1998; Middelburg and Herman 2007). Towards the MTZ, C/N values, PN and PC contents decreased, indicating remineralization in the water column. This remineralization and subsequent nitrification can then cause the observed succession of ammonium, nitrite and nitrous oxide peaks (Figure 4.4a), contributing to the high nitrate concentrations in the MTZ, where high C/N values (9-11/16) indicate low organic matter quality (e.g., Hedges and Keil 1995; Middelburg and Herman 2007). Overall, we conclude that remineralization of marine organic matter, followed by nitrification, produced the nitrous oxide peak in the salinity gradient of the Elbe Estuary. This production was mainly fueled by fresh organic matter entering the estuary from the North Sea.

#### **4.4.3 Hamburg Port: nitrous oxide production in spring and summer**

During all cruises, we measured highest nitrous oxide saturation in the Port of Hamburg. These peaks can be caused by input from a wastewater treatment plant, by deepening and dredging operations, enhanced benthic production or by in-situ production in the water column.

Point sources generally play a minor role in the Elbe Estuary (Hofmann et al. 2005; IKSE 2018). We estimated the wastewater discharge fraction of stream flow according to Büttner et al. (2020) for the wastewater treatment plant (WWTP) Köhlbrandhöft, which treats the wastewater from the Hamburg

metropolitan region, with less than 5 % even under low freshwater inflow. Thus, point sources seemed not to be the cause for the elevated nitrous oxide concentrations.

Dredging can be a potential source of nitrous oxide in the water column. The estuary is continuously deepened and dredged to grant access for large container ships, which stirs up bottom sediments. Ammonium concentrations in the sediment pore water are high (Zander et al. 2020, 2022) and nitrous oxide can be produced by nitrifier-denitrification in the sediments (Deek et al. 2013). However, we found no correlation of high suspended particulate matter concentrations and nitrous oxide saturation, indicating no major influence on nitrous oxide dynamics from channel dredging and deepening.

Several studies identified the Hamburg Port region as a hotspot of biogeochemical turnover: Deek et al. (2013) showed denitrification, where Sanders et al. (2018) measured intense nitrification. Norbistrath et al. (2022) determined intense total alkalinity generation, and Dähnke et al. (2022) found that nitrogen turnover was driven by high particulate organic matter in this region. Brase et al. (2017) identified the Hamburg Port region as a hotspot of nitrous oxide production and hypothesized that simultaneous nitrification and sediment denitrification were responsible. We use our expanded dataset to further evaluate this hypothesis and to identify drivers for nitrous oxide production in the port region.

During all cruises in spring and summer, we measured ammonium and nitrite peaks in the Hamburg Port region (Figure 4.2c, e; exemplary for September 2020 in Figure 4.4b). Several researchers did address the nitrogen turnover and this accumulation of nitrite and ammonium assuming that the sudden increase of water depth in the Port leads to a light limitation and decomposition of riverine organic material (Schroeder 1997; Schöl et al. 2014). This in turn raises ammonium and nitrite concentrations and fosters nitrification in the port region (Sanders et al. 2018; Dähnke et al. 2022).

High nitrite concentrations are favorable for nitrous oxide production by nitrification and nitrifier-denitrification (Quick et al. 2019), while low-oxygen conditions facilitate both nitrification and denitrification. We found that nitrous oxide saturation increased with decreasing discharge ( $R = -0.48$ ; Table 4.5) during spring and summer. This further points towards in-situ nitrous oxide production, because denitrification and nitrification are more intense during longer residence times (e.g., Nixon et al. 1996; Pind et al. 1997; Silvennoinen et al. 2007; Gonçalves et al. 2010). Overall, our data showed the succession of ammonium, nitrite and nitrous oxide production (Figure 4.4; Figure A3.3-Figure A3.13) confirming simultaneous sedimentary denitrification and nitrification in the water column responsible pathways for nitrous oxide production in the Port of Hamburg (Brase et al. 2017).

In spring and summer, we found no linear relationship between  $N_2O_{xs}$  and AOU in the Hamburg Port (Figure 4.3). This may result from combined nitrous oxide production by nitrification and denitrification. However, oxygen saturation and nitrous oxide saturation were inversely correlated in Hamburg Port (Table 4.4 and Table 4.5), suggesting that nitrous oxide production was controlled by oxygen concentrations, and thus was related to oxygen consumption in the port region. Most (75 %) of this oxygen consumption is caused by respiration whereas the remaining 25 % stem from nitrification (Schöl et al. 2014; Sanders et al. 2018). This respiration in turn is determined by remineralization of algal material from the upstream river that is transported to and respired within the port region (Schroeder 1997; Kerner 2000; Schöl et al. 2014), linking estuarine nitrous oxide production to river eutrophication. Fabisik et al. (2023) showed that algae could additionally contribute to nitrous oxide production. In the Elbe, fresh organic matter from the river with low C/N values as well as high PN and PC contents entered the estuary. This organic material was rapidly degraded in the Hamburg Port region (Figure A3.1). Dähnke et al. (2022) found that labile organic matter fueled nitrification but also denitrification in the freshwater part of the Elbe Estuary, which, as shown in our study, results in high nitrous oxide production in the Hamburg Port, leading to the reported negative correlations of PC and PN content with nitrous oxide saturation.

Overall, oxygen conditions mainly controlled nitrous oxide production in the Hamburg Port region in spring and summer. Since respiration of organic matter dominates oxygen drawdown in the port region, we deduce that nitrous oxide production there is linked to the decomposition of phytoplankton produced in the upstream Elbe River regions.

#### **4.4.4 Hamburg Port: Nitrous oxide production in winter**

In winter, low water temperature ( $<6$  °C) should hamper biological production (Koch et al. 1992; Halling-Sorensen and Jorgensen 1993). Indeed, we did not detect a nitrous oxide peak in the MTZ in winter, but we find high nitrous oxide concentrations in the port region. For March 2022, we found a linear increase of  $N_2O_{xs}$  and AOU along with oxygen consumption and increasing ammonium, nitrite and PN concentrations indicating nitrification in the Hamburg Port producing nitrous oxide. Unlike in summer, nitrous oxide concentrations showed a flat increase extending far into the oligohaline section of the estuary (Figure 4.2, Figure A3.1).

However, in March 2021, we found a sharp and sudden increase in nitrous oxide, with a peak concentration that by far exceeded internal biological sources in summer (Figure 4.2h). An ammonium peak in the water column coincided with the nitrous oxide maximum (Figure 4.2f and Figure A3.11). If microbial activity is mostly temperature-inhibited, a local source of nitrous oxide in the port seems the most likely cause.

We considered intensified deepening operations in the Port of Hamburg one potential source of elevated nitrous oxide saturation. Deepening and dredging work occurred in the Hamburg Port region in 2021 (HPA, pers. Comm., Karrasch 2022), but, this also applied to 2022, when we saw no sharp nitrous oxide peak (Figure 4.2h). Furthermore, the regions of deepening and dredging did not match the region of high nitrous oxide concentrations, and turbidity at the time of sampling did not change significantly compared to other cruises. Jointly, this suggests that channel dredging and deepening was not the primary cause for the 2021 winter nitrous oxide peak.

Another possible source of nitrous oxide is the WWTP outflow in the Southern Elbe that joins the main estuary at stream kilometer 626 (Figure 4.1), matching the nitrous oxide peak at stream kilometer 627 (Figure 4.2h). As explained above (Section 4.4.3), the effect of this WWTP on nitrous oxide saturations under normal conditions should be negligible. This peak can be the result of an extraordinary event during our sampling. We indeed found that an extreme rain event occurred on March 11<sup>th</sup> 2021 (HAMBURG WASSER, pers. Comm., Laurich 2022) with a statistical recurrence probability of one to five years (HAMBURG WASSER 2023). This rare event caused aggravated operation conditions in the WWTP at the time of sampling. While the operators could still meet the limits for the effluent levels of nitrate and ammonium, higher than usual ammonium loads exited the treatment plant at this time. We assume that these elevated ammonium WWTP loads, were rapidly converted to nitrous oxide as the warmer and biologically active wastewater entered the Elbe Estuary in March 2021. An important factor for aggravated conditions was a temperature drop in the WWTP caused by cold rain water, we hypothesize that a similar rain event in warmer months would not lead to comparable nitrous oxide peaks.

Therefore, we argue that our March 2021 cruise likely represents an exception due to an extreme weather situation, whereas normal winter conditions in the estuary comply with the nitrous oxide production, like in March 2022.

#### **4.4.5 Seasonally varying N<sub>2</sub>O:DIN dynamic**

We calculated annual nitrous oxide emissions of the Elbe Estuary ranging from  $0.08 \pm 0.03$  Gg-N<sub>2</sub>O yr<sup>-1</sup> to  $0.25 \pm 0.16$  Gg-N<sub>2</sub>O yr<sup>-1</sup> (Table 4.3), which varied from recent nitrous oxide summer emission estimate of  $0.18 \pm 0.01$  Gg-N<sub>2</sub>O yr<sup>-1</sup> by Brase et al. (2017). Estuarine nitrous oxide emissions are affected by tides, diel variations and currents (Barnes et al. 2006; Baulch et al. 2012; Gonçalves et al. 2015), all of which we did not address in our study. Range of possible parametrizations of gas transfer coefficients further complicates a direct comparison of fluxes between studies (Hall Jr. and Ulseth 2020; Rosentreter et al. 2021), which were reflected in the big differences of our emission estimates (Table 4.3). Therefore, a direct comparison to other studies is difficult.

---

In a more general approach, the relationship between nitrous oxide and DIN ( $\text{N}_2\text{O}:\text{DIN}$ ) is used for global estimates of nitrous oxide emissions (Kroeze et al. 2005, 2010; Ivens et al. 2011; Hu et al. 2016). Using publicly available data (Table A3.6 and Table A3.7), we calculated the amount of the annual nitrogen load released as nitrous oxide. Depending on the parametrization used for the gas transfer coefficients, 0.14 % to 0.67 % of the annual DIN loads of the Elbe Estuary were released as nitrous oxide (0.11 % to 0.57 % for TN loads). This is significantly less than the 1 % predicted by Kroeze et al. (2005), but matches results from other estuaries with high agricultural input, e.g. Wells et al. (2018) with 0.3 % to 0.7 % (0.1 % for TN loads) and Robinson et al. (1998) with 0.5 % (0.3 % for TN loads) as well as the 0.11 % to 0.37 % estimated by Maavara et al. (2019), who used TN loads to predict global estuarine emissions.

At our site, highest emissions were estimated in winter (Figure 4.5b) along with highest DIN loads (Figure 4.5c). In spring, summer and late summer, nitrous oxide emissions reduced along with DIN loads (Figure 4.5b, c). However, nitrous oxide release did not scale with the seasonal change of DIN. In winter, 0.10 % to 0.32 % of DIN were released as nitrous oxide, whereas during the other seasons, up to 1.26 % were emitted. Thus, our results corroborate that there is a deviating relationship between DIN and nitrous oxide (Borges et al. 2015; Marzadri et al. 2017; Wells et al. 2018) showing that this relationship even varies seasonally on site due to changing drivers for nitrous oxide production and emissions.

Next to DIN loads, we find that organic matter is an important driver for nitrous oxide production by providing substrate for nitrification. Furthermore, the comparison of our results with previous measurements in the Elbe Estuary revealed that nitrous oxide saturation stopped to scale with DIN input after the 1990s (Section 4.4.1). The significant regime change after the 1990s enabled phytoplankton growth to reestablish in the river (Kerner 2000; Amann et al. 2012; Hillebrand et al. 2018; Rewrie et al. submitted) and led to high nitrification rates in the estuary (Dähnke et al. 2008; Sanders et al. 2018), supporting the overarching control of organic matter on nitrous oxide production and emissions along the Elbe Estuary.

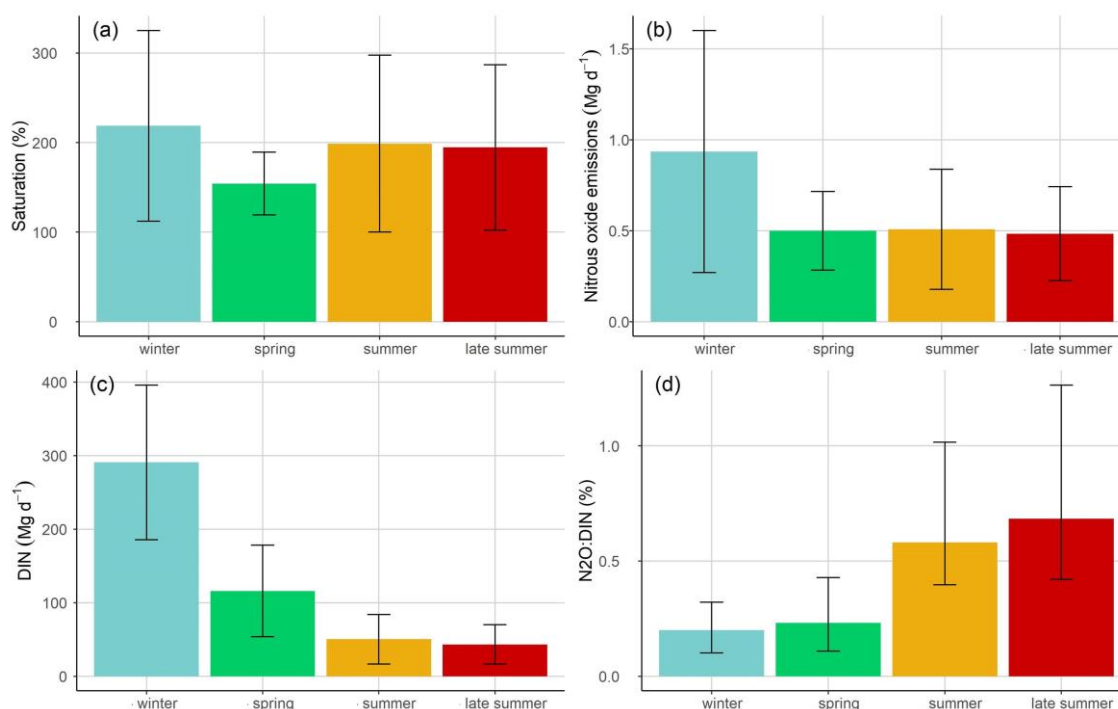


**Figure 4.5.** (a) Average nitrous oxide saturation for each season, (b) average nitrous oxide emissions for each season calculated after Borges et al. (2004), (c) average DIN loads for each season and (d) ratio of nitrous oxide emissions and DIN loads (N<sub>2</sub>O:DIN) for each season. The error bars represent the standard deviations for (a), (b) and (c). The N<sub>2</sub>O:DIN ratios is shown as average values calculated for each parametrization and wind speeds with error bars representing their variability.

## 4.5 Conclusions

Overall, the Elbe is a year-round source of nitrous oxide to the atmosphere, with highest emission occurring in winter, along with high DIN loads and high wind speeds. However, summer nitrous oxide saturation and emissions did not decrease with lower riverine nitrogen input suggesting variable relations of DIN and nitrous oxide (Borges et al. 2015; Marzadri et al. 2017; Wells et al. 2018), and seasonal variability of this ratio caused by changing drivers for nitrous oxide production and emissions. Two hot-spots of nitrous oxide production were found in the Elbe Estuary: the Port of Hamburg and the mesohaline estuary near the estuarine turbidity maximum. Biological nitrous oxide production was enhanced by warmer temperatures and fueled by riverine organic matter in the Hamburg Port or marine organic matter in the MTZ. A comparison with historical nitrous oxide measurements in the Elbe Estuary revealed that nitrous oxide saturation did not decrease with DIN input after the 1990s. The improvement of water quality in the Elbe Estuary enabled phytoplankton growth after the reunification of Germany in 1990s (Kerner 2000; Amann et al. 2012; Hillebrand et al. 2018; Rewrie et al. submitted) and led to a switch from dominant denitrification to high nitrification (Dähnke et al. 2008; Sanders et al. 2018), supporting the overarching control of organic matter on nitrous oxide production along the Elbe Estuary. Thus, our findings indicate that DIN

availability is not the sole control of nitrous oxide production in estuaries with high agricultural input. High organic matter availability due to phytoplankton blooms driven by river eutrophication fuels nitrification and subsequent nitrous oxide emissions, causing a decoupling of the  $\text{N}_2\text{O}:\text{DIN}$  ratio. Therefore, nitrous oxide emissions in heavily managed estuaries with high agricultural loads are clearly linked to eutrophication phenomena. Consequently, reducing nitrogen input alone is not sufficient to minimize nitrous oxide emissions from estuaries. Further measures are needed to prevent the developments of intense phytoplankton blooms in rivers and estuaries. Especially considering climate change projections of more frequent and extensive draughts and warmer temperatures (IPCC 2022), which potentially fuel phytoplankton growth (Scharfe et al. 2009; Kamjunke et al. 2021; IPCC 2022).

### **Acknowledgments**

We thank the crew of *R/V Ludwig Prandtl* for the great support during the cruises. Thanks to Leon Schmidt and the entire working group “Aquatic nutrients cycles” for measuring nutrients and the support during the campaigns. We are thankful for the Hereon FerryBox Team for providing the FerryBox data. Thanks to the working group of Biogeochemistry at the Institute for Geology of the University Hamburg for measuring C/N ratios, PC and PN fractions. We thank Frank Laurich (HAMBURG WASSER) and Dr. Maja Karrasch (Hamburg Port Authority) for their interest in our nitrous oxide measurements and their willingness to provide information. Thanks to Victoria Ortiz (Federal Waterways and Engineering and Research Institute) for providing the respective areas of the Elbe Estuary. Thanks to the NOAA ESRL GML CCGG Group for providing high quality, readily accessible atmospheric nitrous oxide data.



---

## 5 SPM drives the spatial segregation of nitrogen turnover along the hyper-turbid Ems Estuary

*Schulz, G., Sanders, T., van Beusekom, J. E. E., Voynova, Y. G., Schöl, A., and Dähnke, K.: Suspended particulate matter drives the spatial segregation of nitrogen turnover along the hyper-turbid Ems estuary, Biogeosciences, 19, 2007–2024, <https://doi.org/10.5194/bg-19-2007-2022>, 2022.*

### Abstract

Estuaries are nutrient filters and change riverine nutrient loads before they reach coastal oceans. Their morphology have been extensively changed by anthropogenic activities like draining, deepening and dredging to meet economic and social demand, causing significant regime changes like tidal amplifications and in some cases to hyper-turbid conditions. Furthermore, increased nutrient loads, especially nitrogen, mainly by agriculture cause coastal eutrophication. Estuaries can either act as a sink or as a source of nitrate, depending on environmental and geomorphological conditions. These factors vary along an estuary, and change nitrogen turnover in the system. Here, we investigate the factors controlling nitrogen turnover in the hyper-turbid Ems Estuary (Northern Germany), which has been strongly impacted by human activities. During two research cruises in August 2014 and June 2020, we measured water column properties, dissolved inorganic nitrogen, dual stable isotopes of nitrate and dissolved nitrous oxide concentration along the estuary. We found that three distinct biogeochemical zones exist along the estuary. A strong fractionation (26 ‰) of nitrate stable isotopes points towards nitrate removal via water column denitrification in the hyper-turbid tidal river, driven by anoxic conditions in deeper water layers. In the middle reaches of the estuary nitrification gains importance, turning this section into a net nitrate source. The outer reaches are dominated by mixing, with nitrate uptake in 2020. We find that the overarching control on biogeochemical nitrogen cycling, zonation and nitrous oxide production in the Ems Estuary is exerted by suspended particulate matter concentrations and the linked oxygen deficits.

### 5.1 Introduction

Estuaries can significantly alter riverine nutrient loads before they reach adjacent coastal oceans (Crossland et al. 2005; Bouwman et al. 2013). The morphology of estuaries has been extensively altered by humans and anthropogenic activities to meet economic and social demands. Land draining, damming, diking, channel deepening and dredging lead to significant regime changes including tidal

amplification, hyper-turbid conditions and loss of habitats (e.g., Kennish 2005; Winterwerp et al. 2013; de Jonge et al. 2014). High nutrient loads from agriculture, wastewater and urban runoff have induced eutrophication (Galloway et al. 2003; Howarth 2008; van Beusekom et al. 2019), one of the greatest threats to coastal ecosystems worldwide (e.g., Howarth and Marino 2006; Voss et al. 2011).

Depending on the predominant microbial processes, environmental conditions and geomorphological characteristics, estuaries can either act as a sink or as an additional source of nitrate (Middelburg and Nieuwenhuize 2000; Dähnke et al. 2008). In particular, the balance between remineralization, nitrification and denitrification determines the net role of a specific estuary. Previous studies found that biogeochemical changes of dissolved oxygen saturation, residence time or light penetration affect this balance of nutrient uptake and removal (Thornton et al. 2007; Diaz and Rosenberg 2008; Voss et al. 2011; Carstensen et al. 2014).

To disentangle the role of nitrate production and removal processes, stable isotopes are a frequently used tool, because nitrogen turnover processes discriminate heavier isotopes, leading to an enrichment in the pool of remaining substrate. The magnitude of enrichment, the so-called isotope effect, is process specific (Granger et al. 2004; Deutsch et al. 2006; Sigman et al. 2009).

Nitrification and denitrification also produce nitrous oxide ( $N_2O$ ) (Knowles 1982; Tiedje 1988; Wrage et al. 2001; Francis et al. 2007), a potent greenhouse gas that contributes to global warming (IPCC 2007). Estuaries are potential sources of nitrous oxide (Bange 2006) and, together with coastal wetlands, contribute approximately 0.17 to 0.95 Tg  $N_2O$ -N  $yr^{-1}$  to the global nitrous oxide budget of 16.9 Tg  $N_2O$ -N  $yr^{-1}$  (Murray et al. 2015; Tian et al. 2020). Numerous factors control estuarine nitrous oxide emissions. Oxygen depletion, nutrient levels and possibly organic matter composition trigger nitrous oxide production. Therefore, nitrous oxide emissions are linked to eutrophication (de Wilde and de Bie 2000; Galloway et al. 2003; Murray et al. 2015; Quick et al. 2019). The role of nitrous oxide production can vary along an estuary, depending on the environmental and geomorphological properties.

Although the individual nitrogen turnover processes are well understood, the interplay of multiple stressors on the nitrogen cycle needs further investigation (e.g., Billen et al. 2011; Giblin et al. 2013; Sanders and Laanbroek 2018). Therefore, we investigate how biogeochemical water column properties can change the nitrogen turnover, emerging eutrophication and nitrous oxide production along an estuary.

We performed two summer research cruises along the Ems Estuary, a heavily managed estuary in Germany that undergoes anthropogenic pressures from fertilizer input, dredging and channel deepening (de Jonge 1983; Talke and de Swart 2006; Johannsen et al. 2008). This has led to a

significant increase of suspended particulate matter concentration in the inner estuary since the 1950s (de Jonge et al. 2014). We studied water column nutrient and stable isotope composition, as well as suspended particulate matter concentration, in the Ems Estuary to investigate spatial dynamics in nitrogen removal, nitrogen turnover processes and their relation to nitrous oxide production. We have (1) evaluated the biogeochemical zonation of nitrogen turnover along the estuary, (2) identified the dominating nitrogen turnover pathways in individual zones and (3) discussed the controlling factors of nitrogen cycling and emerging nitrous oxide production. Ultimately, with this study, we provide a better insight into the effects of biogeochemical water column properties and biogeochemistry on estuarine nutrient turnover.

## **5.2 Methods**

### **5.2.1 Study site**

The Ems Estuary is situated on the Dutch–German border (Figure 5.1). The estuary is approximately 100 km long and stretches from the weir at Herbrum to the island Borkum. The Ems discharges into the Wadden Sea, a part of the southern North Sea (van Beusekom and de Jonge 1994). The catchment of the Ems is 17 934 km<sup>2</sup> (Krebs and Weilbeer 2008). Agricultural land use is dominant in the catchment (80 %), and urban land use makes up 8% of the catchment (FGG Ems 2015b), with a population density of ~200 km<sup>-2</sup> (FGG Ems 2015c). The Ems is also an important waterway with ports in Delfzijl and Emden, and is used for transport of large vessels from the shipyard in Papenburg to the North Sea (Talke and de Swart 2006).

The Ems is characterized by steep gradients in salinity and tides (Compton et al. 2017). It has an average discharge of 80.8 m<sup>3</sup> s<sup>-1</sup>, with low freshwater discharge in summer and highest discharge between January and April. The Ems is a hyper-turbid estuary with high suspended sediment concentrations (de Jonge et al. 2014; van Maren et al. 2015a), reaching values of 30-40 g L<sup>-1</sup> and more in fluid mud layers (Winterwerp et al. 2013). Channel deepening has led to tidal amplification and an increased upstream sediment transport in the tidal Ems (de Jonge et al. 2014). The increase of suspended matter has lowered light penetration, and has led to decreasing oxygen concentration (Bos et al. 2012). Bos et al. (2012) classified the Ems Estuary as a degraded ecological system with high nutrient loads.

Based on geomorphological characteristics, the Ems can be divided into four sections: the tidal river (kilometer 14-35), Dollard reach (kilometer 35-43), middle reaches (kilometer 43-75) and outer reaches (downstream from kilometer 75; Figure 5.1).

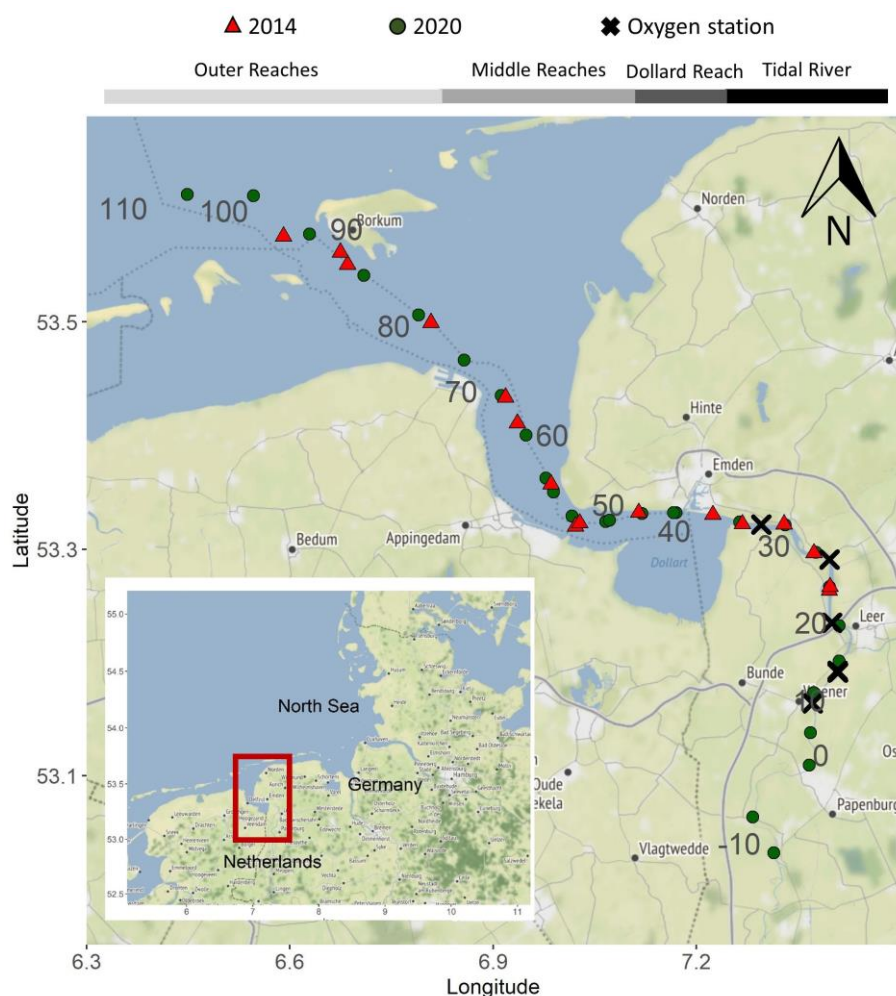


**Figure 5.1.** Map of the Ems Estuary displaying the sampling stations during two summer periods. Red triangles mark cruise stations in 2014, green circles mark cruise stations in 2020 and crosses mark stations with oxygen measurements. The grey numbers show the stream kilometers calculated according to German federal waterways (wsv.de). Background map: © OpenStreetMap contributors 2021. Distributed under the Open Data Commons Open Database License (ODbL) v1.0.

### 5.2.2 Sampling

Water samples were taken during two research cruises with the research vessel *Ludwig Prandtl* in August 2014 and June 2020. Nutrient concentration and suspended particulate matter concentration from the cruise in 2014 have been published in (Sanders and Laanbroek 2018). An onboard membrane pump provided the on-line in-situ FerryBox system with water from 2 m below the surface. The FerryBox system continuously measures dissolved oxygen, water temperature, pH, salinity, fluorescence and turbidity (Petersen et al. 2011). In 2014, the dissolved oxygen measurements from the Ferry-Box were about  $32 \mu\text{mol L}^{-1}$  lower than the Winkler titrations of two discrete samples collected in July 2014. This offset was used to correct the FerryBox optode measurements. Salinity measurements were checked using Optimare Precision Salinometer (Bremerhaven, Germany), and the error of the FerryBox measurements was within 0.01 salinity units.

Discrete water samples were taken from a bypass of the FerryBox system. The samples for nutrient and isotope analysis were filtered immediately through combusted, preweighted GF/F Filters (4 h, 450 °C), and stored frozen in acid-washed (10% HCl, overnight) PE bottles at -20 °C until analyses. The filters were stored at -20 °C for later analysis of suspended particulate matter (SPM; Röttgers et al. 2014),  $^{15}\text{N}$ -SPM and C/N ratios. C/N ratios were measured with an Elemental Analyzer (Eurovector EA 3000) calibrated against a certified acetanilide standard (IVA Analysentechnik, Germany). The standard deviation was 0.05% and 0.005% for carbon and nitrogen respectively. During the 2020 cruise, nitrous oxide gas phase mole fractions were continuously measured in unfiltered water.

### 5.2.3 Dissolved oxygen measurements

During the cruises in 2014 and 2020, we measured dissolved oxygen concentration in surface water using the FerryBox system (see above). For a more detailed view on oxygen dynamics, we also used data provided by the German Federal Institute of Hydrology (BfG unpublished) at the stations in Figure 5.1. Vertical profiles of oxygen concentration were taken at four monitoring stations along the Ems Estuary (Figure 5.1) in August 2014 and June 2020 using an YSI 6660 probe. At these stations, oxygen and temperature were also continuously measured with optodes of miniDot™ (PME, Precision Measurement Engineering) loggers at 0.5m above the bottom at Ems kilometers 11.8 and 24.5 in 2014 and additionally at 18.2 and 33.0 in 2020.

### 5.2.4 Nutrient measurements

Nutrient concentrations (nitrate, nitrite, ammonium, silicate and phosphate) were measured with a continuous flow auto analyzer (AA3, SEAL Analytics) using standard colorimetric and fluorometric techniques (Hansen and Koroleff 1999). Measurement ranges were 0-400  $\mu\text{mol-N L}^{-1}$  for combined nitrate and nitrite, 0-17.8  $\mu\text{mol-N-L}^{-1}$  for nitrite, 0.07-25  $\mu\text{mol-N L}^{-1}$  for ammonium, 0-1000  $\mu\text{mol-Si L}^{-1}$  for silicate and 0-16.1  $\mu\text{mol-P L}^{-1}$  for phosphate.

### 5.2.5 Isotopic analysis

The stable isotope composition of nitrate ( $\delta^{15}\text{N-NO}_3^-$ ,  $\delta^{18}\text{O-NO}_3^-$ ) was measured using the denitrifier method (Sigman et al. 2001; Casciotti et al. 2002), which is based on the isotopic analysis of nitrous oxide. In brief, *Pseudomonas aureofaciens* (ATCC#13985) reduces nitrate and nitrite in the filtered water samples to nitrous oxide. Nitrous oxide was measured by a GasBench II coupled with an isotope ratio mass spectrometer (Delta Plus XP, Thermo Fisher Scientific). Two international standards (USGS34,  $\delta^{15}\text{N-nitrate} = -1.8 \text{ ‰}$ ,  $\delta^{18}\text{O-nitrate} = -27.9 \text{ ‰}$ ; IAEA,  $\delta^{15}\text{N-nitrate} = +4.7 \text{ ‰}$ ,  $\delta^{18}\text{O-nitrate} = +25.6 \text{ ‰}$ ) and one internal standard ( $\delta^{15}\text{N-nitrate} = +7.6 \text{ ‰}$ ,  $\delta^{18}\text{O-nitrate} = +24.4 \text{ ‰}$ ) were used to calibrate the samples. The standard deviation for standards and samples was  $<0.2 \text{ ‰}$ .

( $n = 4$ ) and  $<0.5\%$  ( $n = 4$ ) for  $\delta^{15}\text{N}$ -nitrate and  $\delta^{18}\text{O}$ -nitrate respectively. Nitrite concentration of the samples was usually  $<5\%$ . When nitrite exceeded  $5\%$ , it was removed prior to analysis using sulfamic acid (Granger and Sigman 2009).

An elemental analyzer (Carlo Erba NA 2500) coupled with an isotope ratio mass spectrometer (Finnigan MAT 252) was used to measure  $\delta^{15}\text{N}$ -SPM values. IAEA N1 ( $\delta^{15}\text{N} = 0.4\%$ ), IAEA N2 ( $\delta^{15}\text{N} = +20.3\%$ ) and a certified sediment standard (IVA Analysetechnik, Germany) were used as reference materials.

### 5.2.6 Equilibrator based nitrous oxide measurements and calculations

An nitrous oxide analyzer (Model 914-0022, Los Gatos Res. Inc.) coupled with a seawater/gas equilibrator measured the dry mole fraction of nitrous oxide and water vapor in the water column using off-axis integrated cavity output spectroscopy. The set-up and instrument precision is described in detail in (Brase et al. 2017). The equilibration time of nitrous oxide of approximately 7 min was taken into account for data processing.

For validation of the measurements, we measured two standard gas mixtures of nitrous oxide in synthetic air regularly ( $500.5 \text{ ppb} \pm 5\%$  and  $321.2 \text{ ppb} \pm 3\%$ ). No drift was detected. For further data processing, we calculated 1 min averages of nitrous oxide detected dry mole fraction (ppm). We calculated the dissolved nitrous oxide concentration in water ( $N_2O_{cw}$ ) using the Bunsen solubility function of (Weiss and Price 1980) taking temperature differences between sample inlet and equilibrator into account (Rhee et al. 2009). Nitrous oxide saturation ( $s$ ) was calculated using Eq. 5.1, based on nitrous oxide concentration in water ( $N_2O_{cw}$ ) and atmospheric nitrous oxide ( $N_2O_{eq}$ ).

$$s = 100 \times \frac{N_2O_{cw}}{N_2O_{eq}} \quad (5.1)$$

Atmospheric nitrous oxide was measured regularly during our cruise and was on average  $0.33 \text{ ppm}$  during our cruise in 2020. The gas transfer coefficient ( $k$ ) was calculated based on (Borges et al. 2004), where  $u_{10}$  is wind speed 10m above surface, and  $Sc$  is the Schmidt number (Eq. 5.2). Sea-to-air flux densities ( $f$ ) were calculated using Eq. 5.3.

$$k = 0.24 \times (4.045 + 2.58 u_{10}) \times \left(\frac{Sc}{600}\right)^2 \quad (5.2)$$

$$f = k \times (N_2O_{cw} - N_2O_{air}) \quad (5.3)$$

### 5.2.7 Nitrate mixing calculation

Nitrate concentration from conservative mixing ( $C_{Mix}$ ) between two endmembers was calculated for each sample using the classical mixing model of (Eq. 5.4; Liss 1976).

$$C_{Mix} = f \times C_R + (1 - f)C_M \quad (5.4)$$

Where  $C_R$  and  $C_M$  stand for the concentration of the riverine and marine end-members, respectively, and  $f$  denotes freshwater fractionation in each sample calculated as follows in Eq. 5.5:

$$f = \frac{(S_M - S_{Mix})}{(S_M - S_R)} \quad (5.5)$$

$S_{Mix}$ ,  $S_M$ ,  $S_R$  denote the salinity of the sample, marine and riverine endmembers, respectively. We used the concentration-weighted mean of the isotopic values of the marine ( $\delta_M$ ) and riverine ( $\delta_R$ ) end-members to calculate the theoretical isotope value of samples following conservative mixing ( $\delta_{Mix}$ ; Eq. 5.6; Fry 2002):

$$\delta_{Mix} = \frac{f \times C_R \times \delta_R + (1 - f) \times C_M \times \delta_M}{C_{Mix}} \quad (5.6)$$

### 5.2.8 Isotope effect

During turnover processes, nitrogen isotopes ratios change along a specific isotope effect that helps to identify individual process pathways (Kendall et al. 2007). Isotope effects were calculated with an open-system approach where the reactant nitrate is continuously supplied and partially consumed, and steady state is assumed. This leads to a linear relationship between isotope values of nitrogen and fraction  $f$ , where  $f = ([C]/[C_{initial}])$ . The isotope effect  $\epsilon$  corresponds to the slope of the regression line (Eq. 5.8; Sigman et al. 2009).

$$\epsilon_{substrate} = \frac{\delta^{15}N_{substrate} - \delta^{15}N_{initial}}{(1 - f)} \quad (5.7)$$

$$\epsilon_{product} = \frac{\delta^{15}N_{product} - \delta^{15}N_{initial}}{f} \quad (5.8)$$

Where  $\delta^{15}N_{substrate}$ ,  $\delta^{15}N_{product}$ ,  $\delta^{15}N_{initial}$  denote  $\delta^{15}N$  values of the substrate and product at the time of sampling and the initial value. The remaining fraction of substrate at the time of sampling is described by  $f$ . In the present study, the mixing line determines initial concentrations and isotope values.

### 5.2.9 Statistical analysis

All statistical analyses were done using R packages. Pearson correlation matrices were calculated with `ggcorr` from the Rpackage `GGally` v.2.0.0 (Schloerke et al. 2020). From the R-package `stats` v4.0.2 (R Core Team and contributors worldwide 2020), we used the function `prcomp` for the principal component analysis (PCA). Salinity was not taken into account for the multivariate analysis.

## 5.3 Results

### 5.3.1 Hydrographic properties and dissolved nutrients in surface water

To evaluate controls on nutrient cycling, we first look at the hydrochemical properties that were measured in 2014 and 2020 in surface waters, alongside with nutrient concentrations and nitrogen stable isotope composition (Figure 5.2). Discharge ranged from 59.7 to 67.5  $\text{m}^3 \text{s}^{-1}$  in 2014 and was  $\sim 30 \text{ m}^3 \text{ s}^{-1}$  in 2020. The long-term average discharge is 30–40  $\text{m}^3 \text{ s}^{-1}$  in June and August (Andreas Engels, NLWKN Bst. Aurich, pers. comm., 2021). The mean water temperature was 23 °C in 2014 and 17 °C in 2020. Salinity ranged from  $\sim 0.5$  to  $\sim 32$  in both years. In 2014, the sampling section started with the onset of the salinity gradient (kilometer 20), whereas the most upstream sample in 2020 was taken near Herbrum (kilometer -14; Figure 5.2g). This sample and the sample at stream kilometer -9 were taken with a bucket from shore. The research vessel transect started in Papenburg (kilometer 0).

Nitrate was the major form of dissolved inorganic nitrogen (DIN) and decreased with increasing salinity. Nitrate concentration decreased from 177 to 3.9  $\mu\text{mol L}^{-1}$  in 2014 and from 166 to 4.9  $\mu\text{mol L}^{-1}$  in 2020 (Figure 5.2c).

Ammonium (Figure 5.2a) and nitrite (Figure 5.2b) concentration were generally low in the tidal river, with average concentrations of  $\sim 3$  and 1  $\mu\text{mol L}^{-1}$ , respectively. One sample (June 2020; stream kilometer 25) had an unusually high ammonium concentration of 13  $\mu\text{mol L}^{-1}$ . In the Dollard reach, ammonium and nitrite concentration increased with salinity in 2020, whereas this increase occurred further downstream, i.e., in the middle reaches, in 2014. The highest ammonium concentration was similar in 2014 and 2020, with 8.5  $\mu\text{mol L}^{-1}$  and 10.2  $\mu\text{mol L}^{-1}$  respectively. Whereas in 2020 nitrite concentration reached 1  $\mu\text{mol L}^{-1}$ , with little variability along the transect, in 2014, it reached a maximum of 3.5  $\mu\text{mol L}^{-1}$ , with a distinct peak in the middle and outer reaches.

Incoming nitrate isotope values were elevated in the most upstream regions of the tidal river with values of 15 ‰ for  $\delta^{15}\text{N}$ -nitrate and 6 ‰ for  $\delta^{18}\text{O}$ -nitrate in 2020, and 17 ‰ and 8 ‰ for  $\delta^{15}\text{N}$ -nitrate and  $\delta^{18}\text{O}$ -nitrate in 2014. Isotope values increased further to a local maximum of 25 ‰ and 11 ‰ for  $\delta^{15}\text{N}$ -nitrate and  $\delta^{18}\text{O}$ -nitrate around kilometer 13 in 2020. In 2014, the respective local maxima (22 ‰ and 10 ‰ for  $\delta^{15}\text{N}$ -nitrate and  $\delta^{18}\text{O}$ -nitrate) were shifted to kilometer 35. Further downstream, isotope values decreased, except for a slight increase in the outermost marine samples (Figure 5.2d, e).

In 2020, we also measured dissolved nitrous oxide concentration. Measured values ranged between equilibrium concentrations ( $\sim 9 \text{ nmol L}^{-1}$ ) and supersaturation of up to  $40 \text{ nmol L}^{-1}$  at kilometer 0, which corresponded to a saturation of 400 %. Nitrous oxide then decreased downstream to  $\sim 14 \text{ nmol L}^{-1}$  (140 %) at kilometer 30 and then increased to a local maximum of  $21 \text{ } \mu\text{mol L}^{-1}$  (210 %) in the tidal river/Dollard reach transition at stream kilometer 35. Further downstream, nitrous oxide decreased to near equilibrium concentration towards the North Sea (Figure 5.2f).

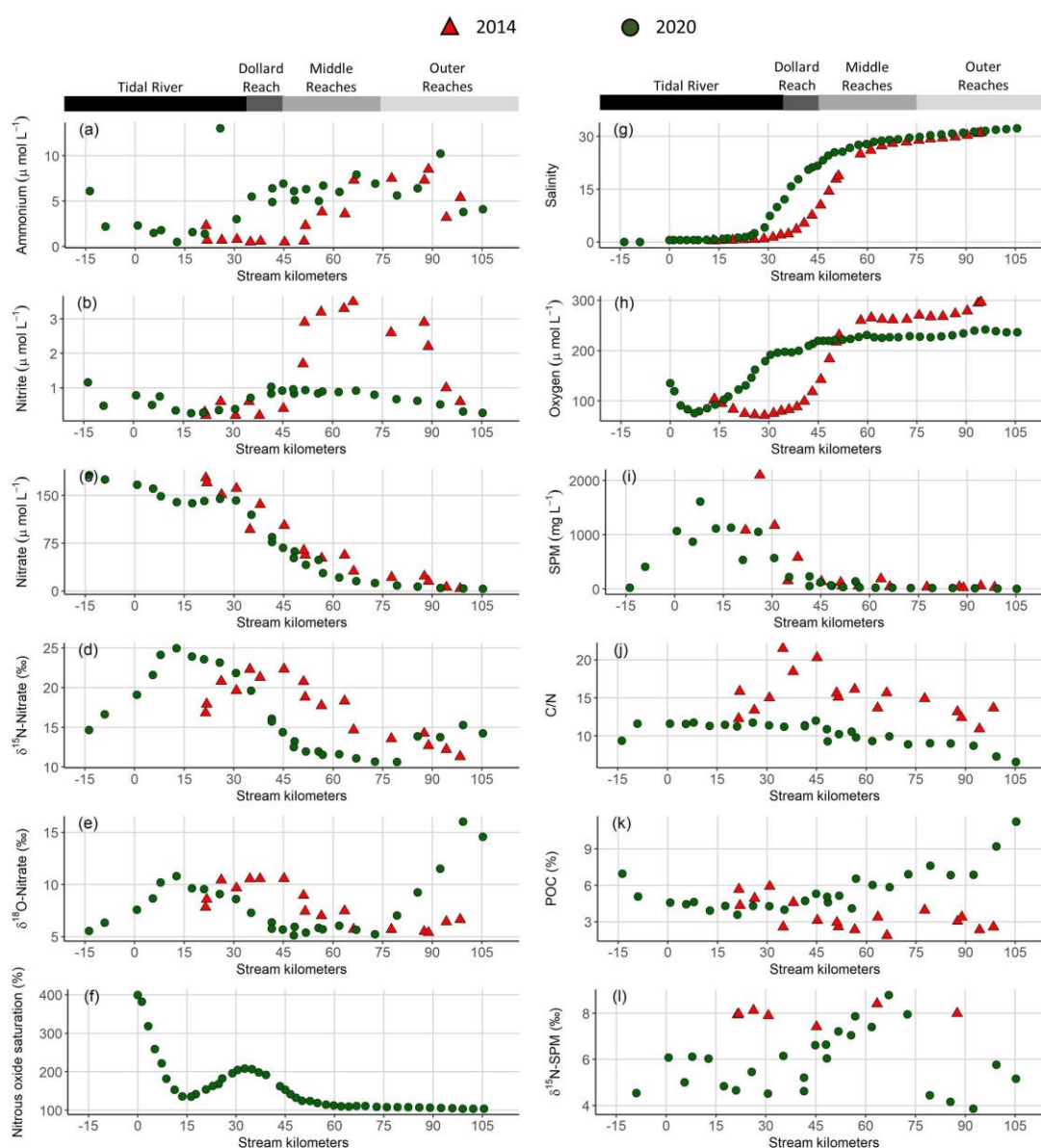


**Figure 5.2.** Near surface water column properties along the Ems Estuary: (a) ammonium concentration, (b) nitrite concentration, (c) nitrate concentration, (d)  $\delta^{15}\text{N}$ -nitrate, (e)  $\delta^{18}\text{O}$ -nitrate, (f) nitrous oxide saturation, (g) salinity, (h) dissolved oxygen concentration, (i) suspended particulate matter concentration (SPM), (j) C/N ratios, (k) particulate organic carbon fraction (POC), (l)  $\delta^{15}\text{N}$ -suspended particulate matter. For clarity, only 10 min means are plotted for the continuous measurements of nitrous oxide (f), oxygen (h) and salinity (g). Red triangles mark stations sampled in 2014 and green circles represent stations in 2020.

### 5.3.2 Suspended particulate matter properties

Near surface suspended particulate matter concentration was highest in the tidal river, reaching values of  $2100 \text{ mg L}^{-1}$  in 2014 and  $1600 \text{ mg L}^{-1}$  in 2020. Suspended particulate matter concentration decreased at the beginning of the Dollard reach region (Figure 5.2i). The  $\delta^{15}\text{N}$ -SPM values showed considerable scatter (Figure 5.2l): around 5 ‰ in the tidal river/Dollard reach, and 9 ‰ in the middle

reaches. In the outer reaches,  $\delta^{15}\text{N}$ -SPM dropped again to  $\sim 5$  ‰. In 2014,  $\delta^{15}\text{N}$ -SPM were elevated (8 ‰), but the database during this cruise is relatively sparse (Figure 5.2l).

In 2020, C/N ratios of suspended particulate matter (Figure 5.2j) were relatively stable in the tidal river ( $\sim 11$ ) and Dollard reach, with a slightly lower value of 9 in the most upstream sample. In the middle reaches, C/N ratios decreased, reaching the lowest value of 6.5 in the most offshore sample. In 2014, C/N values were 11-15 in the tidal river, increasing to values as high as 20 in the Dollard reach and decreasing to  $\sim 11$  approaching the North Sea (Figure 5.2j).

Particular organic carbon fraction (% POC) was high in the most upstream samples in 2020 (Figure 5.2k), decreased to 4.5 % and remained relatively stable in the tidal river and Dollard before it increased in the middle and outer reaches up to 11 %. In 2014, the values in tidal river and Dollard were comparable, but we found a decreasing trend downstream, with a low POC fraction of  $\sim 3$  % in the outermost sample (Figure 5.2k).

### 5.3.3 Dissolved oxygen conditions in the Ems Estuary

In surface water, oxygen concentrations in the tidal river section were low during both cruises, and increased downstream with rising salinity. The lowest values were measured in the tidal river, where the minimum oxygen concentration was  $\sim 72 \mu\text{mol L}^{-1}$  in 2014 and  $76 \mu\text{mol L}^{-1}$  in 2020 (Figure 5.2h), corresponding to a saturation of 27 % and 26 %, respectively.

Oxygen profiles showed strong vertical gradients with decreasing concentration in deeper water layers. The extent of hypoxia in the water column depended on the tidal cycle and location, with lowest bottom water oxygen concentration measured at the most upstream station at stream kilometer 7.2 during low tide in 2020. Detailed profiles can be found in Figure A4.1.

During the continuous near-bottom oxygen measurements, we found anoxic conditions during both of our cruises that lasted for several hours over a tidal cycle (Figure 5.3). Oxygen concentration was generally low at low tide, and elevated at high tide. In 2014, anoxia developed at stream kilometer 11.8 and 18.5, and highest oxygen concentration in bottom water was only  $60 \mu\text{mol L}^{-1}$  (kilometer 24.5) and  $70 \mu\text{mol L}^{-1}$  (kilometer 11.8). At the beginning of August, oxygen concentration at kilometer 11.8 frequently exceeded measured values at kilometer 24.5.

In 2020, oxygen concentration in bottom water was higher, and anoxia was only found at stream kilometer 11.8. At all other stations, oxygen concentration remained above  $40 \mu\text{mol L}^{-1}$  even at low tide.

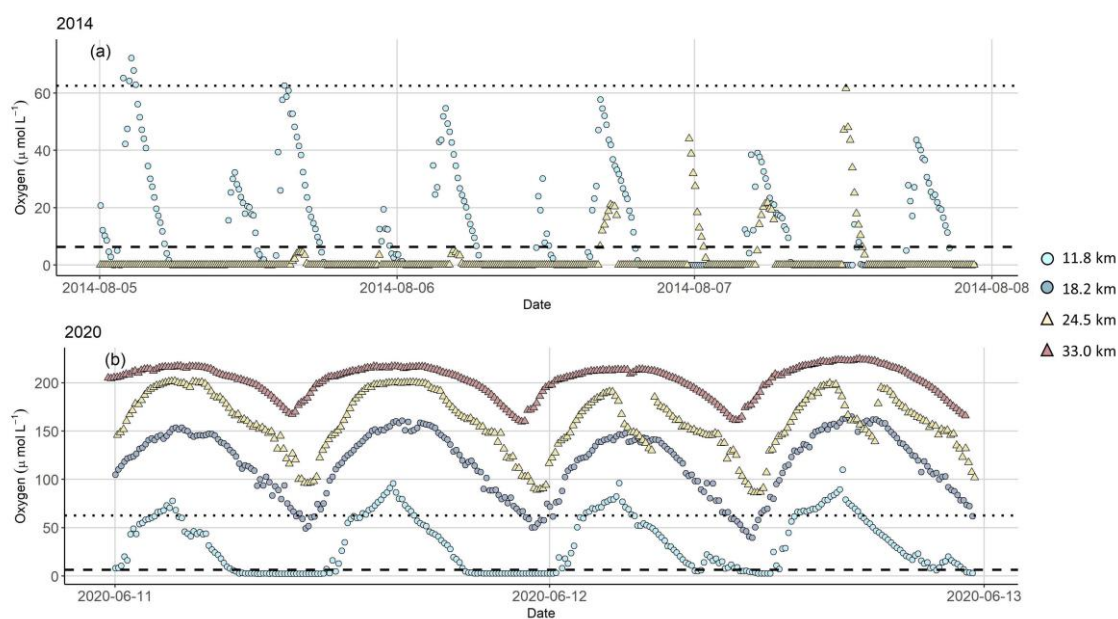


**Figure 5.3.** Dissolved oxygen concentration 0.5 m above riverbed during our research cruises in (a) 2014 and (b) 2020, measured continuously at several stations along the Tidal River. In 2014, oxygen concentration was measured at two stations at stream kilometers 11.8 and 24.5. In 2020, additional measurements were done at stream kilometers 18.2 and 33.0. Symbols and colors mark stream kilometer of each sampling station. White circles are results from a station at stream kilometer 11.8, grey at stream kilometer 18.2, black triangles at stream kilometer 24.5 and grey triangles at stream kilometer 33.0. The dotted line indicates hypoxic conditions at oxygen concentration of  $62.5 \mu\text{mol L}^{-1}$  (Diaz et al. 2019). The dashed line marks oxygen concentration ( $6.25 \mu\text{mol L}^{-1}$ ) below which denitrification occurs (Seitzinger 1988). Note different y-axes in plots (a) and (b).

### 5.3.4 Nitrate mixing

We plotted nitrate versus salinity concentration and nitrate dual isotopes to evaluate mixing properties (Figure 5.4; Fry 2002). We used the most upstream and downstream samples as end-members for each year. In both years, nitrate concentrations plot below the mixing line in the most upstream region with low salinity in both years, corresponding to an enrichment of  $\delta^{15}\text{N}$ -nitrate and  $\delta^{18}\text{O}$ -nitrate in the same region. Above salinity of 20, a slight nitrate source is present, while isotope values decrease. In 2020, the outermost samples have a slightly enriched isotope signature and nitrate concentration below the mixing line (Figure 5.4).

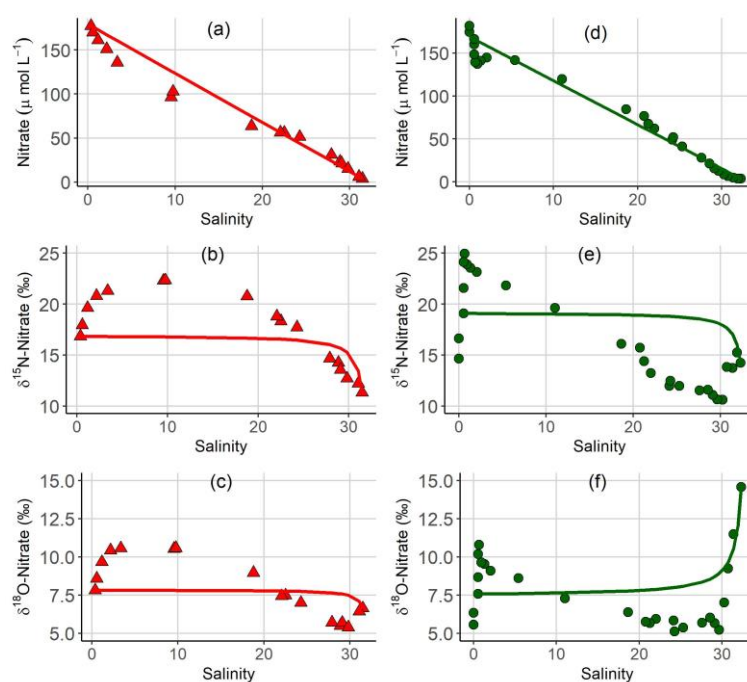


**Figure 5.4.** Nitrate concentrations and isotope values of nitrate plotted versus salinity for (a), (b), (c) in 2014 and (d), (e), (f) in 2020. Lines indicate calculated conservative mixing.

### 5.3.5 Principal component analysis

Together, PC1 and PC2 explained about 80 % of total variance in both years. In 2014, PC1 contributed to 66 % and PC2 to 15 %. PC1 and PC2 explained 61 % and 18 % of total variance in 2020, respectively.

Oxygen, pH, C/N ratios, suspended particulate matter and nitrate concentration contributed largely to PC1 in 2014, just like silicate concentration in 2020 (this parameter was not measured in 2014). Temperature, phosphate and nitrite concentration contributed largely to PC2 in both years, so did  $\delta^{15}\text{N}$ -SPM in 2020. Due to few data,  $\delta^{15}\text{N}$ -SPM could not be included into the principle component analysis of 2014. In 2014, PC2 was also heavily influenced by suspended particulate matter. The PCA overall suggests that the estuary can be divided into three biogeochemically distinct zones (Figure 5.5).

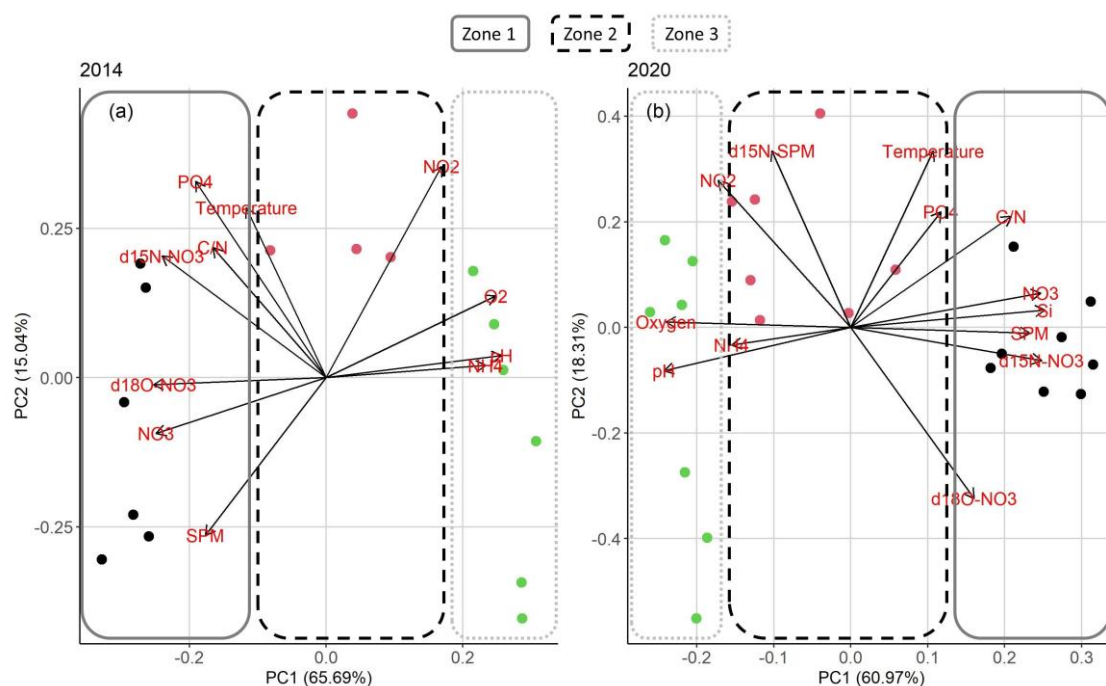


**Figure 5.5.** PCA results for (a) 2014 and (b) 2020. Colors and frames stand for the assignment of the samples into the respective zones. Dark blue circles and a straight frame shows samples in zone 1, red circles and a dashed frame samples from zone 2. Green circles and a dotted frame stand for samples in zone 3.

## 5.4 Discussion

### 5.4.1 Biogeochemical zones in the Ems Estuary

The first goal of this study was to identify distinct biogeochemical zones of nitrogen turnover within the Ems Estuary to see if changing environmental and geomorphological properties affect the occurring processes. The assessment of estuarine mixing curves showed three zones of different nitrogen turnover along the salinity gradient (Figure 5.4).

In both years, 2014 and 2020, nitrate concentration deviated clearly and in a similar manner from the conservative mixing line. In the upper riverine part of the estuary, nitrate concentration fell below the conservative mixing line, indicating nitrate removal (zone 1), followed by a zone with nitrate concentration slightly above the mixing line (zone 2) that acted as a net nitrate source. In the third zone, nitrate mostly followed the conservative mixing line, with nitrate removal and isotopic enrichment near the marine endmember in 2020, indicating nitrate uptake by phytoplankton. In 2014, the identification of the “outer zone” (zone 3) is more complicated, as the outermost samples follow the conservative mixing line in Figure 5.4. However, these outermost samples are distinct from the prevailing processes in zone 2, because they do not show signs of nitrate production, a characteristic of zone 2.

The PCA analysis showed that nitrogen turnover was comparable in both years. However, there are distinct differences between the cruises. Seasonal and interannual variation may cause differences in dissolved inorganic nitrogen distribution and nitrate stable isotope composition. The PCA independently confirms comparable zones of nitrogen turnover for both years. The principle component loadings were also similar for both cruises. The PCA supports the suggested nitrate zonation taking the other biogeochemical properties into account (Figure 5.5). The three biogeochemical zones were mainly divided according to PC1. Contributing parameters were oxygen, nitrate, C/N, suspended particulate matter and silicate, which suggests a tight coupling of nitrate turnover to suspended particulate matter. PC2 helped to differentiate zone 2. Contributing parameters (temperature, nitrite, and phosphate) suggest a link to nutrient uptake processes.

Based on the location of the biogeochemical zones along the Ems (Figure 5.1), we see a connection with the geomorphological characteristics of the Ems Estuary. In both years, zone 1 was located in the hyper-turbid tidal river and the beginning of zone 2 is characterized by increasing ammonium concentration. In 2014, zone 1 included the Dollard reach. In 2020, the Dollard reach was grouped into zone 2, together with the middle reaches. The shift of zone 2 between the cruises may be driven by discharge conditions. In 2014, discharge was significantly higher than in 2020 (about twice the long-term average discharge of 30 to 40 m<sup>3</sup> s<sup>-1</sup> for June and August; Andreas Engels, NLWKN Bst. Aurich, pers. comm., 2021). This may have led to a shift of zone 2 downstream, as was also indicated by the shift in the salinity gradient and suspended particulate matter concentrations. (de Jonge et al. 2014) showed that elevated discharge can relocate estuarine turbidity maxima downstream. Zone 3 was in the outer reaches in 2014 and 2020.

Overall, mixing properties as well as a PCA suggest that there are three distinct biogeochemical zones that act either as sinks (zones 1 and 3) or sources (zone 2) of nitrate along the Ems. These ones are mainly defined by discharge and suspended particulate matter (especially PC1).

#### **5.4.2 Denitrification in the upper estuary**

Zone 1, the most upstream region acted as a nitrate sink in both years, with nitrate concentrations below the conservative mixing line and enriched  $\delta^{15}\text{N}$ -nitrate and  $\delta^{18}\text{O}$ -nitrate values (Figure 5.4d, e). Potential removal mechanisms are nitrate respiration or nitrate assimilation.

High suspended particulate matter values in the hyper-turbid tidal river and Dollard reach (Figure 5.2i) reduced light availability, limiting primary production (Bos et al. 2012). Therefore, nitrate assimilation by phytoplankton in the upper estuary can be ruled out as a relevant nitrate sink.

Denitrification is a potential nitrate sink that can lead to strong isotope enrichment. Denitrification was a dominant loss pathway in the 1980s in other temperate estuaries like the Elbe Estuary (Schröder

et al. 1996), where sediment denitrification removed up to 40 % of the summer nitrate load. We found that  $\delta^{15}\text{N}$ -nitrate and  $\delta^{18}\text{O}$ -nitrate in the Ems Estuary increased with decreasing nitrate concentration.  $\delta^{15}\text{N}$ -nitrate versus  $\delta^{18}\text{O}$ -nitrate plot on a slope of 0.5 in both years (Figure A4.2), which points towards denitrification (Böttcher et al. 1990; Mengis et al. 1999; Granger and Wankel 2016; Wong et al. 2020). A strong fractionation occurred ( $^{15}\epsilon \sim 24 \text{ ‰}$ ;  $R^2 = 0.89$  in 2014 and  $26 \text{ ‰}$ ;  $R^2 = 0.76$  in 2020). While denitrification in sediments leads to little to no fractionation due to a diffusion limitation (Brandes and Devol 1997; Lehmann et al. 2004; Sigman and Fripiat 2019), water column denitrification has an isotope effect that fits our calculations (Kendall et al. 2007; Sigman and Fripiat 2019), and can explain the observed patterns.

Water column denitrification occurs under anaerobic to low oxygen conditions in the water column (Tiedje 1988). According to Seitzinger (1988), denitrification occurs at oxygen concentration below  $6.25 \mu\text{mol L}^{-1}$ . We measured low oxygen concentration in surface water during both years with lowest concentration of  $\sim 70 \mu\text{mol L}^{-1}$  (Figure 5.2h), which is well above the threshold for denitrification. However, vertical oxygen concentration profiles and continuous measurements in the estuary in near-bottom water showed that deeper water became anoxic in both years. Even though these anoxic conditions only developed for a few hours over a tidal cycle, we conclude that water column denitrification was the responsible nitrate sink mechanism in the Ems in 2014 and 2020.

Furthermore, denitrification can also occur on suspended particles. Liu et al. (2013) reported the occurrence of denitrification on suspended particles in oxic waters in a hyper-turbid river. Xia et al. (2016) observed a high oxygen influx around suspended particles and decreasing oxygen concentration. They suggest that oxygen was consumed by nitrification and/or microbial respiration close to the particle's surface and thereby provided redox conditions for coupled nitrification-denitrification to take place. Zhu et al. (2018) detected aggregates of nitrifiers and denitrifiers on suspended particulate matter in the Hangzhou Bay in China. Similarly, Sanders and Laanbroek (2018) propose that coupled nitrification-denitrification processes occur in the upper Ems Estuary, and suggested immediate nitrate consumption driven by suspended particles in the water column.

Overall, we find strong evidence for water column denitrification in zone 1, likely in the anoxic bottom waters. Moreover, coupled nitrification-denitrification can add to this nitrate sink in the hyper-turbid tidal river.

#### **5.4.3 Increasing importance of nitrification in the middle reaches**

The mixing lines along the estuary displayed a significant shift of nitrogen turnover from the “denitrification zone” (zone 1) to zone 2. Nitrate concentrations plotted above the mixing line, indicating a net nitrate source with lighter nitrate isotope values (Figure 5.4).

Nitrate is produced via nitrification, which was no longer oxygen limited in zone 2 due to increasing concentrations compared to the tidal river. A positive correlation between nitrite and ammonium, as well as a negative correlation between nitrite and nitrate for both years indicate nitrate production via nitrification with nitrite as an intermediate product. This is in line with the findings of Sanders and Laanbroek (2018), who found nitrification in water column and sediments in 2014.

However, there is no clear indication of nitrification in the correlations of nitrate concentration and nitrate isotopes. Nitrate isotopes were positively correlated with nitrate concentrations, but such a parallel increase usually does not occur during nitrification. Nitrification produces isotopically depleted nitrate, but the sources of  $\delta^{15}\text{N}$ -nitrate and  $\delta^{18}\text{O}$ -nitrate are independent and increase the overall nitrate pool. At least in 2014, a plot of  $\delta^{15}\text{N}$ -nitrate versus  $\delta^{18}\text{O}$ -nitrate still plots on a slope of 0.5 in 2014, suggesting that denitrification may still be of importance in this zone. During denitrification, nitrate isotope values and concentrations are also negatively correlated, because denitrification consumes light nitrate and elevates the isotope values in the remaining pool.

The positive correlation in our study thus is intriguing. It seems likely that denitrification still occurs in parts of zone 2, either in the oxygen limited conditions in deeper water layers, in the sediments of the adjacent tidal flats (Gao et al. 2010), or driven by still elevated suspended particulate matter concentrations of 185 and 230  $\text{mg L}^{-1}$  in 2014 and 2020, respectively. The net addition of nitrate, however, is a clear sign of nitrification.

Therefore, we aim to explore whether the parallel increase of nitrate concentration and isotope values can be explained by simultaneous nitrification and denitrification. To identify the influence of both processes, we used a mapping approach inspired by Lewicka-Szczebak et al. (2017). A detailed description of the open-system mapping approach and figures are shown in the *Appendix A4*. Briefly, we try to disentangle the influence of nitrification and denitrification in zone 2 based on the open-system isotope effects, where the slope of the linear relationship between nitrate isotope values and remaining fraction of nitrate concentration corresponds to the isotope effect (Sigman et al. 2009). The initial values used for the mapping are derived from the nitrate mixing calculations based on (Fry 2002).

For denitrification, we calculated an isotope effect of  $^{15}\epsilon_{\text{DENIT}} = -26 \text{‰}$  in the “denitrification zone” (zone 1). For nitrification, the expression of the isotope effect depends on the abundance of ammonium. As long as ammonium is limiting, we assume that any ammonium is converted to nitrite and nitrate, so that the apparent isotope effect is that of remineralization. In most parts of zone 2, no ammonium was accumulated. A simultaneous increase of  $\delta^{15}\text{N}$ -SPM, ammonium and nitrite concentration at stream kilometer 50 in 2020 point towards remineralization (Figure 5.2a, b, l). Based on  $\delta^{15}\text{N}$ -SPM, we calculated an isotope effect of  $^{15}\epsilon_{\text{REMIN}} = -1.2\text{‰}$  ( $R^2 = 0.26$ ), which fits with

previous assessments of the isotope effect of ammonification (Möbius 2013). We applied this value for nitrification with prior remineralization. Further downstream, ammonium and nitrite concentrations increased, so we assume that remineralization no longer determines the overall isotope effect of nitrification. Instead, there was a combined influence of ammonium oxidation with an isotope effect  $^{15}\epsilon = -14\text{‰}$  to  $-41\text{‰}$  (Mariotti et al. 1981; Casciotti et al. 2003; Santoro and Casciotti 2011) and nitrite oxidation with  $^{15}\epsilon = +9\text{‰}$  to  $+20\text{‰}$  (Casciotti 2009; Buchwald and Casciotti 2010; Jacob et al. 2017). As we measured elevated ammonium and nitrite concentrations, both processes influenced the fractionation caused by nitrification. Therefore, for total nitrification we assumed a combined isotope effect of  $^{15}\epsilon_{\text{NITRI}} = -10\text{‰}$ , that we used to describe nitrification in samples with accumulated ammonium and nitrite. This number is lower than previously measured for ammonium oxidation, and is based on nitrification rate from incubations performed previously in the Elbe estuary (Sanders and Dähnke 2014).

Based on these input variables, the mapping approach can indeed explain the development of isotope effects and nitrate concentration. In the most upstream samples, nitrate removal exceeded production: in 2014, denitrification removed  $26\ \mu\text{mol L}^{-1}$ , and nitrification added  $10\ \mu\text{mol L}^{-1}$ . In 2020, the mapping approach suggests an addition of  $52\ \mu\text{mol L}^{-1}$  and simultaneous denitrification of  $62\ \mu\text{mol L}^{-1}$ . In the middle of zone 2, nitrification gained in relative importance with an approximated production of  $10\ \mu\text{mol L}^{-1}$  in 2014 and  $20\ \mu\text{mol L}^{-1}$  in 2020, in contrast to denitrification of approximately 3 and  $10\ \mu\text{mol L}^{-1}$ , respectively. In the most downstream samples, mixing was dominant, and we detected neither nitrate production nor reduction.

Overall, nitrification and denitrification determined the evolution of nitrate isotopes and concentration in the estuary. Further downstream of zone 2, nitrification becomes increasingly important, and the relevance of denitrification ceases. Both processes lose in importance towards the North Sea, when mixing turns to be the most important process.

#### **5.4.4 Mixing and nitrate uptake in the outer reaches**

In the “outer zone” (zone 3) the mixing line shows divergent trends for our two cruises (Figure 5.4). While conservative mixing dominates in 2014, 2020 shows nitrate uptake in the North Sea.

For 2020, a plot of  $\delta^{15}\text{N}$ -nitrate versus  $\delta^{18}\text{O}$ -nitrate falls along a slope of 1.5, which points towards simultaneous assimilation and nitrification (Wankel et al. 2006; Dähnke et al. 2010). The isotope effect  $^{15}\epsilon$  of this drawdown is  $-3\text{‰}$ , which also is a sign of assimilation, even though it is at the lower end of values reported for pure cultures (Granger et al. 2004). C/N values close to Redfield ratio in 2020 (Figure 5.2j) also pointed towards primary production in the outer reaches. The stronger signal of nitrate uptake in June 2020 compared to August 2014 is likely caused by a stronger influence of

the spring phytoplankton bloom in the outer reaches (Colijn 1983; Colijn et al. 1987; Brinkman et al. 2015) fueled by continuous nutrient supply from the estuary.

In the mixing plot (Figure 5.4), the outermost isotope samples of our cruise in 2020 fall on the conservative mixing line. The good fit is caused by the calculation with a marine endmember that has an isotopically enriched signature in comparison to average global values (Sigman et al. 2000, 2009) and North Sea winter values of 5 ‰ (Dähnke et al. 2010). The increase of the isotope signature shows that fractionation takes place, likely due to assimilation.

In contrast to the biogeochemical active inner zones, mixing dominated nitrate distribution in the outer reaches of the estuary in 2014. In 2020 however, the outer reaches were a nitrate sink due to ongoing primary production in the coastal North Sea.

#### **5.4.5 Suspended particulate matter as driving force of the spatial zonation**

We identified three biogeochemical zones of nitrogen turnover along the estuary, which differ significantly in their coastal filter function. The tidal river was a nitrate sink with dominating water column denitrification. In the middle reaches, nitrification gained in importance, turning this section in a net nitrate source. In the “outer zone” (zone 3), mixing gained in importance but with a clear nutrient uptake in 2020. Other estuaries with high turbidity show denitrification zones as well (Ogilvie et al. 1997; Middelburg and Nieuwenhuize 2000). This finding and our analysis of the PCA and dominant nitrogen turnover processes suggest that the overarching control on biogeochemical nitrogen cycling and zonation may be suspended particulate matter.

Channel deepening led to tidal amplification and an increased sediment transport in the estuary (Winterwerp et al. 2013; de Jonge et al. 2014; van Maren et al. 2015a; b). Between 1954 and 2005, suspended particulate matter concentration increased on average 2- to 3-fold, and even 10-fold in the tidal river. The turbidity maximum extended to a length of 30 km and moved upstream, into the freshwater tidal river (de Jonge et al. 2014).

High C/N ratios (Figure 5.2j), as well as a low and stable particular organic carbon (POC) fraction of the suspended particulate matter in this region (~4.5 %) in the tidal river and Dollard reach indicate low organic matter quality and a large contribution of mineral associated organic matter of the present organic matter (Figure 5.2k). In 2014, C/N ratios were extremely high, and uncharacteristic for estuarine environments. We attribute this to a potential influence of peat soils or peat debris in sediments (Broder et al. 2012; Loisel et al. 2012; Papenmeier et al. 2013; Wang et al. 2015), which may have been washed into the river due to high discharge. The extremely high C/N ratios should nonetheless be treated with caution, as we cannot entirely rule out sampling artifacts.

Nonetheless, and regardless of organic matter origin, degradation of organic carbon leads to anoxic conditions in the tidal river. Even though the low quality of organic matter fuels only low degradation rates with POC fractions of ~3 % (Figure 5.2k), the extremely high POC concentration ( $>4000 \mu\text{mol L}^{-1}$ ) support the intense oxygen depletion and anoxic conditions in the tidal river. This indicates very refractory material. Talke et al. (2009) found oxygen depletion rates proportional to suspended particulate matter concentrations in the Ems Estuary. Moreover, high suspended particulate matter concentrations depress primary production throughout the inner estuary due to light limitation and this leads to a dominance of heterotrophic processes (Bos et al. 2012).

With decreasing suspended particulate matter concentration, oxygen concentration increases, and the relevance of denitrification ceases in comparison to nitrification. In the “coactive zone” (zone 2) at the transition between Dollard reach and middle reaches, C/N ratios start to decrease, indicating the input of fresh organic matter entering the estuary from the North Sea (van Beusekom and de Jonge 1997, 1998), fueling nitrification in zone 2. Although, the quality of the organic matter improves, oxygen depletion decreases due to reduced suspended particulate matter concentrations leading to lower POC concentrations in comparison to the tidal river. Towards the North Sea, low suspended particulate matter concentration in the outer reaches enables deeper light penetration supporting local primary production (Colijn et al. 1987; Liu et al. 2018), as is also supported by a slight chlorophyll maximum in the outer reaches (Figure A4.11). Given the ongoing import of organic matter from the North Sea to the Wadden Sea and adjacent estuaries, this primary produced organic material probably fuels the remineralization process in the inner estuary.

Changing discharge conditions can lead to a spatial shift of the biogeochemical zones within the estuary. (de Jonge et al. 2014) showed that elevated discharge can relocate the turbidity maximum (MTZ) downstream. As we identified suspended particulate matter concentrations as one of the most important controls on nitrogen turnover in the Ems Estuary, we assume that the described zones will move with shifting suspended particulate matter concentration along the estuary.

Overall, we find that the interplay of nitrification and denitrification and nitrogen assimilation is governed by suspended particulate matter concentration along the Ems Estuary. We expect that changing discharge can lead to spatial offsets in suspended particulate matter concentrations and thus influence the spatial segregation of nitrogen turnover processes.

#### **5.4.6 Nitrous oxide production and its controls in the Ems Estuary**

So far, we elucidated nitrogen turnover in the Ems Estuary. We found that nitrification and denitrification vary spatially in importance. Both processes can produce nitrous oxide, and we accordingly found nitrous oxide peaks in the estuary in areas with significant differences in their nitrogen turnover. Nitrous oxide was measured only in 2020, thus we will use the high-resolution

data from this cruise to examine the importance of nitrification and denitrification for nitrous oxide production along the estuary. We will also discuss controls that favor the emergence of nitrous oxide production areas.

The calculated average sea-to-air flux of  $0.35 \text{ g-N}_2\text{O m}^{-2} \text{ yr}^{-1}$  results in a total nitrous oxide emission of  $0.57 \times 10^8 \text{ g-N}_2\text{O yr}^{-1}$  along the Ems Estuary. In June 1997, a significantly higher average sea-to-air flux density of  $1.23 \text{ g-N}_2\text{O m}^{-2} \text{ yr}^{-1}$  was measured (Barnes and Upstill-Goddard 2011), which amounted to an annual nitrous oxide emission of  $2.0 \times 10^8 \text{ g-N}_2\text{O yr}^{-1}$  over the entire estuary. Upscaling from a single cruise to an entire year is somewhat questionable, but it is interesting to note that the emissions may have halved since the 1990s. Furthermore, our results as well as those from 1997 were obtained from a single survey in June, making the comparison intriguing. Since the 1990s, the DIN load of the Ems Estuary was significantly reduced due to management efforts (Bos et al. 2012). Phytoplankton biomass in the outer reaches (Station Huibergat Oost; van Beusekom et al. 2018) decreased in response to decreasing nutrient loads, possibly contributing to the observed lower nitrous oxide emissions. However, this hypothesis requires further verification in the future.

The nitrous oxide concentrations observed in 2020 can be linked to the prevailing biogeochemical conditions. The first nitrous oxide maximum was located in the upstream region (stream kilometer 0). In this area, we identified water column denitrification as the dominant nitrogen turnover process, and we found relatively low pH values and high nitrate concentration. In their summary paper about nitrous oxide in streams and rivers, Quick et al. (2019) found that these factors are favorable for nitrous oxide production via denitrification. Intermittent oxygen hypoxia and anoxia in the different water depths also enhance nitrous oxide production in the tidal river, which is in line with our tidal oxygen measurements in the Ems. Several studies also showed a positive correlation between nitrous oxide concentration and suspended particulate matter concentration (Tiedje 1988; Liu et al. 2013; Zhou et al. 2019), and suspended particulate matter concentration was also highest in this region of the tidal river. Altogether, we suggest that the Ems is well suited as a region with extremely high nitrous oxide production, triggered by high nutrient loss, intermittent anoxia, and high suspended particulate matter loads.

Further downstream, nitrous oxide concentrations decrease, along with oxygen concentrations, reaching a minimum around kilometer 22. The simultaneous reduction of nitrous oxide and oxygen concentration at first sight seems counterintuitive, but it may be caused by complete denitrification that produces  $\text{N}_2$  instead of nitrous oxide (Knowles 1982).

Based on our data, we cannot clearly say whether the source of nitrous oxide production was in the water column or in the sediments. Other studies, e.g., in the muddy Colne estuary found high nitrous oxide production due to denitrification, but assigned nitrous oxide production only to the sediments

(Ogilvie et al. 1997; Robinson et al. 1998; Dong et al. 2002). Sedimentary denitrification in our study may have contributed to this first nitrous oxide maximum. The beginning of ebb tide during our campaign may have enhanced outgassing of nitrous oxide from the sediment, and low water levels may have caused a mechanical release of nitrous oxide from the sediments caused by our research vessel. Thus, the “denitrification zone” (zone 1) is an important nitrous oxide production zone, but the measured nitrous oxide concentration might in parts be affected by sedimentary processes and might overestimate nitrous oxide production in the water column.

The second nitrous oxide maximum occurred around stream kilometer 35 at the transition between tidal river and Dollard reach. In this area, our mapping approach indicates simultaneous denitrification and nitrification. The nitrous oxide peak coincides with an increase of ammonium and nitrite concentration, as well as a slight rise in nitrate concentration, indicating the onset of nitrification in the water column.

In contrast to conditions leading to the first nitrous oxide peak, not enough fresh organic matter seems to be present in the transition area to support nitrous oxide production. Lower suspended particulate matter concentrations with comparable low POC fraction leads to lower remineralization rates and higher oxygen levels. Low organic matter availability and increasing oxygen concentration favor nitrous oxide production via nitrification (Otte et al. 1999; Sutka et al. 2006). Similarly, Quick et al. (2019) summarized aerobic or oxygen limited conditions with low organic carbon availability favorable for nitrous oxide production via nitrification. As our data suggest additional denitrification, we speculate that in possible anoxic microsites on suspended particles and anoxic deeper water layers, denitrification may have contributed to nitrous oxide production. Overall, we assume that nitrification and denitrification jointly added to nitrous oxide production in this region.

In summary, we find that two nitrous oxide production hotspots exist in the Ems Estuary. Suspended particulate matter plays a big role controlling the nitrous oxide production along the Ems Estuary. In the upstream region, where oxygen depletion occurs due to immense suspended particulate matter concentration, denitrification produces nitrous oxide. At the transition zone between tidal river and Dollard reach, suspended particulate matter concentration is lower, leading to higher oxygen concentration and nitrous oxide production via nitrification. Denitrification prevails in deeper water layers where oxygen concentration is low, and possibly in anoxic microsites close to particles.

## **5.5 Conclusion**

Overall, we find that three distinct biogeochemical zones exist along the Ems. Stable isotope changes point towards water column denitrification in the turbid water column of the tidal river. In the Dollard reach/middle reaches nitrification gains importance turning this section of the estuary into a net nitrate

source. Nitrate uptake occurs in the outer reaches due to primary production in the coastal North Sea, in August 2014 mixing dominated. Our analysis of the dominant nitrogen turnover processes suggest that suspended particulate matter concentration and the linked oxygen deficits exert the overarching control on biogeochemical nitrogen cycling, zonation and nitrous oxide production in the Ems Estuary.

Changing biogeochemical conditions can significantly alter estuarine nutrient processing. Deepening of river channels happens not only in Germany (Kerner 2007; Schuchardt and Scholle 2009; de Jonge et al. 2014; van Maren et al. 2015a) but worldwide (van Maren et al. 2009; Winterwerp et al. 2013; Cox et al. 2019; Grasso and Le Hir 2019; Pareja-Roman et al. 2020), and this can change suspended particulate matter loads and composition in estuaries. Increased suspended particulate matter loads can enhance denitrification, but also trigger nitrous oxide production and enhance oxygen-depleted zones, which is what we observe in the Ems Estuary. Thus, the interplay of suspended particulate matter with riverine nutrient filter function and nitrous oxide emissions should be further evaluated. The common practices of deepening and dredging affect suspended particulate matter and this creates a direct link between pressing social and ecological problems in coastal regions.

### **Acknowledgments**

We thank the crew of *R/V Ludwig Prandtl* for the great support during the cruises. Thanks to Leon Schmidt, who measured the nutrients and helped during the field work. Phillip Wiese is gratefully acknowledge for the isotope analyses of the 2014 sampling. We are thankful for the FerryBox Team: Martina Gehrung for the preparation and Tanja Pieplow for the oxygen measurements. Thanks to the working group of Biogeochemistry at the Institute for Geology for measuring C/N ratios, POC fractions and  $\delta^{15}\text{N}$ -SPM values.



---

## 6 Conclusions and outlook

### 6.1 Conclusion

Estuaries are situated in an area of conflict among ecological, economic and social demands (Bianchi 2007; Kennish 2017), with anthropogenic alterations potentially affecting the estuarine nutrient filter function significantly (Horrigan et al. 1990; Soetaert et al. 2006; Dähnke et al. 2008; Voss et al. 2011). In my thesis, I have examined the effects of different stressors on nitrogen retention, nitrogen turnover, and nitrous oxide production in two heavily managed estuaries in Germany: Elbe and Ems.

The powerful effect of discharge on riverine nitrogen turnover was shown for the Elbe. The reduction in German nitrogen emissions was mirrored in river loads, while discharge conditions were responsible for the strong variability in annual nitrogen loads. Low discharges enhance denitrification and sedimentation in the river and its catchments but also fuel phytoplankton growth, leading to increased DIN uptake and transport of particulate nitrogen downstream. This particulate nitrogen is recycled in the estuary, potentially increasing nitrogen loads and oxygen depletion. At present, decreasing nitrogen input and low discharge conditions lead to low or even depleted riverine nitrate concentrations in the upper freshwater section of the estuary and an upstream shift of heterotrophic processes with accumulated ammonium and low oxygen conditions. Further downstream, in the Port of Hamburg, the increased retention in the river reverses: At low freshwater discharges, nitrate gain increases due to the synergetic effects of fueled riverine phytoplankton blooms and altered suspended particulate matter dynamics.

In estuaries with high agricultural input, eutrophication is linked to nitrous oxide emissions by the overarching control of organic matter on nitrous oxide production. The Elbe Estuary is a year-round source of nitrous oxide, with the highest emissions in winter when DIN loads and wind speeds are high. However, in spring and summer, nitrous oxide saturation and emissions do not decrease with lower DIN loads, suggesting that estuarine in-situ nitrous oxide production is important regardless of the season. Thus, DIN availability is not the sole control of nitrous oxide emissions in estuaries with high agricultural input. High organic matter availability due to phytoplankton blooms promoted by high nutrient loads in the upstream rivers fuel nitrification. The consequence is high nitrous oxide emissions and a decoupling of nitrous oxide and DIN ratios.

Finally, the effects of suspended particulate matter on nitrogen retention, turnover and nitrous oxide emissions were shown in the hyper-turbid Ems Estuary. Suspended particulate matter was identified as the overarching control of nitrogen turnover, leading to a distinct biogeochemical zonation with

water column denitrification occurring in the most turbid section of the estuary. Increased suspended particulate matter loads possibly enhance denitrification but also trigger nitrous oxide production and the development of oxygen-depleted zones, which is what I observed in the Ems Estuary. The common practice of deepening and dredging affects the turbidity state of an estuary (Kerner 2007; Winterwerp et al. 2013; de Jonge et al. 2014) and thus creates a direct link between pressing social and ecological problems in coastal regions.

Generally, the findings of my research indicate the possible connection between multiple stressors on the nitrogen cycle in heavily anthropogenically impacted estuaries, highlighting the need for a holistic approach to water quality improvement, nutrient mitigation and sediment management that considers the impacts of climate change. The Elbe Estuary is an excellent study site for these synergetic effects of different anthropogenic stressors and their biogeochemical feedback. According to climate change predictions (Brasseur et al. 2017; IPCC 2022), low discharge periods will become more frequent and extensive, leading to enhanced retention in the river and catchment. As a consequence, depleted nitrate concentrations in the upper estuary result in an upstream shift of heterotrophic processes causing phytoplankton degradation, oxygen depletion and remineralization. The spread of low-oxygen zones affects biomass, biodiversity and habitats (Diaz et al. 2019). Furthermore, low discharges in combination with high nutrient inputs from agriculture also fuel riverine phytoplankton growth, possibly leading to an increased transport of reactive nitrogen downstream, where it can be reconverted to ammonium or nitrate, fueling eutrophication in a cascade effect (Galloway et al. 2003). This effect is accelerated in the Hamburg Port region, where a sudden light limitation due to increasing water depth results in the decomposition of phytoplankton (Kerner 2000; Schöl et al. 2014). Intense respiration causes oxygen depletion that in combination with a change in organic matter quality and quantity triggers nitrous oxide production and emissions. Considering the most recent construction work for further deepening of the fairway and the regular deepening and dredging operations, as well as the effects of suspended particulate matter in the hyper-turbid Ems Estuary, further sediment management could lead to a spreading of low-oxygen zones, significant water-column denitrification and higher nitrous oxide production.

### **6.2 Outlook**

My thesis revealed the dominance of discharge conditions on estuarine biogeochemical cycling. However, how low discharges affect the general filter function and estuarine nitrogen budget needs to be further evaluated. Long residence times limit quantification of nitrate gain along an estuary by transect measurements. Therefore, an approach is needed that combines high-resolution observations at the head of the estuary with transect measurements and estuarine residence time calculations to

---

track nitrogen inputs from the river to the estuary and to assess the effects of low discharges on the estuarine nutrient filter function.

In light of climate change projections, more frequent and extensive droughts are to be expected (IPCC 2022). In light of the discharge-driven depleted nitrate concentrations in the Elbe Estuary, the question arose whether a nitrate limitation of phytoplankton growth might develop in estuaries with high nutrient inputs. Nitrate limitation could possibly lead to a collapse of phytoplankton blooms, which affects the expansion of oxygen minimum zones impacting biomass, biodiversity, habitat and biogeochemical cycling (Diaz et al. 2019). As I further elaborated the tight coupling between eutrophication and nitrous oxide emissions in estuaries with high agricultural input, the effects on nitrous oxide production and emissions need to be considered as well.

To assess the nitrous oxide emissions in estuaries in more detail, stationary data would help to elucidate the effects of diel variations as well as tidal effects. More long-term data are needed to understand the impact of management efforts on nitrous oxide concentrations, production, and emissions. I propose a measurement strategy with stationary nitrous oxide measurements coupled with transect cruises for a more profound understanding of complex spatial and temporal nitrous oxide dynamics.

In particular, nitrous oxide production in the Hamburg Port region still poses many interesting research questions, as the port acts as a highly reactive bioreactor (e.g., Sanders et al. 2018; Pein et al. 2021; Dähnke et al. 2022; Norbistrath et al. 2022), making it possible to study processes and controlling parameters in a relatively small study site: (1) notably, nitrous oxide production occurred simultaneously in the water column and sediments. Thus, a closer look into the nitrous oxide dynamics, including incubation experiments for rate determination from both sources, is needed to assess the contribution of sediments and the water column to overall nitrous oxide production and their respective controls. Measuring  $\delta^{15}\text{N}^{\text{sp}}\text{-N}_2\text{O}$  site preference has been shown to be a useful tool to distinguish between different nitrous oxide production pathways (e.g., Yamagishi et al. 2007; Breider et al. 2015; Toyoda et al. 2019) and could help to disentangle relevant processes in Hamburg Port. (2) Zander et al. (2020) found a high spatial gradient of organic matter quality along the Hamburg Port and within port basins. They found that organic matter degradability was ten times higher in upstream areas. Considering the overarching control of organic matter on nitrous oxide production that I found, as well as changing residence times, water depth, and light availability in the port basins, the spatial variability of nitrous oxide concentrations, production, and emissions in the Port of Hamburg, including the port basins, should be studied in detail. (3) My results showed the effect of a wastewater treatment plant on nitrous oxide concentrations in the Elbe Estuary during an extreme weather event. The IPCC (2022) expects more frequent and extensive weather extremes, including

both droughts and heavy rainfall. Furthermore, I assume water temperature, riverine nitrogen load and freshwater discharge may influence the importance of input from the wastewater treatment plant on nitrous oxide concentrations and emissions. Therefore, the possible reassessment of inputs from wastewater treatment plants should be considered in light of climate change with the overarching aim of evaluating management measures.

The deepening of river channels occurs not only in Germany (Kerner 2007; de Jonge et al. 2014; van Maren et al. 2015a) but also worldwide (e.g., van Maren et al. 2009; Winterwerp et al. 2013; Cox et al. 2019; Grasso and Le Hir 2019; Pareja-Roman et al. 2020). In the Elbe Estuary, a change in the suspended particulate matter dynamics after the deepening in 1999 was shown by Kerner (2007). A decrease in tidal flow led to longer residence times of fine-grained suspended particles that remained in the freshwater section of the estuary until all degradable organic matter was consumed. Suspended particulate matter accumulated in the Port of Hamburg and longitudinal profile, leading to enhanced oxygen deficits (Kerner 2007). Furthermore, Winterwerp and Wang (2013) and Winterwerp et al. (2013) introduced the theory of estuarine “tipping points” that lead to hyper-turbid conditions induced by extensive deepening and narrowing. High suspended particulate matter concentrations were the overarching control in the “beyond the tipping point” Ems Estuary. Dähnke et al. (2022) showed that suspended particulate matter quantity and quality are also crucial controls in the Elbe Estuary. Therefore, the suspended particulate matter dynamics and possible changes after the most recent deepening of the fairway in the Elbe Estuary should be studied alongside possible effects on the nitrogen cycle, oxygen depletion and nitrous oxide production – as well as in other heavily deepened and dredged estuaries worldwide. Moreover, the effects of sediment operations themselves on the air-water-sediment interaction and on nitrous oxide emissions need to be addressed.

Generally, I elaborated the need for a holistic approach to water quality improvement, nutrient mitigation, and sediment management in heavily managed estuaries. However, this has a direct link to economic and social demands, highlighting the need for an interdisciplinary approach in the socioecological research field of estuaries. A profound understanding of the interaction between ecological parameters and the estuarine nitrogen cycle is necessary to assess complex management studies, and knowledge about the interaction with social, legal, and economic drivers is crucial.

---

## Abbreviations

AOA	Ammonia-oxidizing archaea
AOB	Ammonia-oxidizing bacteria
AOU	Apparent oxygen utilization
BAW	Bundesanstalt für Wasserbau (=Federal Waterways Engineering and Research Institute)
c	Concentration
C	Carbon
CO <sub>2</sub>	Carbon dioxide
DIN	Dissolved inorganic nitrogen
DNRA	Dissimilatory nitrate reduction to ammonium
EEA	European Environmental Agency
Eq.	Equation
FGG	Flussgebietsgemeinschaft (= River Basin Community)
GF/F	Glass fiber filter, grad F
HCl	Hydrochloric acid
HPA	Hamburg Port Authority
i.e.	id est
IAEA	International Atomic Energy Agency
IKSE	Internationale Kommission zum Schutz der Elbe (=International Commission for the Protection of the Elbe River)
INSC	Ministerial Conference on the Protection of the North Sea
IPCC	Intergovernmental Panel on Climate Change
L	Loads
MTZ	Maximum turbidity zone
n	Number
N	Nitrogen
N <sub>2</sub>	Dinitrogen
N <sub>2</sub> O	Nitrous oxide
NH <sub>2</sub> OH	Hydroxylamine
NH <sub>3</sub>	Ammonia
NH <sub>4</sub> <sup>+</sup>	Ammonium

NLWKN	Niedersächsischer Landesbetrieb für Wasserwirtschaft, Küsten- und Naturschutz (=Lower Saxon State Department for Waterway, Coastal and Nature Conservation)
NO	Nitric oxide
NO <sub>x</sub> <sup>-</sup>	Sum of nitrite and nitrate
NO <sub>2</sub> <sup>-</sup>	Nitrite
NO <sub>3</sub> <sup>-</sup>	Nitrate
NOB	Nitrite-oxidizing bacteria
O <sub>2</sub>	Oxygen
OSPAR	Convention for the Protection of the Marine Environment of the North-East Atlantic
p	Level of significance
ppb	Parts per billion
PC	Particulate carbon
PCA	Principal component analysis
PE	Polyethylene
PN	Particulate nitrogen
PO <sub>4</sub> <sup>3-</sup>	Phosphate
POC	Particulate organic carbon
Q	Discharge
R	Pearson correlation coefficient
R/V	Research vessel
Si	Silicate
SPM	Suspended particulate matter
T	Temperature
TN	Total nitrogen
TON	Total organic nitrogen
UBA	Umweltbundesamt (=German Environmental Agency)
USGS	United States Geological Survey
VSMOV	Vienna Standard Mean Ocean Water
WSA	Wasser- und Schifffahrtsamt (=Federal Waterways and Shipping Administration)
WWTP	Wastewater treatment plant
δ	Isotope ratio relative to standard isotope ratio
ε	Fractionation factor

---

## References

- Amann, T., A. Weiss, and J. Hartmann. 2012. Carbon dynamics in the freshwater part of the Elbe estuary, Germany: Implications of improving water quality. *Estuar. Coast. Shelf Sci.* **107**: 112–121. doi:10.1016/j.ecss.2012.05.012
- Amann, T., A. Weiss, and J. Hartmann. 2015. Inorganic Carbon Fluxes in the Inner Elbe Estuary, Germany. *Estuaries Coasts* **38**: 192–210. doi:10.1007/s12237-014-9785-6
- Anderson, D. M., P. M. Glibert, and J. M. Burkholder. 2002. Harmful algal blooms and eutrophication: Nutrient sources, composition, and consequences. *Estuaries* **25**: 704–726. doi:10.1007/BF02804901
- ARGE-Elbe. 2001. Analyse der Nährstoffkonzentrationen, -frachten und -einträge im Elbeeinzugsgebiet. Arbeitsgemeinschaft für die Reinhaltung der Elbe.
- Bange, H. W. 2006. Nitrous oxide and methane in European coastal waters. *Estuar. Coast. Shelf Sci.* **70**: 361–374. doi:10.1016/j.ecss.2006.05.042
- Bange, H. W. 2008. Chapter 2 - Gaseous Nitrogen Compounds (NO, N<sub>2</sub>O, N<sub>2</sub>, NH<sub>3</sub>) in the Ocean D.G. Capone, D.A. Bronk, M.R. Mulholland, and E.J. Carpenter [eds.]. *Nitrogen Mar. Environ.* Second Ed. 51–94. doi:10.1016/B978-0-12-372522-6.00002-5
- Bange, H. W., C. H. Sim, D. Bastian, J. Kallert, A. Kock, A. Mujahid, and M. Müller. 2019. Nitrous oxide (N<sub>2</sub>O) and methane (CH<sub>4</sub>) in rivers and estuaries of northwestern Borneo. *Biogeosciences* **16**: 4321–4335. doi:10.5194/bg-16-4321-2019
- Barnes, J., and N. J. P. Owens. 1999. Denitrification and Nitrous Oxide Concentrations in the Humber Estuary, UK, and Adjacent Coastal Zones. *Mar. Pollut. Bull.* **37**: 247–260. doi:10.1016/S0025-326X(99)00079-X
- Barnes, J., R. Ramesh, R. Purvaja, and others. 2006. Tidal dynamics and rainfall control N<sub>2</sub>O and CH<sub>4</sub> emissions from a pristine mangrove creek. *Geophys. Res. Lett.* **33**. doi:10.1029/2006GL026829
- Barnes, J., and R. C. Upstill-Goddard. 2011. N<sub>2</sub>O seasonal distributions and air-sea exchange in UK estuaries: Implications for the tropospheric N<sub>2</sub>O source from European coastal waters. *J. Geophys. Res. Biogeosciences* **116**. doi:10.1029/2009JG001156
- Baulch, H. M., P. J. Dillon, R. Maranger, J. J. Venkiteswaran, H. F. Wilson, and S. L. Schiff. 2012. Night and day: short-term variation in nitrogen chemistry and nitrous oxide emissions from streams. *Freshw. Biol.* **57**: 509–525. doi:10.1111/j.1365-2427.2011.02720.x
- BAW Oritz, V. 2023. pers. Comm.: Flächen des Elbe Ästuars.
- Beaulieu, J. J., J. L. Tank, S. K. Hamilton, and others. 2011. Nitrous oxide emission from denitrification in stream and river networks. *Proc. Natl. Acad. Sci.* **108**: 214–219. doi:10.1073/pnas.1011464108

- Bergemann, M. 2004. Die Trübungszone in der Tideelbe - Beschreibung der räumlichen und zeitlichen Entwicklung. Wassergütestelle Elbe.
- Bergemann, M., G. Blöcker, H. Harms, M. Kerner, R. Meyer-Nehls, W. Petersen, and F. Schroeder. 1996. Der Sauerstoffhaushalt der Tideelbe. *Küste* **58**: 199–261.
- Bergemann, M., and T. Gaumert. 2008. Elbebericht 2008: Ergebnisse des nationalen Überwachungsprogramms Elbe der Bundesländer über den ökologischen und chemischen Zustand der Elbe nach EG-WRRLsowie der Trendentwicklung von Stoffen und Schadstoffgruppen. Flussgebietsgemeinschaft Elbe (FGG Elbe).
- van Beusekom, J. E. E., J. Carstensen, T. Dolch, and others. 2019. Wadden Sea Eutrophication: Long-Term Trends and Regional Differences. *Front. Mar. Sci.* **6**: 370. doi:10.3389/fmars.2019.00370
- van Beusekom, J. E. E., and V. N. de Jonge. 1994. The role of suspended matter in the distribution of dissolved inorganic phosphate, iron and aluminium in the Ems estuary. *Netherland J. Aquat. Ecol.* **28**: 383–395. doi:10.1007/BF02334208
- van Beusekom, J. E. E., and V. N. de Jonge. 1997. Transformation of phosphorus in the Wadden Sea: Apatite formation. *Dtsch. Hydrogr. Z.* **49**: 297–305. doi:10.1007/BF02764040
- van Beusekom, J. E. E., and V. N. de Jonge. 1998. Retention of phosphorus and nitrogen in the Ems estuary. *Estuaries* **21**: 527–539. doi:10.2307/1353292
- van Beusekom, J. E. E., and V. N. de Jonge. 2002. Long-term changes in Wadden Sea nutrient cycles: importance of organic matter import from the North Sea, p. 185–194. *In* E. Orive, M. Elliott, and V.N. De Jonge [eds.], *Nutrients and Eutrophication in Estuaries and Coastal Waters: Proceedings of the 31st Symposium of the Estuarine and Coastal Sciences Association (ECSA), held in Bilbao, Spain, 3–7 July 2000*. Springer Netherlands. doi: 10.1007/978-94-017-2464-7\_15
- van Beusekom, J., R. Thiel, I. Bobsien, and others. 2018. Aquatische Ökosysteme: Nordsee, Wattenmeer, Elbeästuar und Ostsee, p. 89–107. *In* H. Von Storch, I. Meinke, and M. Claußen [eds.], *Hamburger Klimabericht – Wissen über Klima, Klimawandel und Auswirkungen in Hamburg und Norddeutschland*. Springer. doi: 10.1007/978-3-662-55379-4\_5
- BfG. unpublished. Die vertikale Verteilung von Sauerstoff, Schwebstoff und Nährstoffen in der Tideems von 2014 – 2020. BfG-2077. BfG-2077 Bundesanstalt für Gewässerkunde.
- Bianchi, T. S. 2007. *Biogeochemistry of Estuaries*, Oxford University Press.
- Billen, G., M. Silvestre, B. Grizzetti, and others. 2011. Nitrogen flows from European regional watersheds to coastal marine waters, p. 271–297. *In* A. Bleeker, B. Grizzetti, C.M. Howard, G. Billen, H. Van Grinsven, J.W. Erisman, M.A. Sutton, and P. Grennfelt [eds.], *The European Nitrogen Assessment: Sources, Effects and Policy Perspectives*. Cambridge University Press. doi: 10.1017/CBO9780511976988.016
- BMEL. 2022. Nährstoffbilanzen und Düngemittel - Nährstoffbilanz insgesamt von 1990 bis 2020. MBT-0111260-0000. MBT-0111260-0000 Federal Ministry of Food and Agriculture (BMEL). <https://www.bmel-statistik.de/fileadmin/daten/MBT-0111260-0000.xlsx>. Last accessed: 24.4.2023.
- Boehlich, M. J., and T. Strotmann. 2008. The Elbe Estuary. *Küste* **74**: 288–306.

- Boehlich, M. J., and T. Strotmann. 2019. Das Elbeästuar. *Küste* **87**: Kuratorium für Forschung im Küsteningenieurwesen (KFKI). doi:10.18171/1.087106
- Böhlke, J. K., S. J. Mroczkowski, and T. B. Coplen. 2003. Oxygen isotopes in nitrate: new reference materials for  $^{18}\text{O}$ : $^{17}\text{O}$ : $^{16}\text{O}$  measurements and observations on nitrate-water equilibration. *Rapid Commun. Mass Spectrom.* **17**: 1835–1846. doi:10.1002/rcm.1123
- Böhme, M., H. Guhr, and K. Ockenfeld. 2006. 3.1 Phytoplanktodynamik, p. 33–43. *In* M. Pusch and H. Fischer [eds.], *Stoffdynamik und Habitatstruktur der Elbe*. Weißensee Verlag.
- Borges, A. V., F. Darchambeau, C. R. Teodoru, and others. 2015. Globally significant greenhouse-gas emissions from African inland waters. *Nat. Geosci.* **8**: 637–642. doi:10.1038/ngeo2486
- Borges, A., J.-P. Vanderborght, L.-S. Schiettecatte, F. Gazeau, S. Ferrón-Smith, B. Delille, and M. Frankignoulle. 2004. Variability of gas transfer velocity of  $\text{CO}_2$  in a macrotidal estuary (The Scheldt). *Estuaries* **27**: 593–603. doi:10.1007/BF02907647
- Bos, D., H. Büttger, P. Esselink, Z. Jager, V. N. de Jonge, H. Kruckenberg, D. S. van Maren, and B. Schuchardt. 2012. The ecological state of the Ems estuary and options for restoration.
- Bothe, H., G. Jost, M. Schloter, B. B. Ward, and K. Witzel. 2000. Molecular analysis of ammonia oxidation and denitrification in natural environments. *FEMS Microbiol. Rev.* **24**: 673–690. doi:10.1111/j.1574-6976.2000.tb00566.x
- Böttcher, J., O. Strelbel, S. Voerkelius, and H.-L. Schmidt. 1990. Using isotope fractionation of nitrate-nitrogen and nitrate-oxygen for evaluation of microbial denitrification in a sandy aquifer. *J. Hydrol.* **114**: 413–424. doi:10.1016/0022-1694(90)90068-9
- Bouwman, A. F., M. F. P. Bierkens, J. Griffioen, M. M. Hefting, J. J. Middelburg, H. Middelkoop, and C. P. Slomp. 2013. Nutrient dynamics, transfer and retention along the aquatic continuum from land to ocean: towards integration of ecological and biogeochemical models. *Biogeosciences* **10**: 1–23. doi:10.5194/bg-10-1-2013
- Brandes, J. A., and A. H. Devol. 1997. Isotopic fractionation of oxygen and nitrogen in coastal marine sediments. *Geochim. Cosmochim. Acta* **61**: 1793–1801. doi:10.1016/S0016-7037(97)00041-0
- Brandes, J. A., A. H. Devol, T. Yoshinari, D. A. Jayakumar, and S. W. A. Naqvi. 1998. Isotopic composition of nitrate in the central Arabian Sea and eastern tropical North Pacific: A tracer for mixing and nitrogen cycles. *Limnol. Oceanogr.* **43**: 1680–1689. doi:10.4319/lo.1998.43.7.1680
- Brase, L., H. W. Bange, R. Lendt, T. Sanders, and K. Dähnke. 2017. High Resolution Measurements of Nitrous Oxide ( $\text{N}_2\text{O}$ ) in the Elbe Estuary. *Front. Mar. Sci.* **4**: 162. doi:10.3389/fmars.2017.00162
- Brasseur, G. P., D. Jacob, and S. Schuck-Zöller, eds. 2017. *Klimawandel in Deutschland*, Springer Berlin Heidelberg. doi:10.1007/978-3-662-50397-3
- Breider, F., C. Yoshikawa, H. Abe, S. Toyoda, and N. Yoshida. 2015. Origin and fluxes of nitrous oxide along a latitudinal transect in western North Pacific: Controls and regional significance. *Glob. Biogeochem. Cycles* **29**: 1014–1027. doi:10.1002/2014GB004977

- 
- Bremner, J. M. 1997. Sources of nitrous oxide in soils. *Nutr. Cycl. Agroecosystems* **49**: 7–16. doi:10.1023/A:1009798022569
- Brinkman, A. G., R. Riegman, P. Jacobs, S. Kuhn, and A. Meijboom. 2015. Ems-Dollard primary production research: Full data report. Technical Report Institute for Marine Resources & Ecosystem Studies.
- Brockmann, U. H., and A. Pfeiffer. 1990. Seasonal Changes of Dissolved and Particulate Material in the Turbidity Zone of the River Elbe. *Estuarine Water Quality Management*. Springer. 327–334.
- Brockmann, U., B. Heyden, M. Schütt, A. Starke, D. Topcu, and K.-J. Hesse. 2003. Assessment Criteria for Eutrophication Areas – Emphasis German Bight, *In* Texte Umweltbundesamt. Federal Environmental Agency (Umweltbundesamt).
- Broder, T., C. Blodau, H. Biester, and K. H. Knorr. 2012. Peat decomposition records in three pristine ombrotrophic bogs in southern Patagonia. *Biogeosciences* **9**: 1479–1491. doi:10.5194/bg-9-1479-2012
- Buchwald, C., and K. L. Casciotti. 2010. Oxygen isotopic fractionation and exchange during bacterial nitrite oxidation. *Limnol. Oceanogr.* **55**: 1064–1074. doi:10.4319/lo.2010.55.3.1064
- Buchwald, C., A. E. Santoro, R. H. R. Stanley, and K. L. Casciotti. 2015. Nitrogen cycling in the secondary nitrite maximum of the eastern tropical North Pacific off Costa Rica. *Glob. Biogeochem. Cycles* **29**: 2061–2081. doi:10.1002/2015GB005187
- Burkholder, J. M., D. A. Tomasko, and B. W. Touchette. 2007. Seagrasses and eutrophication. *J. Exp. Mar. Biol. Ecol.* **350**: 46–72. doi:10.1016/j.jembe.2007.06.024
- Büttner, O., J. W. Jawitz, and D. Borchardt. 2020. Ecological status of river networks: stream order-dependent impacts of agricultural and urban pressures across ecoregions. *Environ. Res. Lett.* **15**: 1040b3. doi:10.1088/1748-9326/abb62e
- Cadée, G. C., and J. Hegeman. 1974. Primary production of the benthic microflora living on tidal flats in the dutch wadden sea. *Neth. J. Sea Res.* **8**: 260–291. doi:10.1016/0077-7579(74)90020-9
- Cadée, G. C., and J. Hegeman. 2002. Phytoplankton in the Marsdiep at the end of the 20th century; 30 years monitoring biomass, primary production, and *Phaeocystis* blooms. *J. Sea Res.* **48**: 97–110. doi:10.1016/S1385-1101(02)00161-2
- Capone, D. G., J. A. Burns, J. P. Montoya, A. Subramaniam, C. Barford, T. Gunderson, A. F. Michaels, and E. J. Carpenter. 2005. Nitrogen fixation by *Trichodesmium* spp.: An important source of new nitrogen to the tropical and subtropical North Atlantic Ocean. *Glob. Biogeochem. Cycles* **19**. doi:10.1029/2004GB002331
- Carstensen, J., D. J. Conley, E. Bonsdorff, and others. 2014. Hypoxia in the Baltic Sea: biogeochemical cycles, benthic fauna, and management. *Ambio* **43**: 26–36. doi:10.1007/s13280-013-0474-7
- Casciotti, K. L. 2009. Inverse kinetic isotope fractionation during bacterial nitrite oxidation. *Geochim. Cosmochim. Acta* **73**: 2061–2076. doi:10.1016/j.gca.2008.12.022

- 
- Casciotti, K. L. 2016. Nitrogen and Oxygen Isotopic Studies of the Marine Nitrogen Cycle. *Annu. Rev. Mar. Sci.* **8**: 379–407. doi:10.1146/annurev-marine-010213-135052
- Casciotti, K. L., D. M. Sigman, M. G. Hastings, J. K. Böhlke, and A. Hilkert. 2002. Measurement of the Oxygen Isotopic Composition of Nitrate in Seawater and Freshwater Using the Denitrifier Method. *Anal. Chem.* **74**: 4905–4912. doi:10.1021/ac020113w
- Casciotti, K. L., D. M. Sigman, and B. B. Ward. 2003. Linking Diversity and Stable Isotope Fractionation in Ammonia-Oxidizing Bacteria. *Geomicrobiol. J.* **20**: 335–353. doi:10.1080/01490450303895
- Chilton, D., D. P. Hamilton, I. Nagelkerken, and others. 2021. Environmental Flow Requirements of Estuaries: Providing Resilience to Current and Future Climate and Direct Anthropogenic Changes. *Front. Environ. Sci.* **9**: 764218. doi:10.3389/fenvs.2021.764218
- Clark, J. F., P. Schlosser, H. J. Simpson, M. Stute, R. Wanninkhof, and D. T. Ho. 1995. Relationship between gas transfer velocities and wind speeds in the tidal Hudson River determined by the dual tracer technique, p. 785–800. *In* B. Jähne and E.C. Monahan [eds.], *Air-Water Gas Transfer*. AEON Verlag.
- Cloern, J. E. 2001. Our evolving conceptual model of the coastal eutrophication problem. *Mar. Ecol. Prog. Ser.* **210**: 223–253. doi:10.3354/meps210223
- Cohen, J., C. Small, A. Mellinger, J. Gallup, J. Sachs, P. Vitousek, and H. Mooney. 1997. Estimates of Coastal Populations. *Science* **278**: 1209–1213. doi:10.1126/science.278.5341.1209c
- Colijn, F. 1983. Primary production in the Ems Dollard estuary. State University Groningen.
- Colijn, F., W. Admiraal, J. W. Baretta, and P. Ruardij. 1987. Primary production in a turbid estuary, the Ems-Dollard: field and model studies. *Cont. Shelf Res.* **7**: 1405–1409. doi:10.1016/0278-4343(87)90045-8
- Compton, T. J., S. Holthuijsen, M. Mulder, and others. 2017. Shifting baselines in the Ems Dollard estuary: A comparison across three decades reveals changing benthic communities. *J. Sea Res.* **127**: 119–132. doi:10.1016/j.seares.2017.06.014
- Coplen, T. B. 2011. Guidelines and recommended terms for expression of stable-isotope-ratio and gas-ratio measurement results. *Rapid Commun. Mass Spectrom.* **25**: 2538–2560. doi:10.1002/rcm.5129
- Cornwell, J., W. Kemp, and T. Kana. 1999. Denitrification in coastal ecosystems: Methods, environmental controls, and ecosystem level controls, a review. *Aquat. Ecol.* **33**: 41–54. doi:10.1023/A:1009921414151
- Cox, T. J. S., T. Maris, T. Van Engeland, K. Soetaert, and P. Meire. 2019. Critical transitions in suspended sediment dynamics in a temperate meso-tidal estuary. *Sci. Rep.* **9**: 12745. doi:10.1038/s41598-019-48978-5
- Crossland, C. J., D. Baird, J.-P. Ducrotoy, and others. 2005. The Coastal Zone — a Domain of Global Interactions, p. 1–37. *In* C.J. Crossland, H.H. Kremer, H.J. Lindeboom, J.I. Marshall Crossland, and M.D.A. Tissier [eds.], *Coastal Fluxes in the Anthropocene: The Land-Ocean Interactions in the Coastal Zone Project of the International Geosphere-Biosphere Programme*. Springer. doi:10.1007/3-540-27851-6\_1

- Dähnke, K., E. Bahlmann, and K.-C. Emeis. 2008. A nitrate sink in estuaries? An assessment by means of stable nitrate isotopes in the Elbe estuary. *Limnol. Oceanogr.* **53**: 1504–1511. doi:10.4319/lo.2008.53.4.1504
- Dähnke, K., K.-C. Emeis, A. Johannsen, and B. Nagel. 2010. Stable isotope composition and turnover of nitrate in the German Bight. *Mar. Ecol. Prog. Ser.* **408**: 7–18. doi:10.3354/meps08558
- Dähnke, K., T. Sanders, Y. Voynova, and S. D. Wankel. 2022. Nitrogen isotopes reveal a particulate-matter-driven biogeochemical reactor in a temperate estuary. *Biogeosciences* **19**: 5879–5891. doi:10.5194/bg-19-5879-2022
- Daims, H., E. V. Lebedeva, P. Pjevac, and others. 2015. Complete nitrification by *Nitrospira* bacteria. *Nature* **528**: 504–509. doi:10.1038/nature16461
- Daims, H., S. Lüscher, and M. Wagner. 2016. A New Perspective on Microbes Formerly Known as Nitrite-Oxidizing Bacteria. *Trends Microbiol.* **24**: 699–712. doi:10.1016/j.tim.2016.05.004
- Damashek, J., and C. A. Francis. 2018. Microbial Nitrogen Cycling in Estuaries: From Genes to Ecosystem Processes. *Estuaries Coasts* **41**: 626–660. doi:10.1007/s12237-017-0306-2
- Deek, A., K. Dähnke, J. van Beusekom, S. Meyer, M. Voss, and K.-C. Emeis. 2013. N<sub>2</sub> fluxes in sediments of the Elbe Estuary and adjacent coastal zones. *Mar. Ecol. Prog. Ser.* **493**: 9–21. doi:10.3354/meps10514
- Deutsch, B., I. Liskow, P. Kahle, and M. Voss. 2005. Variations in the  $\delta^{15}\text{N}$  and  $\delta^{18}\text{O}$  values of nitrate in drainage water of two fertilized fields in Mecklenburg-Vorpommern (Germany). *Aquat. Sci.* **67**: 156–165. doi:10.1007/s00027-004-0759-9
- Deutsch, B., M. Mewes, I. Liskow, and M. Voss. 2006. Quantification of diffuse nitrate inputs into a small river system using stable isotopes of oxygen and nitrogen in nitrate. *Org. Geochem.* **37**: 1333–1342. doi:10.1016/j.orggeochem.2006.04.012
- Deutsch, B., M. Voss, and H. Fischer. 2009. Nitrogen transformation processes in the Elbe River: Distinguishing between assimilation and denitrification by means of stable isotope ratios in nitrate. *Aquat. Sci.* **71**: 228–237. doi:10.1007/s00027-009-9147-9
- Devol, A. H. 2008. Chapter 6 - Denitrification Including Anammox, p. 263–301. *In* D.G. Capone, D.A. Bronk, M.R. Mulholland, and E.J. Carpenter [eds.], *Nitrogen in the Marine Environment* (Second Edition). Academic Press. doi:10.1016/B978-0-12-372522-6.00006-2
- Diaz, R. J., and R. Rosenberg. 2008. Spreading Dead Zones and Consequences for Marine Ecosystems. *Science* **321**: 926–929. doi:10.1126/science.1156401
- Diaz, R. J., R. Rosenberg, and K. Sturdivant. 2019. 2.5 Hypoxia in estuaries and semi-enclosed seas, p. 85–102. *In* D. Laffoley and J.M. Baxter [eds.], *Ocean deoxygenation : everyone’s problem*. IUCN. doi:10.2305/IUCN.CH.2019.13.en
- Dlugokencky, E. J., A. M. Croftwell, J. W. Mund, M. J. Croftwell, and K. W. Thoning. 2022. Earth System Research Laboratory Carbon Cycle and Greenhouse Gases Group Flask-Air Sample Measurements of N<sub>2</sub>O at Global and Regional Background Sites, 1967-Present [Data set]. NOAA ESRL GML CCGG Group **Version: 2022-08-18**. doi:10.15138/53G1-X417

- Dong, L. F., D. B. Nedwell, G. J. C. Underwood, D. C. O. Thornton, and I. Rusmana. 2002. Nitrous oxide formation in the Colne estuary, England: the central role of nitrite. *Appl. Environ. Microbiol.* **68**: 1240–1249. doi:10.1128/AEM.68.3.1240-1249.2002
- Dortch, Q. 1990. The interaction between ammonium and nitrate uptake in phytoplankton. *Mar. Ecol. Prog. Ser.* **61**: 183–201. doi:10.3354/meps061183
- EEA. 2019. Nutrient enrichment and eutrophication in Europe's seas — Moving towards a healthy marine environment. 14/2019. 14/2019 European Environment Agency.
- Fabisik, F., B. Guieysse, J. Procter, and M. Plouviez. 2023. Nitrous oxide (N<sub>2</sub>O) synthesis by the freshwater cyanobacterium *Microcystis aeruginosa*. *Biogeosciences* **20**: 687–693. doi:10.5194/bg-20-687-2023
- FGE Ems. 2022. Internationaler Bewirtschaftungsplan nach Wasserrahmenrichtlinie für die Flussgebietseinheit Ems 2021 bis 2027. Flussgebietsgemeinschaft Ems (FGG Ems).
- FGG Elbe. 2018. Nährstoffminderungsstrategie für die Flussgebietsgemeinschaft Elbe. Flussgebietsgemeinschaft Elbe (FGG Elbe).
- FGG Elbe. 2022. FIS der FGG Elbe. Flussgebietsgemeinschaft Elbe (FGG Elbe). <https://www.elbe-datenportal.de/FisFggElbe/content/start/>. Last accessed: 21.05.2023.
- FGG Ems. 2015a. Internationaler Bewirtschaftungsplan nach Artikel 13 Wasserrahmenrichtlinie für die Flussgebietseinheit Ems: Bewirtschaftungszeitraum 2015 - 2021. Flussgebietsgemeinschaft Ems.
- FGG Ems. 2015b. Hochwasserrisikomanagementplan 2015–2021 für den deutschen Anteil der Flussgebietseinheit Ems gemäß § 75 WHG, Flussgebietsgemeinschaft Ems. Flussgebietsgemeinschaft Ems (FGG Ems).
- FGG Ems. 2015c. Internationaler Bewirtschaftungsplan nach Artikel 13 Wasserrahmenrichtlinie für die Flussgebietseinheit Ems: Bewirtschaftungszeitraum 2015–2021, Flussgebietsgemeinschaft Ems. Flussgebietsgemeinschaft Ems (FGG Ems).
- Fraga, F., A. F. Ríos, F. F. Pérez, and F. G. Figueiras. 1998. Theoretical limits of oxygen:carbon and oxygen:nitrogen ratios during photosynthesis and mineralisation of organic matter in the sea. *Sci. Mar.* **62**: 161–168. doi:10.3989/scimar.1998.62n1-2161
- Francis, C. A., J. M. Beman, and M. M. M. Kuypers. 2007. New processes and players in the nitrogen cycle: the microbial ecology of anaerobic and archaeal ammonia oxidation. *ISME J.* **1**: 19–27. doi:10.1038/ismej.2007.8
- Fry, B. 2002. Conservative mixing of stable isotopes across estuarine salinity gradients: A conceptual framework for monitoring watershed influences on downstream fisheries production. *Estuaries* **25**: 264–271. doi:10.1007/BF02691313
- Galloway, J. N., J. D. Aber, J. W. Erisman, S. P. Seitzinger, R. W. Howarth, E. B. Cowling, and B. J. Cosby. 2003. The Nitrogen Cascade. *BioScience* **53**: 341–356. doi:10.1641/0006-3568(2003)053[0341:TNC]2.0.CO;2
- Gao, H., F. Schreiber, G. Collins, and others. 2010. Aerobic denitrification in permeable Wadden Sea sediments. *ISME J.* **4**: 417–426. doi:10.1038/ismej.2009.127

- Garnier, J., A. Cébron, G. Tallec, G. Billen, M. Sebilo, and A. Martinez. 2006. Nitrogen Behaviour and Nitrous Oxide Emission in the Tidal Seine River Estuary (France) as Influenced by Human Activities in the Upstream Watershed. *Biogeochemistry* **77**: 305–326. doi:10.1007/s10533-005-0544-4
- Gaumert, T., and M. Bergemann. 2007. Sauerstoffgehalt der Tideelbe - Entwicklung der kritischen Sauerstoffgehalte im Jahr 2007 und in den Vorjahren, Erörterung möglicher Ursachen und Handlungsoptionen. Flussgebietsgemeinschaft Elbe.
- Gaye, B., B. Nagel, K. Dähnke, T. Rixen, and K.-C. Emeis. 2013. Evidence of parallel denitrification and nitrite oxidation in the ODZ of the Arabian Sea from paired stable isotopes of nitrate and nitrite. *Glob. Biogeochem. Cycles* **27**: 1059–1071. doi:10.1002/2011GB004115
- Geerts, L., K. Wolfstein, S. Jacobs, S. van Damme, and W. Vandenbruwaene. 2012. Zonation of the TIDE estuaries. TIDE toolbox.
- Giblin, A., C. Tobias, B. Song, N. Weston, G. Banta, and V. Rivera-Monroy. 2013. The Importance of Dissimilatory Nitrate Reduction to Ammonium (DNRA) in the Nitrogen Cycle of Coastal Ecosystems. *Oceanography* **26**: 124–131. doi:10.5670/oceanog.2013.54
- Gieskes, W. W. C., and G. W. Kraay. 1977. Primary production and consumption of organic matter in the southern North Sea during the spring bloom of 1975. *Neth. J. Sea Res.* **11**: 146–167. doi:10.1016/0077-7579(77)90003-5
- Giles, H., C. A. Pilditch, S. D. Nodder, J. R. Zeldis, and K. Currie. 2007. Benthic oxygen fluxes and sediment properties on the northeastern New Zealand continental shelf. *Cont. Shelf Res.* **27**: 2373–2388. doi:10.1016/j.csr.2007.06.007
- Gonçalves, C., M. J. Brogueira, and M. F. Camões. 2010. Seasonal and tidal influence on the variability of nitrous oxide in the Tagus estuary, Portugal. *Sci. Mar.* **74**: 57–66. doi:10.3989/scimar.2010.74s1057
- Gonçalves, C., M. J. Brogueira, and M. Nogueira. 2015. Tidal and spatial variability of nitrous oxide (N<sub>2</sub>O) in Sado estuary (Portugal). *Estuar. Coast. Shelf Sci.* **167**: 466–474. doi:10.1016/j.ecss.2015.10.028
- Gosselain, V., J.-P. Descy, and E. Everbecq. 1994. The phytoplankton community of the River Meuse, Belgium: seasonal dynamics (year 1992) and the possible incidence of zooplankton grazing. *Hydrobiologia* **289**: 179–191. doi:10.1007/BF00007419
- Granger, J., and D. M. Sigman. 2009. Removal of nitrite with sulfamic acid for nitrate N and O isotope analysis with the denitrifier method. *Rapid Commun. Mass Spectrom.* **23**: 3753–3762. doi:10.1002/rcm.4307
- Granger, J., D. M. Sigman, M. F. Lehmann, and P. D. Tortell. 2008. Nitrogen and oxygen isotope fractionation during dissimilatory nitrate reduction by denitrifying bacteria. *Limnol. Oceanogr.* **53**: 2533–2545. doi:10.4319/lo.2008.53.6.2533
- Granger, J., D. M. Sigman, J. A. Needoba, and P. J. Harrison. 2004. Coupled nitrogen and oxygen isotope fractionation of nitrate during assimilation by cultures of marine phytoplankton. *Limnol. Oceanogr.* **49**: 1763–1773. doi:10.4319/lo.2004.49.5.1763

- Granger, J., and S. Wankel. 2016. Isotopic overprinting of nitrification on denitrification as a ubiquitous and unifying feature of environmental nitrogen cycling. *Proc. Natl. Acad. Sci.* **113**: E6391–E6400. doi:10.1073/pnas.1601383113
- Grasso, F., and P. Le Hir. 2019. Influence of morphological changes on suspended sediment dynamics in a macrotidal estuary: diachronic analysis in the Seine Estuary (France) from 1960 to 2010. *Ocean Dyn.* **69**: 83–100. doi:10.1007/s10236-018-1233-x
- Gruber, N. 2008. Chapter 1 - The Marine Nitrogen Cycle: Overview and Challenges, p. 1–50. *In* D.G. Capone, D.A. Bronk, M.R. Mulholland, and E.J. Carpenter [eds.], *Nitrogen in the Marine Environment* (Second Edition). Academic Press. doi:10.1016/B978-0-12-372522-6.00001-3
- Guhr, H., B. Karrasch, and D. Spott. 2000. Shifts in the Processes of Oxygen and Nutrient Balances in the River Elbe since the Transformation of the Economic Structure. *Acta Hydrochim. Hydrobiol.* **28**: 155–161. doi:10.1002/1521-401X(200003)28:3<155::AID-AHEH155>3.0.CO;2-R
- de Haas, H., T. C. E. van Weering, and H. de Stigter. 2002. Organic carbon in shelf seas: sinks or sources, processes and products. *Cont. Shelf Res.* **22**: 691–717. doi:10.1016/S0278-4343(01)00093-0
- Hall Jr., R. O., and A. J. Ulseth. 2020. Gas exchange in streams and rivers. *WIREs Water* **7**: e1391. doi:10.1002/wat2.1391
- Halling-Sorensen, B., and S. E. Jorgensen, eds. 1993. 3. Process Chemistry and Biochemistry of Nitrification, p. 55–118. *In* *Studies in Environmental Science*. Elsevier. doi:10.1016/S0166-1116(08)70525-9
- HAMBURG WASSER. 2023. Starkregenindex. sri.hamburgwasser. <https://sri.hamburgwasser.de/>. Last accessed: 04.04.2023.
- HAMBURG WASSER, Laurich, F. 2022. pers. Comm.: N<sub>2</sub>O in der Elbe.
- Hanke, V.-R., and H.-D. Knauth. 1990. N<sub>2</sub>O-Gehalte in Wasser-und Luftproben aus den Bereichen der Tideelbe und der Deutschen Bucht. *75. 75 GKSS-Forschungszentrum*.
- Hansen, H. P., and F. Koroleff. 1999. Determination of nutrients, p. 159–228. *In* *Methods of Seawater Analysis*. John Wiley & Sons, Ltd. doi:10.1002/9783527613984.ch10
- Harley, J. F., L. Carvalho, B. Dudley, K. V. Heal, R. M. Rees, and U. Skiba. 2015. Spatial and seasonal fluxes of the greenhouse gases N<sub>2</sub>O, CO<sub>2</sub> and CH<sub>4</sub> in a UK macrotidal estuary. *Estuar. Coast. Shelf Sci.* **153**: 62–73. doi:10.1016/j.ecss.2014.12.004
- Hedges, J. I., and R. G. Keil. 1995. Sedimentary organic matter preservation: an assessment and speculative synthesis. *Mar. Chem.* **49**: 81–115. doi:10.1016/0304-4203(95)00008-F
- Hein, B., C. Viergutz, J. Wyrwa, V. Kirchesch, and A. Schöl. 2016. Impacts of climate change on the water quality of the Elbe Estuary (Germany). *J. Appl. Water Eng. Res.* **6**: 28–39. doi:10.1080/23249676.2016.1209438
- Hein, S. S. V., V. Sohrt, E. Nehlsen, T. Strotmann, and P. Fröhle. 2021. Tidal Oscillation and Resonance in Semi-Closed Estuaries—Empirical Analyses from the Elbe Estuary, North Sea. *Water* **13**: 848. doi:10.3390/w13060848

- 
- Heisler, J. P., P. Glibert, J. Burkholder, and others. 2008. Eutrophication and Harmful Algal Blooms: A Scientific Consensus. *Harmful Algae* **8**: 3–13. doi:10.1016/j.hal.2008.08.006
- Hereon, H.-Z. hereon, and D. W. DWD. 2023. Schleswig-Holstein u. Hamburg: Mittlere Windgeschwindigkeit (1986-2015)\* | Norddeutscher Klimamonitor. Norddtsch. Klimamonitor. <https://www.norddeutscher-klimamonitor.de/klima/1986-2015/jahr/mittlere-windgeschwindigkeit/schleswig-holstein-hamburg/coastdat-1.html>. Last accessed: 27.04.2023.
- Hillebrand, G., P. Hardenbicker, H. Fischer, W. Otto, and S. Vollmer. 2018. Dynamics of total suspended matter and phytoplankton loads in the river Elbe. *J. Soils Sediments* **18**: 3104–3113. doi:10.1007/s11368-018-1943-1
- Hobbie, J. 2000. Estuarine Science: The key to progress in coastal ecological research, p. 1–16. *In* Estuarine Science: A Synthetic Approach to Research and Practice. Island Press.
- Hoch, M. P., M. L. Fogel, and D. L. Kirchman. 1992. Isotope fractionation associated with ammonium uptake by a marine bacterium. *Limnol. Oceanogr.* **37**: 1447–1459. doi:10.4319/lo.1992.37.7.1447
- Hoefs, J. 2018. Stable Isotope Geochemistry, 8th ed. Springer International Publishing. doi:10.1007/978-3-319-78527-1
- Hofmann, J., H. Behrendt, A. Gilbert, and others. 2005. Catchment–coastal zone interaction based upon scenario and model analysis: Elbe and the German Bight case study. *Reg. Environ. Change* **5**: 54–81. doi:10.1007/s10113-004-0082-y
- Horrigan, S. G., J. P. Montoya, J. L. Nevins, and J. J. McCarthy. 1990. Natural isotopic composition of dissolved inorganic nitrogen in the Chesapeake Bay. *Estuar. Coast. Shelf Sci.* **30**: 393–410. doi:10.1016/0272-7714(90)90005-C
- Houlton, B. Z., and E. Bai. 2009. Imprint of denitrifying bacteria on the global terrestrial biosphere. *Proc. Natl. Acad. Sci.* **106**: 21713–21716. doi:10.1073/pnas.0912111106
- Howarth, R. W. 2008. Coastal nitrogen pollution: A review of sources and trends globally and regionally. *Harmful Algae* **8**: 14–20. doi:10.1016/j.hal.2008.08.015
- Howarth, R. W., and R. Marino. 2006. Nitrogen as the limiting nutrient for eutrophication in coastal marine ecosystems: Evolving views over three decades. *Limnol. Oceanogr.* **51**: 364–376. doi:10.4319/lo.2006.51.1\_part\_2.0364
- HPA, and Freie und Hansestadt Hamburg. 2017. Deutsches Gewässerkundliches Jahrbuch - Elbegebiet, Teil III, Untere Elbe ab der Havelmündung - 2014.
- HPA, Karrasch, M. 2022. pers. Comm.: Anfrage wegen N<sub>2</sub>O Peak - Baggerarbeiten Elbe März 2021 und März 2022.
- Hu, M., D. Chen, and R. A. Dahlgren. 2016. Modeling nitrous oxide emission from rivers: a global assessment. *Glob. Change Biol.* **22**: 3566–3582. doi:10.1111/gcb.13351
- IKSE. 2018. Strategie zur Minderung der Nährstoffeinträge in Gewässer in der internationalen Flussgebietsgemeinschaft Elbe. Internationale Kommission zur Schutz der Elbe.

- 
- INSC. 1987. Second International Conference on the Protection of the North Sea, London, 24-25 November 1987. Proceedings of the International Conference on the Protection of the North Sea. 12.
- IPCC. 2007. Climate Change 2007: The Physical Science Basis. Contribution of Working Group I to the Fourth Assessment Report of the Intergovernmental Panel on Climate Change, S. Solomon, D. Qin, M. Manning, M. Marquis, K. Averyt, M.M.B. Tignor, H.L.R. Miller, and Z. Chen [eds.]. Cambridge University Press.
- IPCC. 2021. Climate Change 2021: The Physical Science Basis. Contribution of Working Group I to the Sixth Assessment Report of the Intergovernmental Panel on Climate Change, V. Masson-Delmotte, P. Zhai, A. Pirani, et al. [eds.]. Cambridge University Press. doi:10.1017/9781009157896
- IPCC. 2022. Climate Change 2022: Impacts, Adaptation and Vulnerability. Contribution of Working Group II to the Sixth Assessment Report of the Intergovernmental Panel on Climate Change, H.-O. Pörtner, D.C. Roberts, M.M.B. Tignor, et al. [eds.]. Cambridge University Press. doi:10.1017/9781009325844
- Ivens, W. P. M. F., D. J. J. Tysmans, C. Kroeze, A. J. Löhr, and J. van Wijnen. 2011. Modeling global N<sub>2</sub>O emissions from aquatic systems. *Curr. Opin. Environ. Sustain.* **3**: 350–358. doi:10.1016/j.cosust.2011.07.007
- Jacob, J., B. Nowka, V. Merten, T. Sanders, E. Spieck, and K. Dähnke. 2017. Oxidation kinetics and inverse isotope effect of marine nitrite-oxidizing isolates. *Aquat. Microb. Ecol.* **80**: 289–300. doi:10.3354/ame01859
- Jacob, J., T. Sanders, and K. Dähnke. 2016. Nitrite consumption and associated isotope changes during a river flood event. *Biogeosciences* **13**: 5649–5659. doi:10.5194/bg-13-5649-2016
- Ji, Q., C. Frey, X. Sun, M. Jackson, Y.-S. Lee, A. Jayakumar, J. C. Cornwell, and B. B. Ward. 2018. Nitrogen and oxygen availabilities control water column nitrous oxide production during seasonal anoxia in the Chesapeake Bay. *Biogeosciences* **15**: 6127–6138. doi:10.5194/bg-15-6127-2018
- Johannsen, A., K. Dähnke, and K. Emeis. 2008. Isotopic composition of nitrate in five German rivers discharging into the North Sea. *Org. Geochem.* **39**: 1678–1689. doi:10.1016/j.orggeochem.2008.03.004
- de Jong, F. 2007. *Marine Eutrophication in Perspective*, Springer. doi:10.1007/3-540-33648-6
- de Jonge, V. N. 1983. Relations Between Annual Dredging Activities, Suspended Matter Concentrations, and the Development of the Tidal Regime in the Ems Estuary. *Can. J. Fish. Aquat. Sci.* **40**: 289–300. doi:10.1139/f83-290
- de Jonge, V. N., and H. Postma. 1974. Phosphorus compounds in the Dutch wadden sea. *Neth. J. Sea Res.* **8**: 139–153. doi:10.1016/0077-7579(74)90014-3
- de Jonge, V. N., and U. Schückel. 2019. Exploring effects of dredging and organic waste on the functioning and the quantitative biomass structure of the Ems estuary food web by applying Input Method balancing in Ecological Network Analysis. *Ocean Coast. Manag.* **174**: 38–55. doi:10.1016/j.ocecoaman.2019.03.013

- de Jonge, V. N., H. M. Schuttelaars, J. E. E. van Beusekom, S. A. Talke, and H. E. de Swart. 2014. The influence of channel deepening on estuarine turbidity levels and dynamics, as exemplified by the Ems estuary. *Estuar. Coast. Shelf Sci.* **139**: 46–59. doi:10.1016/j.ecss.2013.12.030
- Kamjunke, N., L.-M. Beckers, P. Herzsprung, and others. 2022. Lagrangian profiles of riverine autotrophy, organic matter transformation, and micropollutants at extreme drought. *Sci. Total Environ.* **828**: 154243. doi:10.1016/j.scitotenv.2022.154243
- Kamjunke, N., M. Rode, M. Baborowski, J. Kunz, J. Zehner, D. Borchardt, and M. Weitere. 2021. High irradiation and low discharge promote the dominant role of phytoplankton in riverine nutrient dynamics. *Limnol. Oceanogr.* **66**. doi:10.1002/lno.11778
- Kappenberg, J., and H.-U. Fanger. 2007. Sedimenttransportgeschehen in der tidebeeinflussten Elbe, der Deutschen Bucht und in der Nordsee. Report GKSS 2007/20. GKSS 2007/20 GKSS-Forschungszentrum.
- Karl, D., R. Letelier, L. Tupas, J. Dore, J. Christian, and D. Hebel. 1997. The role of nitrogen fixation in biogeochemical cycling in the subtropical North Pacific Ocean. *Nature* **388**: 533–538. doi:10.1038/41474
- Karrasch, B., M. Mehrens, Y. Rosenlöcher, and K. Peters. 2001. The dynamics of phytoplankton, bacteria and heterotrophic flagellates at two Banks near Magdeburg in the River Elbe (Germany). *Limnologica* **31**: 93–107. doi:10.1016/S0075-9511(01)80002-5
- Kassambara, A. 2023. ggpubr: “ggplot2” Based Publication Ready Plots.
- Kempe, S. 1988. Estuaries - their natural and anthropogenic changes, p. 251–285. *In* T. Rosswall, R.G. Woodmansee, and P.G. Risser [eds.], *Scales and Global Change*. John Wiley & Sons Ltd.
- Kendall, C. 1998. Chapter 16 - Tracing Nitrogen Sources and Cycling in Catchments, p. 519–576. *In* C. Kendall and J.J. McDonnell [eds.], *Isotope Tracers in Catchment Hydrology*. Elsevier. doi:10.1016/B978-0-444-81546-0.50023-9
- Kendall, C., E. M. Elliott, and S. D. Wankel. 2007. Tracing Anthropogenic Inputs of Nitrogen to Ecosystems, p. 375–449. *In* *Stable Isotopes in Ecology and Environmental Science*. John Wiley & Sons, Ltd. doi:10.1002/9780470691854
- Kennish, M. J. 2005. Estuaries, Anthropogenic Impacts, p. 434–436. *In* M.L. Schwartz [ed.], *Encyclopedia of Coastal Science*. Springer Netherlands. doi:10.1007/1-4020-3880-1\_140
- Kennish, M. J. 2017. Estuaries: Anthropogenic Impacts, p. 1–9. *In* C.W. Finkl and C. Makowski [eds.], *Encyclopedia of Coastal Science*. Springer International Publishing. doi:10.1007/978-3-319-48657-4\_140-2
- Kerner, M. 2000. Interactions between local oxygen deficiencies and heterotrophic microbial processes in the elbe estuary. *Limnologica* **30**: 137–143. doi:10.1016/S0075-9511(00)80008-0
- Kerner, M. 2007. Effects of deepening the Elbe Estuary on sediment regime and water quality. *Estuar. Coast. Shelf Sci.* **75**: 492–500. doi:10.1016/j.ecss.2007.05.033

- Kerner, M., and A. Spitzky. 2001. Nitrate Regeneration Coupled to Degradation of Different Size Fractions of DON by the Picoplankton in the Elbe Estuary. *Microb. Ecol.* **41**: 69–81. doi:10.1007/s002480000031
- van Kessel, M. A. H. J., D. R. Speth, M. Albertsen, P. H. Nielsen, H. J. M. Op den Camp, B. Kartal, M. S. M. Jetten, and S. Lücker. 2015. Complete nitrification by a single microorganism. *Nature* **528**: 555–559. doi:10.1038/nature16459
- Kirchman, D. L. 1994. The uptake of inorganic nutrients by heterotrophic bacteria. *Microb. Ecol.* **28**: 255–271. doi:10.1007/BF00166816
- Knapp, A. N., P. J. DiFiore, C. Deutsch, D. M. Sigman, and F. Lipschultz. 2008. Nitrate isotopic composition between Bermuda and Puerto Rico: Implications for N<sub>2</sub> fixation in the Atlantic Ocean. *Glob. Biogeochem. Cycles* **22**: GB3014. doi:10.1029/2007GB003107
- Knowles, R. 1982. Denitrification. *Microbiol. Rev.* **46**: 43–70. doi:10.1128/mr.46.1.43-70.1982
- Koch, M. S., E. Maltby, G. A. Oliver, and S. A. Bakker. 1992. Factors controlling denitrification rates of tidal mudflats and fringing salt marshes in south-west England. *Estuar. Coast. Shelf Sci.* **34**: 471–485. doi:10.1016/S0272-7714(05)80118-0
- Köhler, J., M. Bahnwart, and K. Ockenfeld. 2002. Growth and Loss Processes of Riverine Phytoplankton in Relation to Water Depth. *Int. Rev. Hydrobiol.* **87**: 241–254. doi:10.1002/1522-2632(200205)87:2/3<241::AID-IROH241>3.0.CO;2-A
- Korth, F., B. Deutsch, C. Frey, C. Moros, and M. Voss. 2014. Nitrate source identification in the Baltic Sea using its isotopic ratios in combination with a Bayesian isotope mixing model. *Biogeosciences* **11**: 4913–4924. doi:10.5194/bg-11-4913-2014
- Krebs, M., and H. Weilbeer. 2008. Ems-Dollart Estuary. *Küste* **74**: 252–262.
- Kroeze, C., E. Dumont, and S. Seitzinger. 2010. Future trends in emissions of N<sub>2</sub>O from rivers and estuaries. *J. Integr. Environ. Sci.* **7**: 71–78. doi:10.1080/1943815X.2010.496789
- Kroeze, C., E. Dumont, and S. P. Seitzinger. 2005. New estimates of global emissions of N<sub>2</sub>O from rivers and estuaries. *Environ. Sci.* **2**: 159–165. doi:10.1080/15693430500384671
- Lehmann, M. F., D. M. Sigman, and W. M. Berelson. 2004. Coupling the <sup>15</sup>N/<sup>14</sup>N and <sup>18</sup>O/<sup>16</sup>O of nitrate as a constraint on benthic nitrogen cycling. *Mar. Chem.* **88**: 1–20. doi:10.1016/j.marchem.2004.02.001
- Lewicka-Szczebak, D., J. Augustin, A. Giesemann, and R. Well. 2017. Quantifying N<sub>2</sub>O reduction to N<sub>2</sub> based on N<sub>2</sub>O isotopocules – validation with independent methods (helium incubation and <sup>15</sup>N gas flux method). *Biogeosciences* **14**: 711–732. doi:10.5194/bg-14-711-2017
- Liss, P. S. 1976. Conservative and non-conservative behavior of dissolved constituents during estuarine mixing, p. 93–130. *In* D.L. Burton and P.S. Liss [eds.], *Estuarine chemistry*. Academic Press.
- Liu, B., H. E. de Swart, and V. N. de Jonge. 2018. Phytoplankton bloom dynamics in turbid, well-mixed estuaries: A model study. *Estuar. Coast. Shelf Sci.* **211**: 137–151. doi:10.1016/j.ecss.2018.01.010

- 
- Liu, T., X. Xia, S. Liu, X. Mou, and Y. Qiu. 2013. Acceleration of denitrification in turbid rivers due to denitrification occurring on suspended sediment in oxic waters. *Environ. Sci. Technol.* **47**: 4053–4061. doi:10.1021/es304504m
- Loisel, J., A. V. Gallego-Sala, and Z. Yu. 2012. Global-scale pattern of peatland *Sphagnum* growth driven by photosynthetically active radiation and growing season length. *Biogeosciences* **9**: 2737–2746. doi:10.5194/bg-9-2737-2012
- Lutz, S. R., N. Trauth, A. Musolff, B. M. Van Breukelen, K. Knöller, and J. H. Fleckenstein. 2020. How Important is Denitrification in Riparian Zones? Combining End-Member Mixing and Isotope Modeling to Quantify Nitrate Removal from Riparian Groundwater. *Water Resour. Res.* **56**: e2019WR025528. doi:10.1029/2019WR025528
- Maavara, T., R. Lauerwald, G. G. Laruelle, Z. Akbarzadeh, N. J. Bouskill, P. Van Cappellen, and P. Regnier. 2019. Nitrous oxide emissions from inland waters: Are IPCC estimates too high? *Glob. Change Biol.* **25**: 473–488. doi:10.1111/gcb.14504
- van Maren, D. S., T. van Kessel, K. Cronin, and L. Sittoni. 2015a. The impact of channel deepening and dredging on estuarine sediment concentration. *Cont. Shelf Res.* **95**: 1–14. doi:10.1016/j.csr.2014.12.010
- van Maren, D. S., J. C. Winterwerp, and J. Vroom. 2015b. Fine sediment transport into the hyper-turbid lower Ems River: the role of channel deepening and sediment-induced drag reduction. *Ocean Dyn.* **65**: 589–605. doi:10.1007/s10236-015-0821-2
- van Maren, D. S., J. C. Winterwerp, Z. Y. Wang, and Q. Pu. 2009. Suspended sediment dynamics and morphodynamics in the Yellow River, China. *Sedimentology* **56**: 785–806. doi:10.1111/j.1365-3091.2008.00997.x
- Mariotti, A., J. C. Germon, P. Hubert, P. Kaiser, R. Letolle, A. Tardieux, and P. Tardieux. 1981. Experimental determination of nitrogen kinetic isotope fractionation: Some principles; illustration for the denitrification and nitrification processes. *Plant Soil* **62**: 413–430. doi:10.1007/BF02374138
- Marzadri, A., M. M. Dee, D. Tonina, A. Bellin, and J. L. Tank. 2017. Role of surface and subsurface processes in scaling N<sub>2</sub>O emissions along riverine networks. *Proc. Natl. Acad. Sci.* **114**: 4330–4335. doi:10.1073/pnas.1617454114
- McMichael, C., S. Dasgupta, S. Ayeb-Karlsson, and I. Kelman. 2020. A review of estimating population exposure to sea-level rise and the relevance for migration. *Environ. Res. Lett.* **15**: 123005. doi:10.1088/1748-9326/abb398
- Megonigal, J. P., M. E. Hines, and P. T. Visscher. 2004. Anaerobic Metabolism: Linkages to Trace Gases and Aerobic Processes, p. 317–424. *In* W.H. Schlesinger [ed.], *Biogeochemistry*. doi:10.1016/B0-08-043751-6/08132-9
- Mengis, M., S. L. Schiff, M. Harris, M. C. English, R. Aravena, R. Elgood, and A. MacLean. 1999. Multiple Geochemical and Isotopic Approaches for Assessing Ground Water NO<sub>3</sub><sup>-</sup> Elimination in a Riparian Zone. *Groundwater* **37**: 448–457. doi:10.1111/j.1745-6584.1999.tb01124.x
- Middelburg, J. J., and P. M. J. Herman. 2007. Organic matter processing in tidal estuaries. *Mar. Chem.* **106**: 127–147. doi:10.1016/j.marchem.2006.02.007

- 
- Middelburg, J. J., and J. Nieuwenhuize. 2000. Uptake of dissolved inorganic nitrogen in turbid, tidal estuaries. *Mar. Ecol.-Prog. Ser.* **192**: 79–88. doi:10.3354/meps192079
- Möbius, J. 2013. Isotope fractionation during nitrogen remineralization (ammonification): Implications for nitrogen isotope biogeochemistry. *Geochim. Cosmochim. Acta* **105**: 422–432. doi:10.1016/j.gca.2012.11.048
- Murray, R. H., D. V. Erler, and B. D. Eyre. 2015. Nitrous oxide fluxes in estuarine environments: response to global change. *Glob. Change Biol.* **21**: 3219–3245. doi:10.1111/gcb.12923
- Needoba, J. A., and P. J. Harrison. 2004. Influence of Low Light and a Light: Dark Cycle on  $\text{NO}_3^-$  Uptake, Intracellular  $\text{NO}_3^-$ , and Nitrogen Isotope Fractionation by Marine Phytoplankton I. *J. Phycol.* **40**: 505–516. doi:10.1111/j.1529-8817.2004.03171.x
- Nevison, C., J. H. Butler, and J. W. Elkins. 2003. Global distribution of  $\text{N}_2\text{O}$  and the  $\Delta\text{N}_2\text{O}$ -AOU yield in the subsurface ocean. *Glob. Biogeochem. Cycles* **17**: 1119. doi:10.1029/2003GB002068
- Nicholls, R. J., and C. Small. 2002. Improved estimates of coastal population and exposure to hazards released. *Eos Trans. Am. Geophys. Union* **83**: 301–305. doi:10.1029/2002EO000216
- Nightingale, P. D., G. Malin, C. S. Law, A. J. Watson, P. S. Liss, M. I. Liddicoat, J. Boutin, and R. C. Upstill-Goddard. 2000. In situ evaluation of air-sea gas exchange parameterizations using novel conservative and volatile tracers. *Glob. Biogeochem. Cycles* **14**: 373–387. doi:10.1029/1999GB900091
- Nixon, S. W. 1981. Remineralization and Nutrient Cycling in Coastal Marine Ecosystems, p. 111–138. *In* B.J. Neilson and L.E. Cronin [eds.], *Estuaries and Nutrients*. Humana Press. doi:10.1007/978-1-4612-5826-1\_6
- Nixon, S. W., J. W. Ammerman, L. P. Atkinson, and others. 1996. The fate of nitrogen and phosphorus at the land-sea margin of the North Atlantic Ocean. *Biogeochemistry* **35**: 141–180. doi:10.1007/BF02179826
- NLWKN, ed. 2018. *Deutsches Gewässerkundliches Jahrbuch - Weser- und Emsgebiet 2015* (1.11.2014-31.12.2015), Niedersächsischer Landesbetrieb für Wasserwirtschaft, Küsten- und Naturschutz.
- NLWKN Bst. Aurich, and A. Engels. 2021. *Abflussdaten Ems Ästuar (Pegeldaten Gandersum)*.
- Norbisrath, M., J. Pätsch, K. Dähnke, T. Sanders, G. Schulz, J. E. E. van Beusekom, and H. Thomas. 2022. Metabolic alkalinity release from large port facilities (Hamburg, Germany) and impact on coastal carbon storage. *Biogeosciences* **19**: 5151–5165. doi:10.5194/bg-19-5151-2022
- Nunes, R. A., and J. H. Simpson. 1985. Axial convergence in a well-mixed estuary. *Estuar. Coast. Shelf Sci.* **20**: 637–649. doi:10.1016/0272-7714(85)90112-X
- Ogilvie, B., D. B. Nedwell, R. M. Harrison, A. Robinson, and A. Sage. 1997. High nitrate, muddy estuaries as nitrogen sinks: the nitrogen budget of the River Colne estuary (United Kingdom). *Mar. Ecol. Prog. Ser.* **150**: 217–228. doi:10.3354/meps150217
- Opdyke, M. R., M. B. David, and B. L. Rhoads. 2006. Influence of Geomorphological Variability in Channel Characteristics on Sediment Denitrification in Agricultural Streams. *J. Environ. Qual.* **35**: 2103–2112. doi:10.2134/jeq2006.0072

- 
- Orth, R. J., T. J. B. Carruthers, W. C. Dennison, and others. 2006. A Global Crisis for Seagrass Ecosystems. *BioScience* **56**: 987–996. doi:10.1641/0006-3568(2006)56[987:AGCFSE]2.0.CO;2
- OSPAR. 1988. PARCOM recommendation 88/2: On the reduction in inputs of nutrients to the Paris Convention area. 88/2. 88/2 Paris Commission.
- OSPAR. 2021. Strategy of the OSPAR Commission for the Protection of the Marine Environment of the North-East Atlantic 2030 (Agreement 2021-01: North-East Atlantic Environment Strategy (replacing Agreement 2010-03)). OSPAR Agreement 2021-01. OSPAR Agreement 2021-01 OSPAR Commission.
- Otte, S., J. Schalk, J. G. Kuenen, and M. S. M. Jetten. 1999. Hydroxylamine oxidation and subsequent nitrous oxide production by the heterotrophic ammonia oxidizer *Alcaligenes faecalis*. *Appl. Microbiol. Biotechnol.* **51**: 255–261. doi:10.1007/s002530051390
- Papenmeier, S., K. Schrottke, A. Bartholomä, and B. W. Flemming. 2013. Sedimentological and Rheological Properties of the Water–Solid Bed Interface in the Weser and Ems Estuaries, North Sea, Germany: Implications for Fluid Mud Classification. *J. Coast. Res.* **29**: 797–808. doi:10.2112/JCOASTRES-D-11-00144.1
- Pareja-Roman, L. F., R. J. Chant, and C. K. Sommerfield. 2020. Impact of Historical Channel Deepening on Tidal Hydraulics in the Delaware Estuary. *J. Geophys. Res. Oceans* **125**: e2020JC016256. doi:10.1029/2020JC016256
- Pätsch, J., and H.-J. Lenhart. 2011. Daily Loads of Nutrients, Total Alkalinity, Dissolved Inorganic Carbon and Dissolved Organic Carbon of the European Continental Rivers for the Years 1977 – 2009. Institut für Meereskunde der Universität Hamburg.
- Pätsch, J., A. Serna, K. Dähnke, T. Schlarbaum, A. Johannsen, and K.-C. Emeis. 2010. Nitrogen cycling in the German Bight (SE North Sea) — Clues from modelling stable nitrogen isotopes. *Cont. Shelf Res.* **30**: 203–213. doi:10.1016/j.csr.2009.11.003
- Pein, J., A. Eisele, T. Sanders, U. Daewel, E. Stanev, J. E. E. van Beusekom, J. Staneva, and C. Schrum. 2021. Seasonal Stratification and Biogeochemical Turnover in the Freshwater Reach of a Partially Mixed Dredged Estuary. *Front. Mar. Sci.* **8**: 623714. doi:10.3389/fmars.2021.623714
- Petersen, W., F. Schroeder, and F.-D. Bockelmann. 2011. FerryBox - Application of continuous water quality observations along transects in the North Sea. *Ocean Dyn.* **61**: 1541–1554. doi:10.1007/s10236-011-0445-0
- Pind, A., N. Risgaard-Petersen, and N. P. Revsbech. 1997. Denitrification and microphytobenthic NO<sub>3</sub><sup>-</sup> consumption in a Danish lowland stream: diurnal and seasonal variation. *Aquat. Microb. Ecol.* **12**: 275–284. doi:10.3354/ame012275
- Port of Hamburg. 2021. HAFEN HAMBURG: Willkommen auf der offiziellen Webseite des größten deutschen Seehafens. Off. Webseite Hambg. Hafens. <http://www.portblog.de/de/startseite/>. Last accessed: 24.09.2021.
- Quick, A. M., W. J. Reeder, T. B. Farrell, D. Tonina, K. P. Feris, and S. G. Benner. 2019. Nitrous oxide from streams and rivers: A review of primary biogeochemical pathways and environmental variables. *Earth-Sci. Rev.* **191**: 224–262. doi:10.1016/j.earscirev.2019.02.021

- 
- Quiel, K., A. Becker, V. Kirchesch, A. Schöl, and H. Fischer. 2011. Influence of global change on phytoplankton and nutrient cycling in the Elbe River. *Reg. Environ. Change* **11**: 405–421. doi:10.1007/s10113-010-0152-2
- R Core Team and contributors worldwide. 2020. The R Stats Package, Version 4.0.2. RDocumentation - Pcomp.
- Radach, G., and J. Pätsch. 2007. Variability of continental riverine freshwater and nutrient inputs into the North Sea for the years 1977–2000 and its consequences for the assessment of eutrophication. *Estuaries Coasts* **30**: 66–81. doi:10.1007/BF02782968
- Reading, M. J., D. R. Tait, D. T. Maher, and others. 2020. Land use drives nitrous oxide dynamics in estuaries on regional and global scales. *Limnol. Oceanogr.* **65**: 1903–1920. doi:10.1002/lno.11426
- Redfield, A. C., B. H. Ketchum, and F. A. Richards. 1963. The influence of organisms on the composition of sea-water M.N. Hill [ed.]. *Compos. Seawater Comp. Descr. Oceanogr. Sea Ideas Obs. Prog. Study Seas* **2**: 26–77.
- Révész, K., J. K. Böhlke, and T. Yoshinari. 1997. Determination of  $\delta^{18}\text{O}$  and  $\delta^{15}\text{N}$  in Nitrate. *Anal. Chem.* **69**: 4375–4380. doi:10.1021/ac9610523
- Rewrie, L. C. V., B. Baschek, J. E. E. Beusekom, A. Körtzinger, G. Ollesch, and Y. G. Voynova. 2023. Recent inorganic carbon increase in a temperate estuary driven by water quality improvement and enhanced by droughts. *EGUsphere* 1–28. doi:10.5194/egusphere-2023-961
- Rewrie, L. C. V., Y. G. Voynova, J. E. E. van Beusekom, T. Sanders, A. Körtzinger, H. Brix, G. Ollesch, and B. Baschek. submitted. Significant shifts in inorganic carbon and ecosystem state in a temperate estuary (1985 - 2018). *Limnol. Oceanogr.*
- Reynolds, C. S., and J.-P. Descy. 1996. The production, biomass and structure of phytoplankton in large rivers. *Arch Hydrobiol Suppl Large Rivers* **10**: 161–187. doi:10.1127/lr/10/1996/161
- Rhee, T. S. 2000. The process of air-water gas exchange and its application. Texas A&M University.
- Rhee, T. S., A. J. Kettle, and M. O. Andreae. 2009. Methane and nitrous oxide emissions from the ocean: A reassessment using basin-wide observations in the Atlantic. *J. Geophys. Res. Atmospheres* **114**: D12304. doi:10.1029/2008JD011662
- Ritz, S., and H. Fischer. 2019. A Mass Balance of Nitrogen in a Large Lowland River (Elbe, Germany). *Water* **11**: 2383. doi:10.3390/w11112383
- Robinson, A. D., D. B. Nedwell, R. M. Harrison, and B. G. Ogilvie. 1998. Hypernutrified estuaries as sources of  $\text{N}_2\text{O}$  emission to the atmosphere: the estuary of the River Colne, Essex, UK. *Mar. Ecol. Prog. Ser.* **164**: 59–71. doi:10.3354/meps164059
- Rohde, M. M., J. Granger, D. M. Sigman, and M. F. Lehmann. 2015. Coupled nitrate N and O stable isotope fractionation by a natural marine plankton consortium. *Front. Mar. Sci.* **2**: 28. doi:10.3389/fmars.2015.00028

- Rosenhagen, G., M. Schatzmann, and A. Schrön. 2011. Das Klima der Metropolregion auf Grundlage meteorologischer Messungen und Beobachtungen, p. 19–59. *In* H. Von Storch and M. Claussen [eds.], *Klimabericht für die Metropolregion Hamburg*. Springer. doi:10.1007/978-3-642-16035-6\_2
- Rosentreter, J. A., N. S. Wells, A. J. Ulseth, and B. D. Eyre. 2021. Divergent Gas Transfer Velocities of CO<sub>2</sub>, CH<sub>4</sub>, and N<sub>2</sub>O Over Spatial and Temporal Gradients in a Subtropical Estuary. *J. Geophys. Res. Biogeosciences* **126**: e2021JG006270. doi:10.1029/2021JG006270
- Röttgers, R., K. Heymann, and H. Krasemann. 2014. Suspended matter concentrations in coastal waters: Methodological improvements to quantify individual measurement uncertainty. *Estuar. Coast. Shelf Sci.* **151**: 148–155. doi:10.1016/j.ecss.2014.10.010
- Sanders, T. unpublished data.
- Sanders, T., and K. Dähnke. 2014. The Elbe river estuary including the Port of Hamburg - an important Nutrient filter and source for reactive Nitrogen? Proceedings of the EGU General Assembly Conference 2014. EGU2013-5061.
- Sanders, T., and H. J. Laanbroek. 2018. The distribution of sediment and water column nitrification potential in the hyper-turbid Ems estuary. *Aquat. Sci.* **80**: 33. doi:10.1007/s00027-018-0584-1
- Sanders, T., A. Schöl, and K. Dähnke. 2018. Hot Spots of Nitrification in the Elbe Estuary and Their Impact on Nitrate Regeneration. *Estuaries Coasts* **41**: 128–138. doi:10.1007/s12237-017-0264-8
- Santoro, A. E., and K. L. Casciotti. 2011. Enrichment and characterization of ammonia-oxidizing archaea from the open ocean: phylogeny, physiology and stable isotope fractionation. *ISME J.* **5**: 1796–1808. doi:10.1038/ismej.2011.58
- Scharfe, M., U. Callies, G. Blöcker, W. Petersen, and F. Schroeder. 2009. A simple Lagrangian model to simulate temporal variability of algae in the Elbe River. *Ecol. Model.* **220**: 2173–2186. doi:10.1016/j.ecolmodel.2009.04.048
- Schlarbaum, T., K. Dähnke, and K. Emeis. 2011. Dissolved and particulate reactive nitrogen in the Elbe River/NW Europe: a 2-yr N-isotope study. *Biogeosciences* **8**: 3519–3530. doi:10.5194/bg-8-3519-2011
- Schloerke, B., J. Larmarange, F. Briatte, and others. 2020. GGally: Extension to “ggplot2.” RDocumentation - GGally.
- Schoer, J. H. 1990. Determination of the origin of suspended matter and sediments in the Elbe estuary using natural tracers. *Estuaries* **13**: 161–172. doi:10.2307/1351585
- Schöl, A., B. Hein, J. Wyrwa, and V. Kirchesch. 2014. Modelling Water Quality in the Elbe and its Estuary – Large Scale and Long Term Applications with Focus on the Oxygen Budget of the Estuary. *Küste* 203–232.
- Schröder, F., K. H. Wiltshire, D. Klages, B. Mathieu, and H. D. Knauth. 1996. Nitrogen and oxygen processes in sediments of the Elbe Estuary. *Arch. Für Hydrobiol. Suppl* **110**: 311–328.

- Schroeder, F. 1997. Water quality in the Elbe estuary: Significance of different processes for the oxygen deficit at Hamburg. *Environ. Model. Assess.* **2**: 73–82. doi:10.1023/A:1019032504922
- Schuchardt, B., and J. Scholle. 2009. Estuaries. Thematic Report No. 16. 25. 25 Common Wadden Sea Secretariat, Trilateral Monitoring and Assessment Group.
- Schuchardt, B., and J. Scholle. 2017. Estuaries, *In* Wadden Sea Quality Status Report. Common Wadden Sea Secretariat.
- Schuchardt, B., J. Scholle, S. Schulze, and T. Bildstein. 2007. Vergleichende Bewertung der ökologischen Situation der inneren Ästuarie von Eider, Elbe, Weser und Ems: Was hat sich nach 20 Jahren verändert?, p. 15–25. *In* G. Gönnert, B. Pflüger, and J.A. Bremer [eds.], *Von der Geoarchäologie über die Küstendynamik zum Küstenzonenmanagement*.
- Schulz, G., J. E. E. van Beusekom, J. Jacob, S. Bold, A. Schöl, M. Ankele, T. Sanders, and K. Dähnke. submitted. Low discharge intensifies nitrogen retention in rivers – a case study in the Elbe River. *Sci. Total Environ.*
- Schulz, G., T. Sanders, J. E. E. van Beusekom, Y. G. Voynova, A. Schöl, and K. Dähnke. 2022. Suspended particulate matter drives the spatial segregation of nitrogen turnover along the hyper-turbid Ems estuary. *Biogeosciences* **19**: 2007–2024. doi:10.5194/bg-19-2007-2022
- Schulz, G., T. Sanders, Y. G. Voynova, H. W. Bange, and K. Dähnke. 2023. Seasonal variability of nitrous oxide concentrations and emissions along the Elbe estuary. *Biogeosciences Discuss.* 1–21. doi:10.5194/bg-2023-35
- Seitzinger, S. P. 1988. Denitrification in freshwater and coastal marine ecosystems: Ecological and geochemical significance. *Limnol. Oceanogr.* **33**: 702–724. doi:10.4319/lo.1988.33.4part2.0702
- Sharma, N., E. D. Flynn, J. G. Catalano, and D. E. Giammar. 2022. Copper availability governs nitrous oxide accumulation in wetland soils and stream sediments. *Geochim. Cosmochim. Acta* **327**: 96–115. doi:10.1016/j.gca.2022.04.019
- Siedler, G., and H. Peters. 1986. Properties of sea water, Physical properties, p. 233–264. *In* J. Sündermann [ed.], *Oceanography*. Springer.
- Sigman, D. M., M. A. Altabet, D. C. McCorkle, R. Francois, and G. Fischer. 2000. The  $\delta^{15}\text{N}$  of nitrate in the Southern Ocean: Nitrogen cycling and circulation in the ocean interior. *J. Geophys. Res. Oceans* **105**: 19599–19614. doi:10.1029/2000JC000265
- Sigman, D. M., K. L. Casciotti, M. Andreani, C. Barford, M. Galanter, and J. K. Böhlke. 2001. A Bacterial Method for the Nitrogen Isotopic Analysis of Nitrate in Seawater and Freshwater. *Anal. Chem.* **73**: 4145–4153. doi:10.1021/ac010088e
- Sigman, D. M., and F. Fripiat. 2019. Nitrogen Isotopes in the Ocean J.K. Cochran, H.J. Bokuniewicz, and P.L. Yager [eds.]. *Encycl. Ocean Sci.* Third Ed. **1**: 263–278. doi:10.1016/B978-0-12-409548-9.11605-7
- Sigman, D. M., K. L. Karsh, and K. L. Casciotti. 2009. Nitrogen isotopes in the ocean, p. 40–54. *In* J. Steele, S. Thorpe, and K. Turekian [eds.], *Encyclopedia of Ocean Sciences*. Academic Press. doi:10.1016/B978-012374473-9.00632-9

- Silvennoinen, H., S. Hietanen, A. Liikanen, C. F. Stange, R. Russow, J. Kuparinen, and P. J. Martikainen. 2007. Denitrification in the River Estuaries of the Northern Baltic Sea. *AMBIO J. Hum. Environ.* **36**: 134–140. doi:10.1579/0044-7447(2007)36[134:DITREO]2.0.CO;2
- Soetaert, K., J. J. Middelburg, C. Heip, P. Meire, S. V. Damme, and T. Maris. 2006. Long-term change in dissolved inorganic nutrients in the heterotrophic Scheldt estuary (Belgium, The Netherlands). *Limnol. Oceanogr.* **51**: 409–423. doi:10.4319/lo.2006.51.1\_part\_2.0409
- Sommerfield, C. K., and K.-C. Wong. 2011. Mechanisms of sediment flux and turbidity maintenance in the Delaware Estuary. *J. Geophys. Res. Oceans* **116**: C01005. doi:10.1029/2010JC006462
- Statistisches Bundesamt. 2023. Regionales. Stat. Bundesamt. [https://www.destatis.de/DE/Themen/Laender-Regionen/Regionales/\\_inhalt.html](https://www.destatis.de/DE/Themen/Laender-Regionen/Regionales/_inhalt.html). Last accessed: 29.03.2023.
- Strous, M., J. A. Fuerst, E. H. M. Kramer, and others. 1999. Missing lithotroph identified as new planctomycete. *Nature* **400**: 446–449. doi:10.1038/22749
- Sulzman, E. W. 2007. Stable Isotope Chemistry and Measurement: A Primer, p. 1–21. *In* R. Michener and K. Lajtha [eds.], *Stable Isotopes in Ecology and Environmental Science*. John Wiley & Sons, Ltd. doi:10.1002/9780470691854.ch1
- Sutka, R. L., N. E. Ostrom, P. H. Ostrom, J. A. Breznak, H. Gandhi, A. J. Pitt, and F. Li. 2006. Distinguishing Nitrous Oxide Production from Nitrification and Denitrification on the Basis of Isotopomer Abundances. *Appl. Environ. Microbiol.* **72**: 638–644. doi:10.1128/AEM.72.1.638-644.2006
- Talke, S. A., H. E. de Swart, and V. N. de Jonge. 2009. An Idealized Model and Systematic Process Study of Oxygen Depletion in Highly Turbid Estuaries. *Estuaries Coasts* **32**: 602–620. doi:10.1007/s12237-009-9171-y
- Talke, S., and H. E. de Swart. 2006. Hydrodynamics and Morphology in the Ems/Dollard Estuary: Review of Models, Measurements, Scientific Literature, and the Effects of Changing Conditions. R06-01. R06-01 Institute for Marine and Atmospheric Research, University of Utrecht.
- Tang, W., J. C. Tracey, J. Carroll, and others. 2022. Nitrous oxide production in the Chesapeake Bay. *Limnol. Oceanogr.* **67**: 2101–2116. doi:10.1002/lno.12191
- Thornton, D. C. O., L. F. Dong, G. J. C. Underwood, and D. B. Nedwell. 2007. Sediment–water inorganic nutrient exchange and nitrogen budgets in the Colne Estuary, UK. *Mar Ecol Prog Ser* **337**: 63–77. doi:10.3354/meps337063
- Tian, H., R. Xu, J. G. Canadell, and others. 2020. A comprehensive quantification of global nitrous oxide sources and sinks. *Nature* **586**: 248–256. doi:10.1038/s41586-020-2780-0
- Tian, S., B. Gaye, J. Tang, and others. 2022. A nitrate budget of the Bohai Sea based on an isotope mass balance model. *Biogeosciences* **19**: 2397–2415. doi:10.5194/bg-19-2397-2022
- Tiedje, J. M. 1988. Ecology of denitrification and dissimilatory nitrate reduction to ammonium, p. 179–244. *In* A.J.B. Zehnder [ed.], *Biology of anaerobic microorganisms*. John Wiley and Sons.

- Toyoda, S., O. Yoshida, H. Yamagishi, A. Fujii, N. Yoshida, and S. Watanabe. 2019. Identifying the origin of nitrous oxide dissolved in deep ocean by concentration and isotopocule analyses. *Sci. Rep.* **9**: 7790. doi:10.1038/s41598-019-44224-0
- Trimmer, M., J. C. Nicholls, and B. Deflandre. 2003. Anaerobic Ammonium Oxidation Measured in Sediments along the Thames Estuary, United Kingdom. *Appl. Environ. Microbiol.* **69**: 6447–6454. doi:10.1128/AEM.69.11.6447-6454.2003
- UBA. 2015. Reactive nitrogen in Germany, Umweltbundesamt. <https://www.umweltbundesamt.de/en/publikationen/reactive-nitrogen-in-germany>. Last accessed: 24.04.2023.
- UBA. 2017. Wasserwirtschaft in Deutschland - Grundlagen, Belastungen, Maßnahmen, Umweltbundesamt. <https://www.umweltbundesamt.de/publikationen/wasserwirtschaft-in-deutschland-grundlagen>. Last accessed: 24.04.2023.
- UBA. 2020. Stickstoff- und Phosphoreinträge aus Punktquellen und diffusen Quellen in die Oberflächengewässer in Deutschland. Umweltbundesamt. [https://www.umweltbundesamt.de/sites/default/files/medien/384/bilder/dateien/2\\_abb\\_n-p-eintraege\\_2020-09-17.xlsx](https://www.umweltbundesamt.de/sites/default/files/medien/384/bilder/dateien/2_abb_n-p-eintraege_2020-09-17.xlsx). Last accessed: 21.11.2022.
- US EPA, 2006. Volunteer Estuary Monitoring: A Methods Manual. Data and Tools EPA-842-B-06-003. EPA-842-B-06-003 United States Environmental Protection Agency (EPA).
- Voss, M., A. Baker, H. W. Bange, and others. 2011. Nitrogen processes in coastal and marine ecosystems, p. 147–176. *In* A. Bleeker, B. Grizzetti, C.M. Howard, G. Billen, H. Van Grinsven, J.W. Erisman, M.A. Sutton, and P. Grennfelt [eds.], *The European Nitrogen Assessment: Sources, Effects and Policy Perspectives*. Cambridge University Press. doi:10.1017/CBO9780511976988.011
- Voss, M., G. Nausch, and J. Montoya. 1997. Nitrogen stable isotope dynamics in the central Baltic Sea: Influence of deep-water renewal on the N-cycle changes. *Mar. Ecol.-Prog. Ser. - MAR ECOL-PROGR SER* **158**: 11–21. doi:10.3354/meps158011
- Walter, S., H. W. Bange, and D. W. R. Wallace. 2004. Nitrous oxide in the surface layer of the tropical North Atlantic Ocean along a west to east transect. *Geophys. Res. Lett.* **31**: L23S07. doi:10.1029/2004GL019937
- Wang, M., T. R. Moore, J. Talbot, and J. L. Riley. 2015. The stoichiometry of carbon and nutrients in peat formation. *Glob. Biogeochem. Cycles* **29**: 113–121. doi:10.1002/2014GB005000
- Wankel, S. D., C. Kendall, C. A. Francis, and A. Paytan. 2006. Nitrogen sources and cycling in the San Francisco Bay Estuary: A nitrate dual isotopic composition approach. *Limnol. Oceanogr.* **51**: 1654–1664. doi:10.4319/lo.2006.51.4.1654
- Wanninkhof, R. 1992. Relationship between wind speed and gas exchange over the ocean. *J. Geophys. Res. Oceans* **97**: 7373–7382. doi:10.1029/92JC00188
- Ward, B. B. 2008. Chapter 5 - Nitrification in Marine Systems, p. 199–261. *In* D.G. Capone, D.A. Bronk, M.R. Mulholland, and E.J. Carpenter [eds.], *Nitrogen in the Marine Environment (Second Edition)*. Academic Press. doi:10.1016/B978-0-12-372522-6.00005-0

- Waser, N. A. D., P. J. Harrison, B. Nielsen, S. E. Calvert, and D. H. Turpin. 1998a. Nitrogen isotope fractionation during the uptake and assimilation of nitrate, nitrite, ammonium, and urea by a marine diatom. *Limnol. Oceanogr.* **43**: 215–224. doi:10.4319/lo.1998.43.2.0215
- Waser, N., K. Yin, Z. Yu, K. Tada, P. Harrison, D. H. Turpin, and S. Calvert. 1998b. Nitrogen isotope fractionation during nitrate, ammonium and urea uptake by marine diatoms and coccolithophores under various conditions of N availability. *Mar. Ecol.-Prog. Ser. - MAR ECOL-PROGR SER* **169**: 29–41. doi:10.3354/meps169029
- Weilbeer, H., A. Winterscheid, T. Strotmann, I. Entelmann, S. Shaikh, and B. Vaessen. 2021. Analyse der hydrologischen und morphologischen Entwicklung in der Tideelbe für den Zeitraum von 2013 bis 2018. *Küste* **89** 57–129. doi:10.18171/1.089104
- Weiss, R. F. 1970. The solubility of nitrogen, oxygen and argon in water and seawater. *Deep Sea Res. Oceanogr. Abstr.* **17**: 721–735. doi:10.1016/0011-7471(70)90037-9
- Weiss, R. F., and B. A. Price. 1980. Nitrous oxide solubility in water and seawater. *Mar. Chem.* **8**: 347–359. doi:10.1016/0304-4203(80)90024-9
- Wells, N. S., D. T. Maher, D. V. Erler, M. Hipsey, J. A. Rosentreter, and B. D. Eyre. 2018. Estuaries as Sources and Sinks of N<sub>2</sub>O Across a Land Use Gradient in Subtropical Australia. *Glob. Biogeochem. Cycles* **32**: 877–894. doi:10.1029/2017GB005826
- Wertz, S., C. Goyer, D. L. Burton, B. J. Zebarth, and M. H. Chantigny. 2018. Processes contributing to nitrite accumulation and concomitant N<sub>2</sub>O emissions in frozen soils. *Soil Biol. Biochem.* **126**: 31–39. doi:10.1016/j.soilbio.2018.08.001
- von Westernhagen, H., W. Hickel, E. Bauerfeind, U. Niermann, and I. Kröncke. 1986. Sources and effects of oxygen deficiencies in the south-eastern North Sea. *Ophelia* **26**: 457–473. doi:10.1080/00785326.1986.10422006
- de Wilde, H. P., and M. J. de Bie. 2000. Nitrous oxide in the Schelde estuary: production by nitrification and emission to the atmosphere. *Mar. Chem.* **69**: 203–216. doi:10.1016/S0304-4203(99)00106-1
- Winterscheid, A., S. Dietrich, C. Svenson, N. Ohle, and I. Entelmann. 2014. Implications of Freshwater Discharge on Estuarine Sediment Dynamics. *Proceedings of the 11th International Conference on Hydrosience & Engineering, September 28 - October 2, 2014, Hamburg, Germany*. Proceedings of the ICHE 2014. Bundesanstalt für Wasserbau. 495–504.
- Winterwerp, J. C., and Z. B. Wang. 2013. Man-induced regime shifts in small estuaries—I: theory. *Ocean Dyn.* **63**: 1279–1292. doi:10.1007/s10236-013-0662-9
- Winterwerp, J. C., Z. B. Wang, A. van Braeckel, G. van Holland, and F. Kösters. 2013. Man-induced regime shifts in small estuaries—II: a comparison of rivers. *Ocean Dyn.* **63**: 1293–1306. doi:10.1007/s10236-013-0663-8
- WMO. 2018. Scientific Assessment of Ozone Depletion: 2018. 58. 58 World Meteorological Organization.
- Wolfstein, K., and L. Kies. 1999. Composition of suspended particulate matter in the Elbe estuary: Implications for biological and transportation processes. *Dtsch. Hydrogr. Z.* **51**: 453–463. doi:10.1007/BF02764166

- 
- Wong, W. W., A. Applegate, S. C. Poh, and P. L. M. Cook. 2020. Biogeochemical attenuation of nitrate in a sandy subterranean estuary: Insights from two stable isotope approaches. *Limnol. Oceanogr.* **65**: 3098–3113. doi:10.1002/lno.11576
- Wrage, N., G. L. Velthof, M. L. van Beusichem, and O. Oenema. 2001. The role of nitrifier denitrification in the production of nitrous oxide. *Soil Biol. Biochem.* **33**: 1723–1732. doi:10.1016/S0038-0717(01)00096-7
- Wunderlich, A., R. Meckenstock, and F. Einsiedl. 2012. Effect of Different Carbon Substrates on Nitrate Stable Isotope Fractionation During Microbial Denitrification. *Environ. Sci. Technol.* **46**: 4861–4868. doi:10.1021/es204075b
- Xia, X., T. Liu, Z. Yang, G. Michalski, S. Liu, Z. Jia, and S. Zhang. 2016. Enhanced nitrogen loss from rivers through coupled nitrification-denitrification caused by suspended sediment. *Sci. Total Environ.* **579**: 47–59. doi:10.1016/j.scitotenv.2016.10.181
- Xue, D., J. Botte, B. De Baets, and others. 2009. Present limitations and future prospects of stable isotope methods for nitrate source identification in surface- and groundwater. *Water Res.* **43**: 1159–1170. doi:10.1016/j.watres.2008.12.048
- Yamagishi, H., M. B. Westley, B. N. Popp, S. Toyoda, N. Yoshida, S. Watanabe, K. Koba, and Y. Yamanaka. 2007. Role of nitrification and denitrification on the nitrous oxide cycle in the eastern tropical North Pacific and Gulf of California. *J. Geophys. Res. Biogeosciences* **112**: G02015. doi:10.1029/2006JG000227
- Zander, F., A. Groengroeft, A. Eschenbach, T. J. Heimovaara, and J. Gebert. 2022. Organic matter pools in sediments of the tidal Elbe river. *Limnologia* **96**: 125997. doi:10.1016/j.limno.2022.125997
- Zander, F., T. Heimovaara, and J. Gebert. 2020. Spatial variability of organic matter degradability in tidal Elbe sediments. *J. Soils Sediments* **20**: 2573–2587. doi:10.1007/s11368-020-02569-4
- ZDM. 2022. Abfluss - Neu Darchau Wasserstraßen- und Schifffahrtsamt Elbe [ed.]. [https://www.kuestendaten.de/DE/Services/Messreihen\\_Dateien\\_Download/Download\\_Zeit\\_reihen\\_node.html](https://www.kuestendaten.de/DE/Services/Messreihen_Dateien_Download/Download_Zeit_reihen_node.html). Last accessed: 05.05.2023.
- Zhou, Y., X. Xu, R. Han, L. Li, Y. Feng, S. Yeerken, K. Song, and Q. Wang. 2019. Suspended particles potentially enhance nitrous oxide (N<sub>2</sub>O) emissions in the oxic estuarine waters of eutrophic lakes: Field and experimental evidence. *Environ. Pollut.* **252**: 1225–1234. doi:10.1016/j.envpol.2019.06.076
- Zhu, W., C. Wang, J. Hill, Y. He, B. Tao, Z. Mao, and W. Wu. 2018. A missing link in the estuarine nitrogen cycle?: Coupled nitrification-denitrification mediated by suspended particulate matter. *Sci. Rep.* **8**: 2282. doi:10.1038/s41598-018-20688-4



---

## Appendix

Appendix A1: Supplementary material for Chapter 2: “Low discharges intensify nitrogen retention in rivers – a case study in the Elbe River” .....	128
Appendix A2: Supplementary material for Chapter 3: “How low discharges affect estuarine nitrogen turnover – a case study in the freshwater Elbe Estuary” .....	133
Appendix A3: Supplementary material for Chapter 4: “Seasonal variability of nitrous oxide concentrations and emissions along a temperate estuary” .....	138
Appendix A4: Supplementary material for Chapter 5: “Suspended particulate matter drives the spatial segregation of nitrogen turnover along the hyper turbid Ems Estuary” .....	148

---

**Appendix A1**

**Table A1.1.** Number of samples in the FGG Elbe data set separated into interval sampling and longitudinal profiles as well as number of samples our weir sampling for each year from 1985 to 2009

	FGG Elbe data set		Hereon
	Interval sampling	Longitudinal profiles	Interval sampling
1985	52	11	0
1986	52	11	0
1987	52	8	0
1988	0	8	0
1989	0	8	0
1990	0	8	0
1991	0	8	0
1992	0	8	0
1993	0	8	0
1994	26	5	0
1995	26	7	0
1996	23	6	0
1997	23	6	0
1998	26	7	0
1999	26	6	0
2000	25	6	0
2001	26	6	0
2002	26	7	0
2003	26	6	0
2004	26	6	0
2005	26	6	0
2006	26	6	0
2007	12	6	0
2008	18	6	0
2009	18	6	0

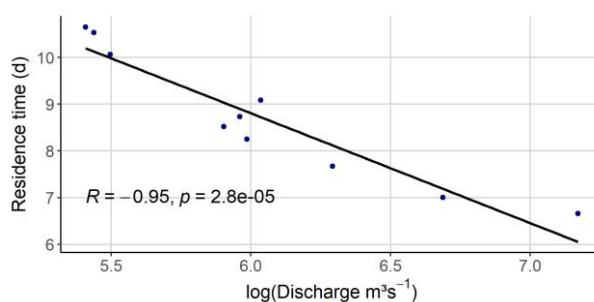
---

**Table A1.2.** Number of samples in the FGG Elbe data set separated into interval sampling and longitudinal profiles as well as number of samples our weir sampling for each year from 2010 to 2021

	FGG Elbe data set		Hereon
	Interval sampling	Longitudinal profiles	Interval sampling
2010	17	15	0
2011	19	6	13
2012	18	7	25
2013	19	6	45
2014	19	5	25
2015	19	5	20
2016	19	5	19
2017	0	5	15
2018	0	10	21
2019	0	6	17
2020	0	0	15
2021	19	6	9

**Table A1.3.** Calculated average summer residence times (T) from Schmilka (stream kilometer 4.0) to weir in Geesthacht (stream kilometer 585.9). The values are based on 12 simulations each starting from 1<sup>st</sup> of June to 31<sup>st</sup> of August with one value per week. Average summer discharge ( $Q_{\text{summer}}$ ) was calculated based on daily discharge measurements at station Neu Darchau (stream kilometer 536, FGG Elbe 2022) from June to August.

Year	2010	2011	2012	2013	2014	2015	2016	2017	2018	2019
$T_{\text{summer}}$ (d)	7.01	7.67	8.25	6.66	8.73	10.06	8.52	9.08	10.65	10.53
$Q_{\text{summer}}$ ( $\text{m}^3 \text{s}^{-1}$ )	802.5	540.4	397.8	1302.0	387.7	243.7	366.3	417.7	223.1	229.9

**Figure A1.1.** Relation of logarithmic annual summer discharge ( $Q_{\text{summer}}$ ) measured at Neu Darchau (stream kilometer 536) and average summer residence time (T) from Schmilka (stream kilometer 4.0) to weir in Geesthacht (stream kilometer 585.9). Pearson correlations coefficient (R) and p-value are shown.

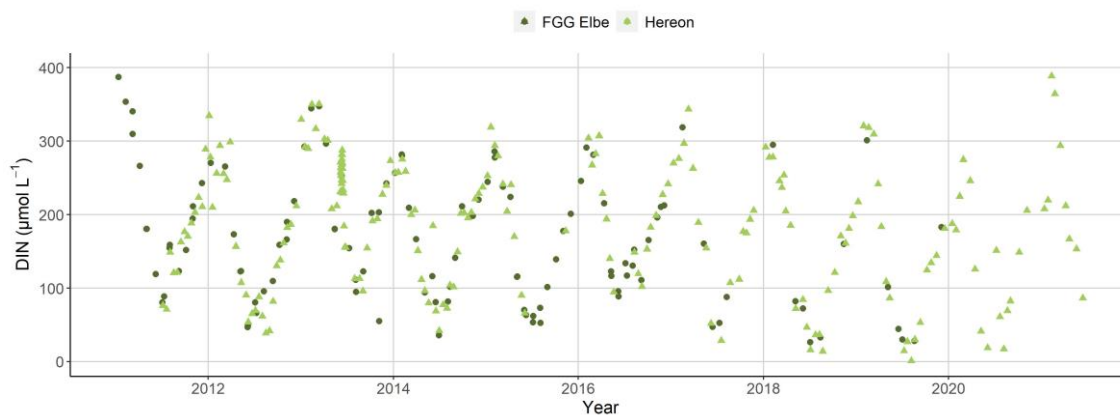


**Figure A1.2.** Comparison of DIN concentrations obtained from the FGG Elbe and Hereon data set at the weir in Geesthacht from 2011 to 2021: FGG Elbe data is shown in dark green circle and Hereon samples in light green triangles.

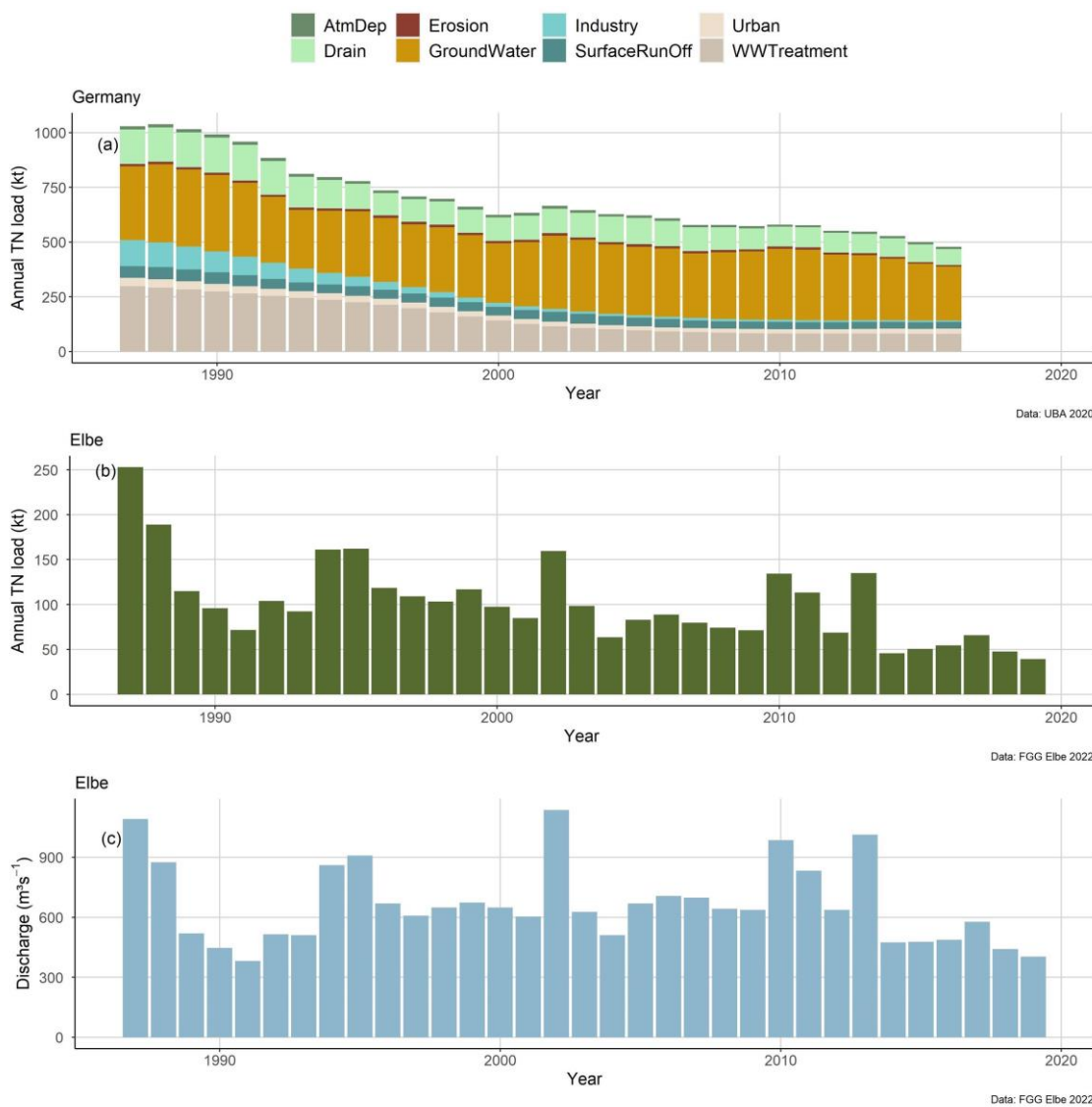


**Figure A1.3.** (a) Annual total nitrogen emission from Germany, data provided from UBA (2020), (b) annual total nitrogen loads from entering the Elbe estuary at the weir Geesthacht, (c) annual average discharge.

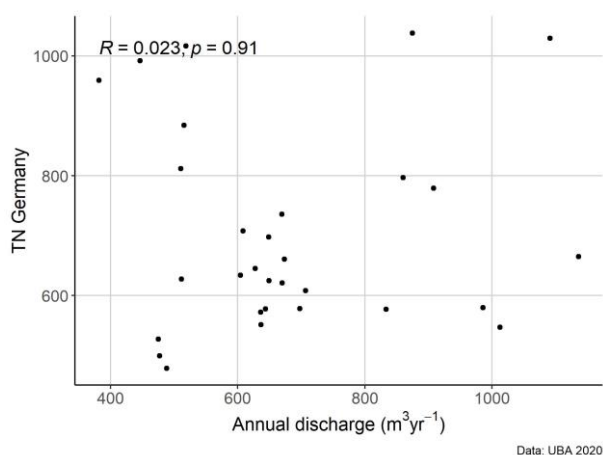


**Figure A1.4.** Internal correlation between annual German TN emissions and annual discharge

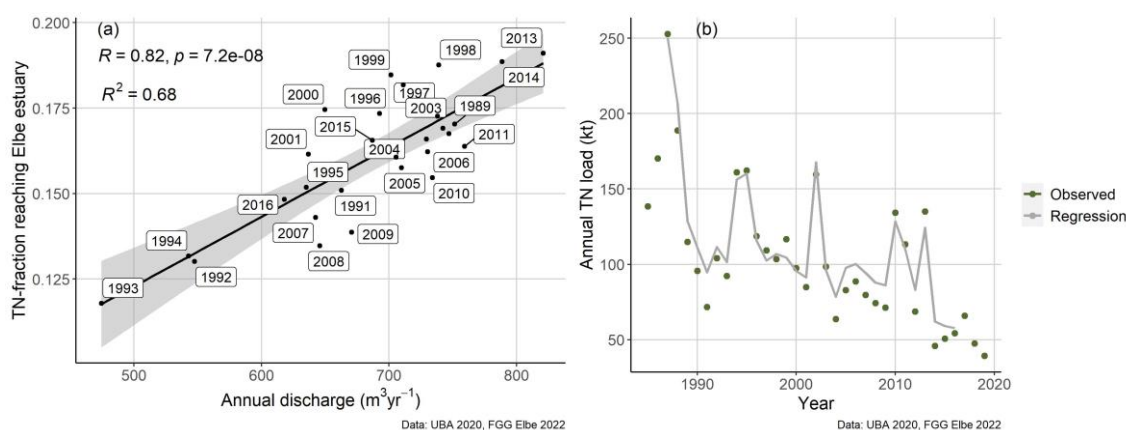


**Figure A1.5.** (a) Fraction of annual German TN emissions to surface water reaching the Elbe Estuary at the weir in Geesthacht with regression line (Eq. 2.3), p-value, Pearson correlation coefficient and  $R^2$ -value, (b) Annual TN loads at the weir Geesthacht: The points show the calculated loads based on the FGG Elbe (2022) data set (Section 3.3). The grey line indicates the results derived from our regression based analysis (Eq. 2.4). Please note that UBA (2020) only provided data from 1987 to 2016 and we calculated TN loads from 1985 to 2019.

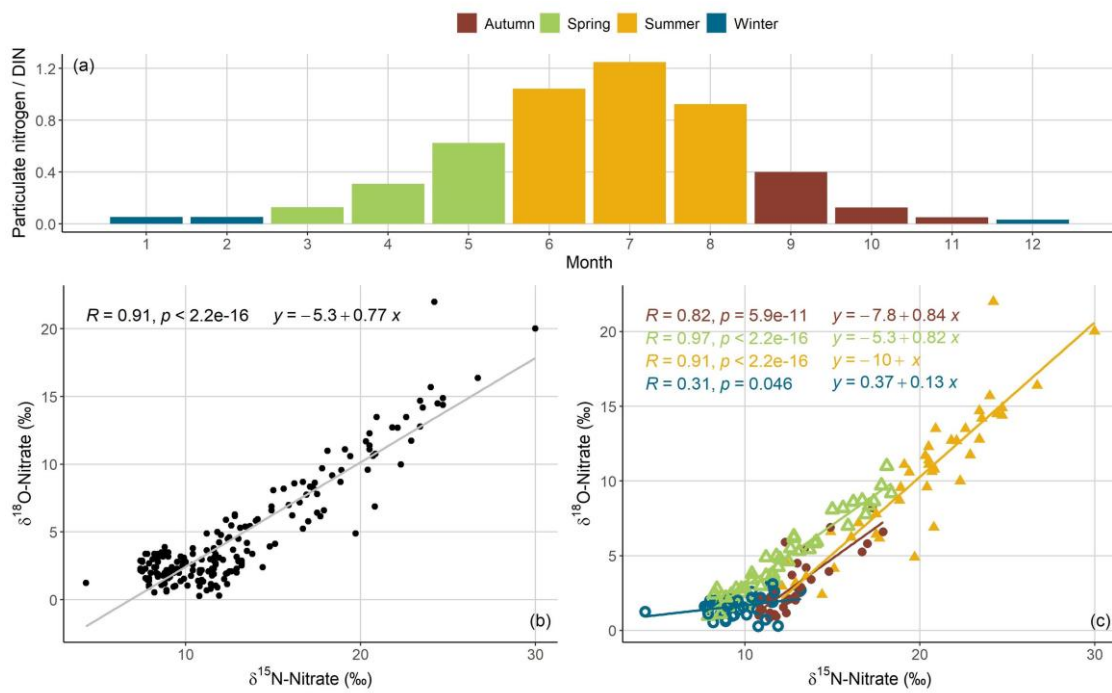


**Figure A1.6.** (a) Average monthly ratio of particulate nitrogen concentration and DIN concentrations that we used to distinguish seasons. (b)  $\delta^{18}\text{O}$ -nitrate plotted against  $\delta^{15}\text{N}$ -nitrate for the entire data set. (c)  $\delta^{18}\text{O}$ -nitrate plotted against  $\delta^{15}\text{N}$ -nitrate without flooding event in summer 2013 and separated into seasons. Blue circle show winter values (January, February and December). Green triangles represent spring values (March to May). Summer values (June to August) are shown in yellow triangles and autumn measurements (September to November) are red circles. Pearson correlations and p-values are shown in the plot.

## Appendix A2

### Isotope correction

Since the studies of Johannsen et al. (2008) and Schlarbaum et al. (2011), the internationally accepted  $\delta^{18}\text{O}$ -nitrate value of the IAEA reference material has been revised and changed from 22.7 ‰ (Révész et al. 1997) to 25.6 ‰ (Böhlke et al. 2003). Thus, we corrected for this offset, and also included an additional offset of -0.6 ‰ to account for a change in the referencing scheme from a single-point-correction to a bracketing correction (Knapp et al. 2008).

**Table A2.1.** Campaign dates with stream kilometers sampled (salinity <1), average water temperatures, average discharges and average DIN loads for each sampling stretch. Water temperatures and DIN loads results from measurements on board. The average discharge is obtained from the nearest gauge Neu Darchau at stream kilometer 536.

Cruise	Campaign Dates	Stream kilometers	Water temperature (°C)	Average discharge (m <sup>3</sup> s <sup>-1</sup> )	Average DIN load (μmol L <sup>-1</sup> )
2011/08	24.-25.08.2011	606 – 694	20.2	686	139.5
2012/05	24.05.2012	610 – 674	17.8	405	124.3
2012/06	13.&28.06.2012	606 – 678	17.9	347	105.5
2012/08	08.08.2012	610 – 680	21.2	418	93.1
2013/05	15.-16.05.2013	606 – 694	16.2	794	212.8
2013/07	24.-25.07.2013	610 – 694	23.6	568	134.4
2013/08	28.08.2013	606 – 674	20.6	377	113.6
2014/05	08.05.2014	610 – 668	15.5	385	127.2
2015/06	11.06.2015	612 – 670	18.7	276	96.6
2017/08	01.-02.08.2017	613 – 692	21.6	607	95.9
2019/06	04.-05.06.2019	610 – 677	19.6	423	107.2
2019/07	01.08.2019	607 – 656	23.6	171	59.2
2020/06	20.06.2020	609 – 668	21.3	331	60.7
2021/05	04.-05.05.2021	610 – 681	11.1	411	169.7
2021/07	27.-28.07.2021	620 – 693	22.8	721	180.0
2022/05	23.-24.05.2022	610 – 676	18.7	336	99.0
2022/06	15.06.2022	611 – 668	19.7	241	50.2

**Table A2.2.** Available data set for each cruise: X – data available, O – uncorrected data available, (blank) – no data available

	2011/08	2012/05	2012/06	2012/08	2013/05	2013/07	2013/08	2014/05	2015/06	2017/08	2019/06	2019/07	2020/06	2021/05	2021/07	2022/05	2022/06
T	X	X	X	X	X	X	X	X	X	X	X	X	X	X	X	X	X
O <sub>2</sub>	O	O	O	O	O	O	O	O	O	X	X	X	X	X	X	X	X
Si					X	X	X	X		X	X	X	X	X	X	X	X
PO <sub>4</sub> <sup>+</sup>					X	X	X	X		X	X	X	X	X	X	X	X
NH <sub>4</sub> <sup>+</sup>	X	X	X	X	X	X	X	X	X	X	X	X	X	X	X	X	X
NO <sub>2</sub> <sup>-</sup>	X	X	X	X	X	X	X	X	X	X	X	X	X	X	X	X	X
NO <sub>3</sub> <sup>-</sup>	X	X	X	X	X	X	X	X	X	X	X	X	X	X	X	X	X
δ <sup>15</sup> N-NO <sub>3</sub> <sup>-</sup>	X	X	X	X	X	X	X	X	X	X	X	X	X	X	X	X	X
δ <sup>18</sup> O-NO <sub>3</sub> <sup>-</sup>	X	X	X	X	X	X	X	X	X	X	X	X	X	X	X	X	X
SPM		X			X	X				X	X	X	X	X	X	X	X
PC		X			X	X				X	X	X	X	X	X	X	X
PN		X			X	X				X	X	X	X	X	X	X	X
C/N		X			X	X				X	X	X	X	X	X	X	X
δ <sup>15</sup> N-SPM		X			X	X				X	X	X	X	X	X	X	X

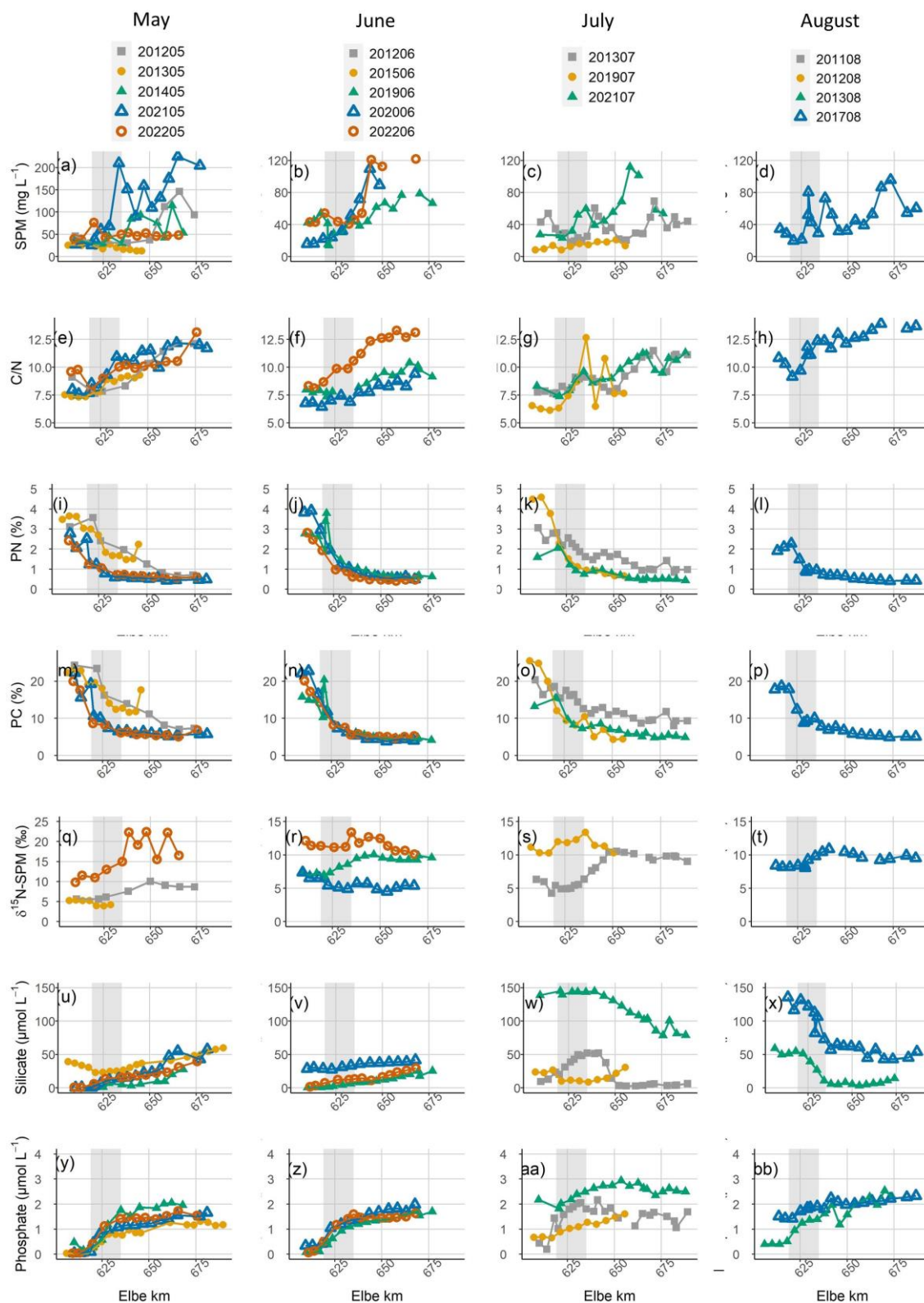


**Figure A2.1.** Suspended particulate matter concentrations in (a) May, (b) June, (c) July and (d) August; C/N ratios in (e) May, (f) June, (g) July and (h) August; PN fractions in (i) May, (j) June, (k) July and (l) August; PC fractions in (m) May, (n) June, (o) July and (p) August;  $\delta^{15}\text{N}$ -SPM values in (q) May, (r) June, (s) July and (t) August; silicate concentrations in (u) May, (v) June, (w) July and (x) August; phosphate concentrations in (y) May, (z) June, (aa) July and (bb) August. The grey background indicates the Port of Hamburg.

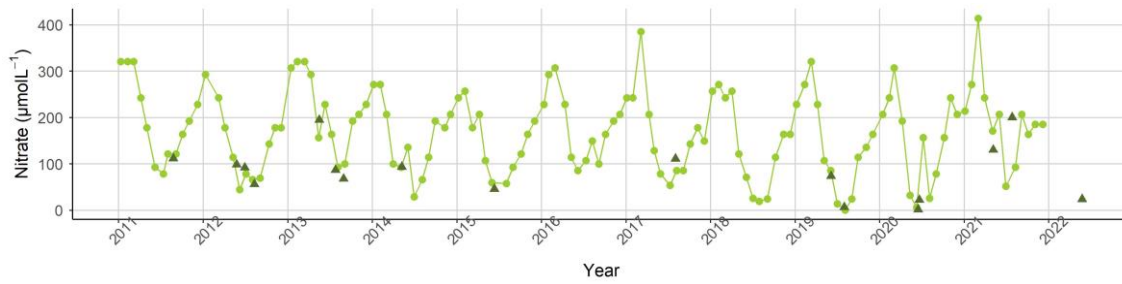


**Figure A2.2.** Comparison of nitrate concentration measured by the FGG Elbe at station Zollenspieker (stream kilometer 598.7) and the most upstream samples of our transect cruises (~ stream kilometer 610). Zollenspieker data is shown in light green and circles. Transect cruise concentrations are displayed by dark green triangles.

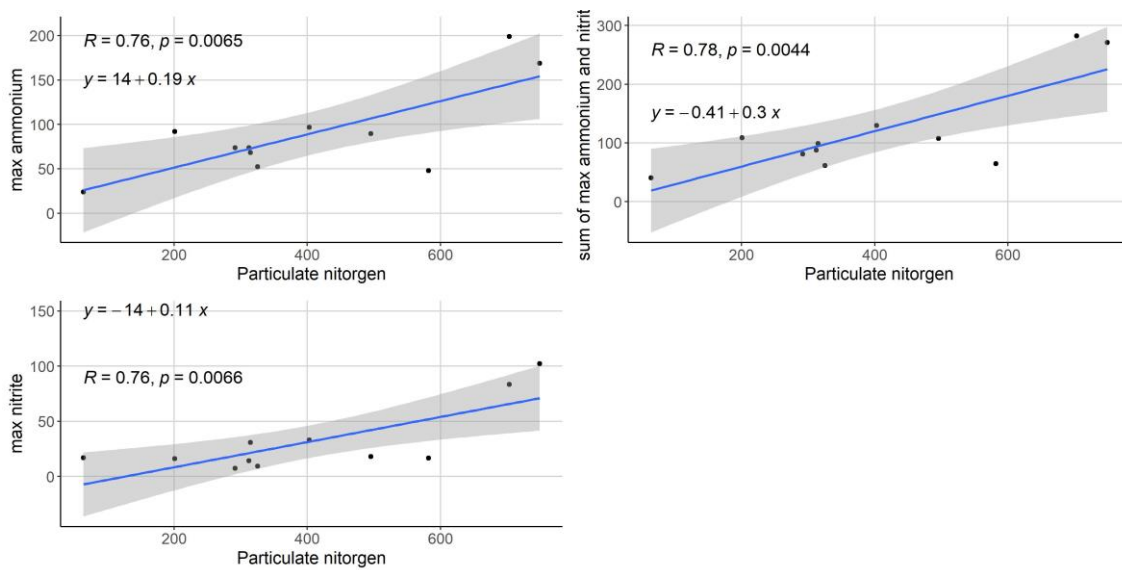


**Figure A2.3.** Maximum ammonium, nitrite as well as combined ammonium and nitrite loads plotted against riverine particulate nitrogen loads. Our most upstream samples lead as riverine values. All values are in  $g\ s^{-1}$ . Pearson correlations (R), p-values and the equations for the regression line are shown.

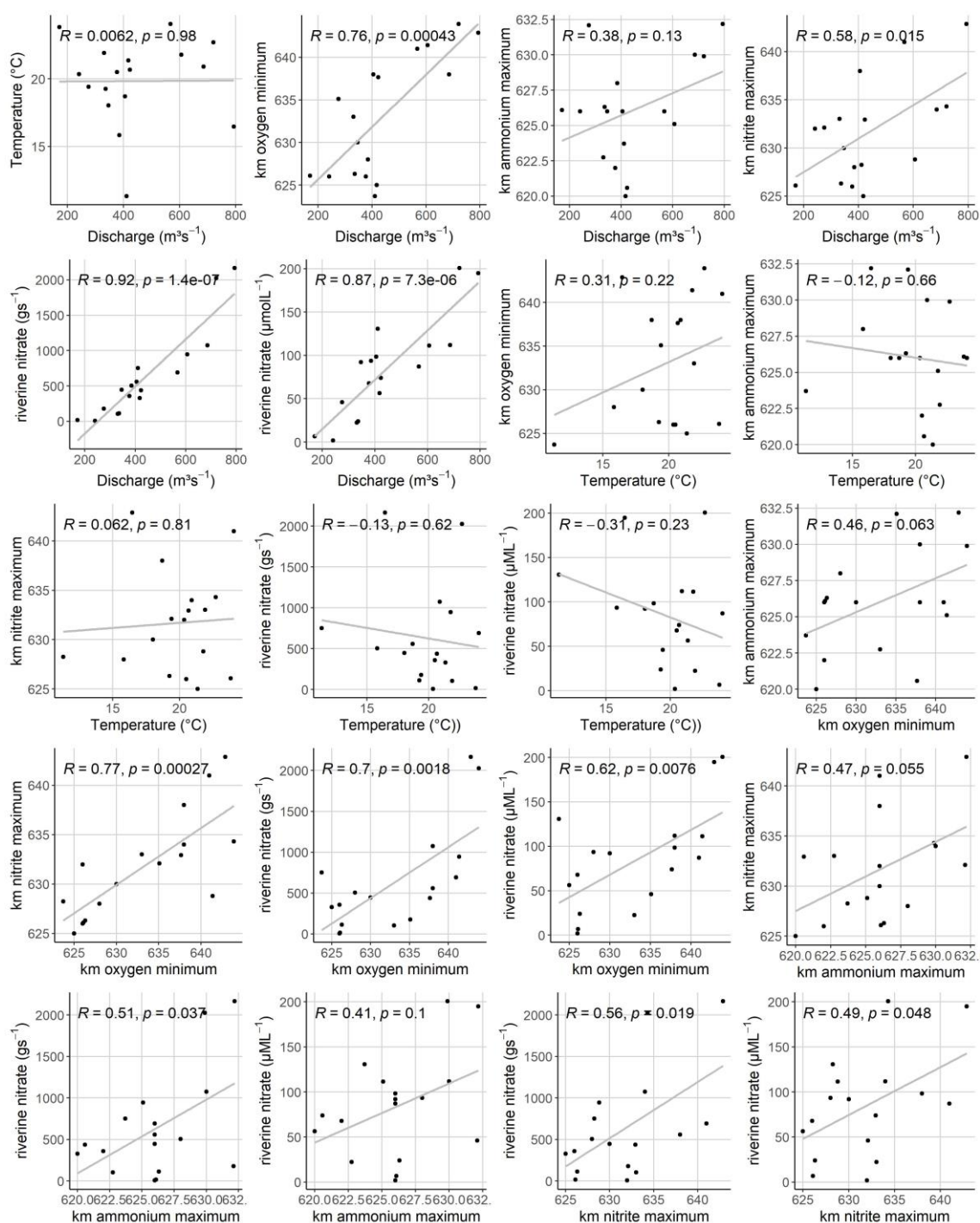


**Figure A2.4.** Pearson correlation coefficients (R) and p-values for discharge, temperature, position of the oxygen minimum, position of the ammonium maximum, position of the nitrite maximum, riverine nitrate concentrations and loads.

## Appendix A3

**Table A3.1.** Applied oxygen correction for each cruise: The corrections were made using the salinity corrected optode measurements from the FerryBox (O<sub>2</sub>) in comparison with Winkler titrations. Changes in oxygen corrections arose due to several optode changes in the time period from 2017 to 2022.

Cruise	Correction	Winkler titrations	R <sup>2</sup>
2017/08	+24.05 ± 1.52	7	
2019/06	+35.19 ± 5.97	9	
2019/07	+35.19 ± 5.97	9	
2020/06	-2.38	19	0.99
2020/09	-2.38	19	0.99
2021/03	0.97 × O <sub>2</sub> + 43.91	22	0.94
2021/05	1.12 × O <sub>2</sub> + 13.41	36	0.97
2021/07	1.12 × O <sub>2</sub> + 13.41	36	0.97
2022/03	1.12 × O <sub>2</sub> + 13.41	36	0.97

**Table A3.2.** Calculated average N<sub>2</sub>O saturation, sea-to-air fluxes calculated following Nightingale et al. (2000) and atmospheric N<sub>2</sub>O dry mole fractions during our cruises for the Elbe estuary

Campaign Dates	Average saturation (%)	N <sub>2</sub> O flux densities (μmol m <sup>-2</sup> d <sup>-1</sup> )		
		Cruise wind	Annual wind	Seasonal wind
28.-29.04.15	160.8 ± 37.9	20.9 ± 13.3	9.2 ± 5.9	11.5 ± 7.3
02.-04.06.15	203.8 ± 112.7	16.6 ± 18.2	14.9 ± 16.3	15.4 ± 16.9
01.-02.08.17	221.0 ± 106.5	10.9 ± 9.7	17.3 ± 15.4	18.1 ± 16.2
04.-05.06.19	192.6 ± 66.0	10.1 ± 7.3	13.4 ± 9.7	13.9 ± 10.0
30.07.-01.08.19	232.5 ± 155.3	15.0 ± 17.9	18.3 ± 21.8	19.9 ± 23.7
19.-20.06.20	193.9 ± 74.1	19.4 ± 15.6	13.3 ± 10.8	13.8 ± 11.2
09.-11.09.20	160.5 ± 53.6	13.1 ± 11.8	8.7 ± 7.9	11.4 ± 10.3
10.-12.03.21	242.5 ± 141.6	80.1 ± 80.5	23.2 ± 23.3	37.0 ± 37.1
04.-05.05.21	145.6 ± 28.8	33.5 ± 21.2	7.1 ± 4.5	7.8 ± 4.9
27.-28.07.21	172.6 ± 37.2	12.4 ± 6.5	10.4 ± 5.4	11.3 ± 5.9
01.-02.03.22	196.5 ± 47.0	6.8 ± 3.4	15.6 ± 7.8	24.8 ± 12.4

**Table A3.3.** Calculated average N<sub>2</sub>O saturation, sea-to-air fluxes calculated following Wanninkhof (1992) and atmospheric N<sub>2</sub>O dry mole fractions during our cruises for the Elbe estuary

Campaign Dates	Average saturation (%)	N <sub>2</sub> O flux densities ( $\mu\text{mol m}^{-2} \text{d}^{-1}$ )		
		Cruise wind	Annual wind	Seasonal wind
28.-29.04.15	160.8 ± 37.9	24.3 ± 15.4	9.8 ± 6.2	12.6 ± 8.0
02.-04.06.15	203.8 ± 112.7	17.8 ± 19.5	15.8 ± 17.2	16.4 ± 18.0
01.-02.08.17	221.0 ± 106.5	10.7 ± 9.6	18.3 ± 16.3	19.3 ± 17.2
04.-05.06.19	192.6 ± 66.0	10.3 ± 7.4	14.2 ± 10.2	14.8 ± 10.7
30.07.-01.08.19	232.5 ± 155.3	15.4 ± 18.4	19.3 ± 23.1	21.3 ± 25.4
19.-20.06.20	193.9 ± 74.1	21.5 ± 17.3	14.1 ± 11.4	14.7 ± 11.9
09.-11.09.20	160.5 ± 53.6	14.6 ± 13.2	9.2 ± 8.4	12.5 ± 11.3
10.-12.03.21	242.5 ± 141.6	96.3 ± 96.8	24.6 ± 24.7	41.4 ± 41.6
04.-05.05.21	145.6 ± 28.8	41.2 ± 26.0	7.5 ± 4.7	8.4 ± 5.3
27.-28.07.21	172.6 ± 37.2	13.4 ± 7.0	11.0 ± 5.7	12.1 ± 6.3
01.-02.03.22	196.5 ± 47.0	6.3 ± 3.1	16.5 ± 8.2	27.8 ± 13.9

**Table A3.4.** Calculated average N<sub>2</sub>O saturation, sea-to-air fluxes calculated following Clark et al. (1995) and atmospheric N<sub>2</sub>O dry mole fractions during our cruises for the Elbe estuary

Campaign Dates	Average saturation (%)	N <sub>2</sub> O flux densities ( $\mu\text{mol m}^{-2} \text{d}^{-1}$ )		
		Cruise wind	Annual wind	Seasonal wind
28.-29.04.15	160.8 ± 37.9	21.6 ± 13.7	10.4 ± 6.6	12.6 ± 8.0
02.-04.06.15	203.8 ± 112.7	18.4 ± 20.1	16.8 ± 18.4	17.3 ± 19.0
01.-02.08.17	221.0 ± 106.5	13.7 ± 12.2	19.5 ± 17.4	20.3 ± 18.1
04.-05.06.19	192.6 ± 66.0	12.1 ± 8.7	15.1 ± 10.9	15.6 ± 11.3
30.07.-01.08.19	232.5 ± 155.3	17.6 ± 21.0	20.6 ± 24.6	22.1 ± 26.4
19.-20.06.20	193.9 ± 74.1	20.8 ± 16.7	15.1 ± 12.1	15.5 ± 12.5
09.-11.09.20	160.5 ± 53.6	14.0 ± 12.6	9.9 ± 8.9	12.4 ± 11.2
10.-12.03.21	242.5 ± 141.6	81.7 ± 82.1	26.2 ± 26.3	39.3 ± 39.4
04.-05.05.21	145.6 ± 28.8	34.1 ± 21.5	8.0 ± 5.1	8.7 ± 5.5
27.-28.07.21	172.6 ± 37.2	13.6 ± 7.1	11.7 ± 6.1	12.5 ± 6.6
01.-02.03.22	196.5 ± 47.0	9.7 ± 4.8	17.6 ± 8.8	26.3 ± 13.2

**Table A3.5.** Areas for different sections of the Elbe Estuary used for N<sub>2</sub>O emission estimates

Section	Stream kilometer (km)	Area (km <sup>2</sup> )
Limnic	585 – 615	8
Port	615 – 632	22
Oligohaline	632 – 704	162
Mesohaline	704 – 727	110
Polyhaline	727 – 750	148
Total	585 – 750	450

**Table A3.6.** Annual DIN and TN loads calculated according to Pätsch and Lenhart (2011) from 2015 to 2021. We used publicly available data provided by FGG Elbe (2022). For 2022, data is not publicly available yet.

Year	DIN (Gg yr <sup>-1</sup> )	TN (Gg yr <sup>-1</sup> )
2015	41.4	59.4
2016	47.5	60.3
2017	53.9	70.2
2018	40.7	51.1
2019	36.7	43.1
2020	36.8	44.5
2021	55.0	63.0
Mean	44.6	55.0

**Table A3.7.** Calculated average seasonal DIN and TN loads from 2015 to 2021

Season	Months	DIN (g d <sup>-1</sup> )	TN (g d <sup>-1</sup> )
Winter	March	$2.91 \times 10^8 \pm 1.05 \times 10^8$	$3.34 \times 10^8 \pm 9.40 \times 10^7$
Spring	April & May	$1.17 \times 10^8 \pm 6.24 \times 10^7$	$1.58 \times 10^8 \pm 7.62 \times 10^7$
Summer	June & July	$5.03 \times 10^7 \pm 3.36 \times 10^7$	$7.37 \times 10^7 \pm 3.99 \times 10^7$
Late summer	August & September	$4.33 \times 10^7 \pm 2.69 \times 10^7$	$6.25 \times 10^7 \pm 3.58 \times 10^7$

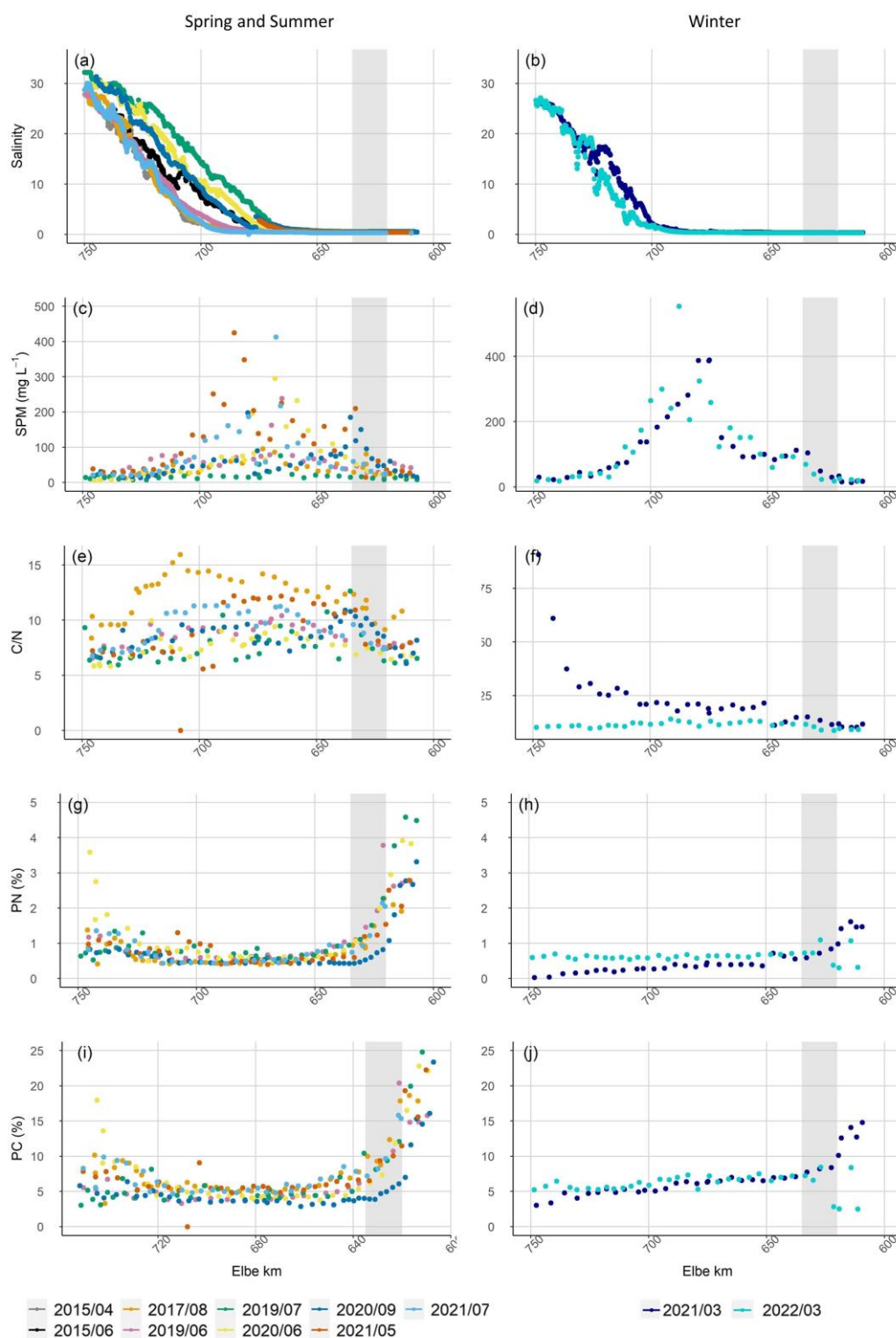


**Figure A3.1.** Salinity along the Elbe estuary (a) in spring/summer and (b) in winter. Suspended particulate matter (SPM) concentration in ( $\text{mg L}^{-1}$ ) along the Elbe estuary in (c) spring/summer and (d) in winter. Particulate carbon to nitrogen ratio (C/N) along the Elbe estuary in (e) in spring/summer and (f) in winter. Particulate nitrogen (PN) content in (%) in (g) spring/summer and (h) winter. Particulate carbon (PC) content in (%) in (i) spring/summer and (j) winter. All values are potted against stream kilometers. The Hamburg Port region is shown with a gray background. C/N ratios were measured with an Elemental Analyzer (Eurovector EA 3000) calibrated against a certified acetanilide standard (IVA Analysentechnik, Germany). The standard deviation was 0.05% and 0.005% for carbon and nitrogen respectively. Please note that there are no data for the suspended particulate matter composition in 2015.

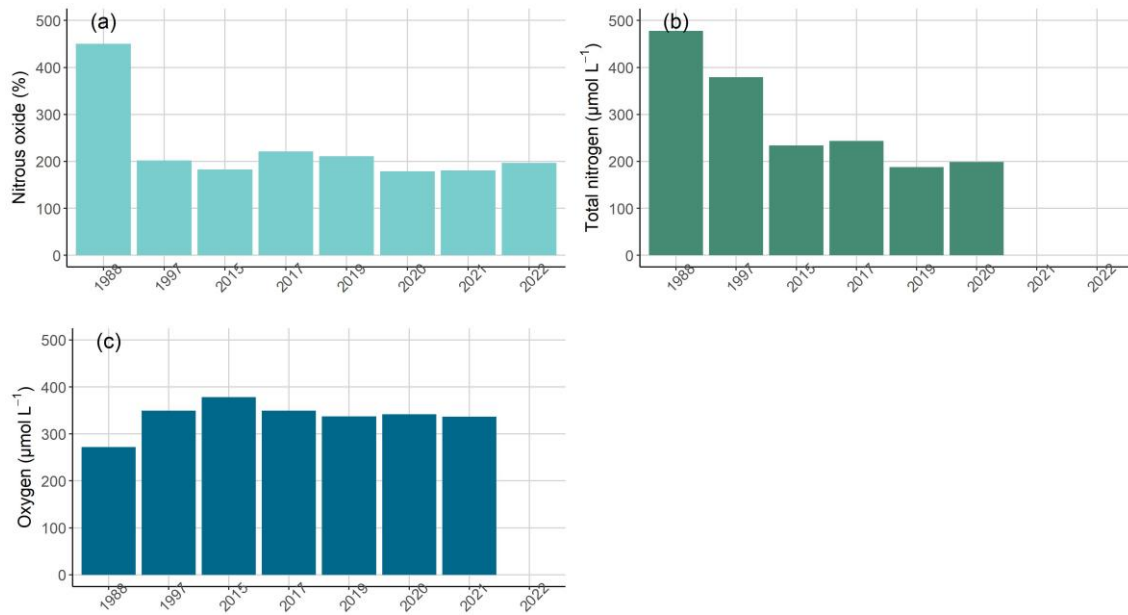


**Figure A3.2.** (a) Comparison of average  $\text{N}_2\text{O}$  saturation transect measurements with previous research from the Elbe Estuary, (b) the total nitrogen concentration and (c) oxygen concentration. Average annual oxygen concentration and total nitrogen concentration are shown for the station Zollenspieker at the beginning of the estuary (stream kilometer 598.7) and publicly available (FGG Elbe 2022). Values for 2022 and total nitrogen concentration for 2021 are not presented as the data is not publicly available yet.

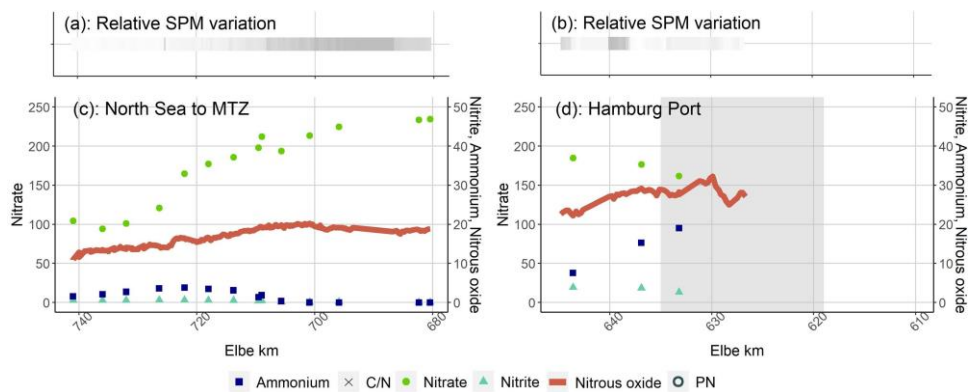


**Figure A3.3.** Succession of N-bearing substances coming from the North Sea and in the Port of Hamburg in April 2015: Relative change of SPM concentrations (a) from the North Sea and (b) in the Port of Hamburg. Nitrate in  $\mu\text{mol L}^{-1}$ , nitrite in  $\mu\text{mol L}^{-1}$ , ammonium in  $\mu\text{mol L}^{-1}$  and nitrous oxide concentrations in  $\text{nmol L}^{-1}$  plotted against stream kilometers (c) from the North Sea and (d) in the Port of Hamburg. The grey area in (d) and (f) shows the position of the Port of Hamburg.

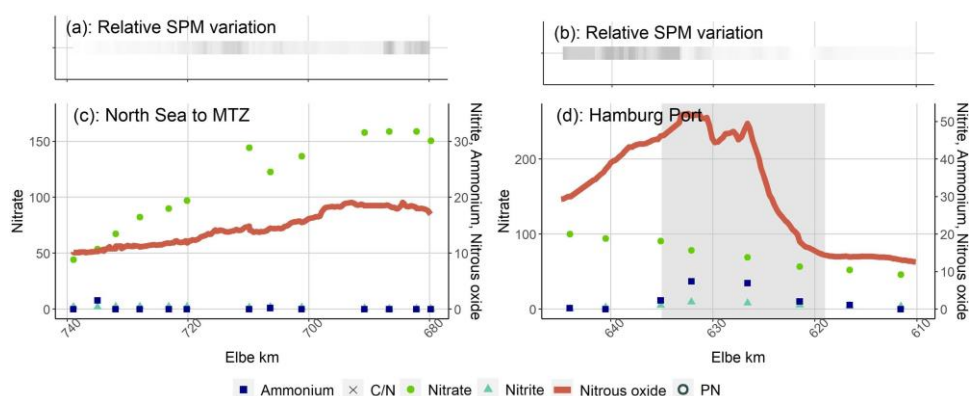


**Figure A3.4.** Succession of N-bearing substances coming from the North Sea and in the Port of Hamburg in June 2015: Relative change of SPM concentrations (a) from the North Sea and (b) in the Port of Hamburg. Nitrate in  $\mu\text{mol L}^{-1}$ , nitrite in  $\mu\text{mol L}^{-1}$ , ammonium in  $\mu\text{mol L}^{-1}$  and nitrous oxide concentrations in  $\text{nmol L}^{-1}$  plotted against stream kilometers (c) from the North Sea and (d) in the Port of Hamburg. The grey area in (d) and (f) shows the position of the Port of Hamburg.

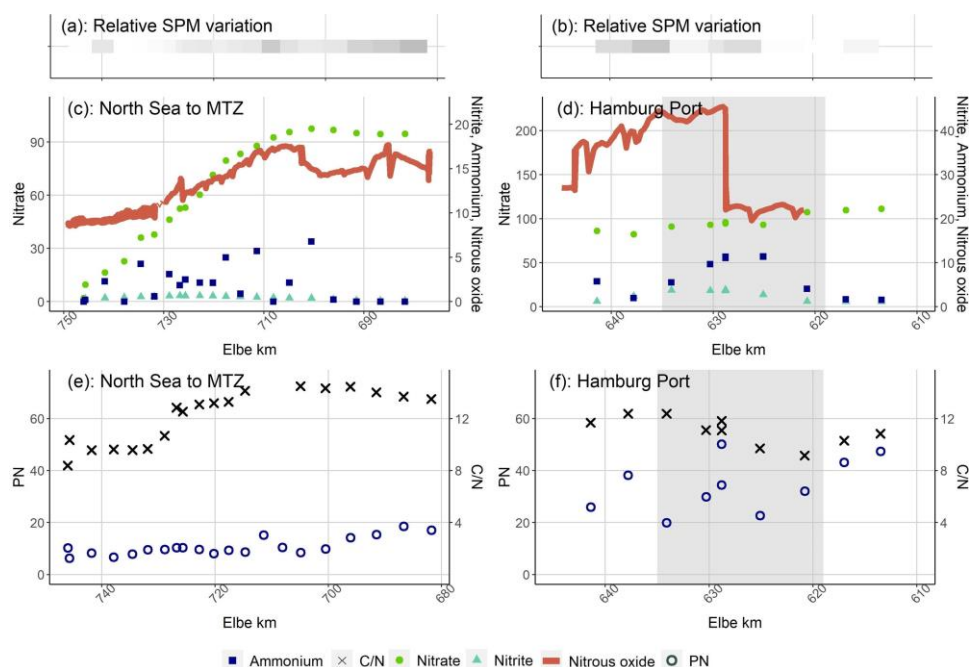


**Figure A3.5.** Succession of N-bearing substances coming from the North Sea and in the Port of Hamburg in August 2017: Relative change of SPM concentrations (a) from the North Sea and (b) in the Port of Hamburg. Nitrate in  $\mu\text{mol L}^{-1}$ , nitrite in  $\mu\text{mol L}^{-1}$ , ammonium in  $\mu\text{mol L}^{-1}$  and nitrous oxide concentrations in  $\text{nmol L}^{-1}$  plotted against stream kilometers (c) from the North Sea and (d) in the Port of Hamburg. Particulate nitrogen concentrations in  $\mu\text{mol L}^{-1}$  and C/N values plotted against stream kilometers (e) from the North Sea and (f) in the Port of Hamburg. The grey area in (d) and (f) shows the position of the Port of Hamburg.

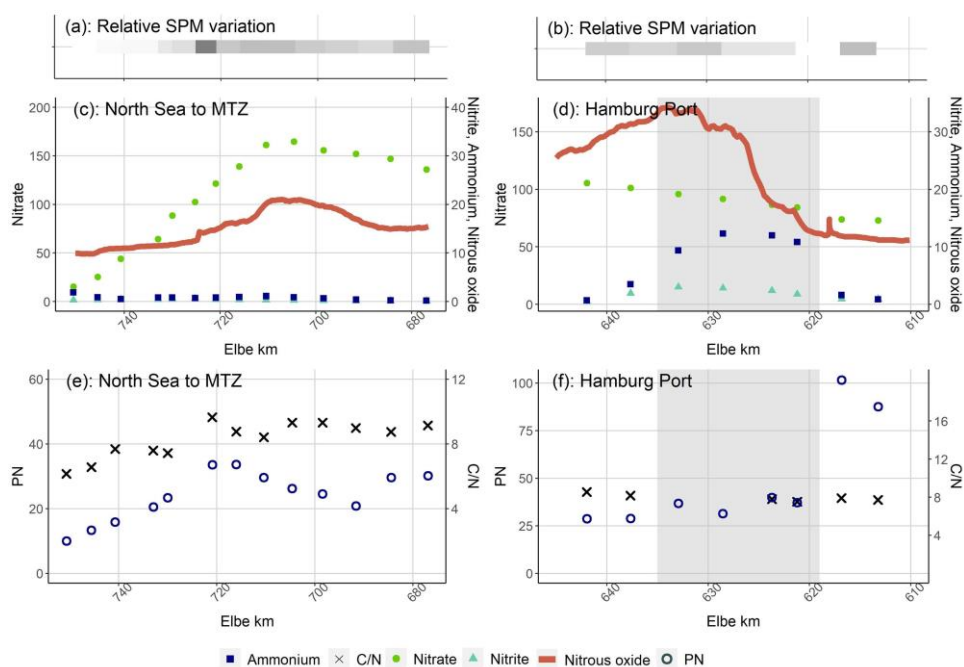


**Figure A3.6.** Succession of N-bearing substances coming from the North Sea and in the Port of Hamburg in June 2019: Relative change of SPM concentrations (a) from the North Sea and (b) in the Port of Hamburg. Nitrate in  $\mu\text{mol L}^{-1}$ , nitrite in  $\mu\text{mol L}^{-1}$ , ammonium in  $\mu\text{mol L}^{-1}$  and nitrous oxide concentrations in  $\text{nmol L}^{-1}$  plotted against stream kilometers (c) from the North Sea and (d) in the Port of Hamburg. Particulate nitrogen concentrations in  $\mu\text{mol L}^{-1}$  and C/N values plotted against stream kilometers (e) from the North Sea and (f) in the Port of Hamburg. The grey area in (d) and (f) shows the position of the Port of Hamburg.

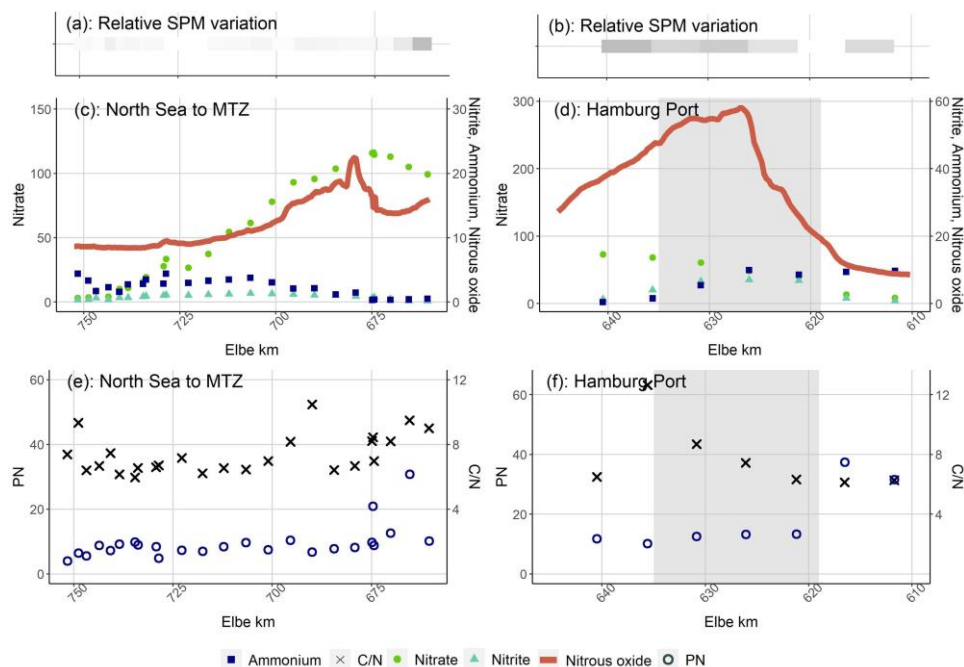


**Figure A3.7.** Succession of N-bearing substances coming from the North Sea and in the Port of Hamburg in July 2019: Relative change of SPM concentrations (a) from the North Sea and (b) in the Port of Hamburg. Nitrate in  $\mu\text{mol L}^{-1}$ , nitrite in  $\mu\text{mol L}^{-1}$ , ammonium in  $\mu\text{mol L}^{-1}$  and nitrous oxide concentrations in  $\text{nmol L}^{-1}$  plotted against stream kilometers (c) from the North Sea and (d) in the Port of Hamburg. Particulate nitrogen concentrations in  $\mu\text{mol L}^{-1}$  and C/N values plotted against stream kilometers (e) from the North Sea and (f) in the Port of Hamburg. The grey area in (d) and (f) shows the position of the Port of Hamburg.

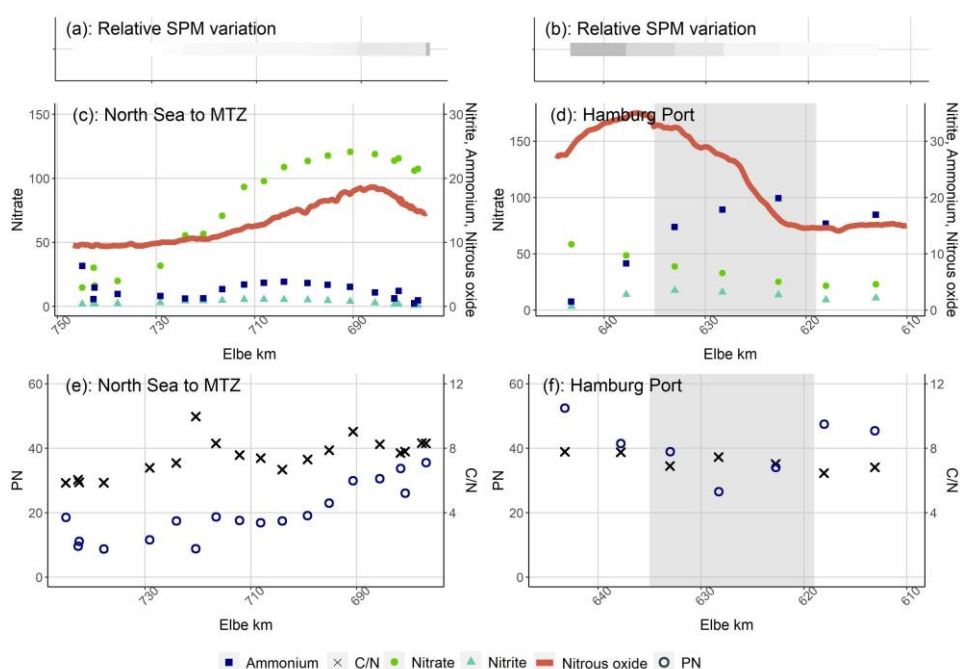


**Figure A3.8.** Succession of N-bearing substances coming from the North Sea and in the Port of Hamburg in June 2020: Relative change of SPM concentrations (a) from the North Sea and (b) in the Port of Hamburg. Nitrate in  $\mu\text{mol L}^{-1}$ , nitrite in  $\mu\text{mol L}^{-1}$ , ammonium in  $\mu\text{mol L}^{-1}$  and nitrous oxide concentrations in  $\text{nmol L}^{-1}$  plotted against stream kilometers (c) from the North Sea and (d) in the Port of Hamburg. Particulate nitrogen concentrations in  $\mu\text{mol L}^{-1}$  and C/N values plotted against stream kilometers (e) from the North Sea and (f) in the Port of Hamburg. The grey area in (d) and (f) shows the position of the Port of Hamburg.

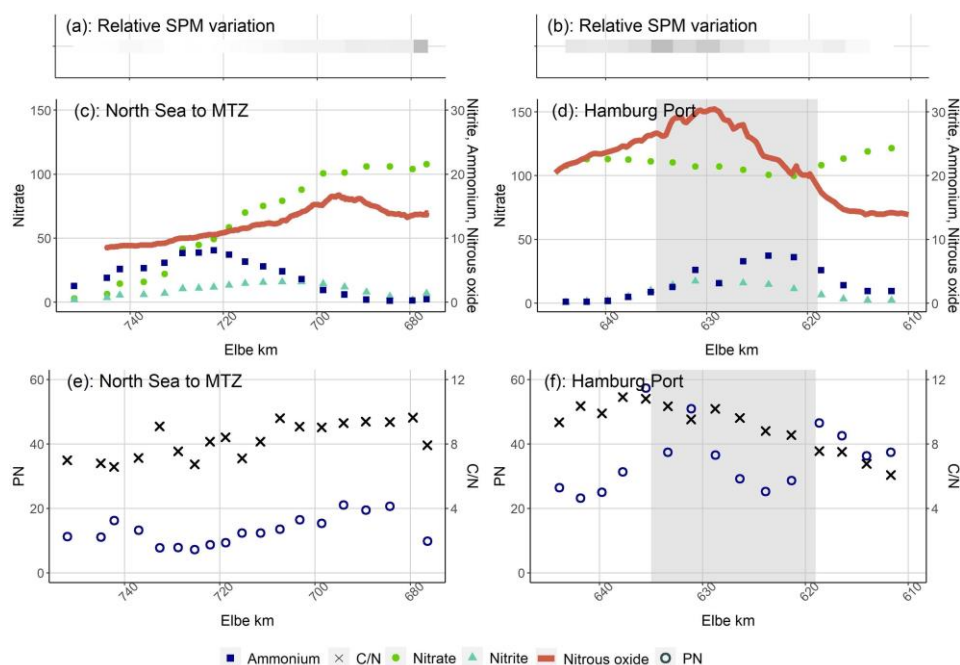


**Figure A3.9.** Succession of N-bearing substances coming from the North Sea and in the Port of Hamburg in September 2020: Relative change of SPM concentrations (a) from the North Sea and (b) in the Port of Hamburg. Nitrate in  $\mu\text{mol L}^{-1}$ , nitrite in  $\mu\text{mol L}^{-1}$ , ammonium in  $\mu\text{mol L}^{-1}$  and nitrous oxide concentrations in  $\text{nmol L}^{-1}$  plotted against stream kilometers (c) from the North Sea and (d) in the Port of Hamburg. Particulate nitrogen concentrations in  $\mu\text{mol L}^{-1}$  and C/N values plotted against stream kilometers (e) from the North Sea and (f) in the Port of Hamburg. The grey area in (d) and (f) shows the position of the Port of Hamburg.

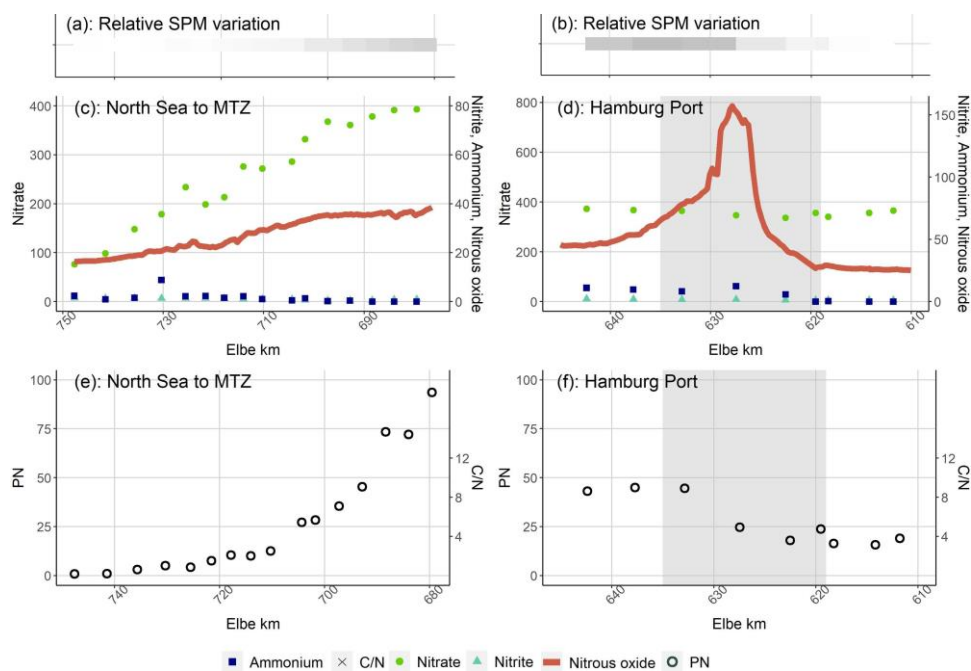


**Figure A3.10.** Succession of N-bearing substances coming from the North Sea and in the Port of Hamburg in March 2021: Relative change of SPM concentrations (a) from the North Sea and (b) in the Port of Hamburg. Nitrate in  $\mu\text{mol L}^{-1}$ , nitrite in  $\mu\text{mol L}^{-1}$ , ammonium in  $\mu\text{mol L}^{-1}$  and nitrous oxide concentrations in  $\text{nmol L}^{-1}$  plotted against stream kilometers (c) from the North Sea and (d) in the Port of Hamburg. Particulate nitrogen concentrations in  $\mu\text{mol L}^{-1}$  and C/N values plotted against stream kilometers (e) from the North Sea and (f) in the Port of Hamburg. The grey area in (d) and (f) shows the position of the Port of Hamburg.

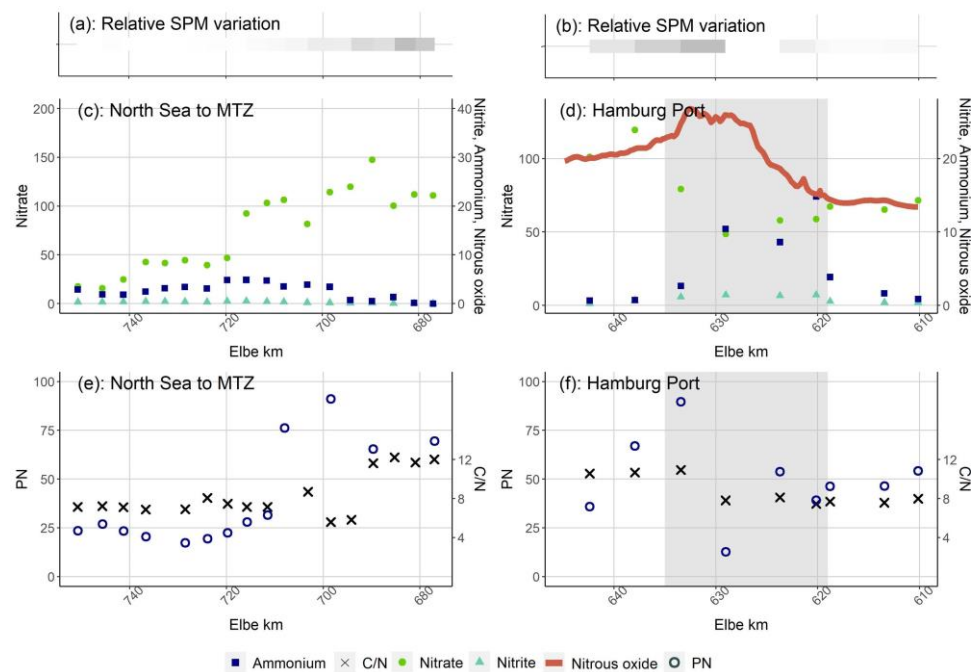


**Figure A3.11.** Succession of N-bearing substances coming from the North Sea and in the Port of Hamburg in May 2021: Relative change of SPM concentrations (a) from the North Sea and (b) in the Port of Hamburg. Nitrate in  $\mu\text{mol L}^{-1}$ , nitrite in  $\mu\text{mol L}^{-1}$ , ammonium in  $\mu\text{mol L}^{-1}$  and nitrous oxide concentrations in  $\text{nmol L}^{-1}$  plotted against stream kilometers (c) from the North Sea and (d) in the Port of Hamburg. Particulate nitrogen concentrations in  $\mu\text{mol L}^{-1}$  and C/N values plotted against stream kilometers (e) from the North Sea and (f) in the Port of Hamburg. The grey area in (d) and (f) shows the position of the Port of Hamburg.

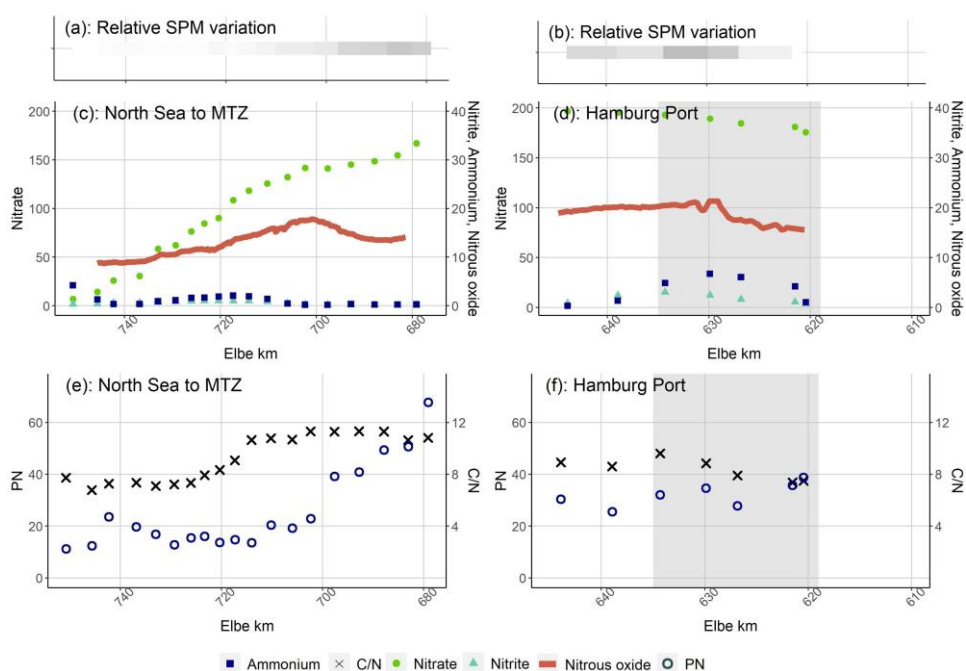


**Figure A3.12.** Succession of N-bearing substances coming from the North Sea and in the Port of Hamburg in June 2021: Relative change of SPM concentrations (a) from the North Sea and (b) in the Port of Hamburg. Nitrate in  $\mu\text{mol L}^{-1}$ , nitrite in  $\mu\text{mol L}^{-1}$ , ammonium in  $\mu\text{mol L}^{-1}$  and nitrous oxide concentrations in  $\text{nmol L}^{-1}$  plotted against stream kilometers (c) from the North Sea and (d) in the Port of Hamburg. Particulate nitrogen concentrations in  $\mu\text{mol L}^{-1}$  and C/N values plotted against stream kilometers (e) from the North Sea and (f) in the Port of Hamburg. The grey area in (d) and (f) shows the position of the Port of Hamburg.

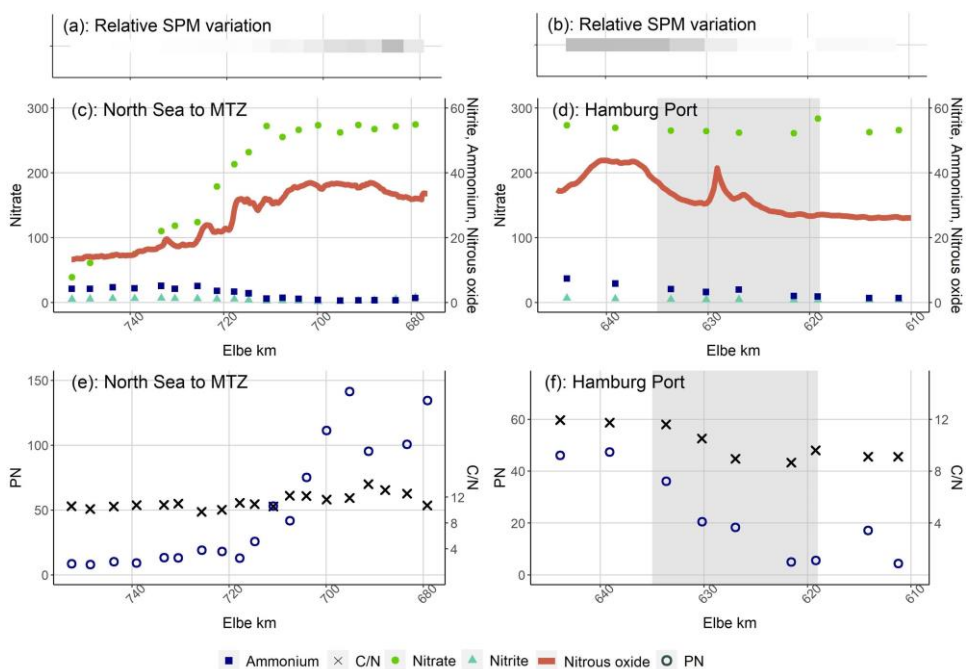


**Figure A3.13.** Succession of N-bearing substances coming from the North Sea and in the Port of Hamburg in March 2022: Relative change of SPM concentrations (a) from the North Sea and (b) in the Port of Hamburg. Nitrate in  $\mu\text{mol L}^{-1}$ , nitrite in  $\mu\text{mol L}^{-1}$ , ammonium in  $\mu\text{mol L}^{-1}$  and nitrous oxide concentrations in  $\text{nmol L}^{-1}$  plotted against stream kilometers (c) from the North Sea and (d) in the Port of Hamburg. Particulate nitrogen concentrations in  $\mu\text{mol L}^{-1}$  and C/N values plotted against stream kilometers (e) from the North Sea and (f) in the Port of Hamburg. The grey area in (d) and (f) shows the position of the Port of Hamburg.

## Appendix A4

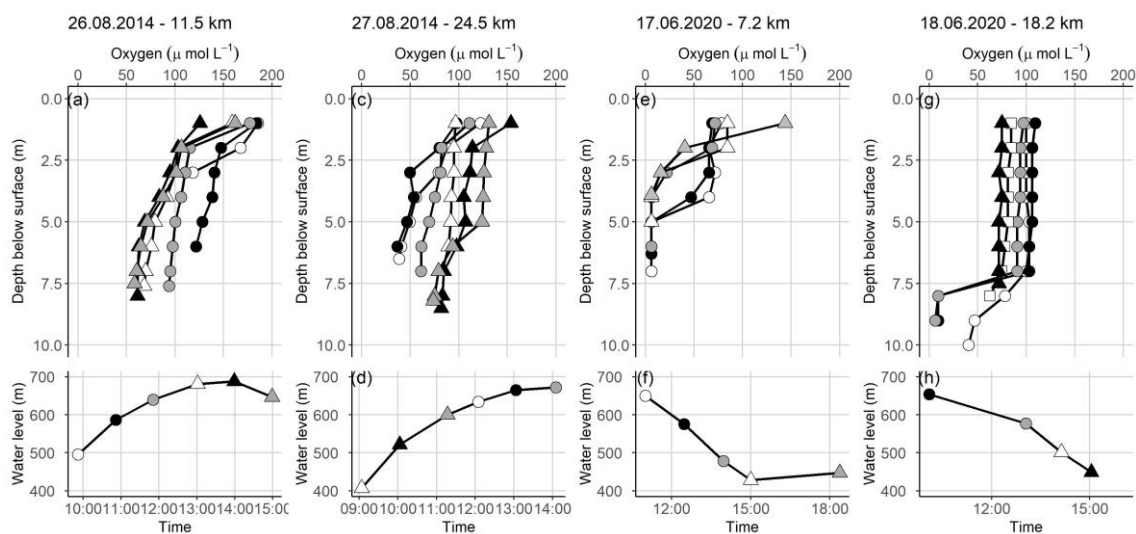


**Figure A4.1.** Vertical profiles of oxygen concentration in 2014 and 2020 at different stations along the Tidal River and Dollard Reach: a) vertical profile measured in 2014 at a station at stream kilometer 11.5, with b) the water levels over time at the station, c) vertical profile measured in 2014 at a station at stream kilometer 24.5, with d) the water levels over time at the station, e) vertical profile measured in 2020 at a station at stream kilometer 7.2, with f) the water levels over time at the station, g) vertical profile measured in 2020 at a station at stream kilometer 18.2, with h) the water levels over time at the station

The lowest concentration in bottom water in 2014 was  $58 \mu\text{mol L}^{-1}$  at stream km 11.5, and  $36 \mu\text{mol L}^{-1}$  at km 24. In 2020, oxygen concentration was low in surface water at stream km 7.2, and anoxia occurred in bottom water over a full tidal cycle. Downstream, at km 18.2,  $\text{O}_2$  concentration decreased 6 m below the surface, and anoxic conditions were reached at low water levels

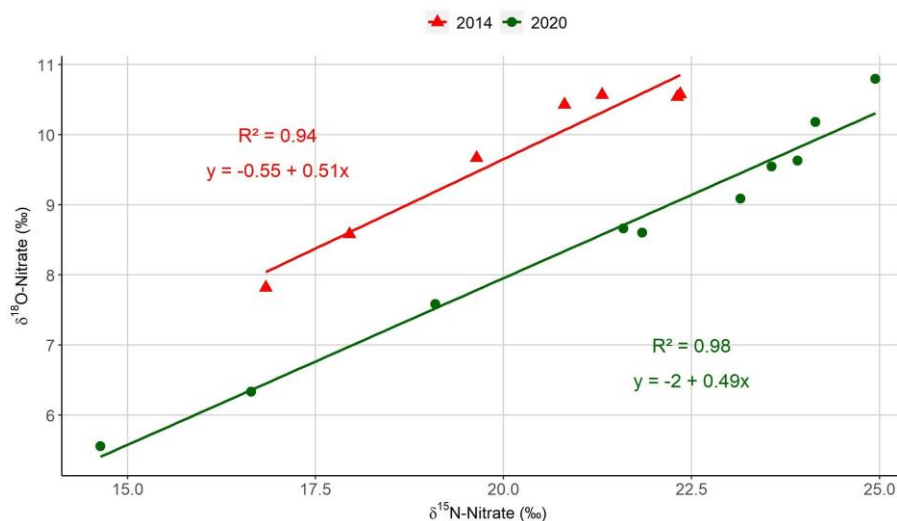


**Figure A4.2.** Plot of  $\delta^{18}\text{O-nitrate}$  vs  $\delta^{15}\text{N-nitrate}$  in the Tidal River of the Ems estuary in 2014 and 2020 with regression line, coefficient of determination and linear regression equation. Point shapes and colors mark stream kilometer of each sampling station.

### Mapping approach

We used a mapping approach inspired by Lewicka-Szczebak et al. (2017) using open-system approach for calculations of isotope effects. In an open-system approach the isotope effect can be described as the slope of the linear relationship between isotope values of nitrogen and fraction  $f$  (Chapter 2.8) (Sigman et al. 2009). The remaining fraction of substrate  $f$  is determined by  $f = ([C]/[C_{initial}])$ . We used our calculated mixing values (Chapter 2.7) as initial concentration and isotope values. In following, we explain our procedure in detail using a sample (ID: 702, km 41.50, 2020) as an example.

We calculated nitrate mixing concentration and the theoretical isotope value of samples following conservative mixing between two endmembers (Liss 1976). For our example we derived:

$$s = \frac{(32.31-18.64)}{(32.31-0)} = 0.423 \quad (\text{A4.1})$$

$$C_{Mix} = s \times C_R + (1 - s)C_M = 0.423 \times 181.70 \mu\text{mol L}^{-1} + (1 - 0.423) \times 3.60 \mu\text{mol L}^{-1} = 78.94 \mu\text{mol L}^{-1} \quad (\text{A4.2})$$

$$\begin{aligned} \delta_{Mix} &= \frac{s \times C_R \times \delta_R + (1 - s) \times C_M \times \delta_M}{C_{Mix}} = \delta_{Mix} \quad (\text{A4.3}) \\ &= \frac{0.423 \times 181.70 \mu\text{mol L}^{-1} \times 14.64 \text{‰} + (1 - 0.423) \times 3.60 \mu\text{mol L}^{-1} \times 14.23 \text{‰}}{78.94 \mu\text{mol L}^{-1}} \\ &= 14.62 \text{‰} \end{aligned}$$

We use  $\delta^{15}\text{N-NO}_3^-_{\text{MIX}}$  as initial isotope value and  $c(\text{NO}_3^-)_{\text{MIX}}$ . The remaining fraction for these values is  $f=1$ , since no nitrate is converted during pure mixing processes. Following figure is derived for our example:

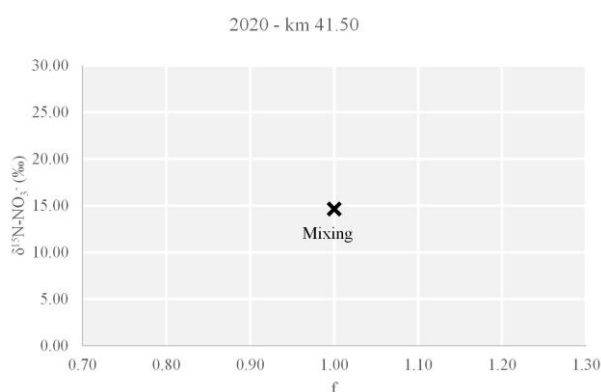


**Figure A4.3.** Calculates mixing  $\delta^{15}\text{N-NO}_3^-$  versus the remaining fraction of nitrate for the example sample

We know that nitrogen isotopes ratios change along a specific isotope effect. We determined following relevant isotope effects for the Ems estuary:  $^{15}\epsilon_{DENIT} = -26 \text{ ‰}$ ,  $^{15}\epsilon_{REMIN} = -1.2 \text{ ‰}$ . As long as ammonium concentration is low, we applied this  $^{15}\epsilon_{REMIN}$  value for nitrification with prior remineralisation. As soon as, ammonium and nitrite concentrations increased, we assume that remineralisation no longer determines the overall isotope effect of nitrification. We expect a combined influence of ammonium oxidation with an isotope effect  $^{15}\epsilon = -14$  to  $-41 \text{ ‰}$  (Mariotti et al. 1981; Casciotti et al. 2003; Santoro and Casciotti 2011) and nitrite oxidation with  $^{15}\epsilon = +9$  to  $+20 \text{ ‰}$  (Casciotti 2009; Buchwald and Casciotti 2010; Jacob et al. 2017) that leads to an assumed isotope effect of  $^{15}\epsilon_{NITRI} = -10 \text{ ‰}$  (Sanders unpublished data).

In our example sample, ammonium and nitrite concentration already increased, so we used  $-10 \text{ ‰}$  as slope for our nitrification line and  $-26 \text{ ‰}$  for the denitrification line. Which leads to the following figure.

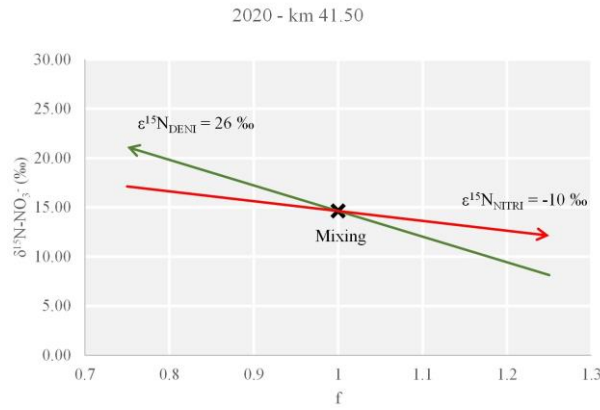


**Figure A4.4.** Calculated mixing  $\delta^{15}\text{N-NO}_3^-$  versus the remaining fraction of nitrate for the example sample. The red line indicates the isotope effect of nitrification with  $^{15}\epsilon_{NITRI} = -10 \text{ ‰}$  with the mixing sample as intersect. The green lines indicates the isotope effect of denitrification with  $^{15}\epsilon_{DENIT} = 26 \text{ ‰}$  with the mixing sample as intersect.

We can describe the linear equations for both processes ( $\text{EQ}_{DENIT, \text{mix}}$  and  $\text{EQ}_{NITRI, \text{mix}}$ ) using the isotope effect as slope and the calculated mixing value as intersect. Leading to following equations:

$$\text{EQ}_{DENIT, \text{mix}}:$$

$$\begin{aligned} \delta^{15}N_{\text{mix}, DENIT} &= m_{DENIT} \times f + b_{DENIT, \text{mix}} \rightarrow b_{DENIT, \text{mix}} = \delta^{15}N_{\text{mix}, DENIT} - m_{DENIT} \times f \\ &= 14.64 \text{ ‰} + 26 \times 1 = 40.64 \end{aligned} \quad (\text{A4.4})$$

$$\text{EQ}_{NITRI, \text{mix}}$$

$$\begin{aligned} \delta^{15}N_{\text{mix}, NITRI} &= m_{NITRI} \times f + b_{NITRI, \text{mix}} \rightarrow b_{NITRI, \text{mix}} = \delta^{15}N_{\text{mix}, NITRI} - m_{NITRI} \times f = \\ &14.64 \text{ ‰} + 10 \times 1 = 24.64 \end{aligned} \quad (\text{A4.5})$$

If only one of the processes occurred, the isotope value of our measured sample would lie on one of the regression lines. However, as the following plot shows, this is not the case for our example. The remaining fraction  $f$  of the sample is derived by  $f = ([C]/[C_{initial}])$ .

$$f = \frac{C_M}{C_{Mix}} = \frac{84.60 \mu\text{mol L}^{-1}}{78.94 \mu\text{mol L}^{-1}} = 1.07 \quad (\text{A4.6})$$

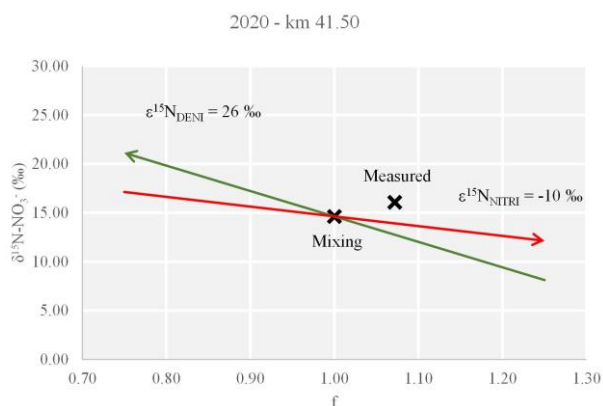


**Figure A4.5.** Calculated mixing  $\delta^{15}\text{N-NO}_3^-_{\text{mix}}$  and measured  $\delta^{15}\text{N-NO}_3^-_{\text{sample}}$  versus the remaining fraction of nitrate for the example sample. The red line indicates the isotope effect of nitrification with  $^{15}\epsilon_{\text{NITRI}} = -10 \text{‰}$  with the mixing sample as intersect. The green lines indicates the isotope effect of denitrification with  $^{15}\epsilon_{\text{DENI}} = 26 \text{‰}$  with the mixing sample as intersect.

After plotting the measured value, we calculate linear equations for each process using the measured values as the intersect ( $\text{EQ}_{\text{DENI,meas}}$  and  $\text{EQ}_{\text{NITRI,meas}}$ ). Leading to following results:

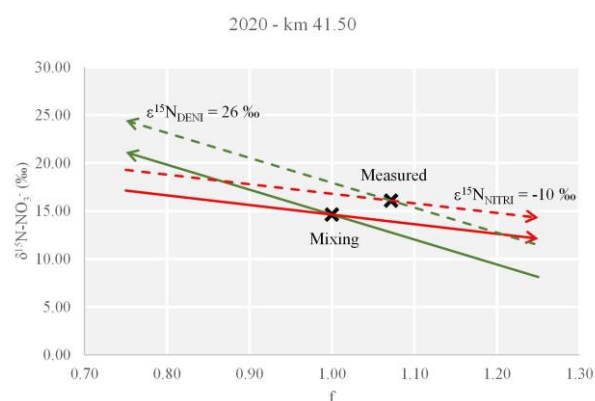


**Figure A4.6.** Calculated mixing  $\delta^{15}\text{N-NO}_3^-_{\text{mix}}$  and measured  $\delta^{15}\text{N-NO}_3^-_{\text{sample}}$  versus the remaining fraction of nitrate for the example sample. The red line indicates the isotope effect of nitrification with  $^{15}\epsilon_{\text{NITRI}} = -10 \text{‰}$  with the mixing sample as intersect. The green lines indicates the isotope effect of denitrification with  $^{15}\epsilon_{\text{DENI}} = 26 \text{‰}$  with the mixing sample as intersect. The dashed red line indicates the isotope effect of nitrification with  $^{15}\epsilon_{\text{NITRI}} = -10 \text{‰}$  with the measured sample as intersect. The dashed green lines indicates the isotope effect of denitrification with  $^{15}\epsilon_{\text{DENI}} = 26 \text{‰}$  with the measured sample as intersect.

EQ<sub>DENI, meas</sub>:

$$\delta^{15}N_{meas, DENI} = m_{DENI} \times f + b_{DENI, meas} \rightarrow b_{DENI, meas} = \delta^{15}N_{meas, DENI} - m_{DENI} \times f = 16.09 \text{ ‰} + 26 \times 1.07 = 43.95 \quad (\text{A4.7})$$

EQ<sub>NITRI, meas</sub>

$$\delta^{15}N_{mix, NITRI} = m_{NITRI} \times f + b_{NITRI, meas} \rightarrow b_{NITRI, meas} = \delta^{15}N_{meas, NITRI} - m_{NITRI} \times f = 16.09 \text{ ‰} + 10 \times 1.07 = 26.80 \quad (\text{A4.8})$$

We determine intersects of a linear equation derived by the mixing value as intersect and an equation derived by the measured sample to calculate the amount of nitrate processes via the different pathways. Therefore, two different approaches are possible for this purpose that lead to the same results.

a) Calculating  $f_{DENI}$ : The intersection of EQ<sub>DENI, mix</sub> and EQ<sub>NITRI, meas</sub> leads to  $f_{DENI}$ . The difference between  $f$  and  $f_{DENI}$  results in  $f_{NITRI}$ . To calculate the amount of nitrate consumed/produced via each process, we use the deviation from the initial fractionation.

$f_{DENI}$ :

$$\delta^{15}N_{DENI} = m_{DENI} \times f_{DENI} + b_{DENI, mix} = m_{NITRI} \times f_{DENI} + b_{NITRI, meas}$$

$$-26 \times f_{DENI} + 40.64 = -10 \times f_{DENI} + 26.80 \quad (\text{A4.9})$$

$$f_{DENI} = \frac{40.64 - 26.80}{26 - 10} = 0.86$$

$f_{NITRI}$ :

$$f_{NITRI} = f - f_{DENI} = 1.07 - 0.86 = 0.21 \quad (\text{A4.10})$$

$c(\text{NO}_3^-)_{DENI}$

$$C_{DENI} = (f_{ini} - f_{DENI}) \times C_{Mix} = (1 - 0.86) \times 78.94 \text{ } \mu\text{mol L}^{-1} = 10.73 \text{ } \mu\text{mol L}^{-1} \quad (\text{A4.11})$$

$c(\text{NO}_3^-)_{NITRI}$

$$C_{NITRI} = f_{NITRI} \times C_{Mix} = 0.21 \times 78.94 \text{ } \mu\text{mol L}^{-1} = 16.39 \text{ } \mu\text{mol L}^{-1} \quad (\text{A4.12})$$

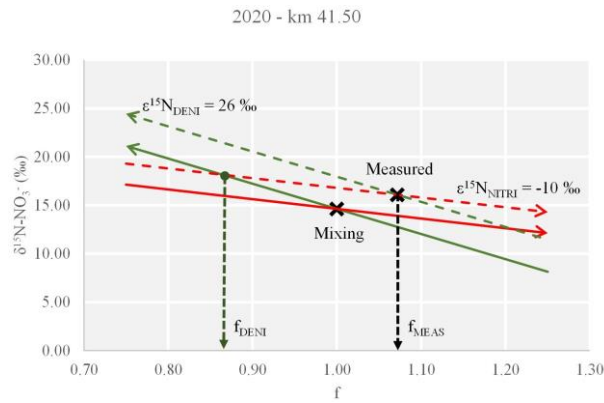


**Figure A4.7.** Calculated mixing  $\delta^{15}\text{N-NO}_3^-_{\text{mix}}$  and measured  $\delta^{15}\text{N-NO}_3^-_{\text{sample}}$  versus the remaining fraction of nitrate for the example sample. The red line indicates the isotope effect of nitrification with  $\epsilon^{15}\text{N}_{\text{NITRI}} = -10 \text{ ‰}$  with the mixing sample as intersect. The green lines indicates the isotope effect of denitrification with  $\epsilon^{15}\text{N}_{\text{DENI}} = 26 \text{ ‰}$  with the mixing sample as intersect. The dashed red line indicates the isotope effect of nitrification with  $\epsilon^{15}\text{N}_{\text{NITRI}} = -10 \text{ ‰}$  with the measured sample as intersect. The dashed green lines indicates the isotope effect of denitrification with  $\epsilon^{15}\text{N}_{\text{DENI}} = 26 \text{ ‰}$  with the measured sample as intersect.

b) Calculating  $f_{\text{NITRI}}$ : The intersection of  $\text{EQ}_{\text{REMIN,mix}}$  and  $\text{EQ}_{\text{DENI,meas}}$  leads to  $f_{\text{NITRI}}$ . The difference between  $f$  and  $f_{\text{NITRI}}$  results in  $f_{\text{DENI}}$ . To calculate the amount of nitrate consumed/produced via each process, we use the deviation from the initial fractionation.

$$f_{\text{NITRI}}:$$

$$\delta^{15}\text{N}_{\text{NITRI}} = m_{\text{DENI}} \times f_{\text{NITRI}} + b_{\text{DENI,meas}} = m_{\text{NITRI}} \times f_{\text{NITRI}} + b_{\text{NITRI,mix}}$$

$$-26 \times f_{\text{NITRI}} + 43.95 = -10 \times f_{\text{NITRI}} + 24.63 \quad (\text{A4.13})$$

$$f_{\text{NITRI}} = \frac{43.95 - 24.63}{26 - 10} = 1.21$$

$$f_{\text{DENI}}:$$

$$f_{\text{DENI}} = f_{\text{NITRI}} - f = 1.21 - 1.07 = 0.14 \quad (\text{A4.14})$$

$$c(\text{NO}_3^-)_{\text{NITRI}}$$

$$C_{\text{NITRI}} = (f_{\text{NITRI}} - f_{\text{ini}}) \times C_{\text{MIX}} = (1.21 - 1) \times 78.94 \mu\text{mol L}^{-1} = 16.39 \mu\text{mol L}^{-1} \quad (\text{A4.15})$$

$$c(\text{NO}_3^-)_{\text{DENI}}$$

$$C_{\text{DENI}} = f_{\text{DENI}} \times C_{\text{MIX}} = 0.14 \times 78.94 \mu\text{mol L}^{-1} = 10.73 \mu\text{mol L}^{-1} \quad (\text{A4.16})$$

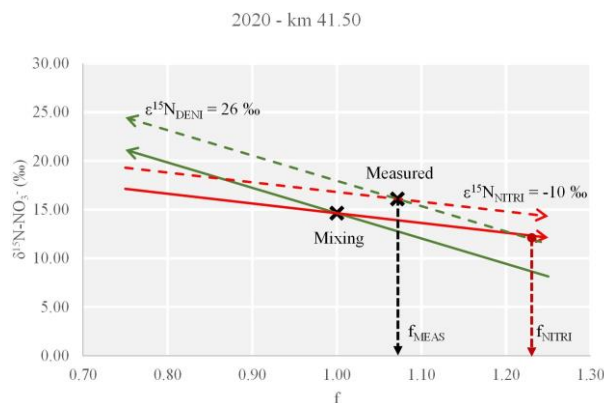


**Figure A4.8.** Calculated mixing  $\delta^{15}\text{N-NO}_3^-_{\text{mix}}$  and measured  $\delta^{15}\text{N-NO}_3^-_{\text{sample}}$  versus the remaining fraction of nitrate for the example sample. The red line indicates the isotope effect of nitrification with  $\epsilon^{15}\text{N}_{\text{NITRI}} = -10 \text{ ‰}$  with the mixing sample as intersect. The green lines indicates the isotope effect of denitrification with  $\epsilon^{15}\text{N}_{\text{DENI}} = 26 \text{ ‰}$  with the mixing sample as intersect. The dashed red line indicates the isotope effect of nitrification with  $\epsilon^{15}\text{N}_{\text{NITRI}} = -10 \text{ ‰}$  with the measured sample as intersect. The dashed green lines indicates the isotope effect of denitrification with  $\epsilon^{15}\text{N}_{\text{DENI}} = 26 \text{ ‰}$  with the measured sample as intersect.

**Table A4.1.** Measured and calculated mixing values for samples in zone 2 in 2014 used for the open-system mapping approach

2014	MEAS		MIX	
km	$c(\text{NO}_3^-)$ $\mu\text{mol L}^{-1}$	$\delta^{15}\text{N-NO}_3^-$ ‰	$c(\text{NO}_3^-)$ $\mu\text{mol L}^{-1}$	$\delta^{15}\text{N-NO}_3^-$ ‰
26.20	151.00	20.81	167.32	16.83
30.73	161.00	19.64	172.84	16.84
66.18	31.10	14.67	23.86	16.04
77.62	21.30	13.56	17.17	15.68
87.53	23.30	14.25	18.40	15.77
88.80	15.10	12.70	13.16	15.29

**Table A4.2.** Results of the open-system mapping approach for samples in zone 2 in 2014

2014	DENI			NITRI			DENI		NITRI			
Km	$F_{\text{Mix}}$	$F_{\text{Meas}}$	m	$b_{\text{mix}}$	$b_{\text{meas}}$	m	$b_{\text{mix}}$	$b_{\text{meas}}$	f	$\text{NO}_3^-$ $\mu\text{M}$ $\text{L}^{-1}$	f	$\text{NO}_3^-$ $\mu\text{M}$ $\text{L}^{-1}$
26.20	1.00	0.90	-26.0	42.83	44.28	-1.2	18.03	21.90	0.84	26.07	1.06	9.75
30.73	1.00	0.93	-26.0	42.84	43.85	-1.2	18.04	20.75	0.89	18.92	1.04	7.08
66.18	1.00	1.30	-26.0	42.04	48.56	-10.0	26.04	27.71	0.90	2.48	1.41	9.72
77.62	1.00	1.24	-26.0	41.68	45.81	-10.0	25.68	25.96	0.98	0.30	1.26	4.43
87.53	1.00	1.27	-26.0	41.77	47.18	-10.0	25.77	26.92	0.93	1.32	1.34	6.23
88.80	1.00	1.15	-26.0	41.29	42.54	-10.0	25.29	24.18	1.07	-0.91	1.08	1.03

**Table A4.3.** Measured and calculated mixing values for samples in zone 2 in 2020 used for the open-system mapping approach

2020 km	MEAS		MIX	
	c(NO <sub>3</sub> <sup>-</sup> ) μmol L <sup>-1</sup>	δ <sup>15</sup> N-NO <sub>3</sub> <sup>-</sup> ‰	c(NO <sub>3</sub> <sup>-</sup> ) μmol L <sup>-1</sup>	δ <sup>15</sup> N-NO <sub>3</sub> <sup>-</sup> ‰
30.64	141.80	21.85	151.83	14.64
35.25	119.50	19.62	120.89	14.64
41.50	84.60	16.09	78.94	14.63
41.50	76.60	15.73	67.08	14.63
44.83	67.50	14.39	64.45	14.63
48.12	51.90	12.49	48.02	14.62
48.37	62.20	13.23	60.35	14.62
55.61	48.90	11.96	48.58	14.62

**Table A4.4.** Results of the open-system mapping approach for samples in zone 2 in 2020

2020 Km	DENI			NITRI			DENI		NITRI			
	F <sub>Mix</sub>	F <sub>Meas</sub>	m	b <sub>mix</sub>	b <sub>meas</sub>	m	b <sub>mix</sub>	b <sub>meas</sub>	f	NO <sub>3</sub> <sup>-</sup> μM L <sup>-1</sup>	f	NO <sub>3</sub> μM L <sup>-1</sup>
30.64	1.00	0.93	-26.0	40.64	46.13	-10.0	24.64	31.18	0.59	62.11	1.34	52.08
35.25	1.00	0.99	-26.0	40.64	45.32	-10.0	24.64	29.50	0.70	36.76	1.29	35.36
41.50	1.00	1.07	-26.0	40.63	43.95	-10.0	24.63	26.80	0.86	10.727	1.208	16.387
41.50	1.00	1.14	-26.0	40.63	45.42	-10.0	24.63	27.15	0.84	10.56	1.30	20.08
44.83	1.00	1.05	-26.0	40.63	41.62	-10.0	24.63	24.86	0.99	0.96	1.06	4.02
48.12	1.00	1.08	-26.0	40.62	40.59	-10.0	24.62	23.30	1.08	-3.96	1.00	-0.09
48.37	1.00	1.03	-26.0	40.62	40.03	-10.0	24.62	23.54	1.07	-4.10	0.96	-2.25
55.61	1.00	1.01	-26.0	40.62	38.13	-10.0	24.62	22.03	1.16	-7.87	0.84	-7.55

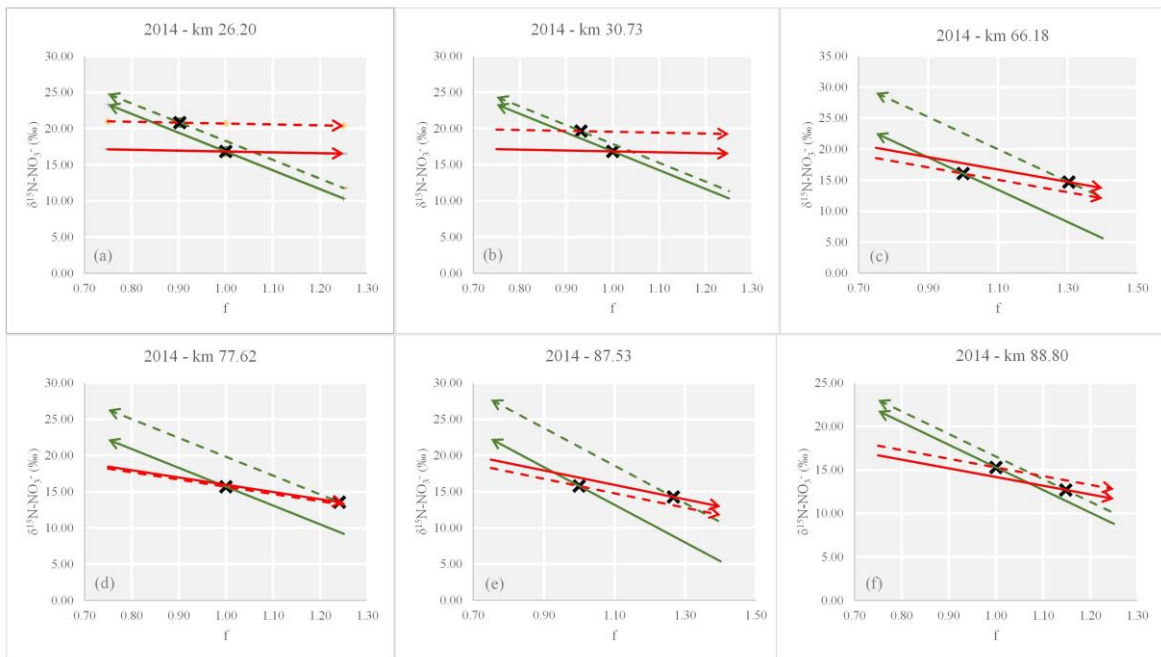


**Figure A4.9.** Plots derived by our open-system mapping approach for samples in 2014 (a) at stream kilometer 26.20, (b) at stream kilometer 30.73 (c) at stream kilometer 66.18, (d) at stream kilometer 77.62, (e) at stream kilometer 87.53, (f) at stream kilometer 88.80. Line color and arrow direction indicate the turnover-process. Green lines with arrows oriented upwards to the left are denitrification lines. Red lines with arrows oriented downwards to the right are nitrification lines. Straight lines indicate linear regression with mixing values as intercept and dashed lines linear regressions with the measured samples as intersect.

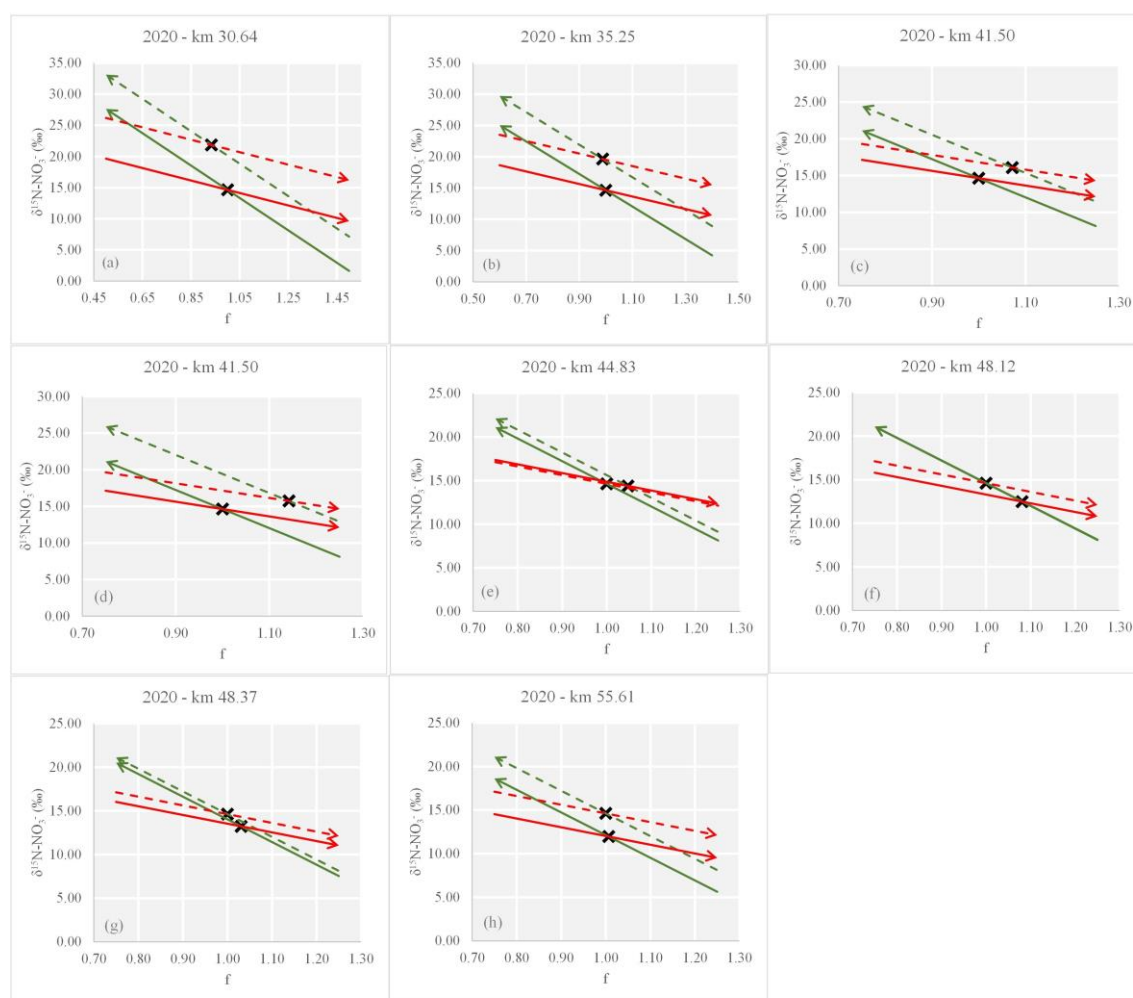


**Figure A4.10.** Plots derived by our open-system mapping approach for samples in 2020 (a) at stream kilometer 30.64, (b) at stream kilometer 35.25, (c) at stream kilometer 41.50, (d) at stream kilometer 41.50, (e) at stream kilometer 44.83, (f) at stream kilometer 48.12, (g) at stream kilometer 48.37, (h) at stream kilometer 55.61. Line color and arrow direction indicate the turnover-process. Green lines with arrows oriented upwards to the left are denitrification lines. Red lines with arrows oriented downwards to the right are nitrification lines. Straight lines indicate linear regression with mixing values as intercept and dashed lines linear regressions with the measured samples as intersect.

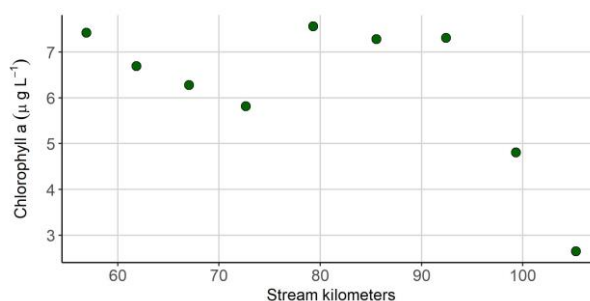


**Figure A4.11.** Chlorophyll a concentration in the Outer Reaches /zone 3 during our cruise in 2020. For chlorophyll a, water was filtered through combusted, pre-weighted GF/F Filters (4 h, 450 °C) and stored frozen for later analysis in our laboratory. The slight chlorophyll maximum supports our assumption of nitrate uptake due to ongoing primary production in the Outer Reaches.



---

## List of publications

The thesis is composed of four individual scientific publications, which are either published (chapter 4), submitted (chapter 1 and 3) or in preparation for submission (chapter 2) in a peer-review journal. Following, publications that arose in course of this thesis are listed and the co-authors contributions are further specified.

**Schulz, G., van Beusekom, J. E. E., Jacob, J., Bold, S., Schöl, A., Ankele, M., Sanders, T., and Dähnke, K.:** *Low discharges intensifies nitrogen retention in rivers – a case study in the Elbe River, Science of The Total Environment, 904, 166740, <https://doi.org/10.1016/j.scitotenv.2023.166740>, 2023.*

KD designed this study. JJ, MA, TS and GS took and analyzed samples at the weir in Geesthacht. SB gathered and organized large parts of the Hereon data set. GS, JJ, JEEvB, TS and KD did the first data interpretation and evaluation. KD, TS, MA, SB, AS, JJ and JEEvB contributed with scientific and editorial recommendations. GS prepared the manuscript with contributions of all co-authors.

**Schulz, G., Sanders, T., Russnak, V., van Beusekom, J. E. E., and Dähnke, K.:** *A decade of summers: How low discharges affects estuarine nitrate turnover – a case study in the freshwater Elbe Estuary, [in preparation].*

GS, TS and KD designed this study. TS, GS, and VR were responsible for cruise sampling and measurements. GS, TS, JEEvB, and KD did the first data interpretation and evaluation. KD, JEEvB, VR and TS contributed with scientific and editorial recommendations. GS prepared the manuscript with contributions of all co-authors.

**Schulz, G., Sanders, T., Voynova, Y. G., Bange, H. W., and Dähnke, K.:** *Seasonal variability of nitrous oxide concentrations and emissions in a temperate estuary, Biogeosciences, 20, 3229–3247, <https://doi.org/10.5194/bg-20-3229-2023>, 2023.*

GS, TS and KD designed this study. GS did the sampling and measurements for cruises from 2020 to 2022 as well as the data interpretation and evaluation. TS was responsible for the sampling and measurements for cruises done in 2017 and 2019. YGV provided the oxygen data correction from the FerryBox data. KD, HWB, YGV and TS contributed with scientific and editorial recommendations. GS prepared the manuscript with contributions of all co-authors.

**Schulz, G., Sanders, T., van Beusekom, J. E. E., Voynova, Y. G., Schöl, A., and Dähnke, K.:** *Suspended particulate matter drives the spatial segregation of nitrogen turnover along the hyper-turbid Ems estuary, Biogeosciences, 19, 2007–2024, <https://doi.org/10.5194/bg-19-2007-2022>, 2022.*

GS, TS and KD designed this study. GS did the sampling, sample measurement and analyses for the cruise of 2020 as well as the data interpretation and evaluation. TS did the sampling and sample measurement for the cruise in 2014. YGV provided the oxygen data and correction from the FerryBox. AS provided the oxygen data from German Federal Institute of Hydrology. KD, AS, YGV, JEEvB and TS contributed with scientific and editorial recommendations. GS prepared the manuscript with contributions from all co-authors.

Further, following papers were published or in preparation for submission, in which I worked on as a co-author independently of my doctoral thesis.

*Norbisrath, M., Pätsch, J., Dähnke, K., Sanders, T., Schulz, G., van Beusekom, J. E. E., and Thomas, H.: Metabolic alkalinity release from large port facilities (Hamburg, Germany) and impact on coastal carbon storage, Biogeosciences, 19, 5151 – 5165, <https://doi.org/10.5194/bg-19-5151-2022>, 2022.*

MN, KD, and HT designed the study. MN did the sampling, sample measurements and analyses, and data interpretation and evaluation and prepared the manuscript. JP did the biogeochemical simulation by using the 3D-ECOHAM model. GS performed stable isotope measurements, data analysis, and interpretation and added to the method description. KD, TS, JP, JEEvB, and HT provided scientific and editorial recommendations. MN wrote the manuscript with input from all co-authors.

*Ingeniero, R. C. O., Schulz, G., and Bange, H.W.: Dissolved Nitric Oxide in the Lower Elbe Estuary and the Hamburg Port Region, [in preparation].*

RI conceptualized and designed the study, carried out field sampling and analysis, and authored the manuscript. GS managed the research cruise, performed laboratory analyses of supplementary biogeochemical parameters, and contributed a critical review of the manuscript. HB assisted with study conceptualization, supervision, and a critical review of the manuscript.

---

## Acknowledgments

I would like to thank everyone who supported me throughout my doctoral period. Through their ongoing support, guidance and inspiration, I was able to truly enjoy my time as a doctoral student and had great fun doing science.

First, I thank Dr. Kirstin Dähnke for her excellent supervision, her many fruitful ideas and discussions, and the opportunities to join research cruises and conferences even under difficult pandemic conditions.

I thank Dr. Birgit Gaye and Prof. Hermann Bange for participating on my supervisor panel with their continuous support, guidance and helpful suggestions.

I especially thank Dr. Tina Sanders, who introduced me to the laboratory and campaign work, helped me design my studies with many valuable discussions, and guided me throughout my entire doctoral period.

Many thanks to Dr. Justus van Beusekom for his many inspiring ideas, discussions, and especially his help in the final stages of writing my PhD thesis.

I am grateful for the entire “Aquatic Nutrient Cycles” group for many joyful lunch breaks as well as for creating an inspiring and safe work environment. I thank Leon Schmidt, Markus Ankele and Andreas Neumann for their support in the laboratory, on the research cruises, on scientific questions or truly any other problem. Furthermore, I want to thank all of my great coauthors, who helped to write the papers that became the chapters of my thesis, as well as my CLICCs C3 working group: Martin Döring, Johannes Pein and Eva Schick for our safe and pleasant meetings, which gave me a view beyond the natural science horizon.

A special thanks goes to my fellow PhD candidates: Fabrizio Minutolo, Vanessa Russnak and Eva Husman for their assistance during research cruises, laboratory work, and helpful discussions as well as for proofreading parts of my thesis. I greatly appreciate the everlasting mutual support (except for wizard games).

I also thank the crew of the *R/V Ludwig Prandtl* for always providing a great support during our cruises and for the pancakes on board.

Finally, I greatly appreciate all the moral support I received by my family and friends. A special thanks goes to my boyfriend Andreas, who moved to Hamburg for me and always made sure I found a balance between work and social life but was also patient during stressful times.